AIRFOIL VIBRATION DAMPERS PROGRAM
CONTRACT NO. NAS8-36720

FINAL REPORT

Prepared For:

NASA/George C. Marshall Space Flight Center
Marshall Space Flight Center, Alabama

11 November 1991

Prepared By:

R. M. Cook, Project Engineer
Advanced Rotating Machinery Projects
Rocketdyne Division
Rockwell International

Approved By:

R.F. Sutton, Manager
Advanced Rotating Machinery Projects

A. Csomor
Program Manager
NLS Turbomachinery

TABLE OF CONTENTS

LIST OF FIGURES

LIST OF FIGURES (Continued)

LIST OF FIGURES (Continued)

LIST OF FIGURES (Continued)

LIST OF FIGURES (Continued)

LIST OF TABLES

ACKNOWLEDGEMENTS

The technical effort reported in this document was performed at the Rocketdyne Division of the Rockwell International Corporation under the program management and direction of Mr. A. Csomor, Program Manager. The effort was organized as a project in the Advanced Rotating Machinery Projects organization under the supervision of Mr. R. F. Sutton, Manager. Mr. R. M. Cook was the cognizant Project Engineer. The analytical and technical effort was performed by Mr. G. A. Davis and Mr. S. S. Gage, who performed the BLDAMP code implementation, dynamic analyses, and data reduction and organization. Mr. D. L. Bice was the Test Engineer for the testing, which was performed in the Rocketdyne Engineering Development Laboratory. Griffin Consulting served as consultants to Rocketdyne, with Mr. J. H. Griffin and Mr. C-H. Menq performing the code development function.

FORWARD

The attainable service life of a turbine blade is very sensitive to the amplitude of vibratory stress which, under resonant conditions, is inversely proportional to the amount of damping in the system. Inherent damping in turbine-bladed disk assemblies is relatively small. Therefore, the introduction of effective damping is instrumental in reducing alternating stress and extending blade life.

The most commonly-used technique to increase the damping in turbine blades is to provide for vibrational energy dissipation, through the use of friction interfaces between adjacent blades. Many different damping configurations, based on this concept, have been used in the past; the designs of which were largely based on empirical data and on experience with previous applications. There have been several published attempts to analytically evaluate these designs. For the most part, they consist of simple studies, aimed at understanding the damping phenomenon, and do not provide useful design tools. Therefore, the objectives of this program are to develop and to experimentally validate the analytical tools necessary for the evaluation of friction dampers on a detail design level. Secondly, it is hoped that the extensive experimental database generated in this program can be used by future code developers to improve upon the analytical work presented herein and by designers to help in the preliminary sizing of friction dampers for turbine blade applications.

ABSTRACT

The Airfoil Vibration Damper program has consisted of an analysis phase and a testing phase. During the analysis phase, a state-of-the-art computer code was developed, which can be used to guide designers in the placement and sizing of friction dampers. The use of this computer code was demonstrated by performing representative analyses on turbine blades from the High Pressure Oxidizer Turbopump (HPOTP) and High Pressure Fuel Turbopump (HPFTP) of the Space Shuttle Main Engine (SSME). The testing phase of the program consisted of performing friction damping tests on two different cantilever beams. Data from these tests provided an empirical check on the accuracy of the computer code developed in the analysis phase.

Results of the analysis and testing showed that the computer code can accurately predict the performance of friction dampers. In addition, a valuable set of friction damping data was generated, which can be used to aid in the design of friction dampers, as well as provide benchmark test cases for future code developers.

1.0 INTRODUCTION AND SUMMARY

Turbine blades are subjected to severe loading conditions during normal operation, consisting of a combination of thermal, centrifugal, power bending, and oscillatory forces. The oscillatory forces are caused by disturbances in the hot-gas flow due to upstream and downstream obstructions, which generally occur at some multiple of pump speed. Dynamic excitation of the turbine blade occurs, as it passes through these flow disturbances during rotation of the disk. Although it is desirable to design turbine blades to avoid coincidence of natural frequencies and flow stream excitation frequencies, aerodynamic constraints imposed on the blade airfoil make it nearly impossible to design a completely resonant-free blade. Natural frequencies exist in almost all blade applications on the SSME. These natural frequencies are in close proximity to excitation frequencies in the hot-gas stream. Therefore, the turbine blade designer is forced to rely on additional damping to improve turbine blade fatigue life. Usually this takes the form of friction dampers, consisting of small, centrifugally-loaded, metal plates. These plates connect each blade to the two adjacent blades and provide damping, as vibration occurs, by frictional scrubbing.

Historically, friction dampers have been designed using empirical data obtained from spin rig and engine testing. Analytical methods of determining friction damper performance have been developed, but these have proven to be either too expensive (transient time-history methods) or too simplistic (single-mode, steady-state harmonic balance methods) for practical use. Therefore, the computer code BLDAMP was developed to economically predict turbine blade friction damper performance. The code is not limited by the size of the finite-element representation of the blade. It includes the effects of as many as eight modes of vibration, as well as allowing input of any arbitrary forcing function.

In addition to the analytical task described above, laboratory testing was completed to determine the effectiveness of friction damping in the reduction of vibratory stresses in a cantilever beam. This testing was done to provide a good empirical database with which to validate the computer code and also to serve as a benchmark for future code developers and damper designers. The tests were performed using two different sized beams; one with a low natural frequency and one with a high natural frequency. Two different dampers of the same geometry, but different materials, were tested on each of the beams to determine their influence on beam response. Results showed that friction damping can be extremely effective in reducing the response levels of vibrating structures. Friction damping was found to provide the greatest reduction in dynamic response when the damper was located near the tip of the beam and also when the normal load was above a critical value.

The friction damping test results were compared with analytical predictions made using the computer program BLDAMP, which was developed in an earlier phase of this program. The comparison showed good agreement between test and analysis results. However, the analytical predictions were highly dependent on friction coefficient. Since friction coefficients were not readily available for the materials used in the test program, this parameter was used to tune the analytical results to match test data.

2.0 TECHNICAL DISCUSSION

2.1 BLDAMP COMPUTER CODE

2.1.1 Summary

The computer code BLDAMP, developed by Griffin Consulting for the task of predicting the performance of friction dampers, was installed on the Rocketdyne CDC computer system. It was thoroughly exercised, using the High-pressure Fuel Turbopump (HPFTP) first-stage turbine blade of the Space Shuttle Main Engine (SSME) as a sample case. Several modifications were made to improve ease of use and output format, as part of the code implementation. The new user manual, as well as a complete listing of the modified code, is included in this report.

Computer predictions for the performance of the HPFTP first-stage turbine blade dampers are included as a sample exercise to demonstrate the various options of BLDAMP. The results presented herein should not be used for design purposes, as the forcing functions used in the analysis were rough assumptions, which were not based on engine measurements or hydrodynamic analysis of the flow field surrounding the blades.

2.1.2 Code Description and Use. BLDAMP is a special purpose computer code developed by Griffin Consulting. It analytically predicts the performance of turbine blade friction dampers. The theoretical development of the method used by the code is reproduced from portions of Reference 1 and is included as an appendix (Section 6.1) of this report.

Input to the code consists of modal parameters, which describe the dynamic characteristics of a turbine blade. These parameters are derived either from an analytical representation of the blade or from a modal test. Damper stiffness properties and friction data are also input as problem parameters. A complete description of all the required input data for running BLDAMP, as well as a listing of the code, is provided in Section 6.2 of the Appendix.

The code is capable of performing three different types of computer analyses. Each analysis type is described briefly below. Sample cases are also presented to illustrate the option. The sample cases were provided by the code developer and were subsequently rerun with identical results, using the Rocketdyne version of the code.

2.1.2.1 Frequency Response Analysis. This option computes the peak response of a friction damper, due to a sinusoidal forcing function over a frequency range of interest for a given normal load. The response is printed in a table of amplitude (stress or displacement) versus frequency. A sample plot of the output data from the program is presented in Figure 2.1-1 for a two degree of freedom oscillator. It is important to understand that the damper normal load, for which the curve of Figure 2.1-1 is calculated, is actually half of the centrifugal load for a single damper. This distinction is made because, for each damper, half of the load is supported by each blade. The program still considers two dampers attached to the blade. However, both the input and output data refer to a normal force which is only half of the centrifugal load of one damper.

2.1.2.2 Optimum Normal Force Analysis. The optimum normal force analysis option computes the resonant response of a blade under sinusoidal loading at various damper normal force values. Printed output consists of a table of peak response versus normal force. Thus, an optimum damper normal force can be obtained using this

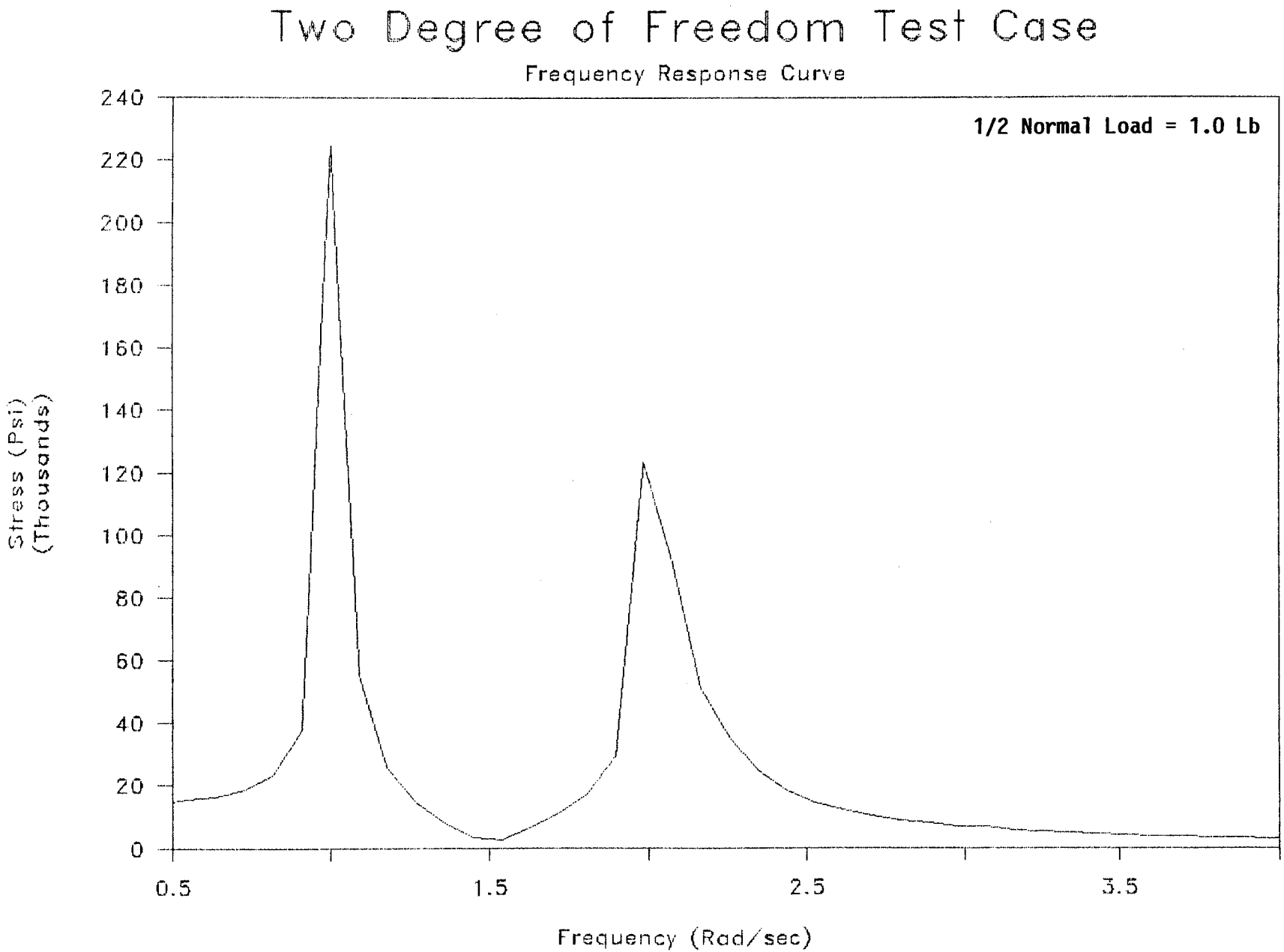

Figure 2.1-1 Two degree of freedom frequency response plot

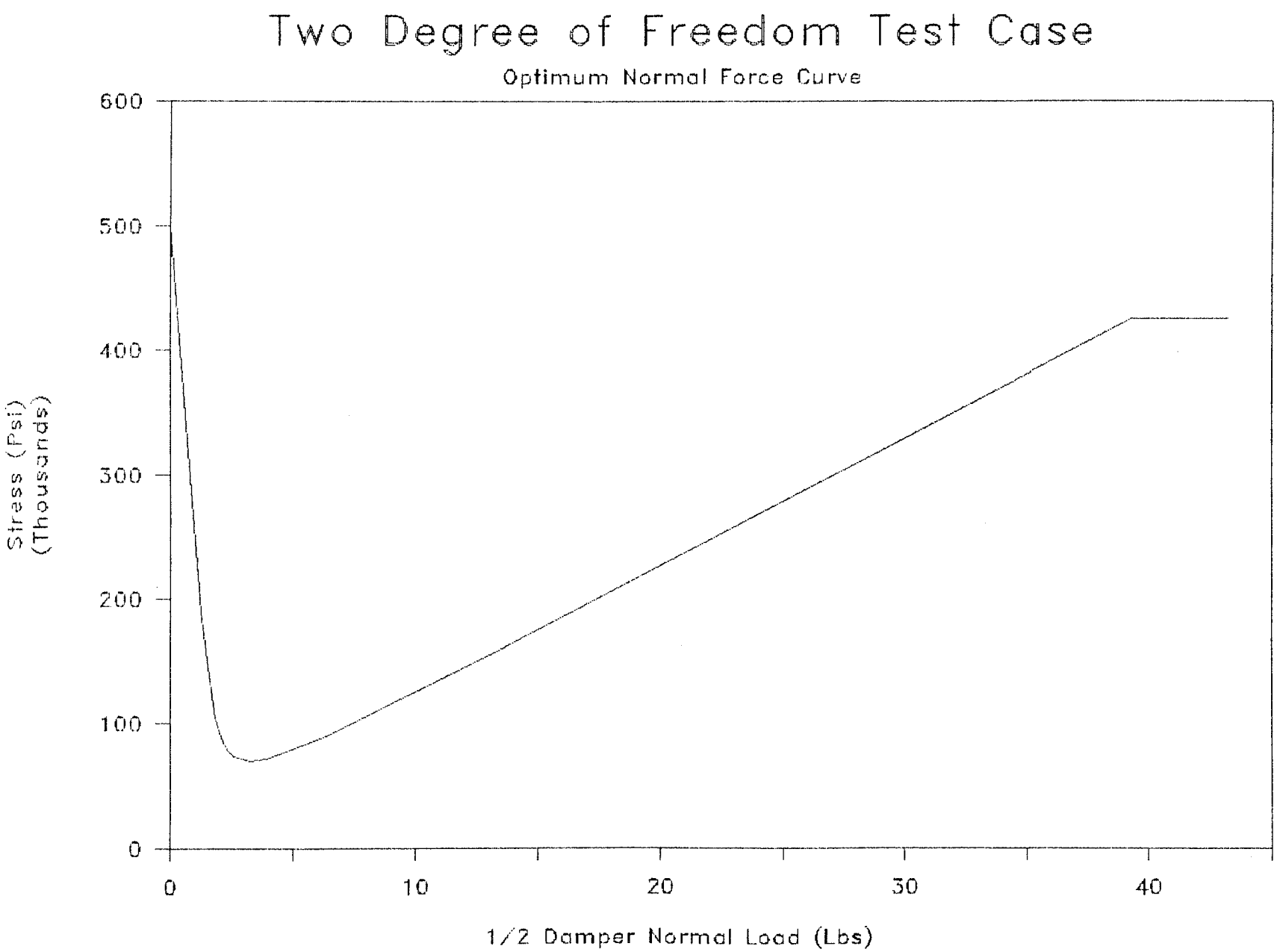

Figure 2.1-2 Two degree of freedom optimum normal force curve

option. An optimum normal force plot is shown in Figure 2.1-2 for the two degree of freedom oscillator. Again, note that the normal force values given in the curve are equal to one-half of the centrifugal load due to a single damper.

2.1.2.3 Damper Performance Analysis. The damper performance analysis option determines the response of a frictionally-damped turbine blade, as a function of the response of the same blade with no friction damper. It is easy to determine the improvement gained by the addition of friction dampers from information of this type. A damper performance curve for a two degree of freedom oscillator is presented in Figure 2.1-3. It clearly shows the effectiveness of friction damping.

2.1.3 HPFTP Damper Optimization. An SSME blade was used as a test case to exercise the code and to gain experience with systems having the same dynamic characteristics as actual rocket engine turbine blades. The blade chosen for analysis was the HPFTP first-stage turbine blade (P/N R0019821). Modal results from an existing finite-element model of the blade were available for use. The only unavailable information was the modal stress distribution, which was not calculated during the initial analysis. In lieu of rerunning the original analysis to obtain modal stresses, it was determined that blade tip displacement would be an adequate measure of blade response to be used in the calculations. Normally, an equivalent alternating stress at some critical location is used as a tracking parameter and indicator of the level of response. At a later date, modal stress information became available. The displacement-based optimization curves were used, in conjunction with this new information, to obtain rough estimates of the optimum damper normal force for the HPFTP turbine blade.

Geometry plots of the blade model used in the analysis are shown in Figure 2.1-4. Boundary conditions consisted of restraining the model along two rows of nodes at the shank root, while material properties used in the analysis reflect those at SSME operational temperature. Comparison with blade-in-block holographic modal test results shows an average error of only 6.3 percent for the first 6 modes. Centrifugal stiffening effects were not included in the analysis. Modal information was derived from the model and was used as input to BLDAMP. A Campbell diagram based on the computer-generated results from the model is presented in Figure 2.1-5. This Campbell diagram should not be used for design purposes. The official Campbell diagram for the HPFTP first-stage blade is based on spin test results. It correctly includes the effects of centrifugal stiffening and disk/fir tree interface flexibility. The analysis presented herein does not attempt to address these issues, but is intended to serve only as an illustrative example on the use and capabilities of the computer program BLDAMP.

The frequency response option of BLDAMP was exercised by forcing the blade second mode with a 13N sinusoidal forcing function. Frequencies ranged from approximately 6,000 to 12,000 Hz. The forcing function was chosen such that the generalized force for the second mode was of such a magnitude as to cause a unit displacement of the blade tip on an undamped blade being forced at resonance. All other generalized forces were chosen to be zero. Note that undamped refers to no friction damping, in the context of this report. A viscous damping ratio of 0.01 was used in all cases, both with and without friction damping present. Figure 2.1-6 presents a comparison of the frequency response plots for the undamped- and frictionally-damped blades. The resonant response of the blade second mode, which occurs at approximately 10,100 Hz, is clearly shown in the figure. The frequency shifts to a higher value with the addition of friction damping to the system. This expected result is opposite to the effect of viscous damping, which reduces the resonant frequency as damping is increased.

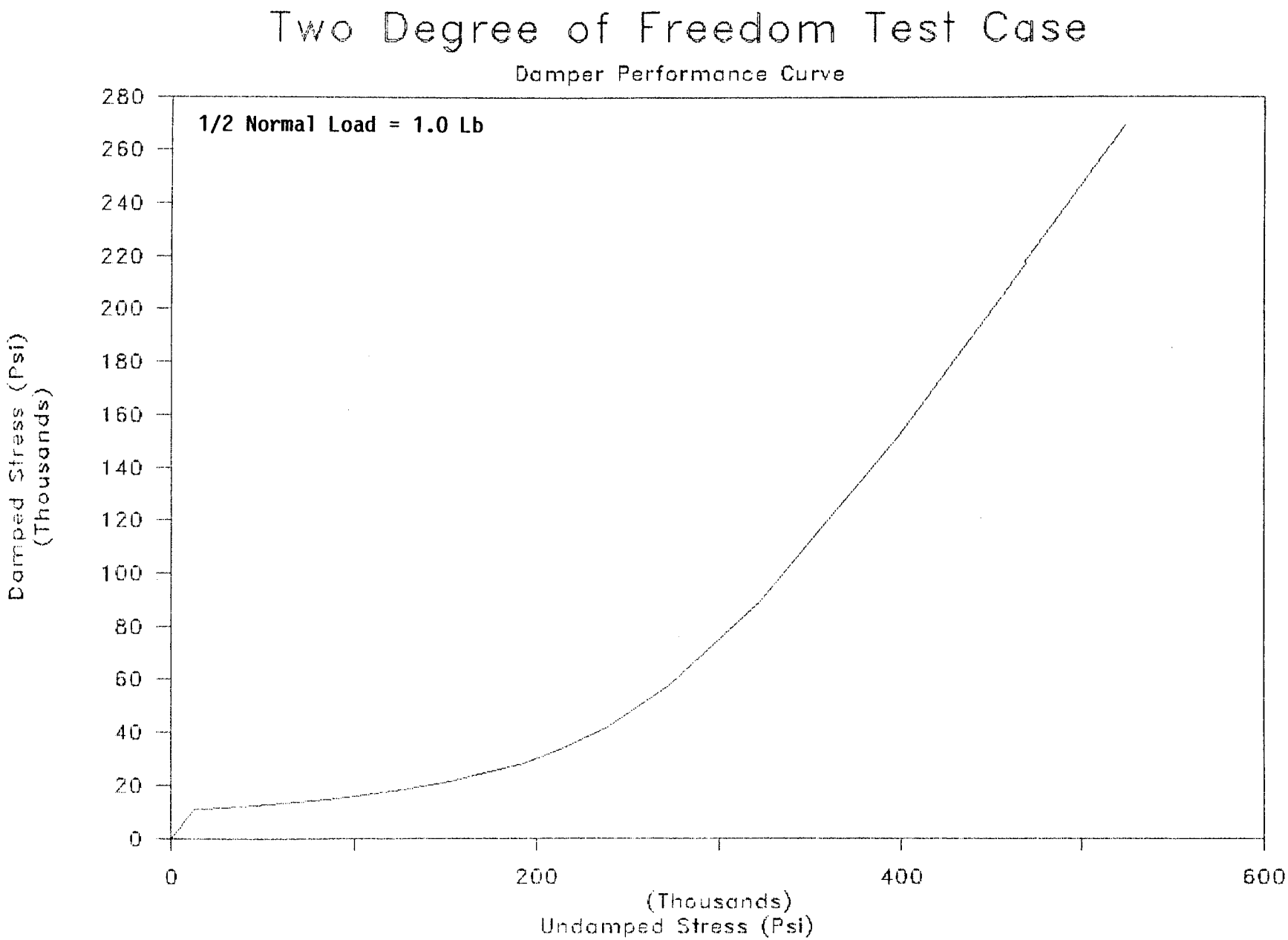

Figure 2.1-3 Two degree of freedom damper performance curve for vibration in mode 1

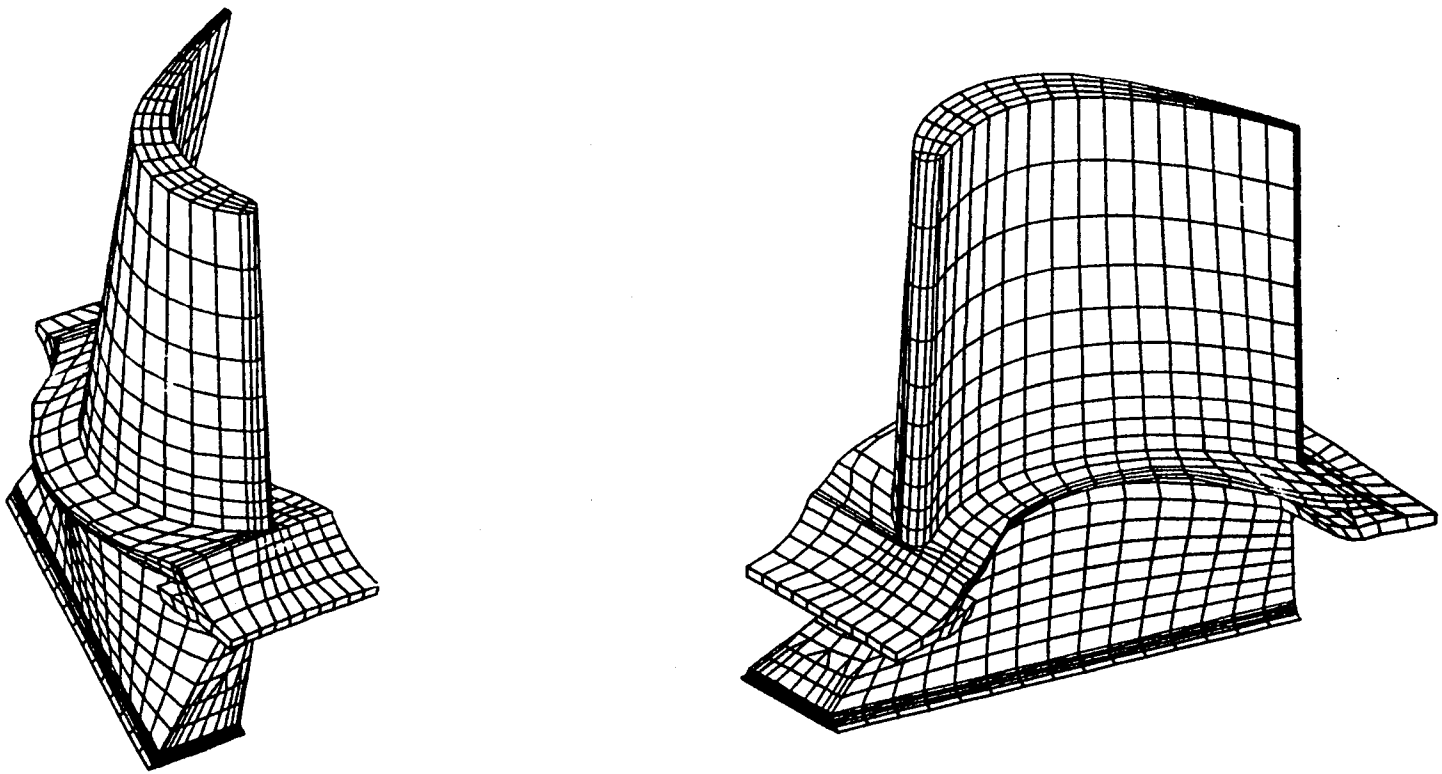

Figure 2.1-4 HPFTP first stage turbine blade finite element model

P/N R0019821

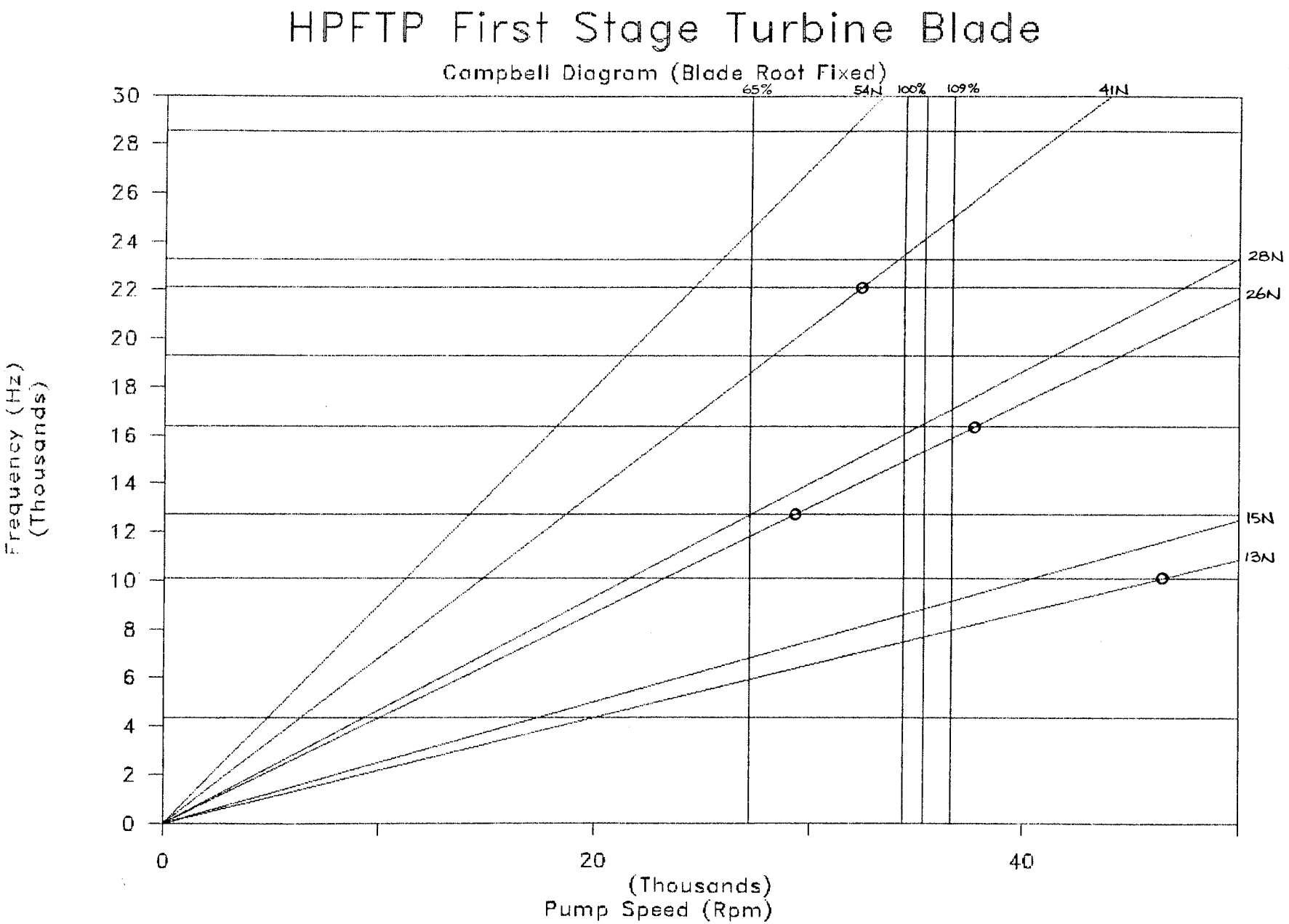

Figure 2.1-5 HPFTP first stage turbine blade Campbell diagram

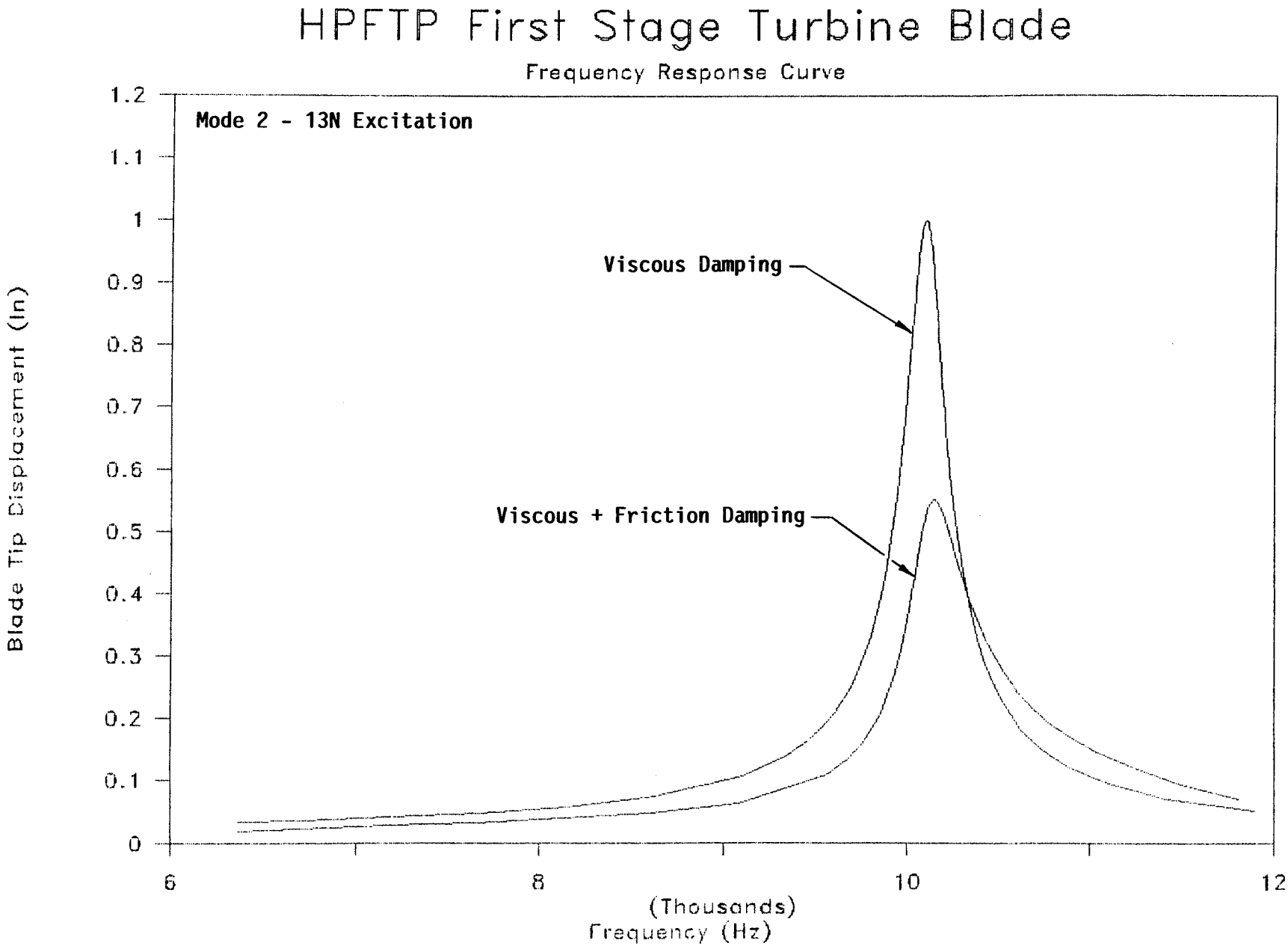

Figure 2.1-6 HPFTP first stage turbine blade frequency response

The optimum normal force option of the code was exercised to a greater extent than any other option, during the study of the HPFTP blade. Four different resonant points were investigated. They are shown by the circled areas on the Campbell diagram of Figure 2.1-5. Recall from previous discussion that these points do not represent actual engine interference points, because the blade model reflects the root-fixed condition. During this phase of the study, the damper stiffness and coefficient of friction were varied to determine the effect on optimum normal load. Results are presented in Figures 2.1-7 through 2.1-10. They reveal the classic damper curve, clearly showing the desired optimum damper normal force. These figures are normalized, such that the response of the blade tip is 1.0 inches under a no-damper configuration. Scaling to another displacement and normal load can be done in a linear fashion. For example, consider the second blade mode being excited by 13N. Consulting Figure 2.1-7 at a damper stiffness of 500,000 lb/in and an undamped tip displacement of 0.001 inches, the optimum 1/2 normal load for this mode is approximately 13 pounds, which gives an optimum total damper load of 26 pounds. For comparison, the current HPFTP damper normal force is shown in Figure 2.1-11, as a function of pump speed. It is 210 pounds at 36,000 rpm. However, this does not imply that the current damper is too heavy, because of the initial assumption on the magnitude of the forcing function. If an undamped tip deflection twice as large had been assumed, then the optimum normal force would also be doubled. It is also apparent from Figures 2.1-7 through 2.1-10 that the optimum normal force varies, depending on the mode which is being damped.

Another set of curves can be generated, from the families shown in Figures 2.1-7 through 2.1-10, by considering only the optimum points and by choosing damper stiffness as the independent variable. These are shown in Figures 2.1-12 through 2.1-15. Here, the generalized force is scaled such that it drives the undamped blade to a peak tip deflection of 0.001 inches at resonance. These curves are highly dependent on the value of force used. For example, if the driving force magnitude is great enough to cause a tip displacement of 0.002 inches in an undamped blade, then the optimum damper loads shown in the figures will double. Therefore, it is clear that, when using the optimum damper force approach, the forcing function magnitude must be known to a relatively high degree of accuracy to obtain meaningful results.

As mentioned previously, modal stresses for the blade became available after the curves of Figures 2.1-7 through 2.1-15 were generated. The maximum alternating stress was then determined from the modal stress information for each of the first six modes, assuming a tip deflection of 0.001 inches. The results for each of the four interference points were then scaled to an undamped stress level of 15,000 psi, which was assumed to be representative of an undamped turbine blade stress level. The results of this scaling are presented in Figures 2.1-16 through 2.1-19, which represent the best estimate of the optimum damper weight for the HPFTP first-stage blade.

The damper performance curve option of the code was used on a limited basis during this study. Results of several cases, ran for the second mode under 13N excitation, are presented in Figure 2.1-20. They show the relative merits of the frictionally-damped blade, as compared to the undamped blade.

2.1.4 Comments on the Use of BLDAMP. The computer code BLDAMP represents a significant improvement in capability over previous methods of analyzing friction dampers. An estimate of the optimum friction damper size, for a given blade design, can be made in a very short period of time, using this code. However, the code is not without its problems. BLDAMP is very sensitive to the input data for the analysis. Small input changes can make the difference in obtaining a correct or incorrect answer.

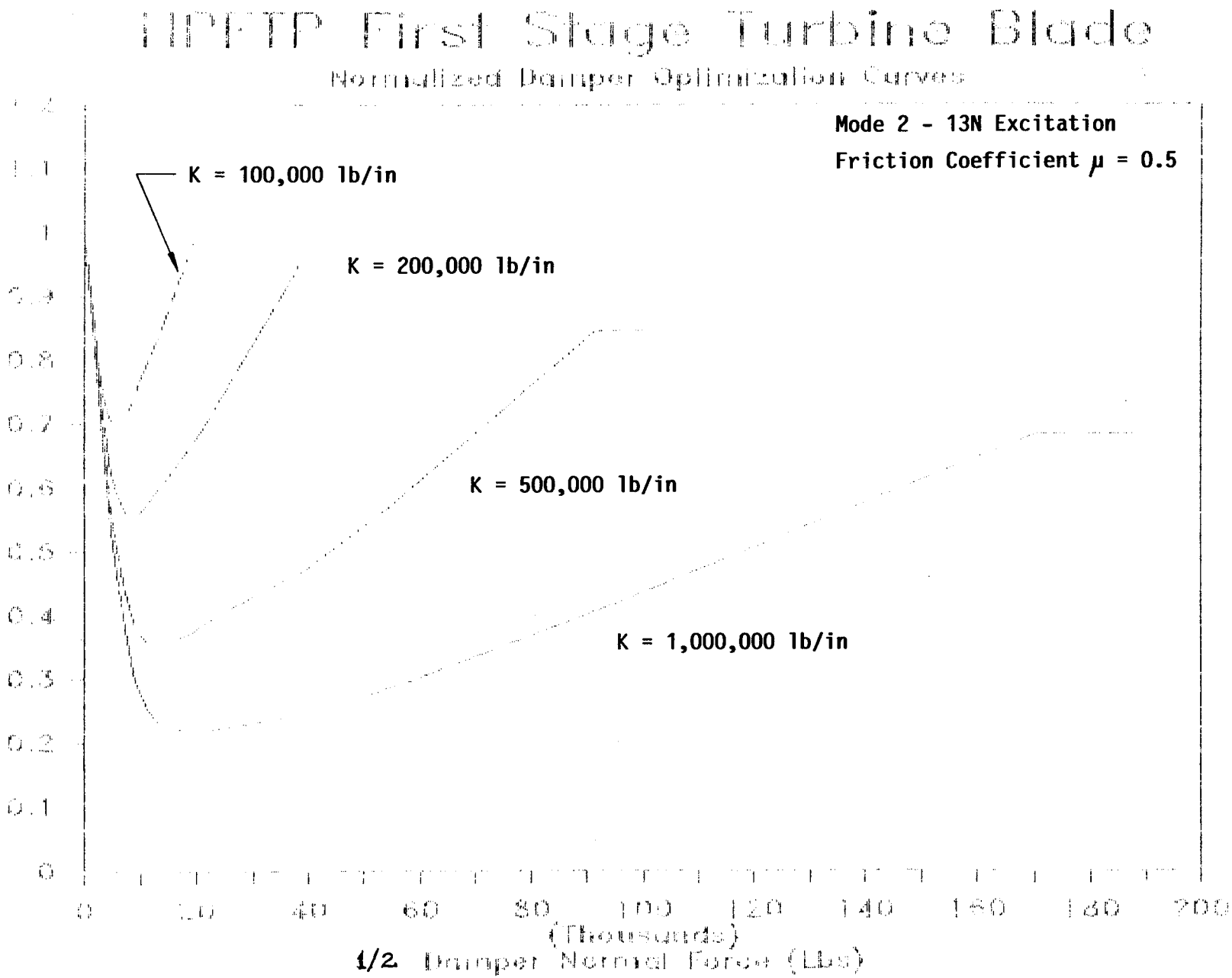

Figure 2.1-7 HPFTP turbine blade damper optimization curve for mode 2

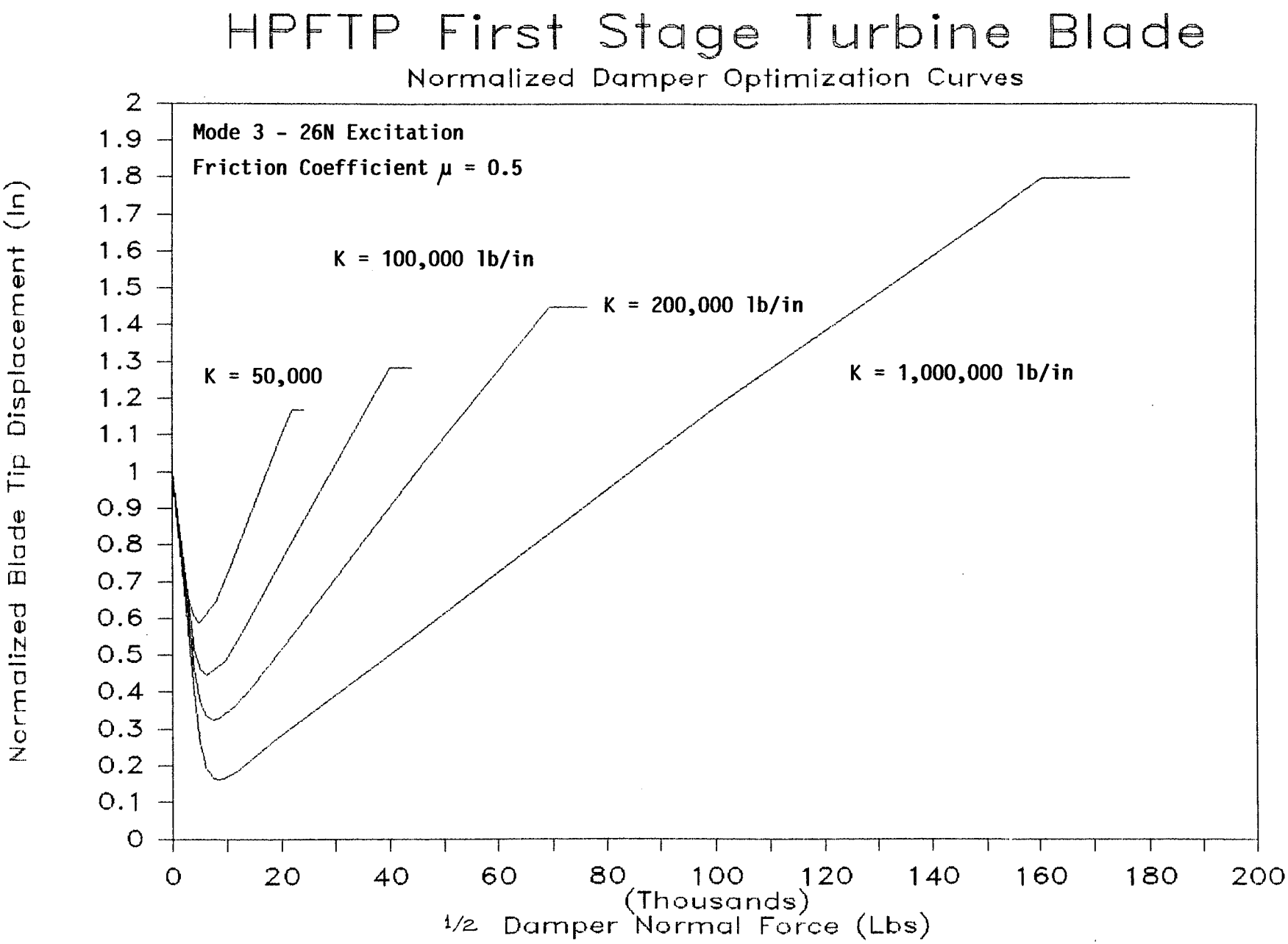

Figure 2.1-8 HPFTP turbine blade damper optimization curve for mode 3

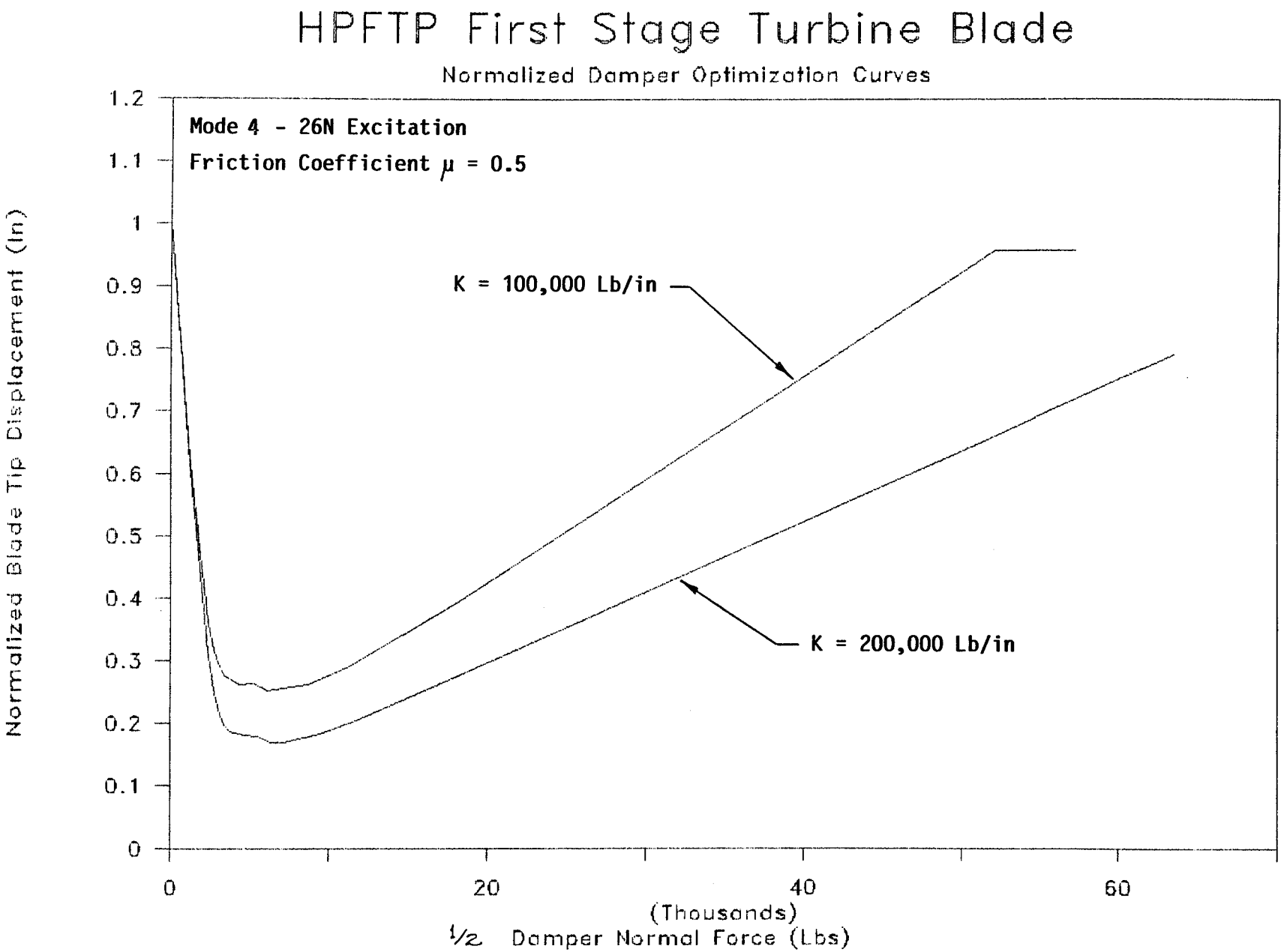

Figure 2.1-9 HPFTP turbine blade damper optimization curve for mode 4

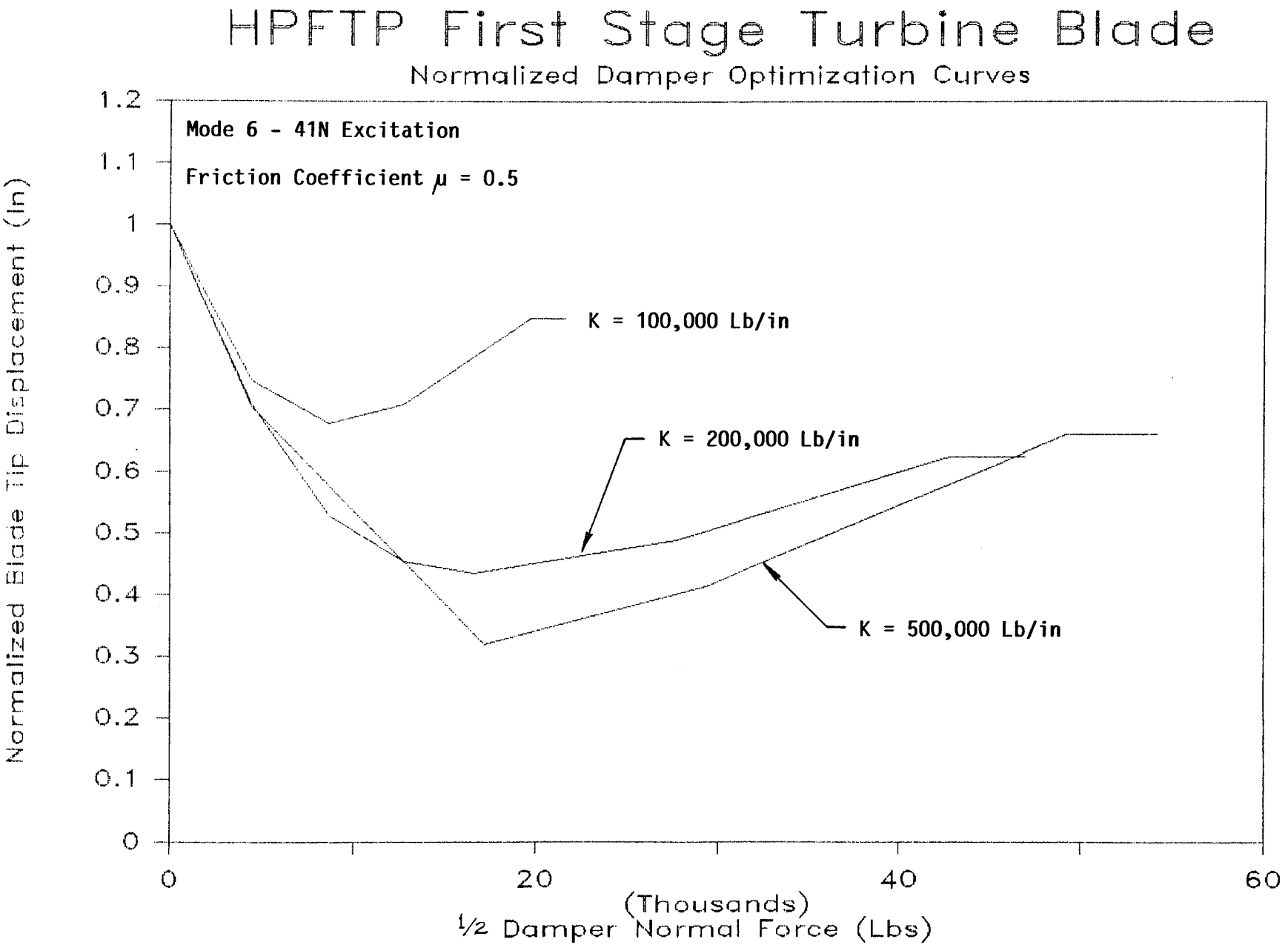

Figure 2.1-10 HPFTP turbine blade damper optimization curve for mode 6

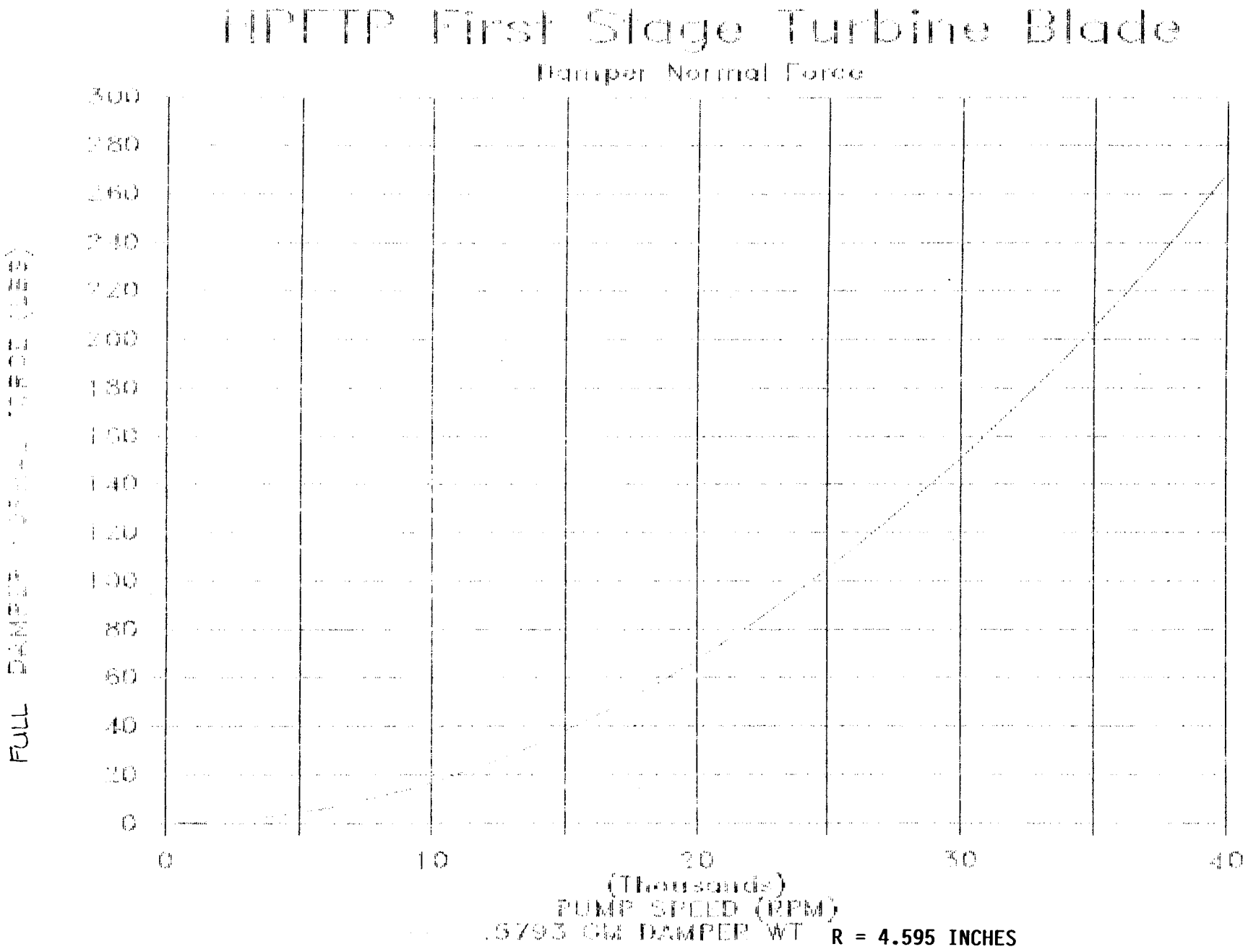

Figure 2.1-11 HPFTP turbine blade damper normal force

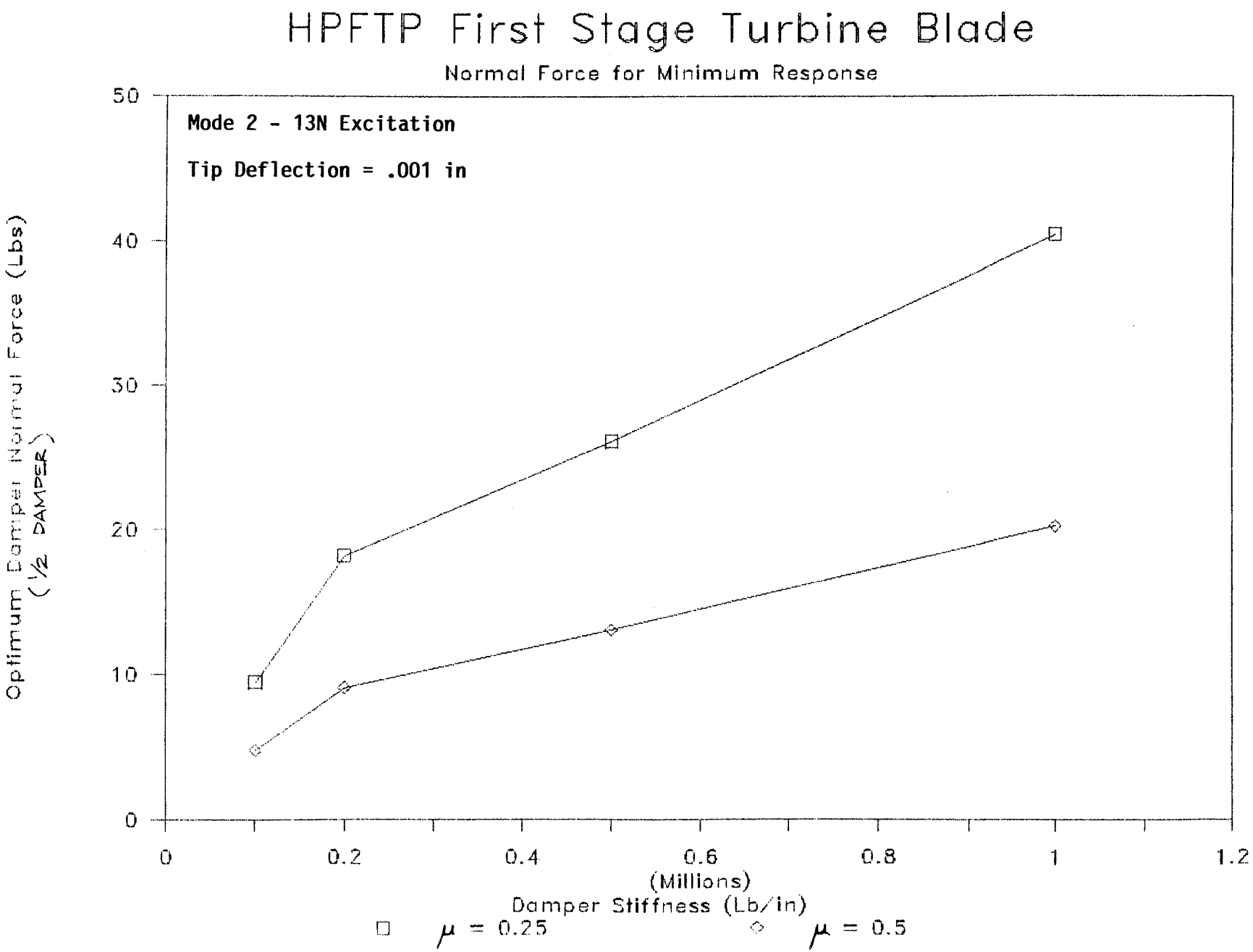

Figure 2.1-12 HPFTP turbine blade optimum normal force for mod. 2

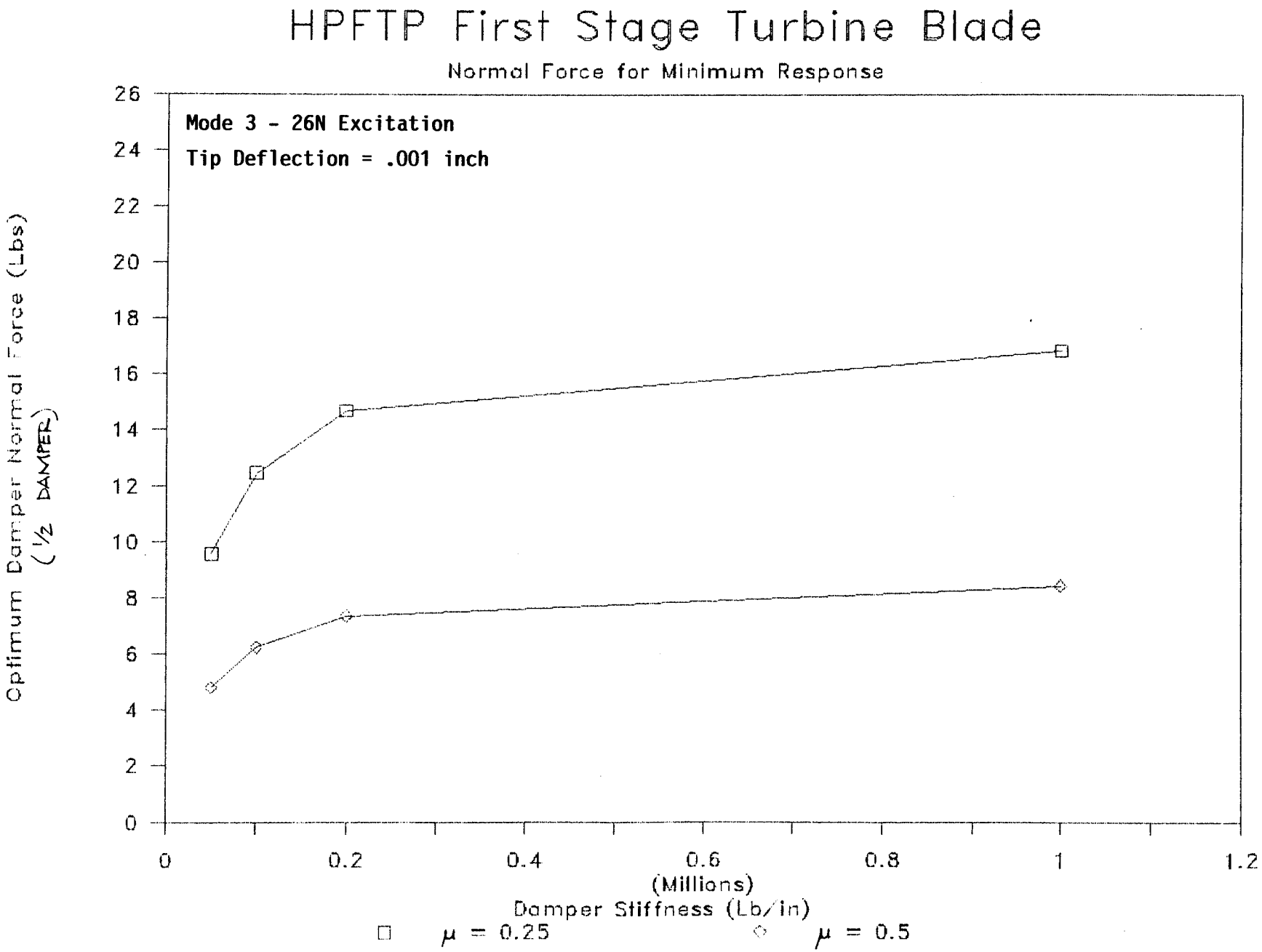

Figure 2.1-13 HPFTP turbine blade optimum normal force for mode 3 based on an undamped tip deflection of .001 inches

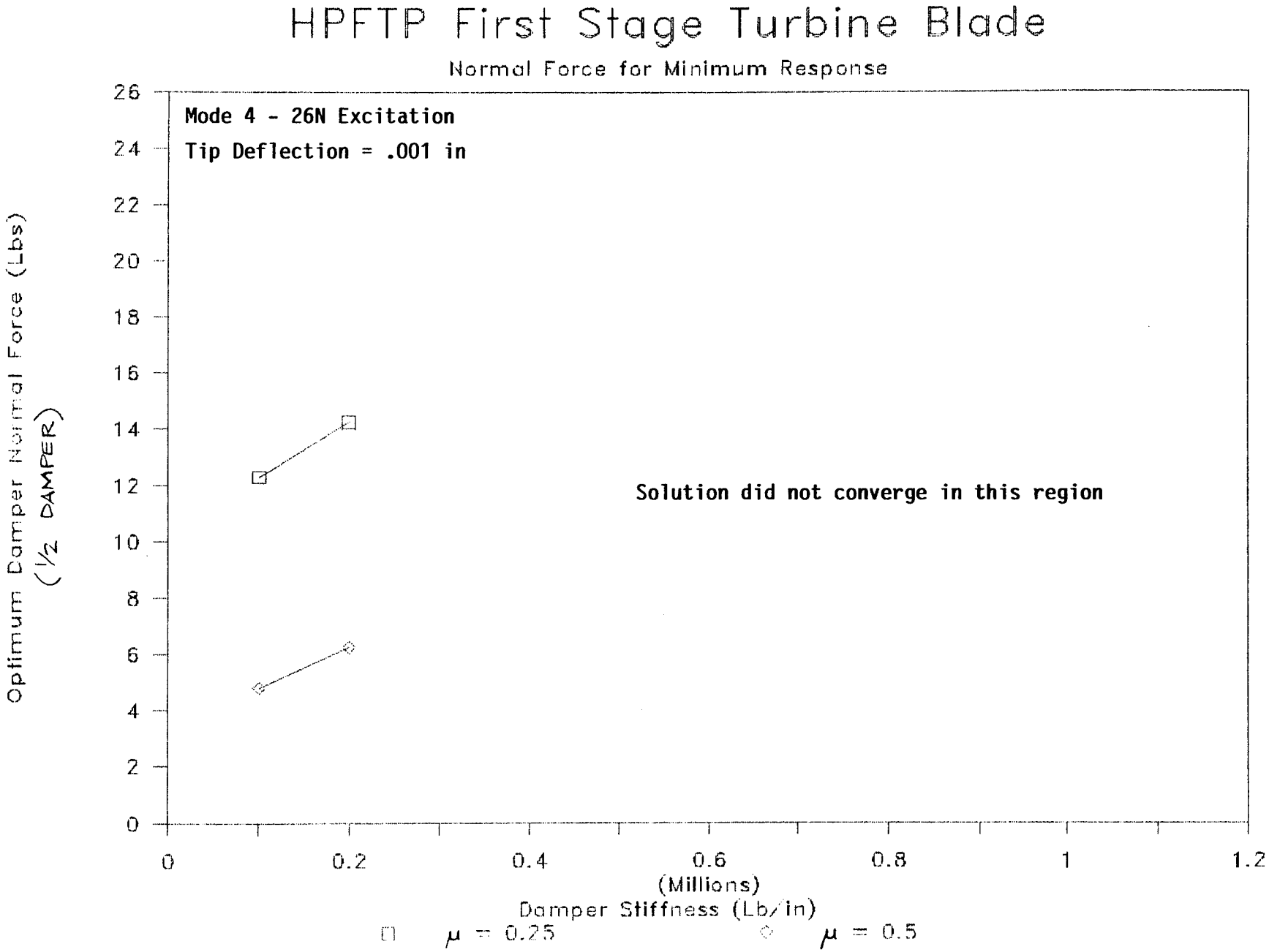

Figure 2.1-14 HPFTP turbine blade optimum normal force for mode 4

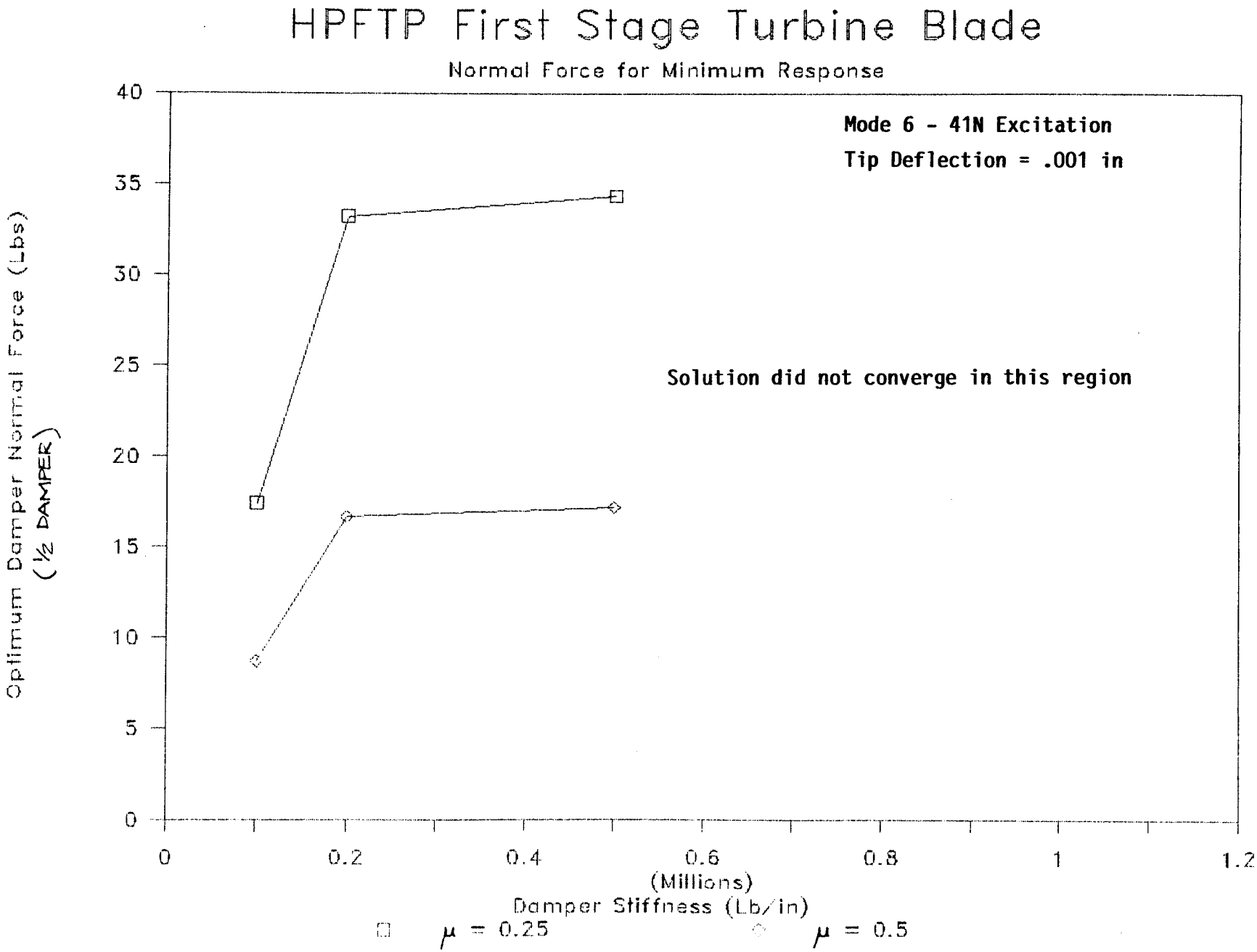

Figure 2.1-15 HPFTP turbine blade optimum normal force for mode 6 based on an undamped tip deflection of .001 inches

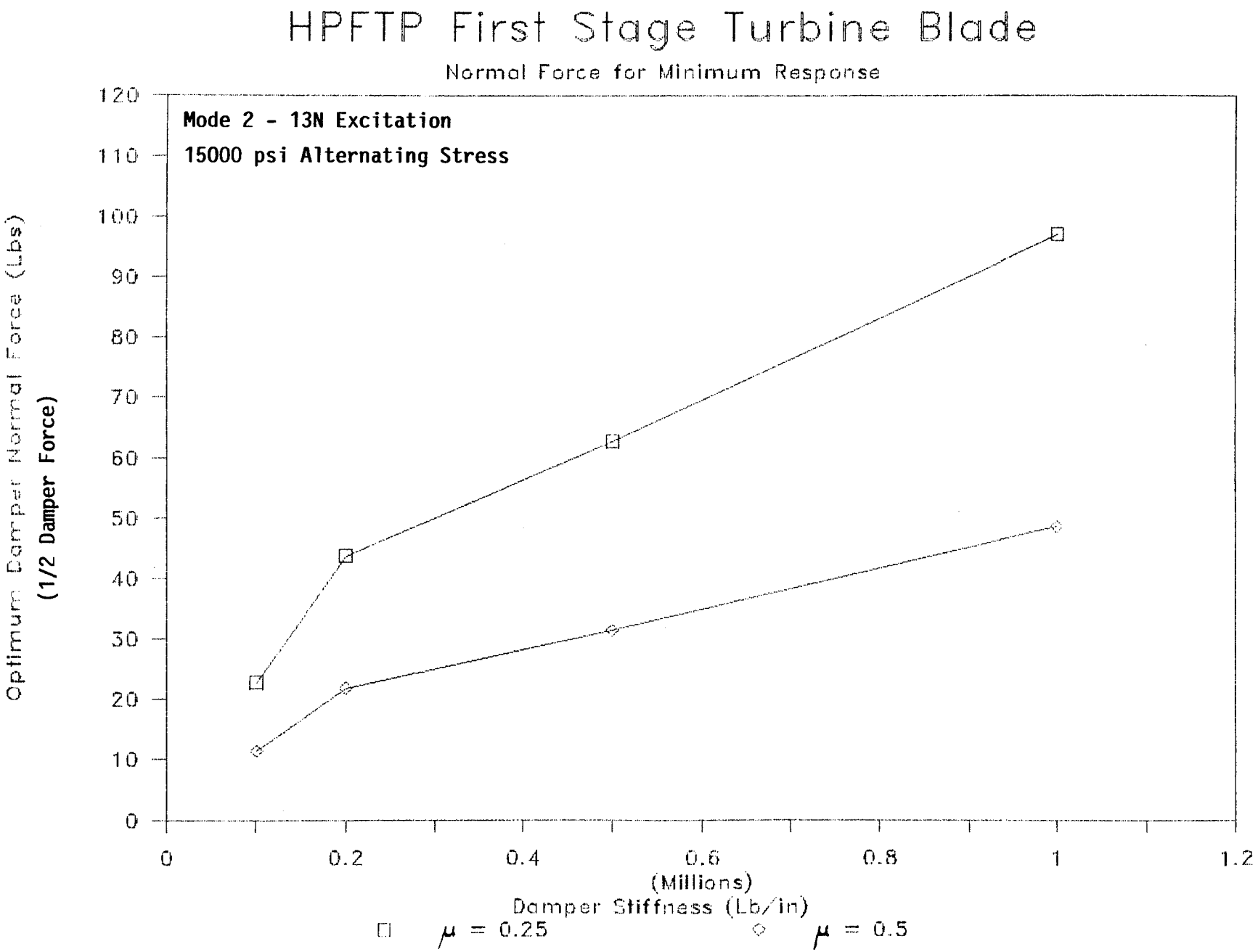

Figure 2.1-16 HPFTP turbine blade optimum normal force for mode 2

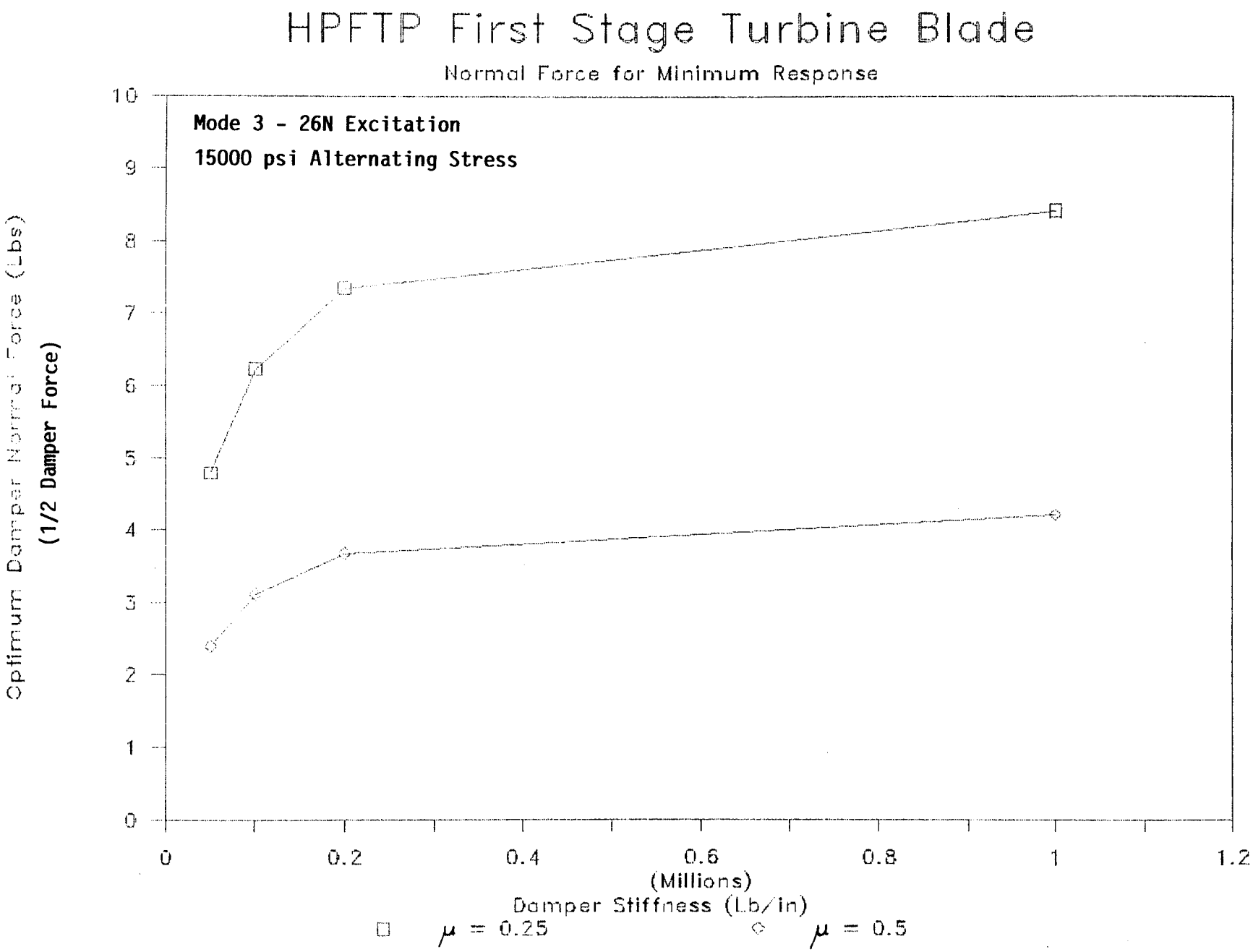

Figure 2.1-17 HPFTP turbine blade optimum normal force for mode 3 based on an undamped blade stress of 15000 psi

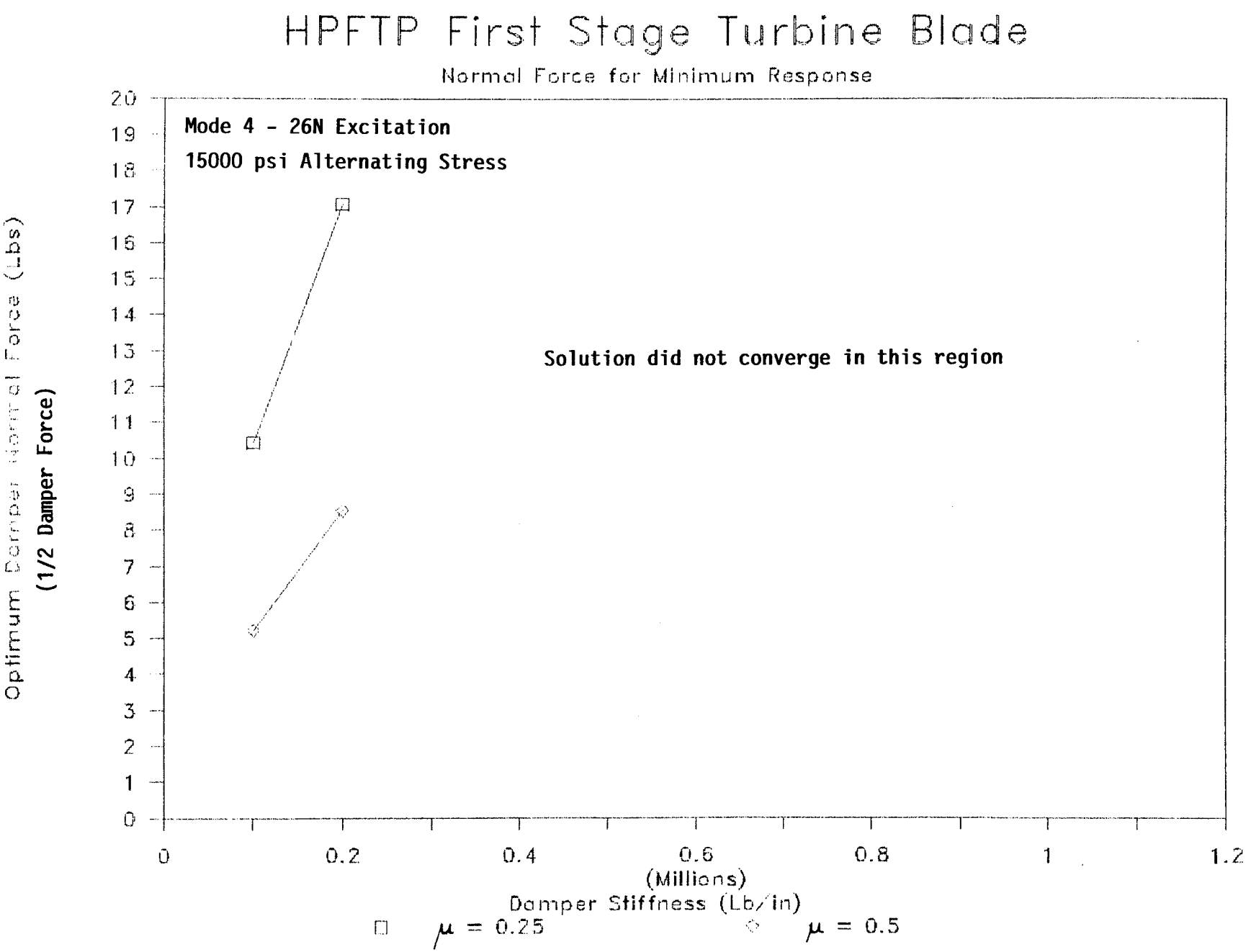

Figure 2.1-18 HPFTP turbine blade optimum normal force for mode 4

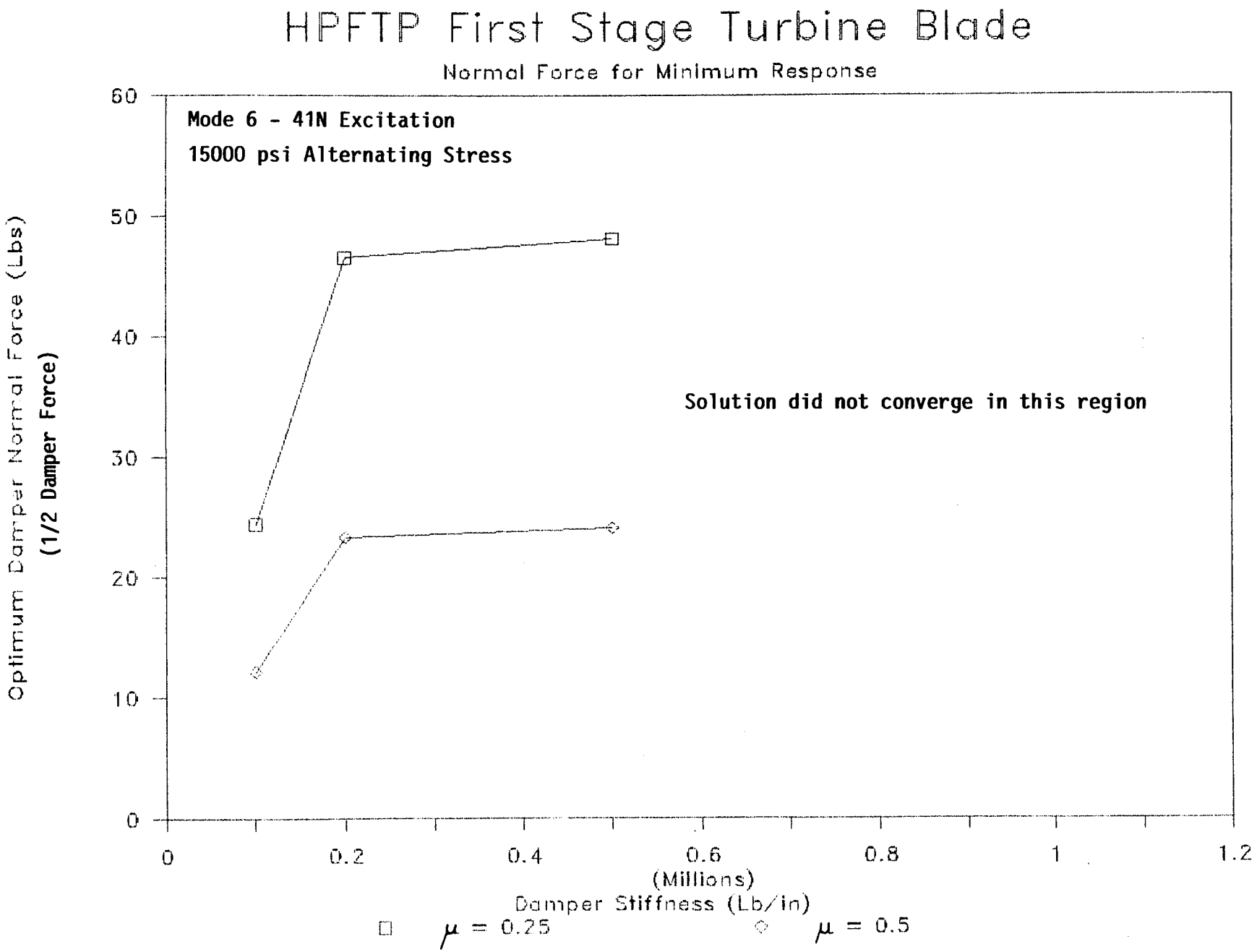

Figure 2.1-19 HPFTP turbine blade optimum normal force for mode 6 based on an undamped blade stress of 15000 psi

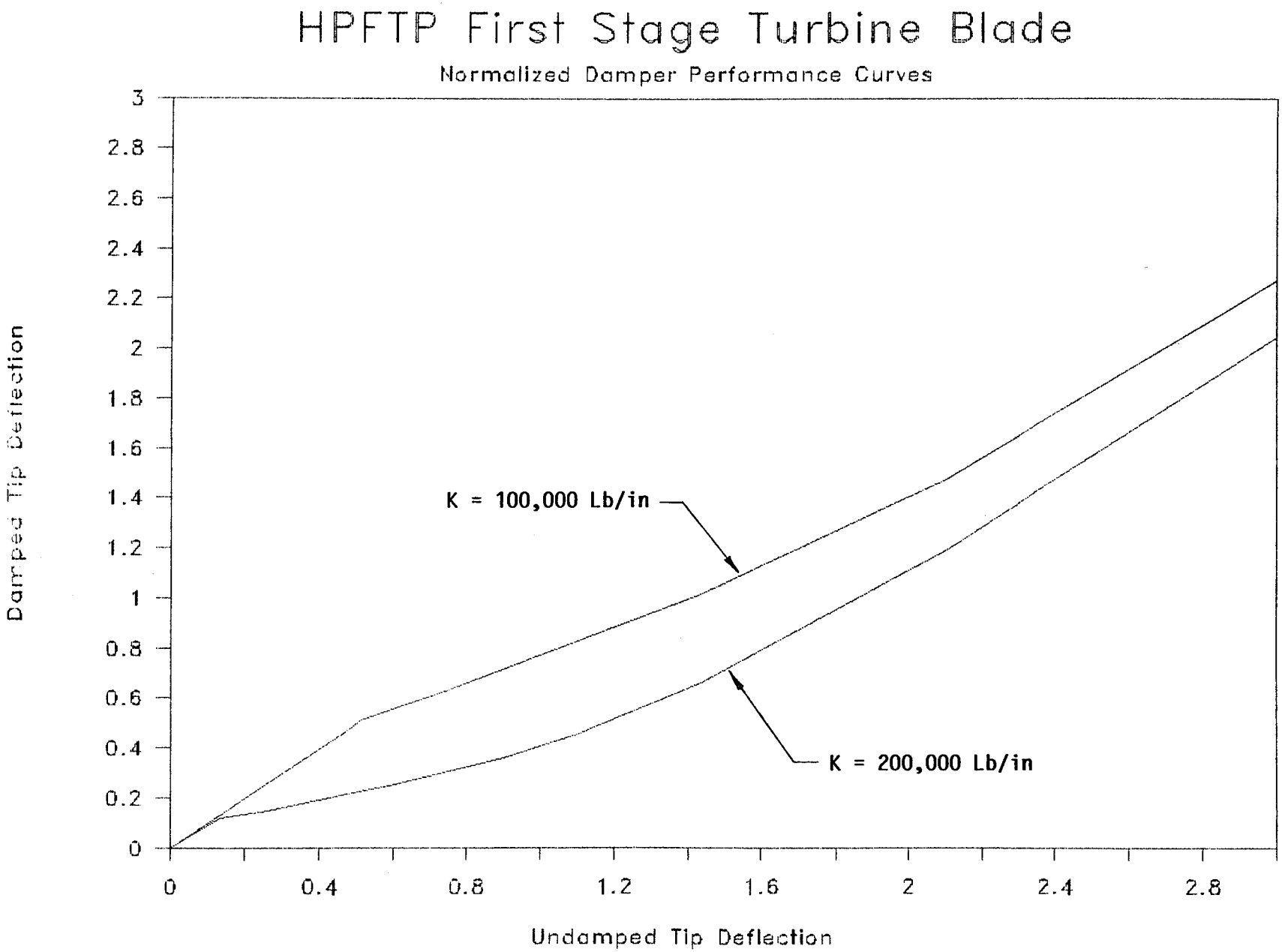

Figure 2.1-20 HPFTP turbine blade damper performance curve for mode 2

In particular BLDAMP fails to converge to a solution at higher values of damper stiffness. As an example, the damper stiffness for the HPFTP blade has been calculated to be 1,000,000 lb/in. Yet, the program will not converge at stiffnesses larger than 200,000 lb/in for the fourth mode (See Figures 2.1-9 and 2.1-14). In other cases, the program will converge to an answer that is obviously incorrect. This can be observed from Figure 2.1-10, where the k = 500,000 lb/in case does not give reasonable results. Although BLDAMP is a great improvement over previous methods of damper analysis, additional work is needed to improve the convergence properties of the program.

Other problems, which were discovered when using BLDAMP during this study, are listed below.

1. The analysis does not converge at intermediate values of damper stiffness and then does converge at higher stiffnesses.

2. Sometimes the program prints too few points to define the normal force curve. It needs user control of the normal force spacing.

3. The analysis does not converge for low values of input force. Problems are anticipated when using realistic forcing functions.

2.1.5 Conclusions. The computer code BLDAMP has been modified and installed on the Rocketdyne CDC computer system. Sample cases have been run, which exactly match those provided by the code developer, Griffin Consulting. In addition, more realistic cases have been run, using the HPFTP first-stage turbine blade as a test case. Results of the study show that the program is easy to use and provides answers which appear to be reasonable. Based on an assumed forcing function, which gives an alternating stress of 15,000 psi on an undamped blade, the optimum damper weight was calculated to be approximately 140, 10, 25, and 100 lbs for modes 2, 3, 4, and 6, respectively. All of these values are less than the current 210 lb damper weight. However, these damper weights are to be used only for illustrative purposes, because the forcing function used for the analysis is not accurate.

2.2 FRICTION DAMPING TEST RESULTS

2.2.1 Initial Testing

2.2.1.1 Summary. A laboratory test was completed to determine the effectiveness of friction damping in the reduction of vibratory stresses in a cantilever beam. The test was performed using two different sized beams; one with a low natural frequency and one with a high natural frequency. Two different dampers of the same geometry, but different materials, were tested on each of the beams to determine their influence on beam response. Results showed that friction damping can be extremely effective in reducing the response levels of vibrating structures. Friction damping was found to provide the greatest reduction in dynamic response when the damper was located near the tip of the beam and also when the normal load was above a critical value.

2.2.1.2 Test Objectives. The objectives of the vibration test were to measure the performance of friction dampers and to quantify certain parameters that were found to be important. These parameters are friction coefficient, damper stiffness, damper location, and beam driving force. The test was also intended to serve as a database for comparison with analytical results, obtained using the BLDAMP computer code.

2.2.1.3 Test Hardware and Setup. The test was repeated on two entirely different cantilever beams; one which was designed to operate at relatively low frequencies, ranging from 300 Hz to 500 Hz, and another which was designed for the 2,000-3,000 Hz frequency range. The low-frequency test beam (long beam) shown in Figure 2.2-1, had a measured first natural frequency of 344 Hz and a second natural frequency of 1,790 Hz, with no dampers installed. The large natural frequency spacing ensured no coupling between modes. The high-frequency test beam (short beam), shown in Figure 2.2-2, had measured undamped natural frequencies of 2,556 Hz and 4,082 Hz.

During testing, the friction damper was installed in a selected position underneath one of the tangs, which were machined as integral parts of each beam. Figure 2.2-3 shows a damper as installed in one of the test beams and Figure 2.2-4 shows the dimensions of the damper, of which several samples were constructed of both Haynes 188 and silicon nitride. Only one of the two material types and only one damper were used on any single test run. The choice of Haynes 188 was made because this has been used successfully at Rocketdyne as a damper material on both the high-pressure oxidizer and high-pressure fuel turbopumps. Silicon nitride was chosen as an experimental material for its low coefficient of friction, low density, and high stiffness. These properties are all desirable in friction dampers, because past experience has shown that heavy dampers, or dampers with high friction coefficients, are subject to lockup. Also damper stiffness has been shown analytically to provide better damper performance.

The dampers were designed to rest in a groove machined into the stationary part of the test fixture (Figures 2.2-1 through 2.2-3). The knife-edge portion of the damper was designed to fit tightly into the groove, thus precluding any damper motion relative to the base. This design allows only sliding motion at the interface between the damper and the test beam. The normal force was applied to the back side of the damper by means of a cable or string arrangement, which acted through a damper holder. The damper holder, shown in Figure 2.2-5, was identical for low- and high-frequency beams. It served to transfer the load from the cable to the damper in a uniform fashion.

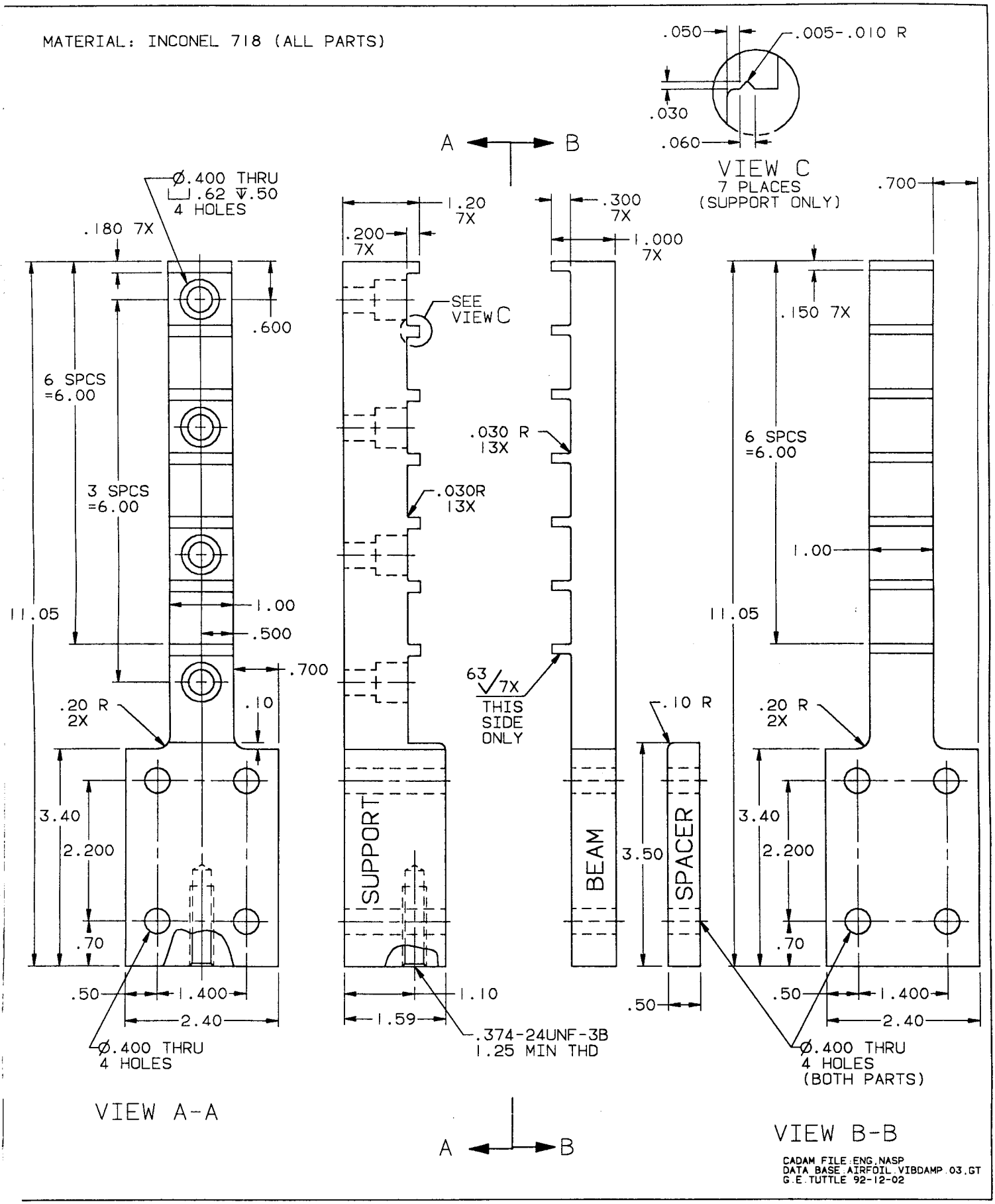

Figure 2.2-1 Low frequency test beam, support, and spacer

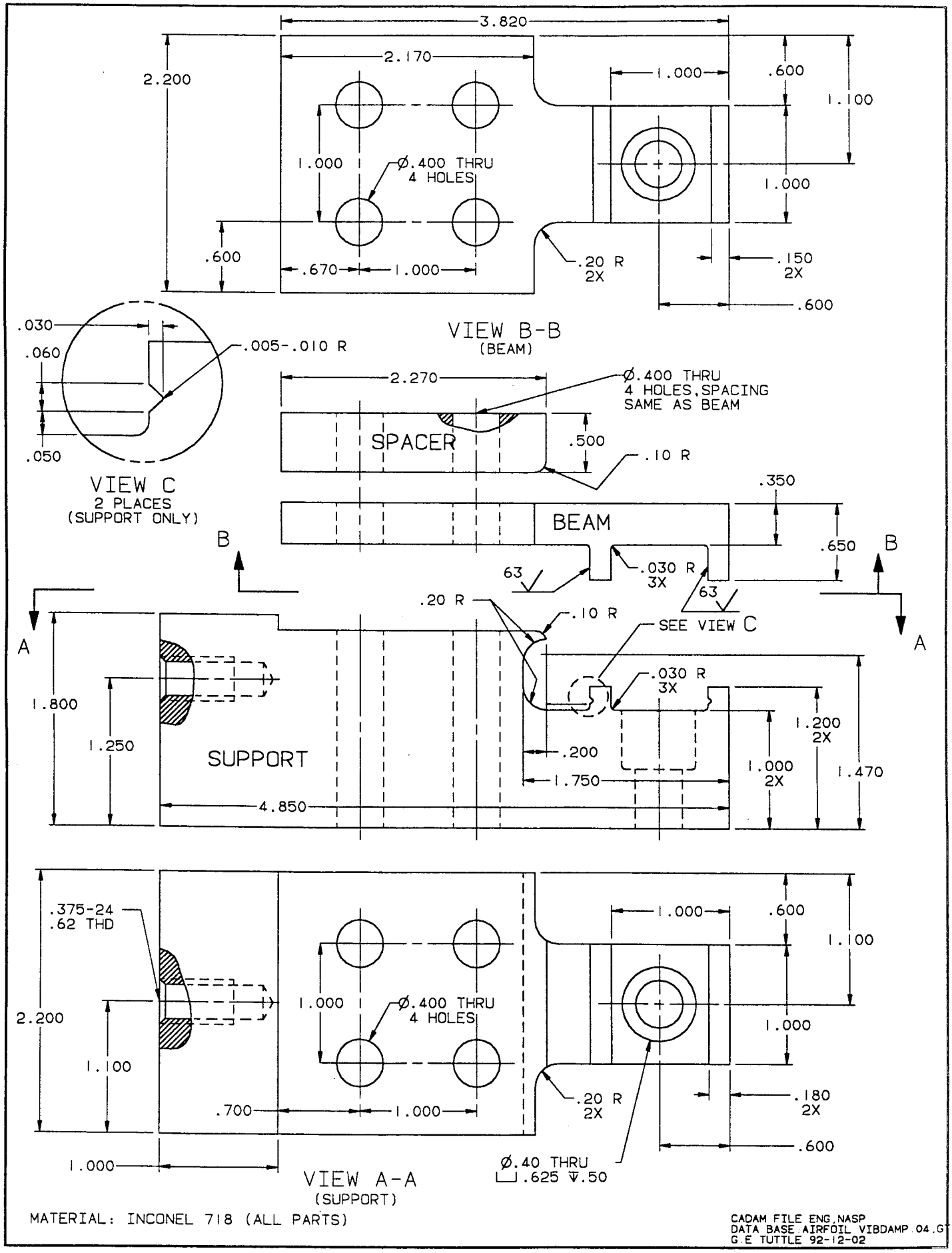

Figure 2.2-2 High frequency test beam, support, and spacer

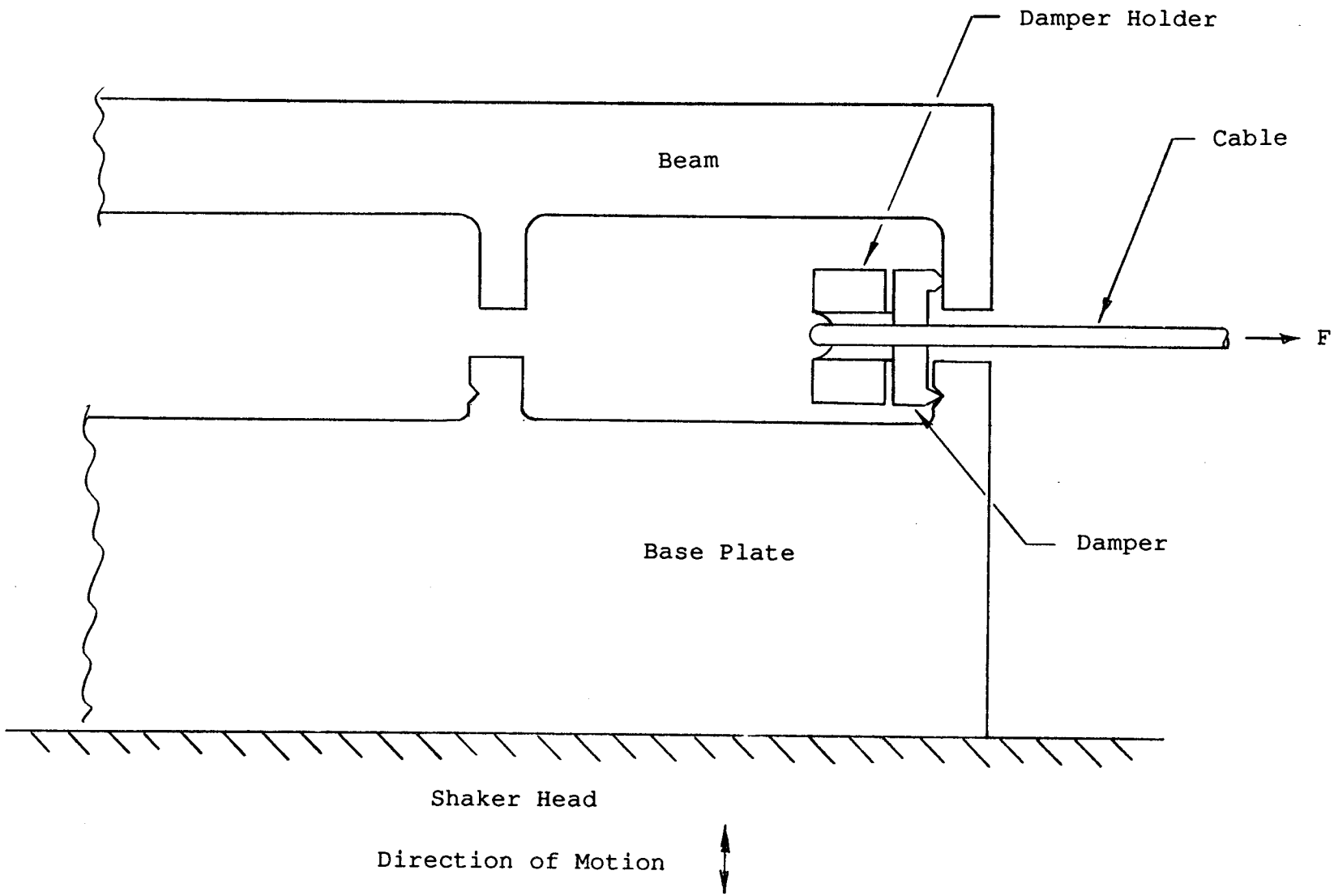

Figure 2.2-3 Details of damper installation and loading method

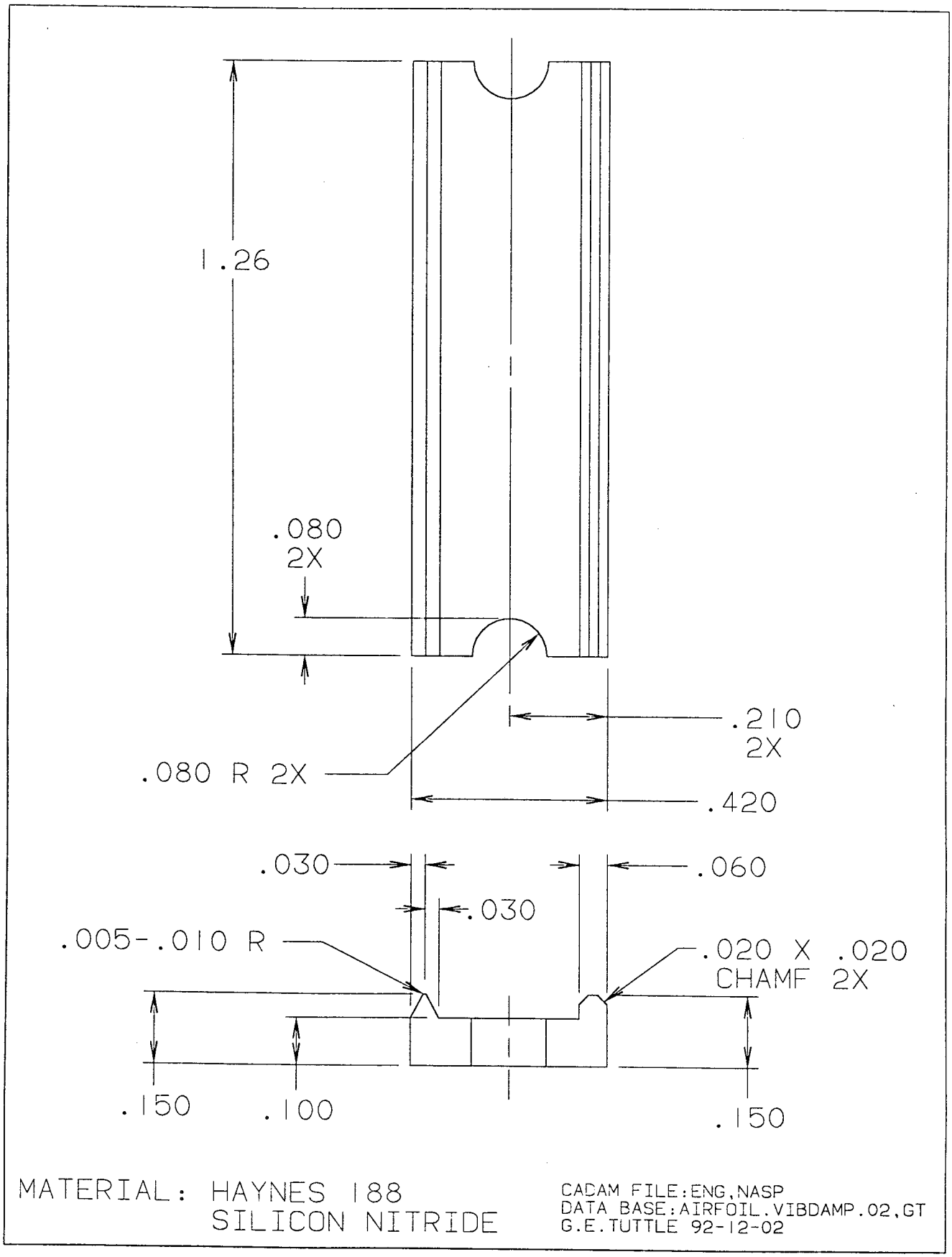

Figure 2.2-4 Damper for high and low frequency beams

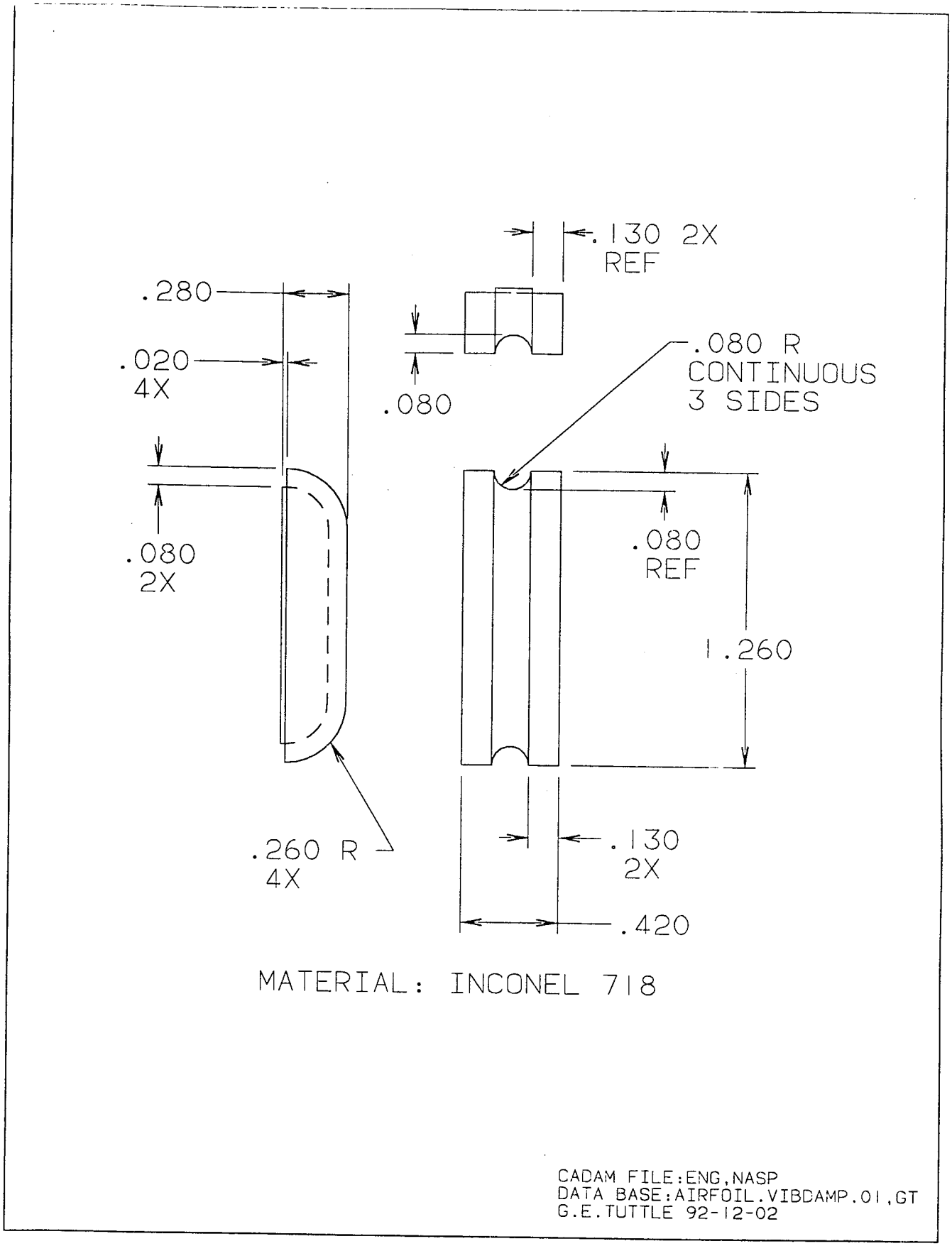

Figure 2.2-5 Damper holder for high and low frequency beams

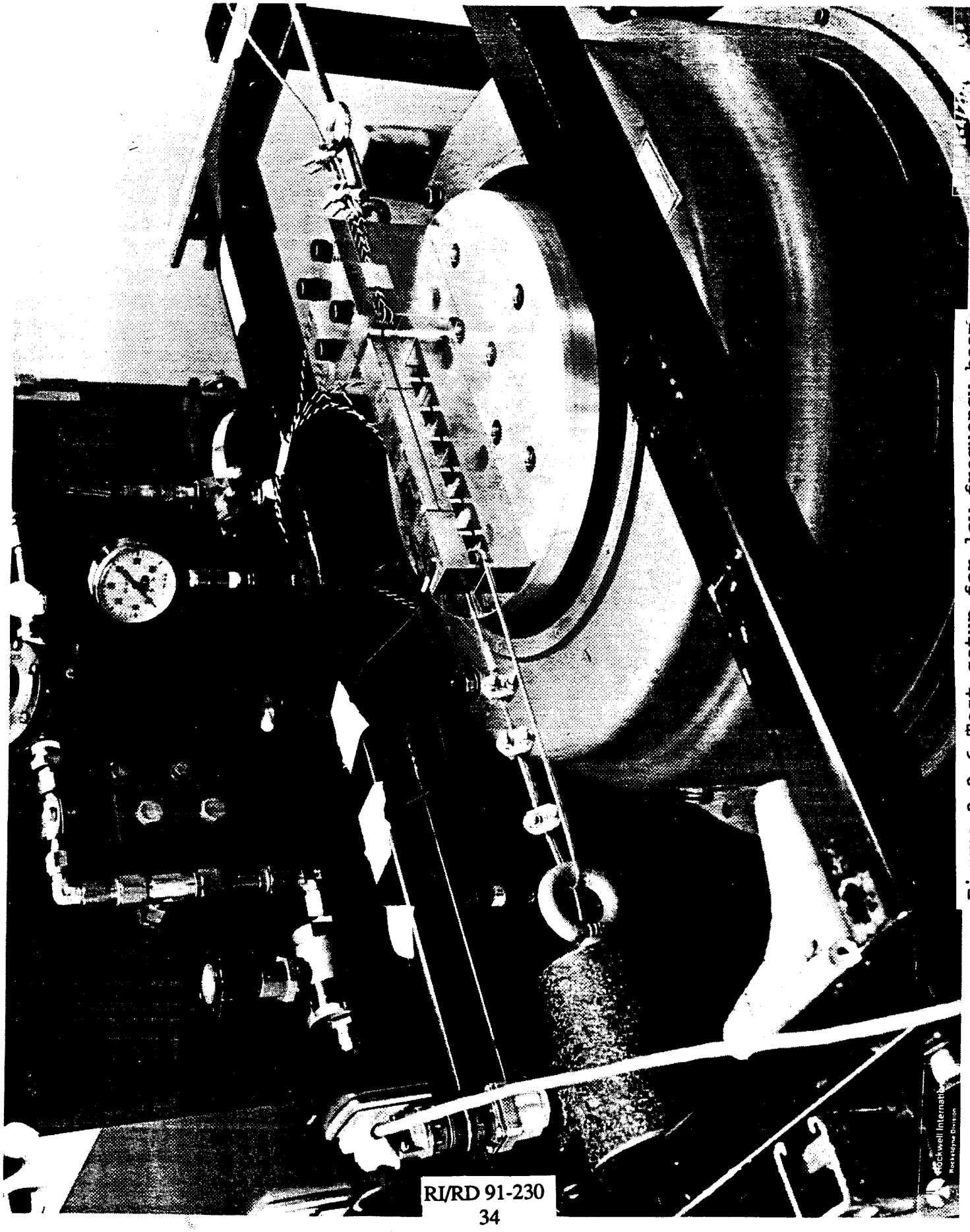

Figure 2.2-6 Test setup for low frequency beam

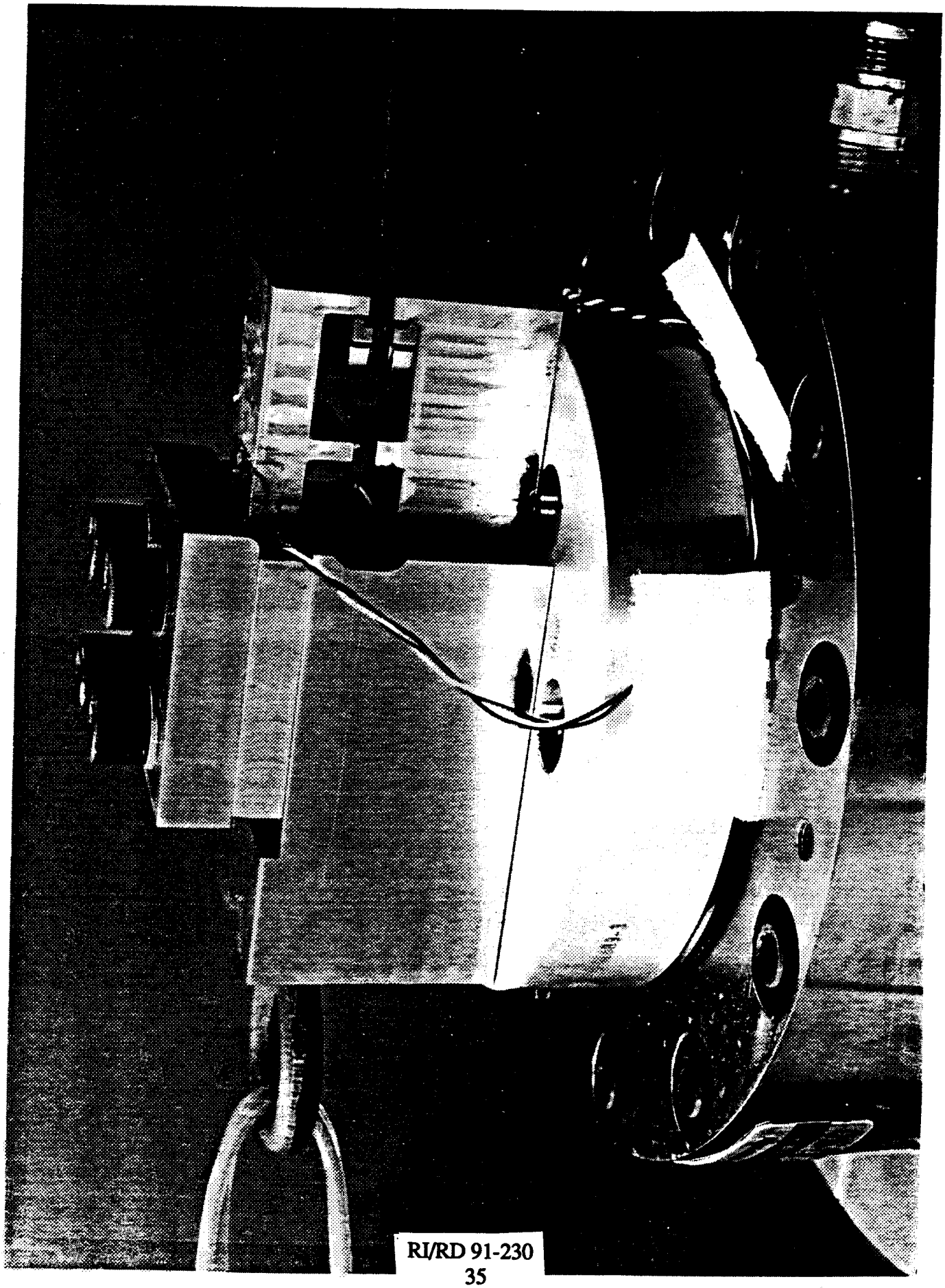

Figure 2.2-7 Test setup for high frequency beam

The test setup consisted of a cantilevered beam bolted to a shaker table, as shown in Figures 2.2-6 and 2.2-7. The low-frequency beam was tested using a MB C-10 shaker in EDL (Engineering Development Laboratory) Vibration Room 3. Later, a Ling A249 shaker in Vibration Room 4 was used. The high-frequency beam was tested using a Wilcox Research D125L-M shaker. As can be seen from the figures, the test setup had provisions for placing a friction damper at any one of several locations along the span of the beam. Dampers were loaded by means of a cable and load cell, or by a string and pulley arrangement, as shown in Figures 2.2-8 and 2.2-9. The load cell was used primarily for the higher loads, while the string and pulley were used for the lower loads. Loads were measured either by the load cell or by a small spring scale. Application of the loads was accomplished by addition of weights to a small bucket, or by tightening a bolt attached to the load cell.

2.2.1.4 Test Instrumentation. Each beam was instrumented with strain gages and accelerometers, positioned as shown in Figures 2.2-10 and 2.2-11. All data channels were recorded on magnetic tape during the test . A schematic of the instrumentation and data-gathering system is shown in Figure 2.2-12.

2.2.1.5 Modal Testing. Both high- and low-frequency beams were modal tested to determine natural frequencies and mode shapes. Testing was accomplished with the HP Modal Analyzer system, using the calibrated hammer method. Measurements were taken with and without a damper installed, to determine the range of resonant frequencies to expect when performing the actual damper sine-sweep testing. The data were also used to determine the damper stiffness, as will be discussed later. When the damper was installed, a large normal force was used to keep the damper from slipping during the test. This was done to ensure that the test with the damper installed represented an upper bound to the frequency which could occur. Table 2.2-1 presents a list of the modal frequencies found from the test. Figures 2.2-13 through 2.2-17 show typical mode shapes and frequency response functions of the beams, both with and without the damper installed. All mode shapes, measured in the test, consisted of beam bending in the vertical plane.

2.2.1.6 Damper Stiffness. Damper stiffness was determined by measuring the natural frequency of the beam, both with and without the damper installed Then a finite-element model of the beam was used to determine the additional stiffness necessary to cause the observed frequency shift. The finite-element model was calibrated by comparing analytical frequencies with measured frequencies, without the damper installed. The model was modified until a satisfactory match was obtained. When the beam was tested with the damper installed, a large normal force was used to ensure that the damper was completely locked. This had the effect of placing a spring to ground at the damper position. The stiffness of the damper spring was found by using the finite-element model to recompute the natural frequencies of the beam, as a function of damper stiffness. Then the stiffness was determined which gave the correct frequency, as measured in the test. This procedure was repeated at each damper location. An average stiffness of 450,000 lb/in resulted for the Haynes 188 damper. The stiffness of the silicon nitride damper was determined from the Haynes damper stiffness, by using the modulus ratio between the two materials. This resulted in a stiffness for the silicon nitride damper of 675,000 lb/in.

2.2.1.7 Damper Effectiveness Testing. Testing to determine the effectiveness of friction dampers was accomplished by performing a sine sweep through the frequency range of the first beam bending mode and recording the accelerometer and strain gage responses. The tests were first performed without the damper installed and then with the damper installed. The damper normal load was selected prior to the test. Then it was held constant throughout the sine sweep. For the next sweep, a new value of damper normal force was used. The test was then repeated at the same input level. Typical

Table 2.2-1

BEAM NATURAL FREQUENCIES WITH AND WITHOUT DAMPERS INSTALLED
MODAL TEST RESULTS

LOW FREQUENCY BEAM

CONFIGURATION	MODE 1	MODE 2
No Damper	344 Hz	1790 Hz
Haynes 188 Damper at Tang 1	405 Hz	>2000 Hz
Haynes 188 Damper at Tang 3	712 Hz	>2000 Hz
Haynes 188 Damper at Tang 5	1288 Hz	1605 Hz (1)
Haynes 188 Damper at Tang 7	1416 Hz	>2000 Hz

HIGH FREQUENCY BEAM

CONFIGURATION	MODE 1	MODE 2
No Damper	2556 Hz	4082 Hz
Haynes 188 Damper at Tang 1	2633 Hz	4402 Hz
Haynes 188 Damper at Tang 2	4335 Hz	6052 Hz

Notes: (1) Tang 5 location was very close to the nodal point for the low frequency beam 2nd bending mode.

(2) When dampers were installed a large normal force was applied to lock the damper and prevent sliding during the modal test. Testing was done using very light hammer raps to excite the beams.

(3) All modes are beam bending modes.

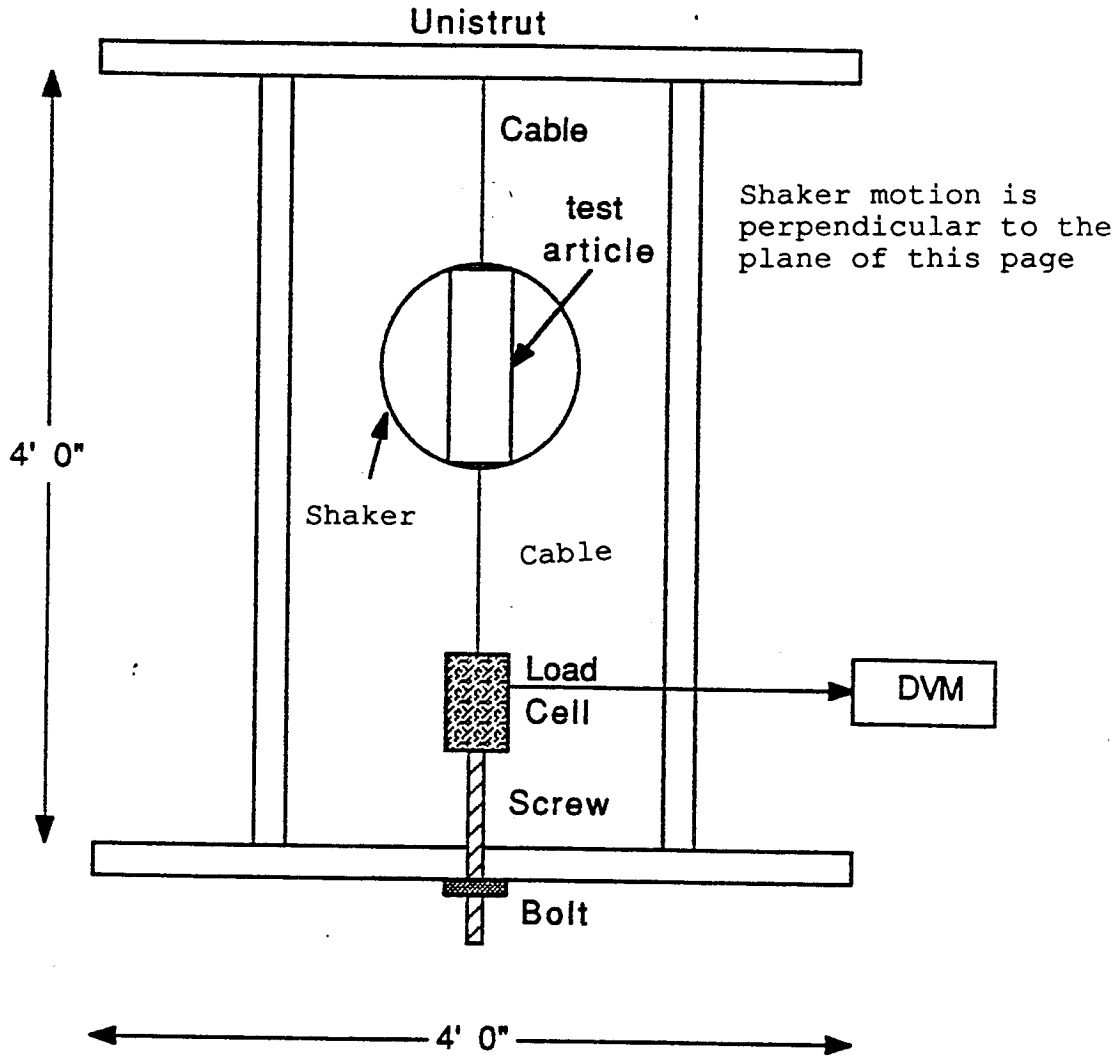

Figure 2.2-8 Top view of damper loading mechanism

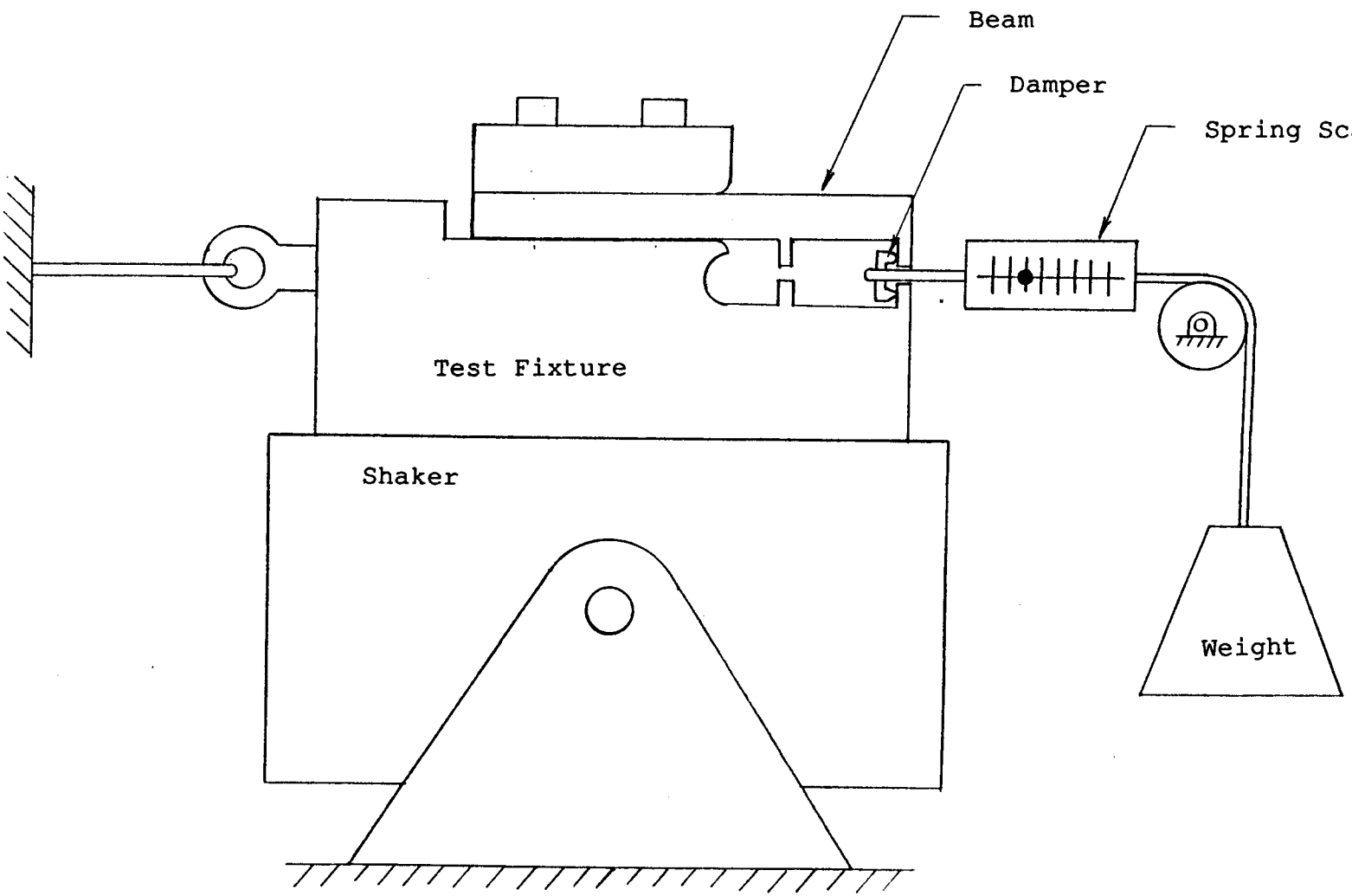

Figure 2.2-9 High frequency beam damper loading mechanism

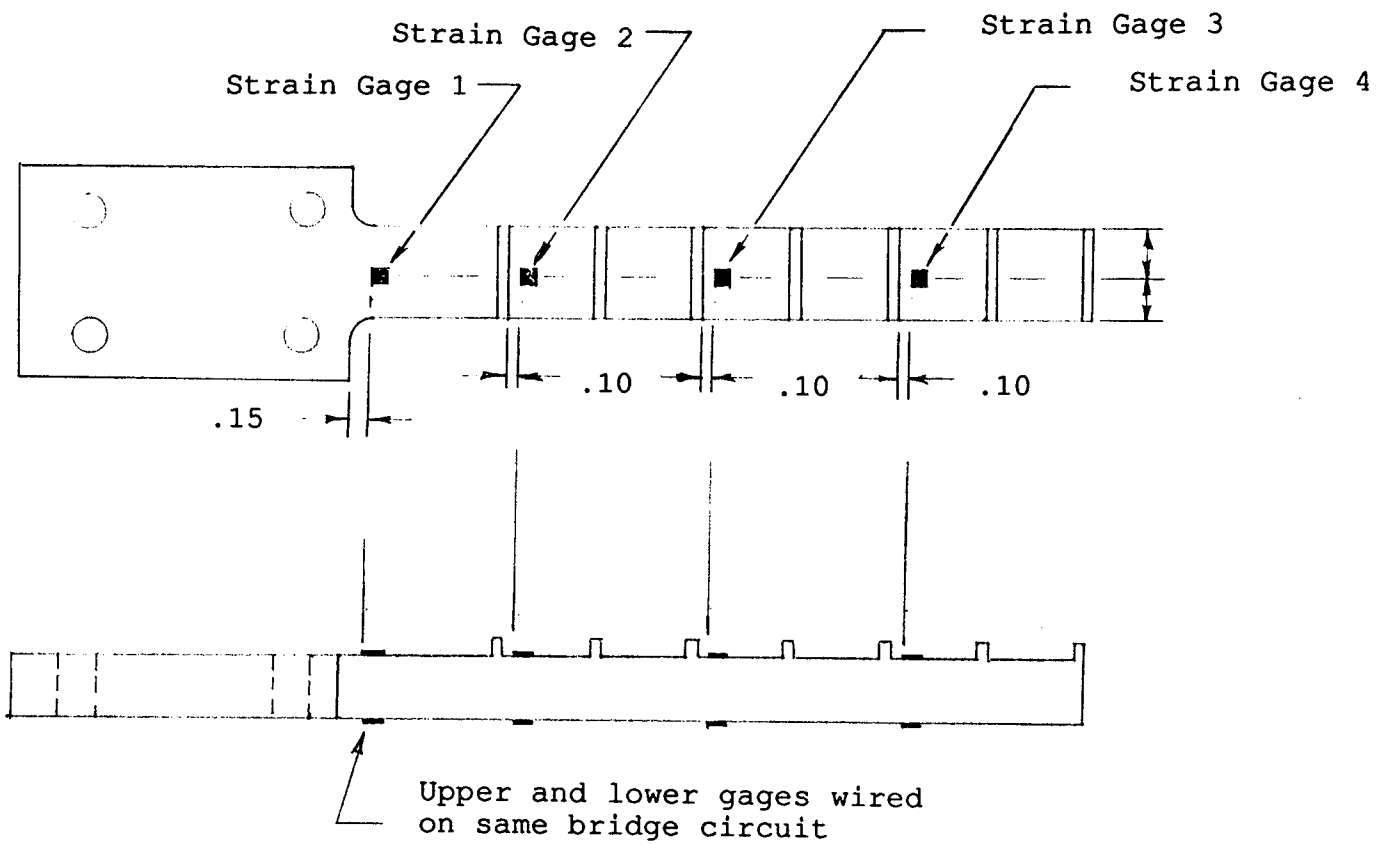

Figure 2.2-10 Low frequency beam strain gage instrumentation

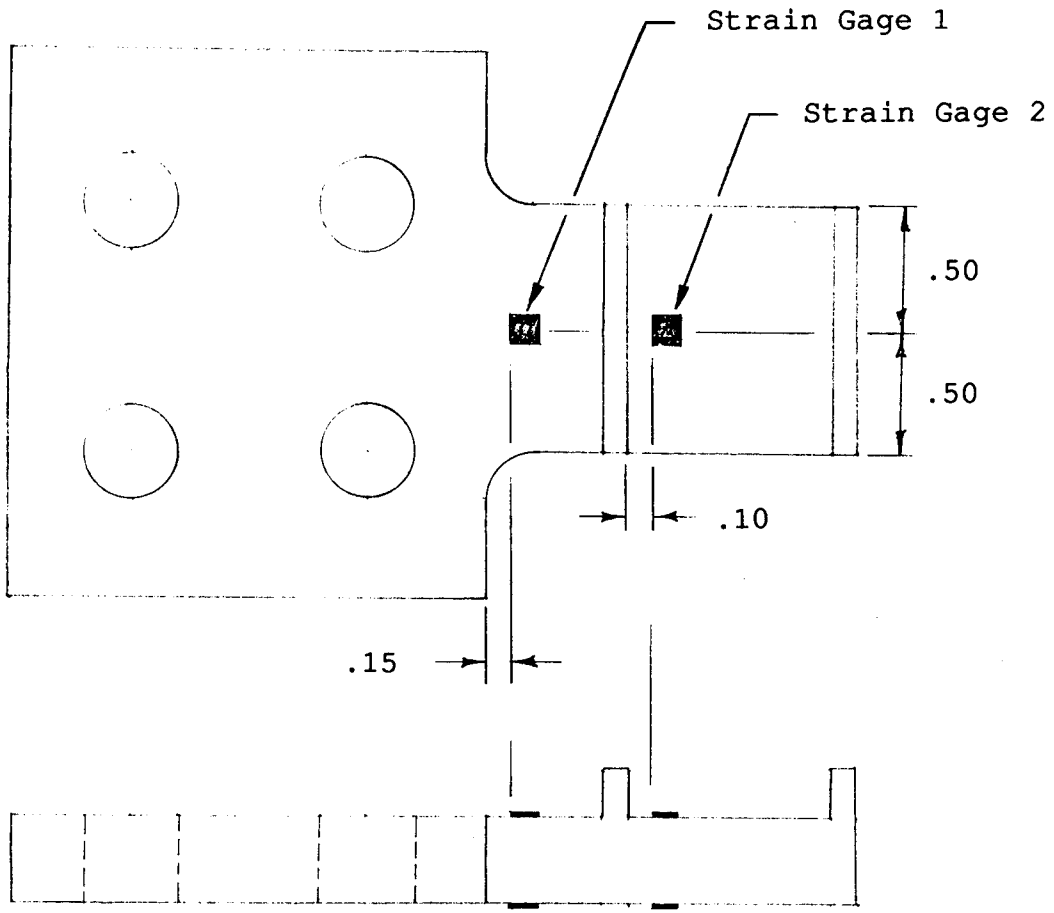

Figure 2.2-11 High frequency beam strain gage instrumentation

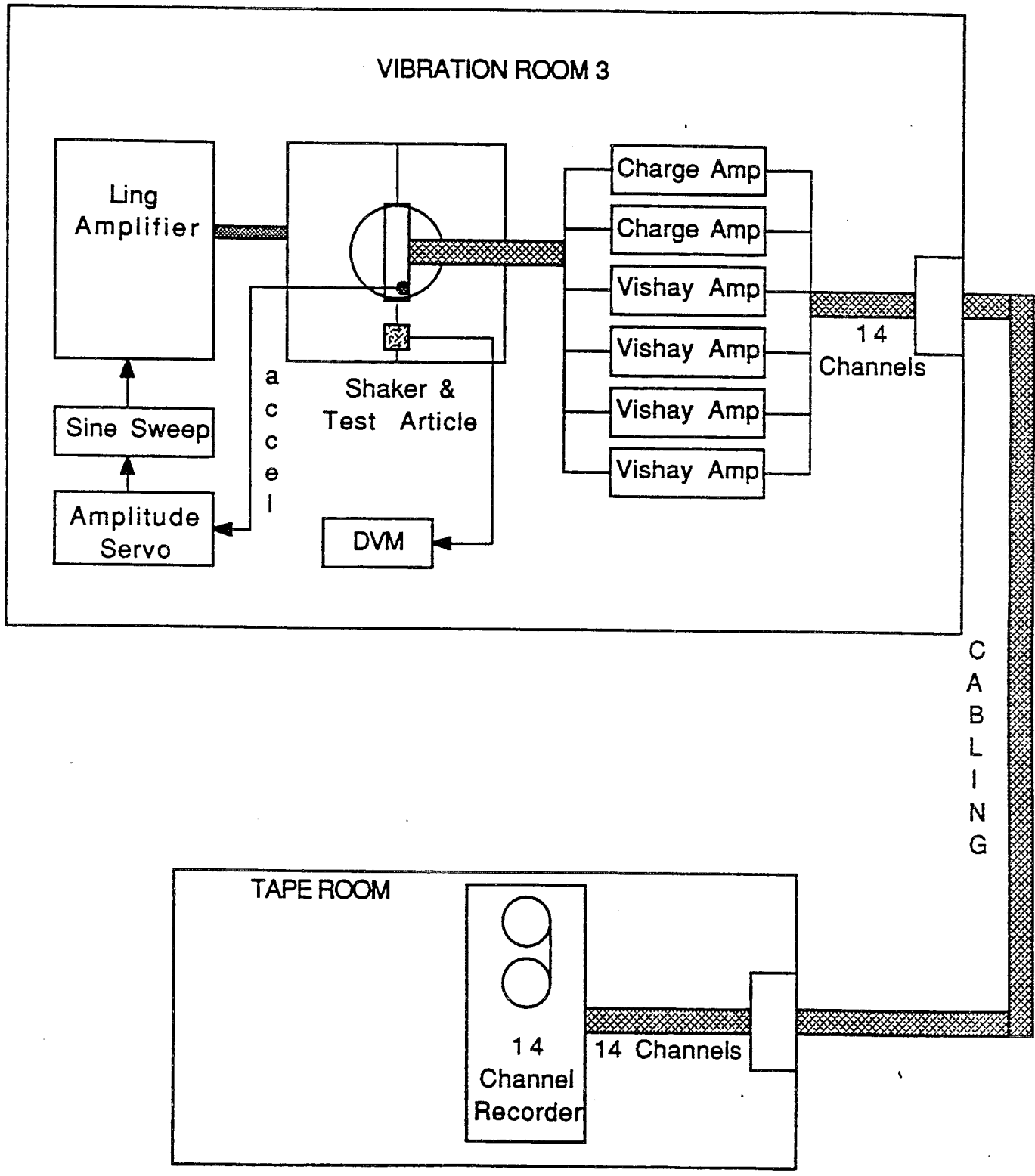

Figure 2.2-12 Data recording system

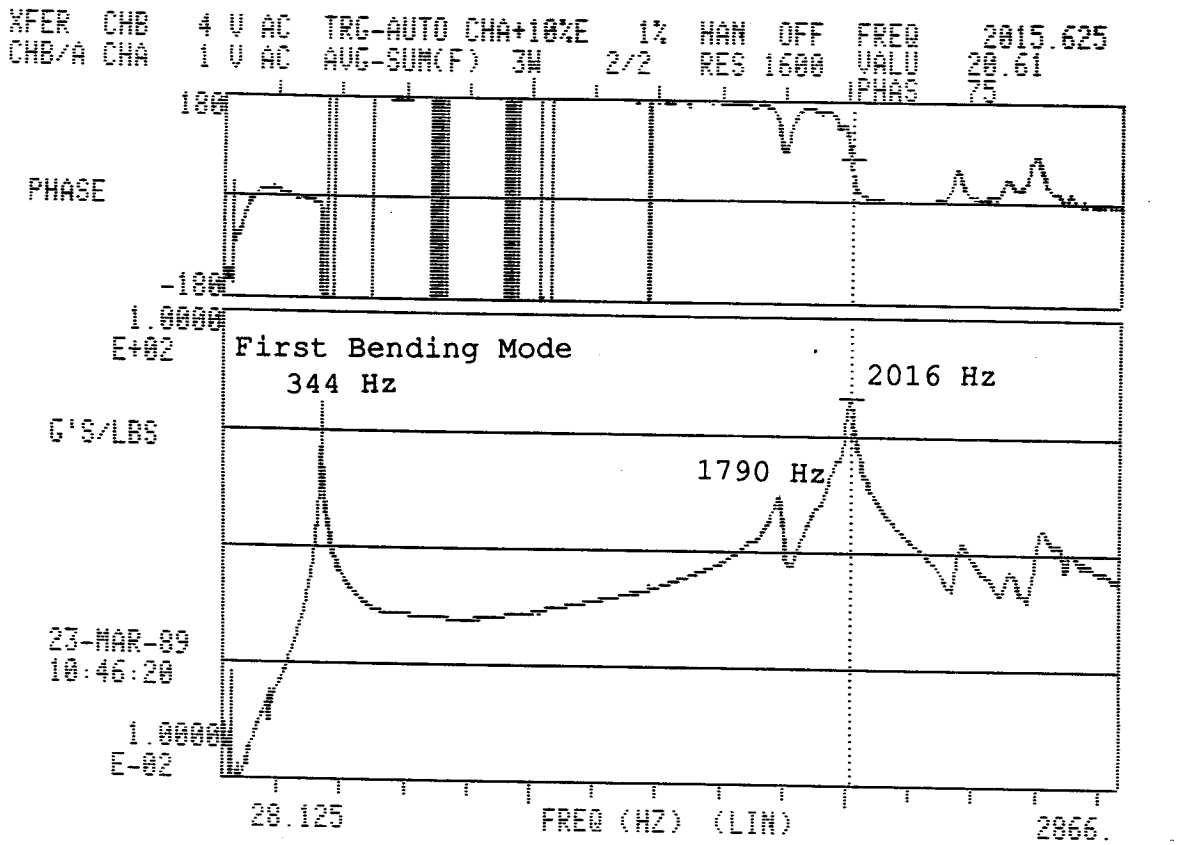

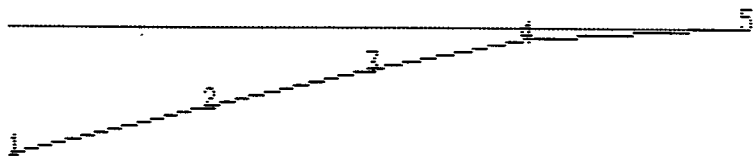

2Y+ REAL,F= 342.000 HZ (0.0, 0.0, 1.0, 0.0)=VIEW

Figure 2.2-13 Frequency response function and mode shape of low frequency beam without damper

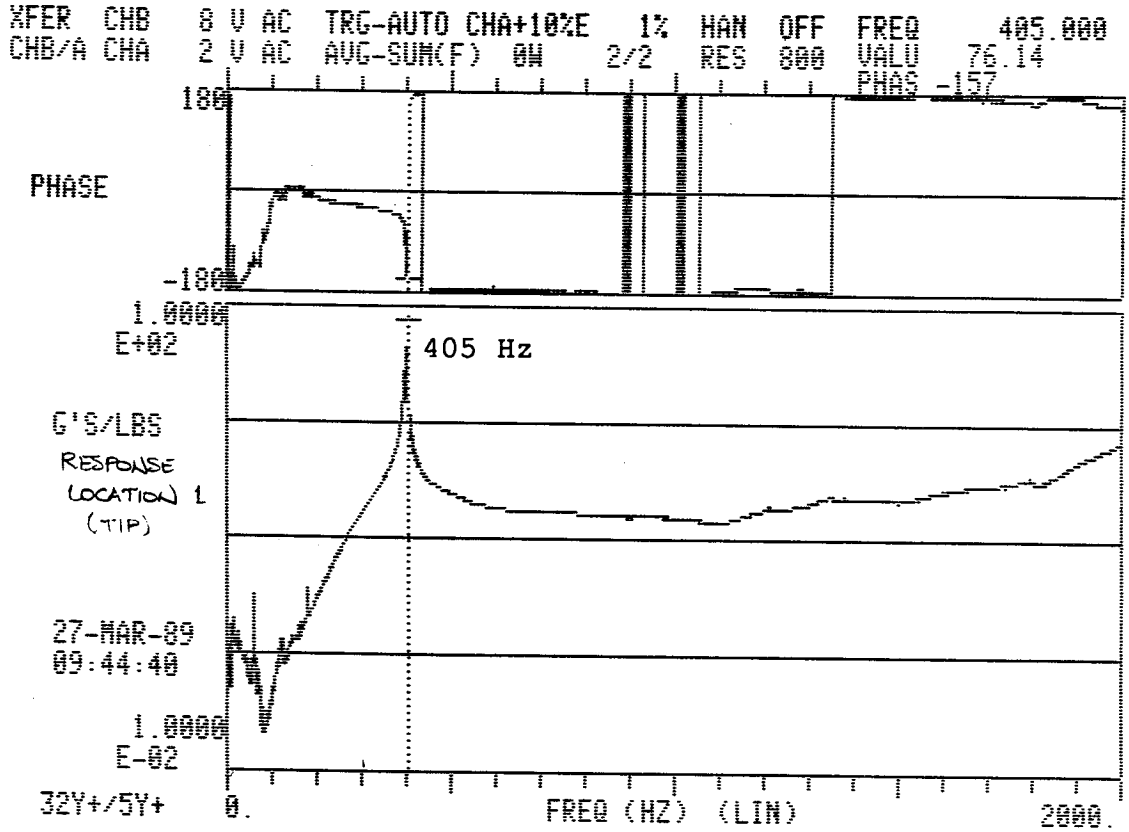

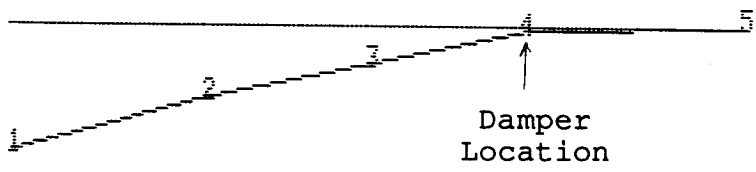

(Tang 1)

N = 500 lbs

42Y+ REAL,F= 402.000 HZ (0.0, 0.0, 1.0, 0.0)=VIEW

Figure 2.2-14 Frequency response function and mode shape of low frequency beam with locked damper at tang 1

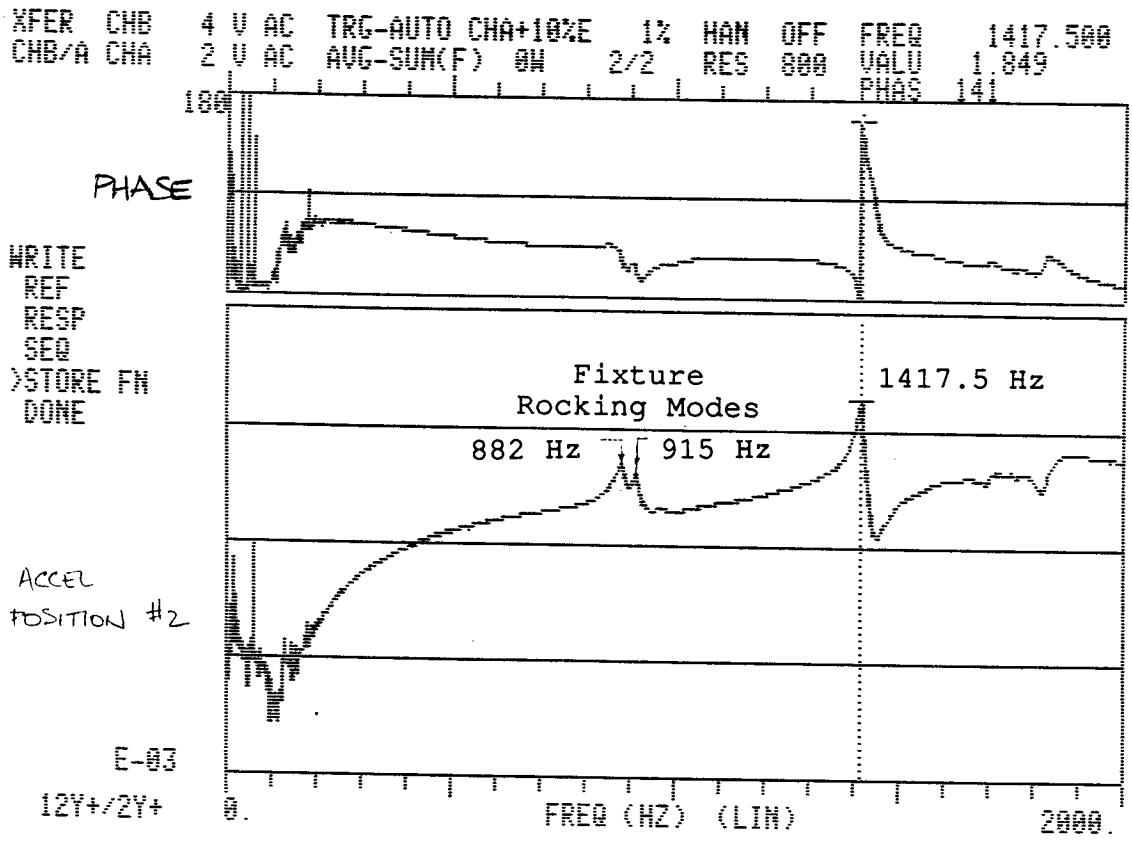

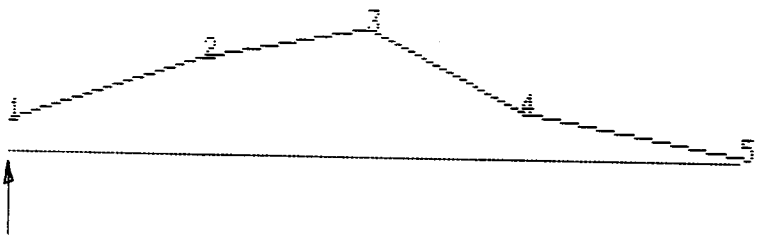

Damper
Location

(Tang 7)

N = 540 lbs

4: 12Y+ REAL,F= 1416.000 HZ (0.0, 0.0, 1.0, 0.0)=VIEW

Figure 2.2-15 Frequency response function and mode shape of low frequency beam with locked damper at tang 7

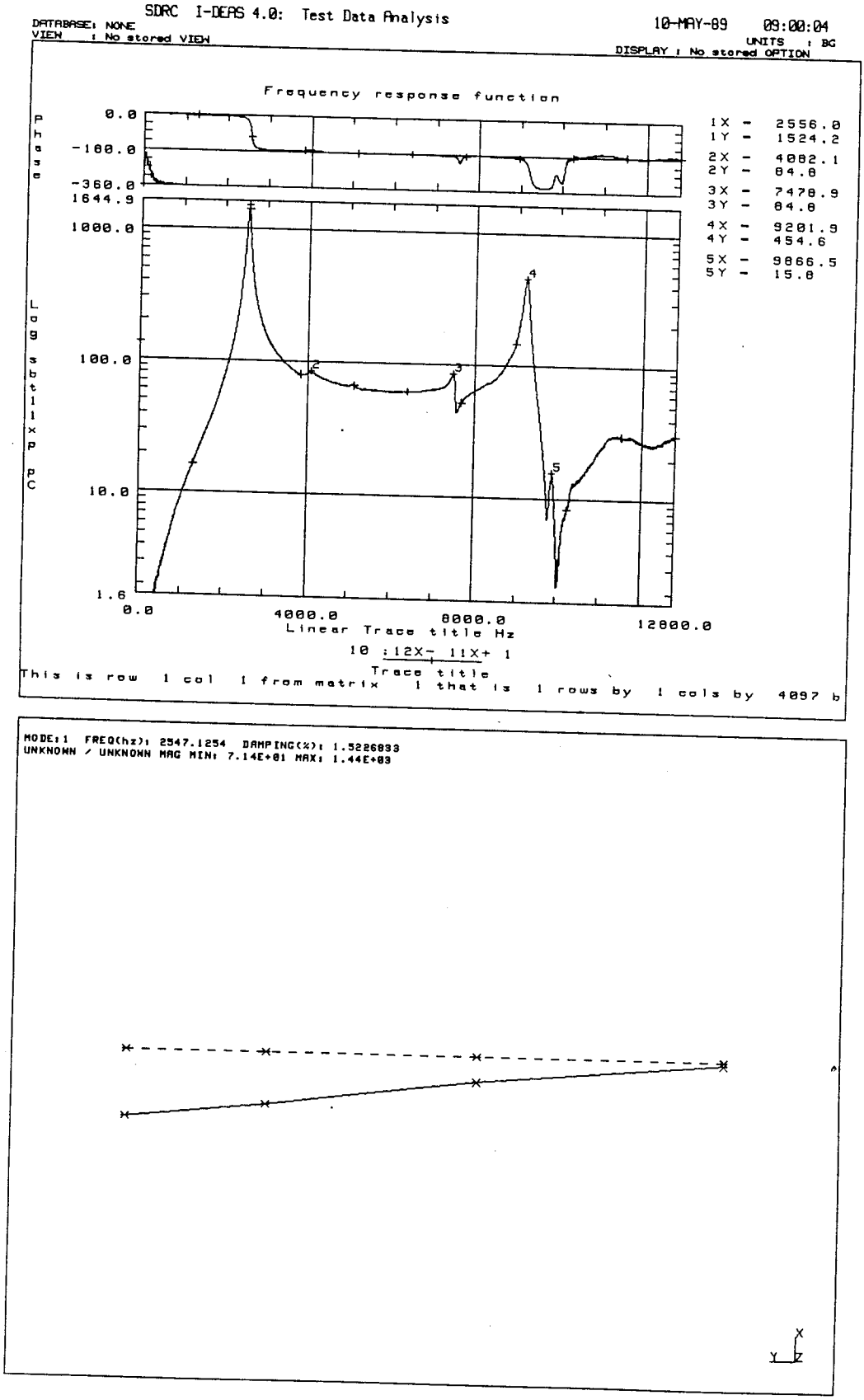

Figure 2.2-16 Frequency response function and mode shape of high frequency beam without damper

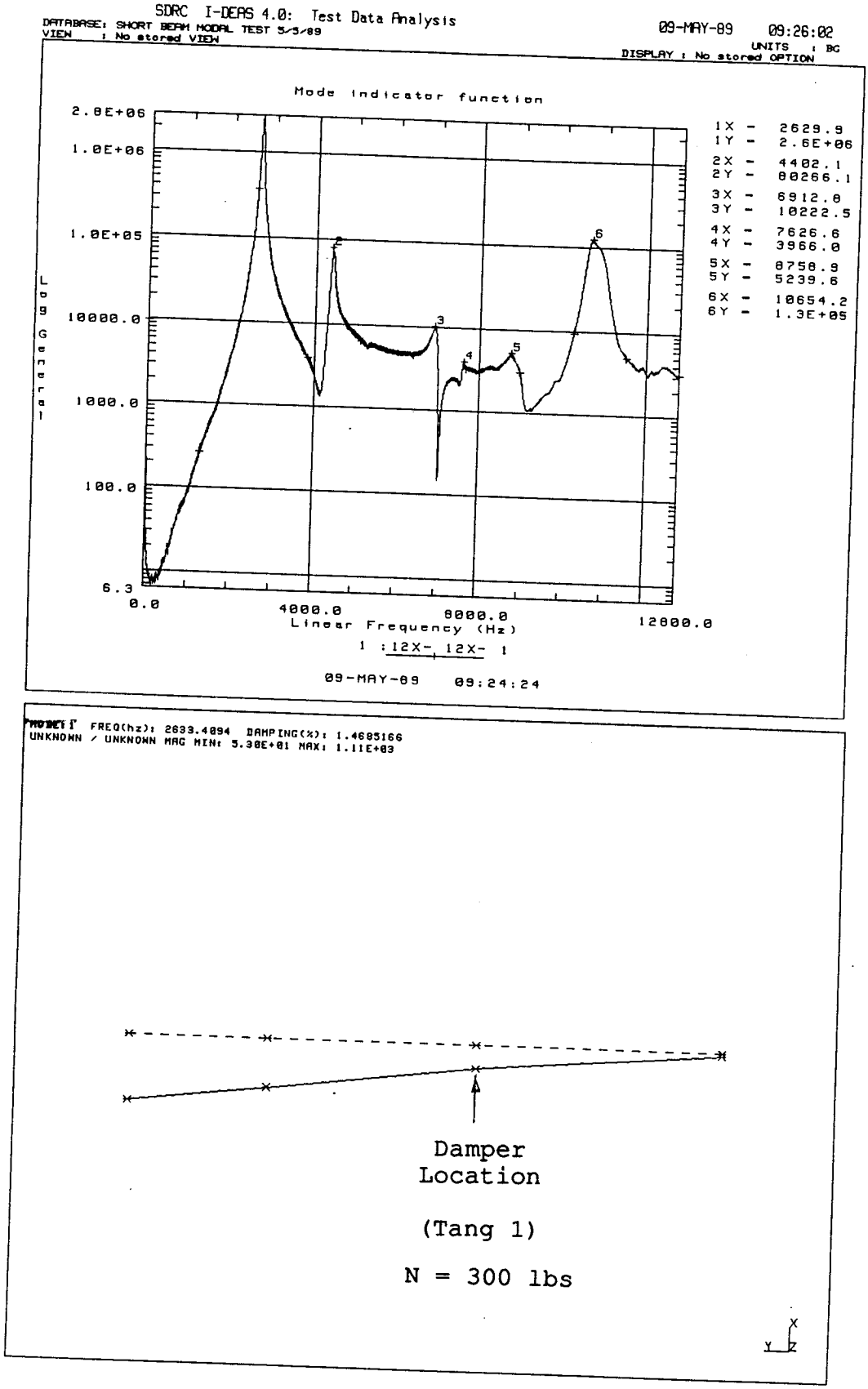

Figure 2.2-17 Frequency response function and mode shape of high frequency beam with damper at tang 1

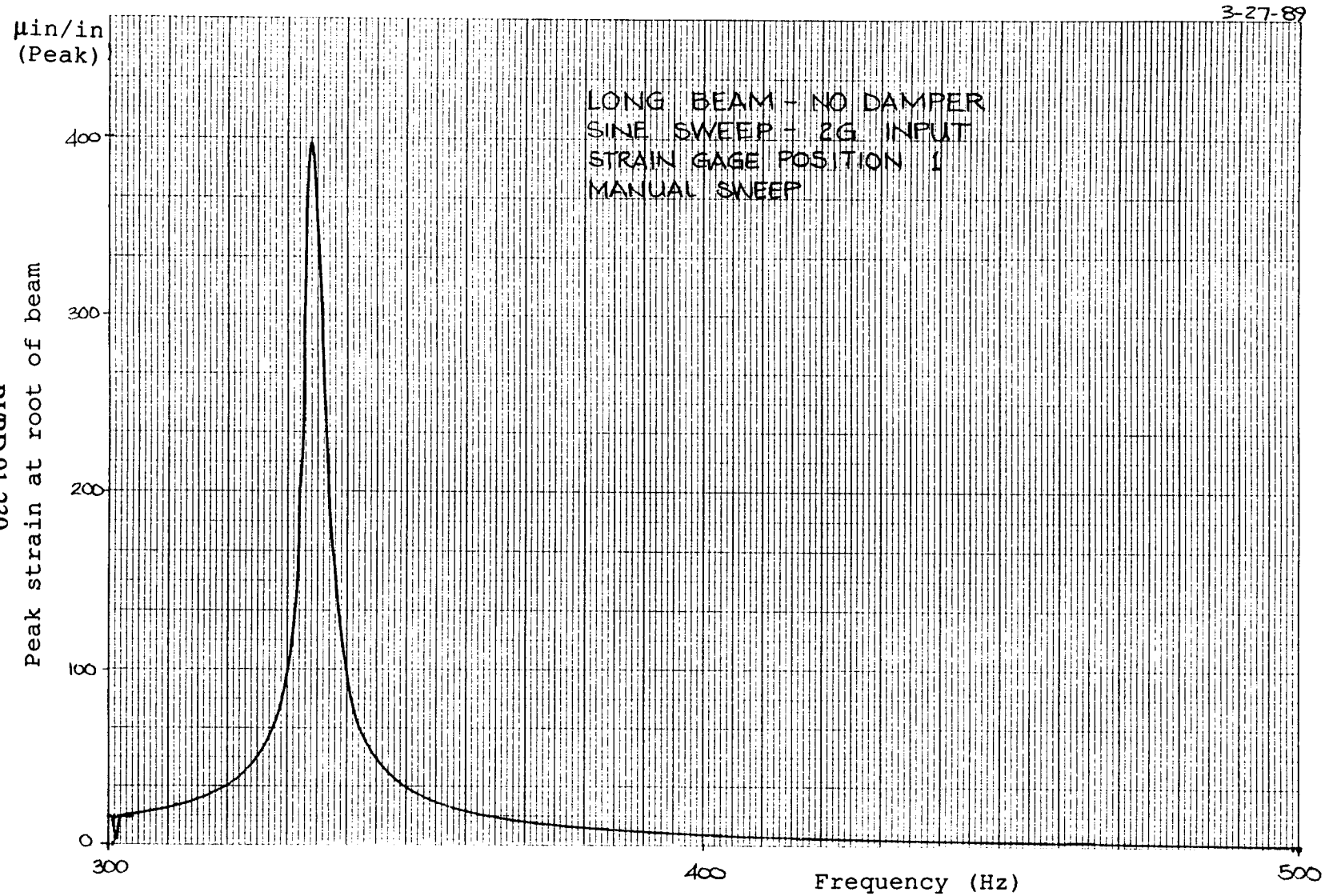

Figure 2.2-18 Response of low frequency beam without damper

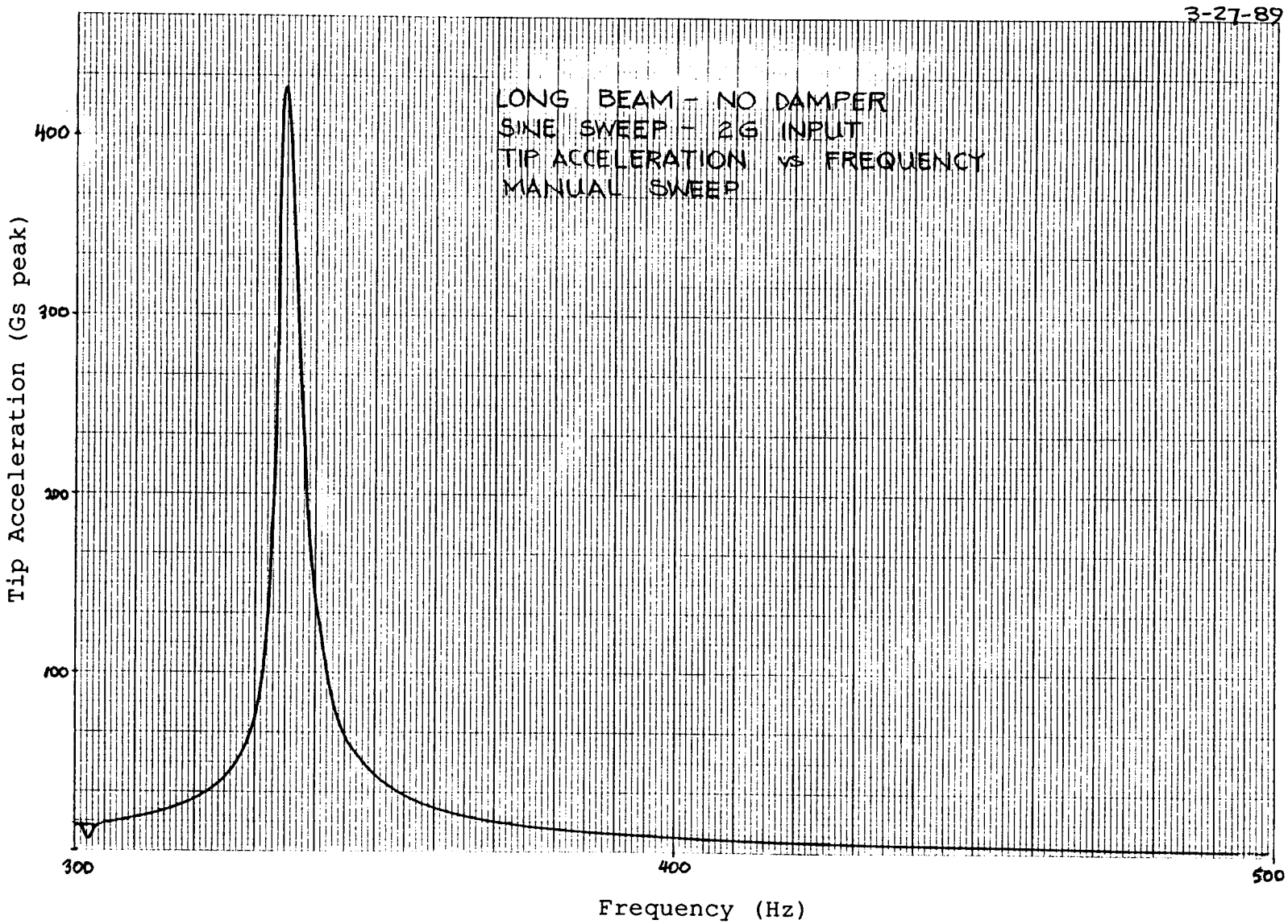

Figure 2.2-19 Response of low frequency beam without damper

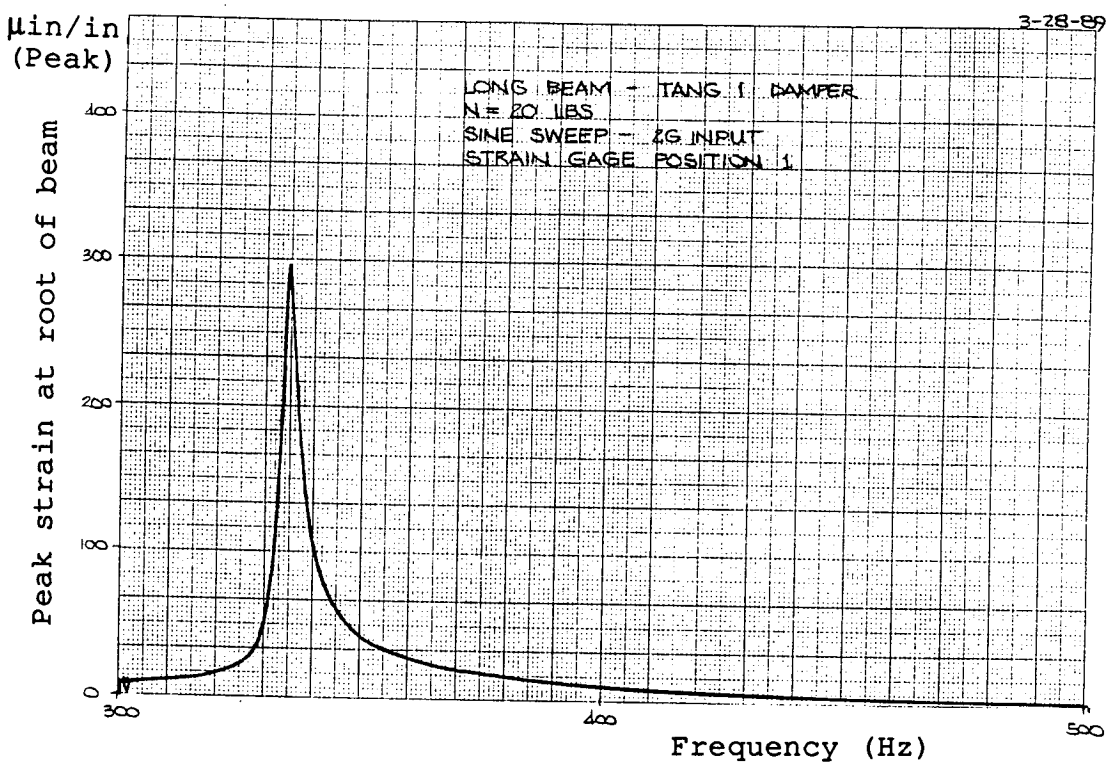

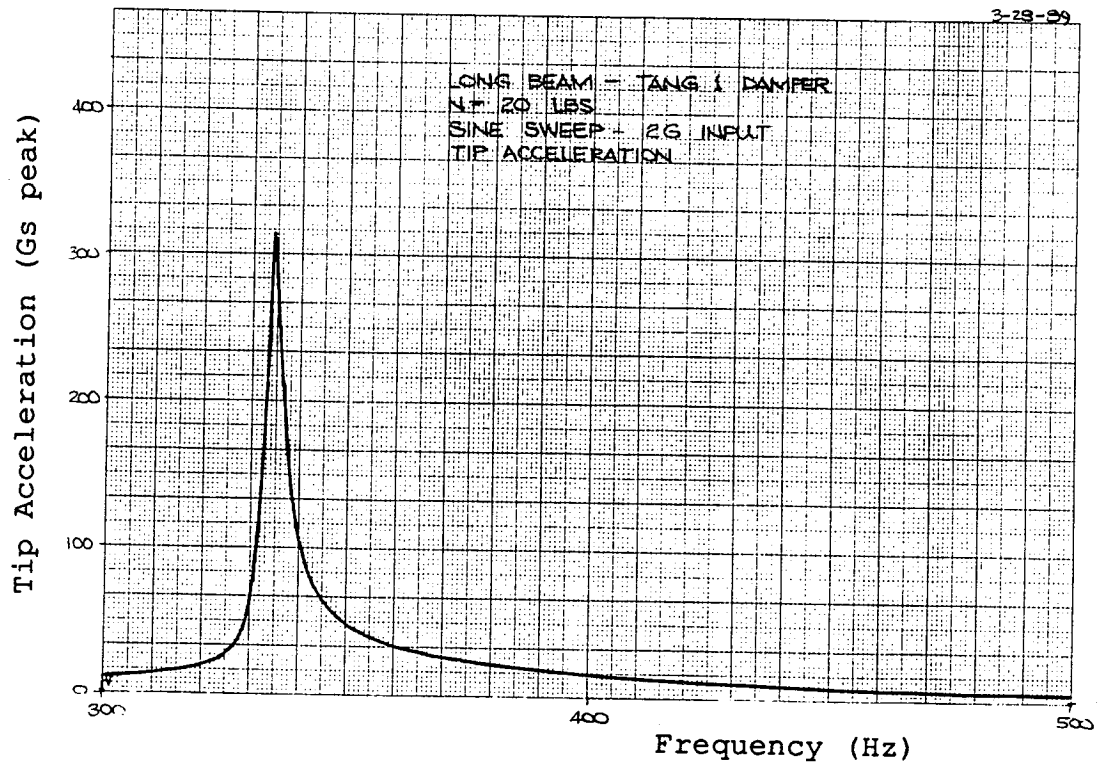

Figure 2.2-20 Response of low frequency beam with damper at tang 1 and normal force of 20 pounds

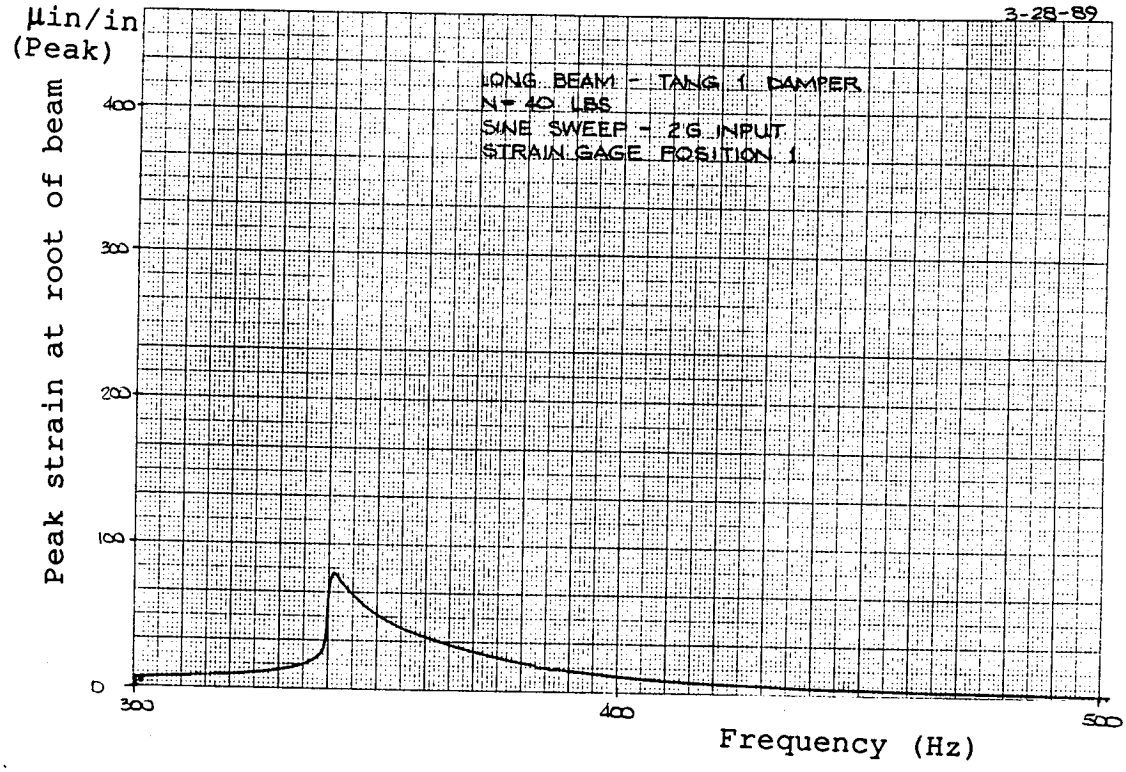

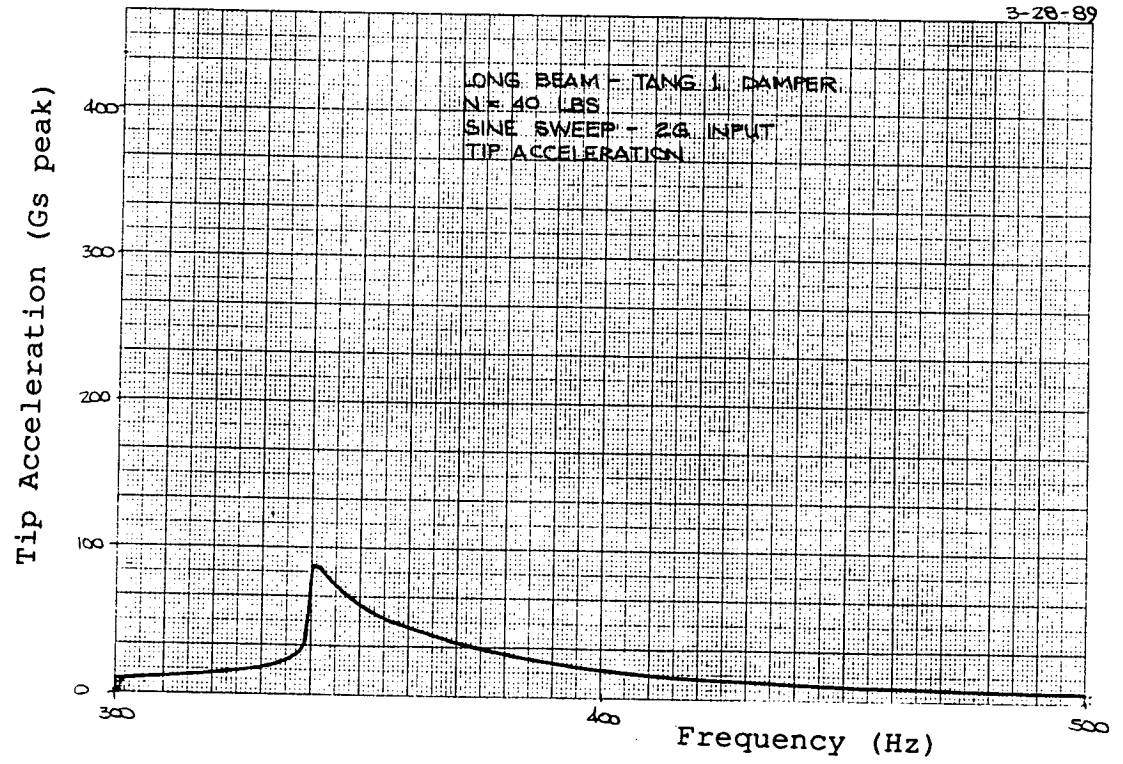

Figure 2.2-21 Response of low frequency beam with damper at tang 1 and normal force of 40 pounds

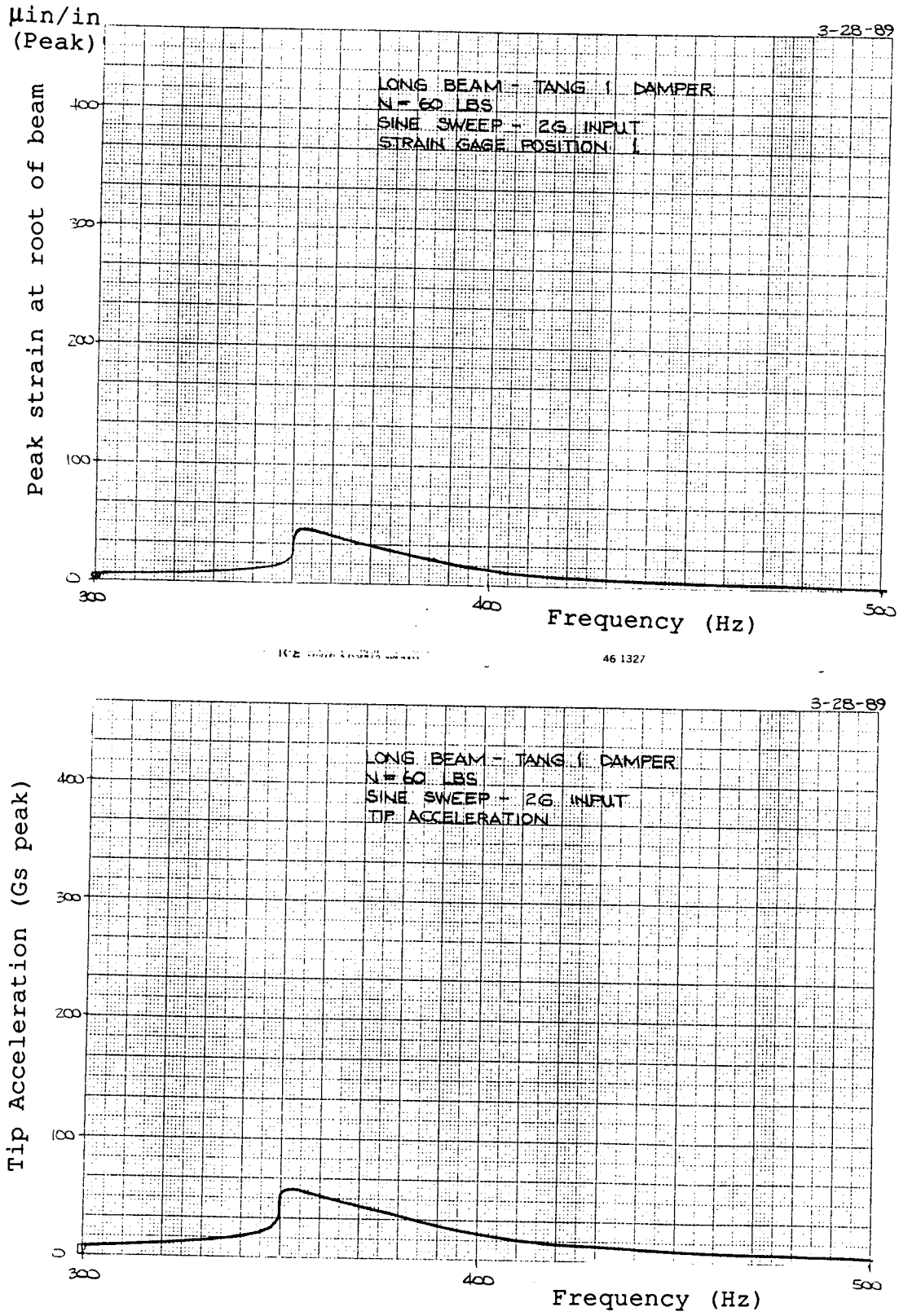

Figure 2.2-22 Response of low frequency beam with damper at tang 1 and normal force of 60 pounds

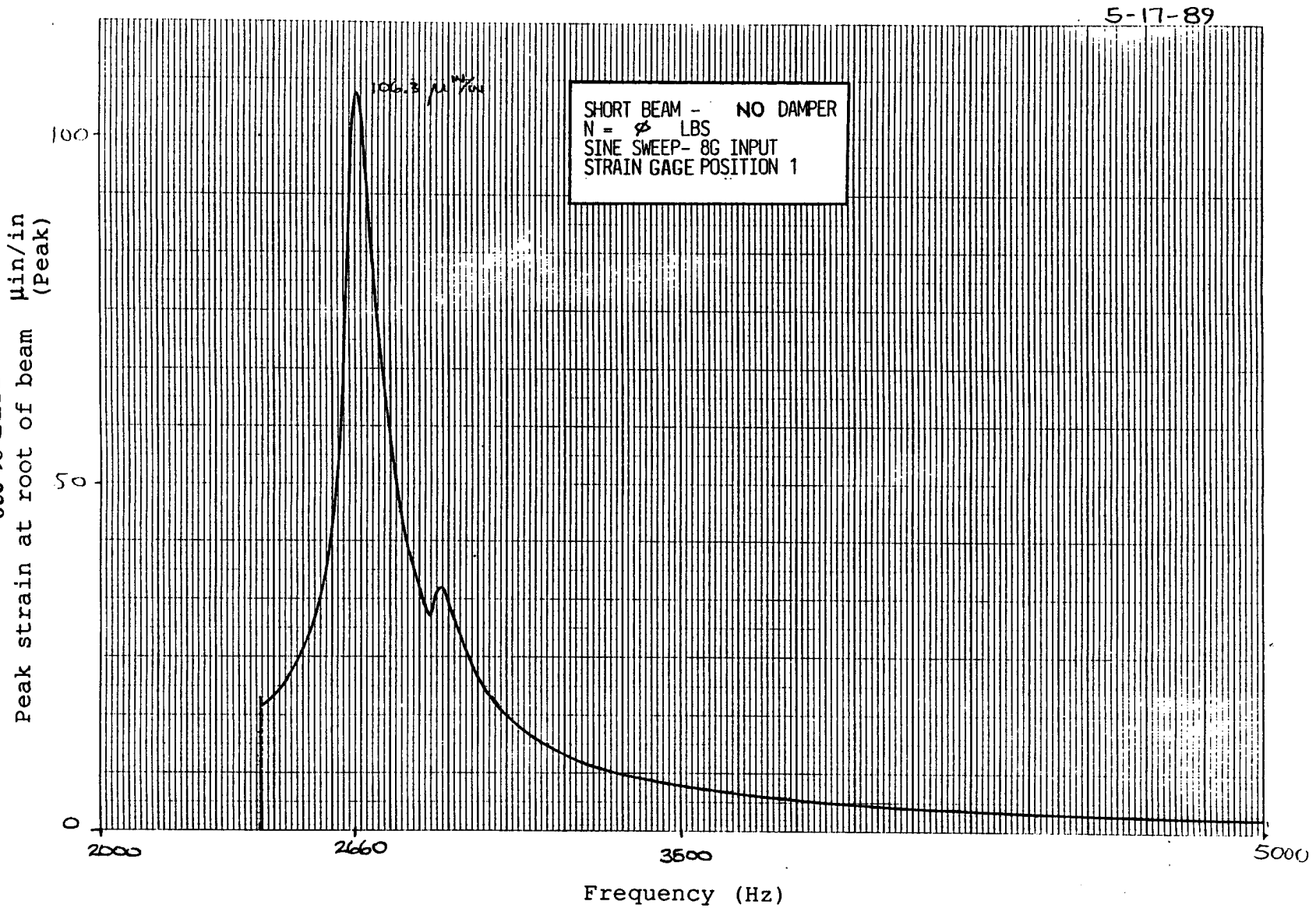

Figure 2.2-23 Response of high frequency beam without damper

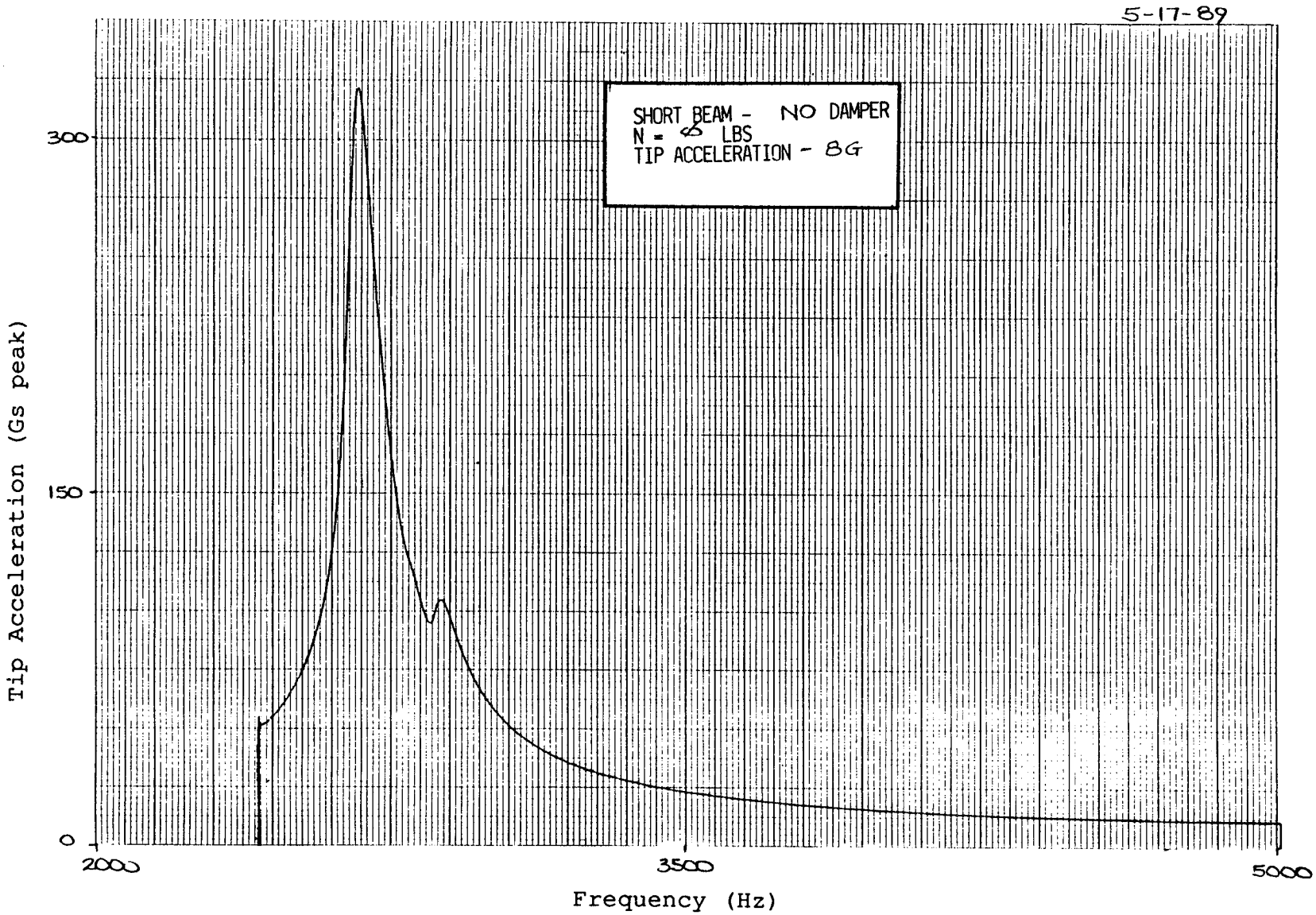

Figure 2.2-24 Response of high frequency beam without damper

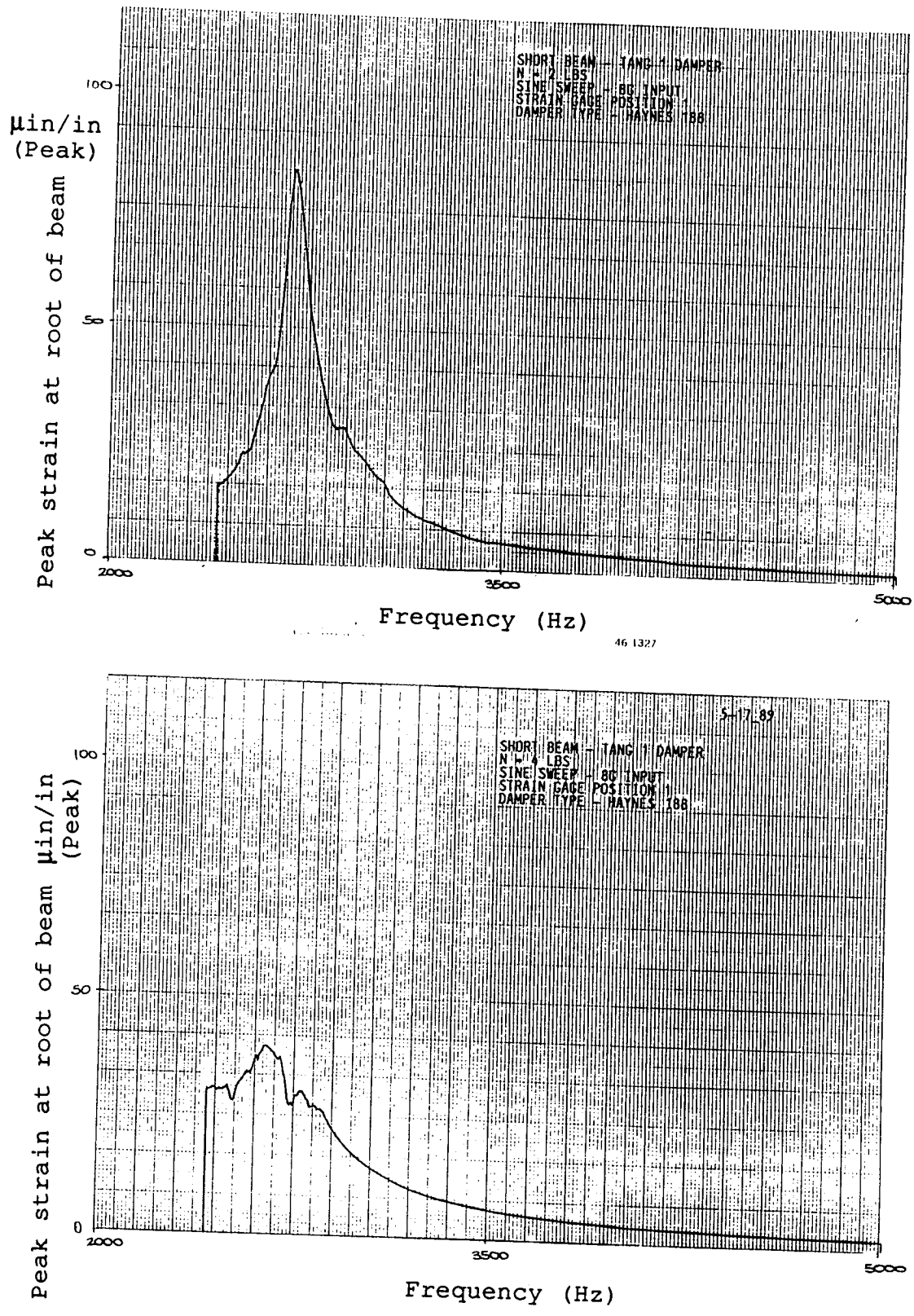

Figure 2.2-25 Response of high frequency beam with damper at tang 1 and normal loads of 2 and 4 pounds

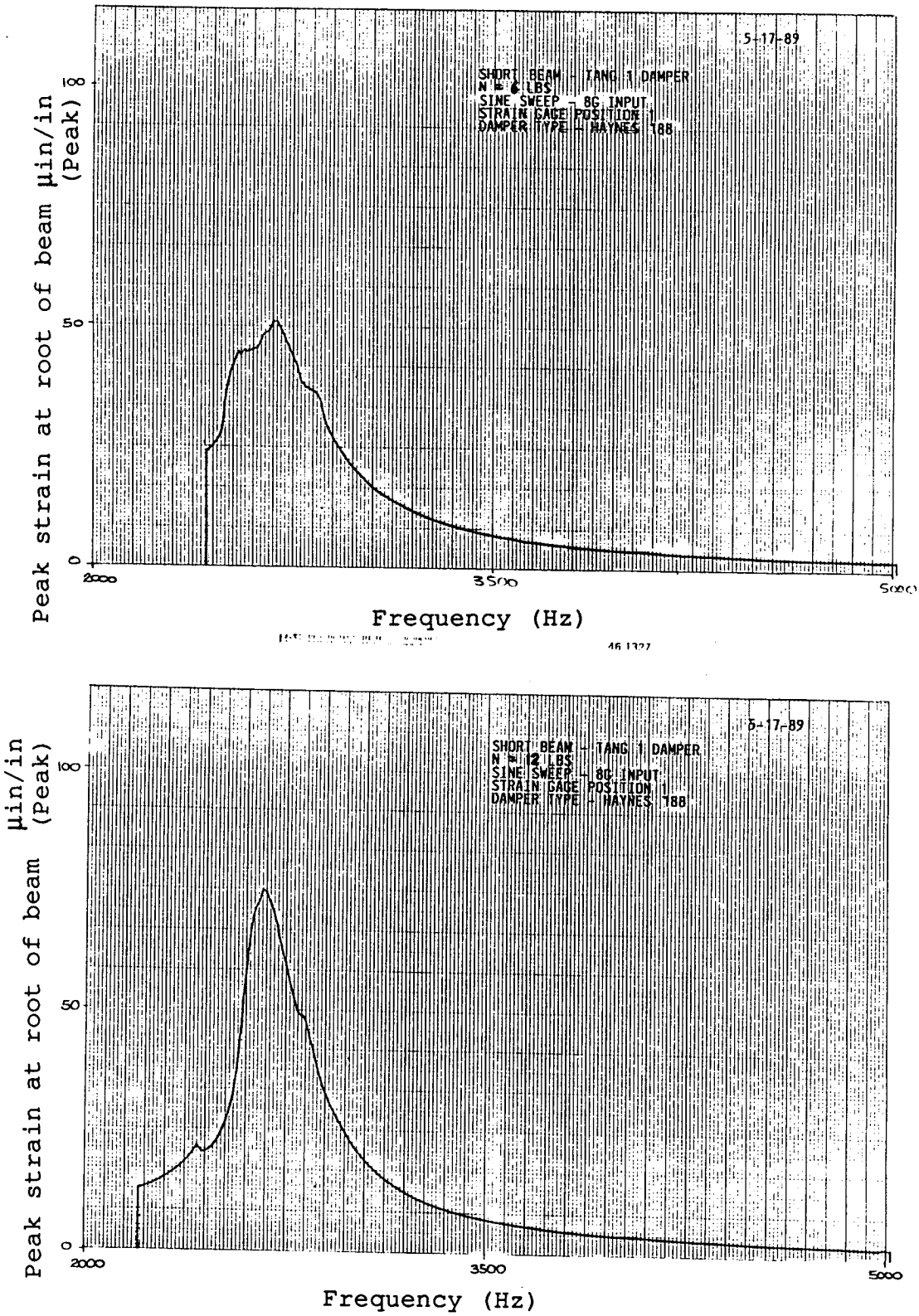

Figure 2.2-26 Response of high frequency beam with damper at tang 1 and normal loads of 6 and 12 pounds

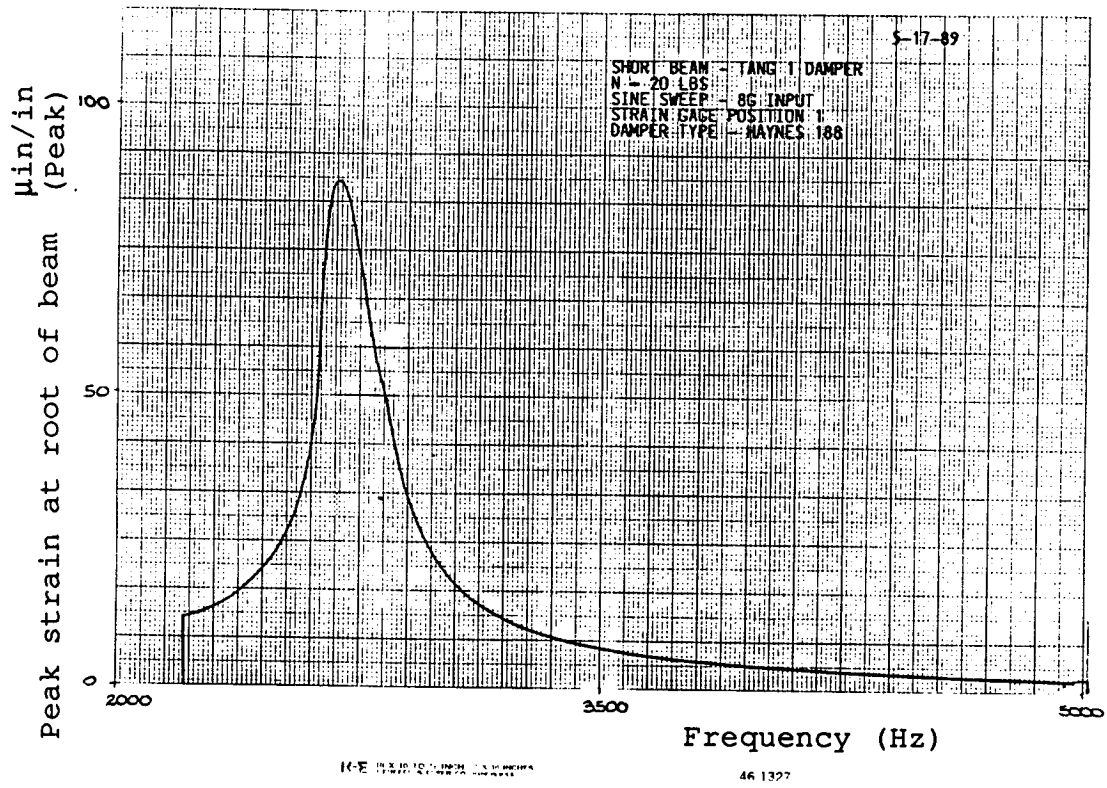

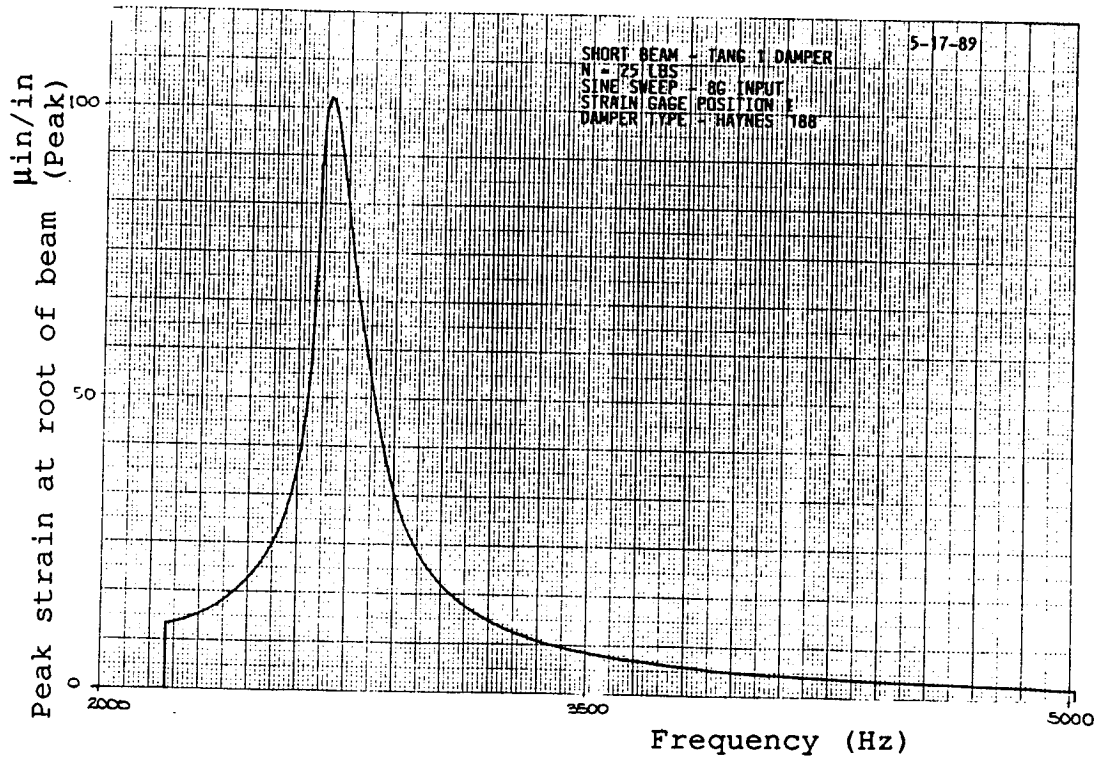

Figure 2.2-27 Response of high frequency beam with damper at tang 1 and normal loads of 20 and 25 pounds

response plots are shown in Figures 2.2-18 through 2.2-27 for both damped and undamped beams. The input was increased after testing was completed at a given excitation level, so that the effects at higher vibration levels could be determined.

2.2.1.8 Test Results. Results of the testing were plotted in the form of stress versus normal force curves for each damper position and type. These curves are presented in Figures 2.2-28 through 2.2-37 for the low-frequency beam (long beam) and Figures 2.2-38 through 2.2-44 for the high-frequency beam (short beam). The stress was determined from strain gages located at the root of the beam for all the cases shown. The normal force, presented in these curves, represents the total force applied to the damper by the cable. The actual force, at the interface between the damper and vibrating beam, is half of the total force. The curves show the classic friction damper behavior, which consists of a reduction in vibratory response as normal force is increased up to a critical value. References 5 and 6 show a large increase in response at normal loads greater than the critical value. However, in this test, a flat or slight increase in response was observed as normal force was increased. This is due to the relatively high stiffness of the damper, which has the effect of flattening the response curve.

Viscous damping ratios were computed for each beam, without dampers installed, using the half power point method. Damping ratios were also computed at each of the two vibration input levels used for the beams. These are shown in Table 2.2-2 and range from 0.005 to 0.006 for the low-frequency beam and from 0.008 to 0.015 for the high-frequency beam.

The major observation from the test data is that friction damping can be extremely effective in reducing vibratory response. Tenfold reductions in response were commonly observed during testing, as can be seen from the summary given in Table 2.2-3. In addition, it was found that the effectiveness of the dampers increases, as the damper is moved to locations closer to the tip of the beam. This expected result occurs because the beam motion is larger at the tip and can be expected to dissipate more energy at that location. This can be seen from a comparison of Figures 2.2-29 and 2.2-33, which show the response of the low-frequency beam with dampers at tangs 1 and 3, respectively. Also, from these two figures, it can be seen that the optimum normal force is significantly reduced, as the damper is moved from tang 1 to tang 3, i.e., closer to the tip of the beam. Further testing with the damper located outboard of tang 3 was attempted with mixed results. For these configurations, the beam response was consistently low level. However, the data quality and test-to-test repeatability were poor. It was found that, because of feedback caused by the stick-slip motion of the damper, the shaker control system was unable to keep the base moving in a sinusoidal fashion at the desired input level.

The character of the damper performance curve for the silicon nitride damper was found to be somewhat different than for the Haynes 188 dampers, as can be seen by comparing Figures 2.2-28 and 2.2-29 with Figures 2.2-30 and 2.2-31. From Figures 2.2-28 and 2.2-30 it is clear that the silicon nitride damper requires a much larger normal load to reach the optimum point than the Haynes 188 damper. This is indicative of a low friction coefficient, which is expected for this material. On the other hand, Figures 2.2-29 and 2.2-31 show the optimum normal force to be about equal for the two dampers. A closer evaluation of the curve of Figure 2.2-31 leads one to believe that the last two data points are in error and that the actual optimum point is much farther to the right than shown. This is supported by the fact that at 2G input (Figure 2.2-30) the optimum normal force was found to be 250 lbs. Therefore, at 5G input (Figure 2.2-31) the optimum must be greater than 250 lbs.

Testing on the low-frequency beam at the outboard damper locations and on the high-frequency beam at all damper locations proved to be very difficult, because of damper

Table 2.2-2

CRITICAL DAMPING RATIOS WITHOUT FRICTION DAMPERS INSTALLED

LOW FREQUENCY BEAM

EXCITATION LEVEL	DAMPING RATIO
2G	.005
5G	.006

HIGH FREQUENCY BEAM

EXCITATION LEVEL	DAMPING RATIO
8G	.015
12G	.008

Table 2.2-3

PEAK RESPONSES WITH AND WITHOUT DAMPERS

LOW FREQUENCY BEAM

INPUT	STRESS (N=0)	STRESS (N=Optimum)	N	TANG	DAMPER
2G	11.7 ksi	1.2 ksi	70 lbs	1	Haynes
5G	23.2 ksi	3.8 ksi	120 lbs	1	Haynes
2G	11.9 ksi	1.4 ksi	250 lbs	1	Si/Nitride
5G	23.2 ksi	7.4 ksi	1200 lbs	1	Si/Nitride
2G	11.7 ksi	0.2 ksi	12 lbs	3	Haynes
5G	23.2 ksi	0.6 ksi	25 lbs	3	Haynes
2G	11.9 ksi	1.4 ksi	18 lbs	3	Si/Nitride
5G	23.2 ksi	--	--	3	Si/Nitride
2G	11.7 ksi	--	--	5	Haynes
2G	11.7 ksi	--	--	5	Si/Nitride

HIGH FREQUENCY BEAM

INPUT	STRESS (N=0)	STRESS (N=Optimum)	N	TANG	DAMPER
8G	2.8 ksi	0.2 ksi	60 lbs	1	Haynes
12G	6.8 ksi	0.8 ksi	50 lbs	1	Haynes
8G	2.9 ksi	0.9 ksi	75 lbs	1	Si/Nitride
12G	6.8 ksi	0.7 ksi	50 lbs	1	Si/Nitride
8G	2.9 ksi	0.5 ksi	50 lbs	2	Si/Nitride
12G	6.1 ksi	0.6 ksi	45 lbs	2	Haynes
12G	6.9 ksi	0.6 ksi	35 lbs	2	Si/Nitride

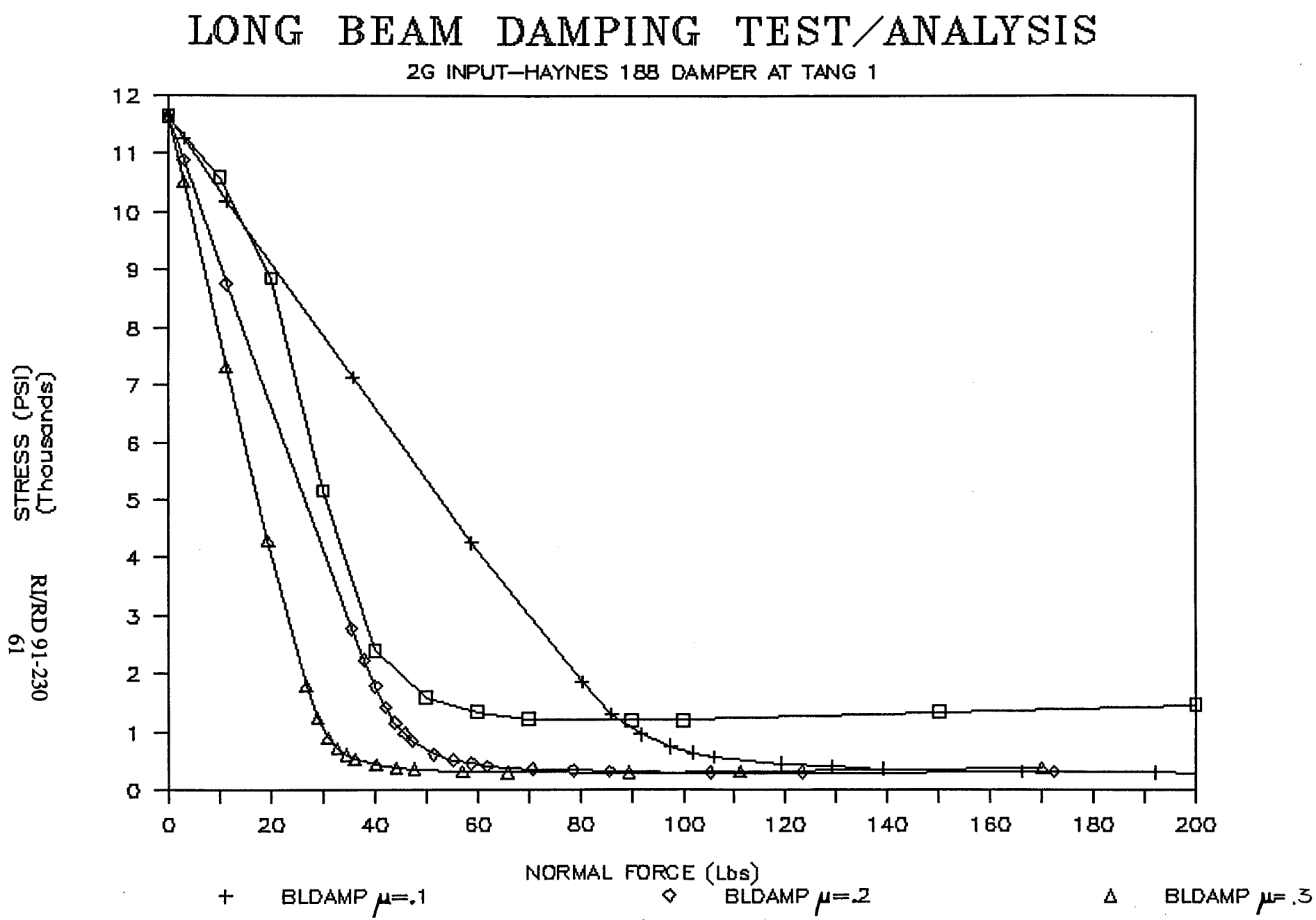

Figure 2.2-28 Low frequency beam optimum normal force curve for 2G input and Haynes 188 damper at tang 1

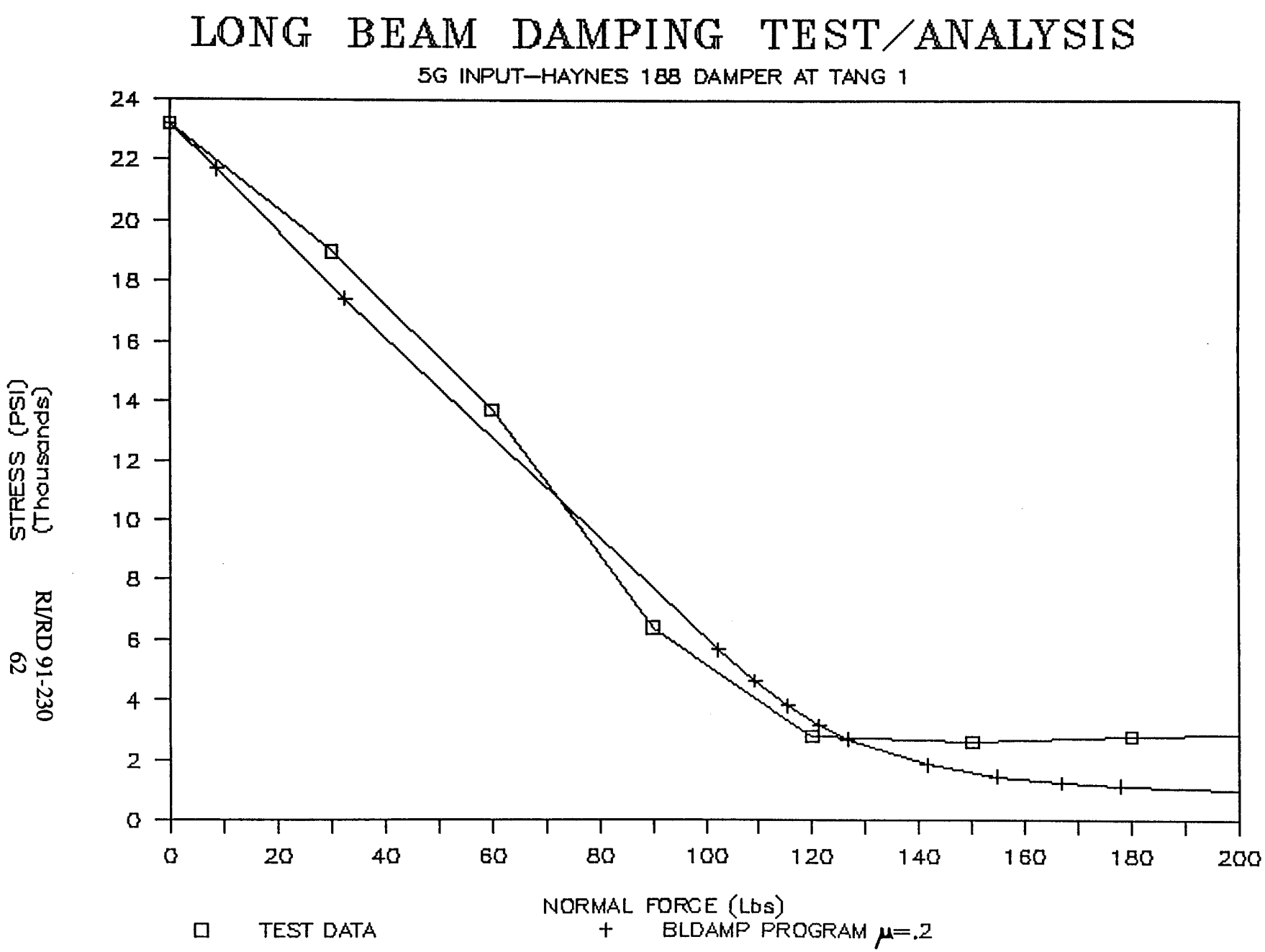

Figure 2.2-29 Low frequency beam optimum normal force curve

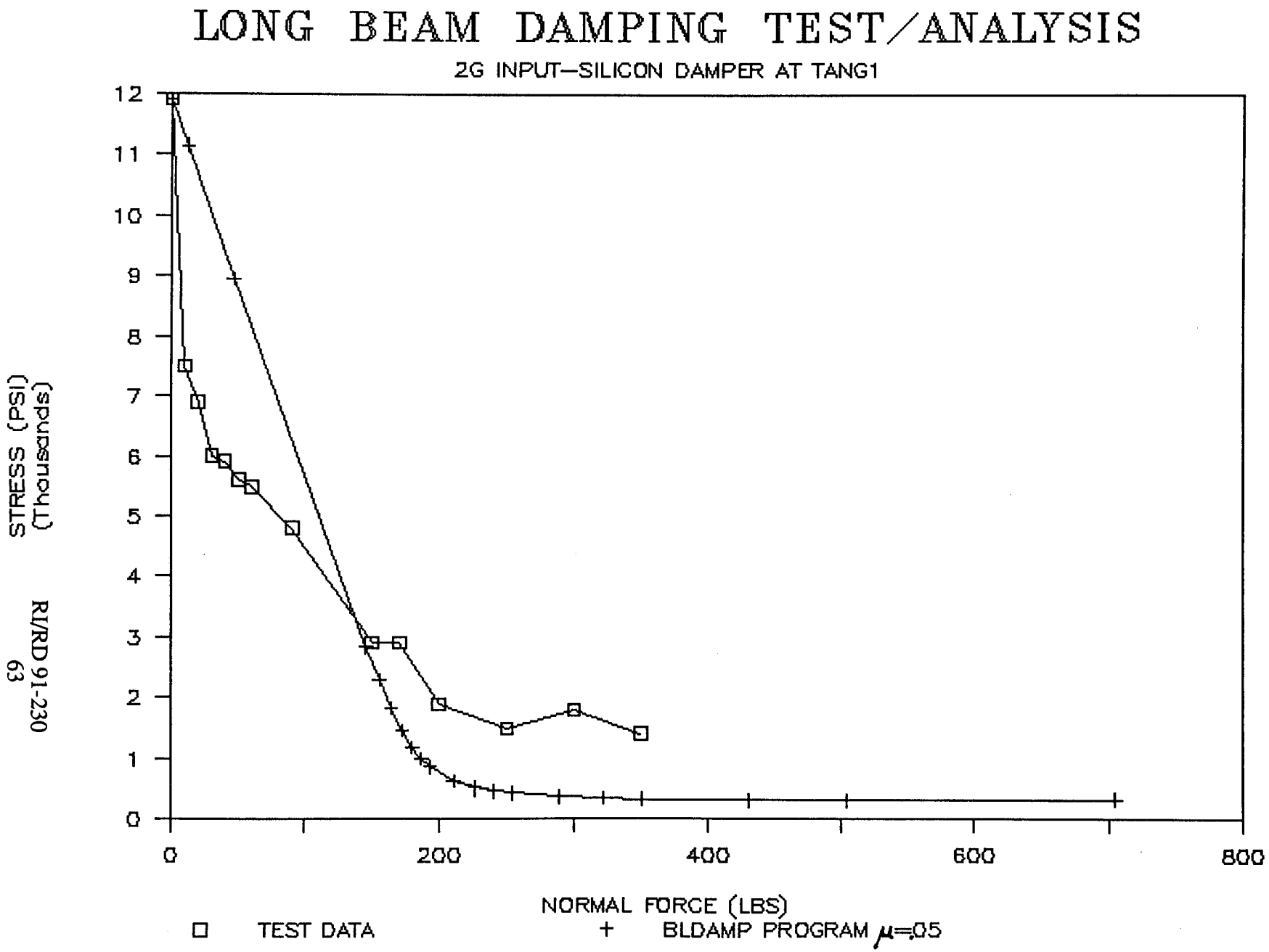

Figure 2.2-30 Low frequency beam optimum normal force curve for 2G input and Silicon Nitride damper at tang 1

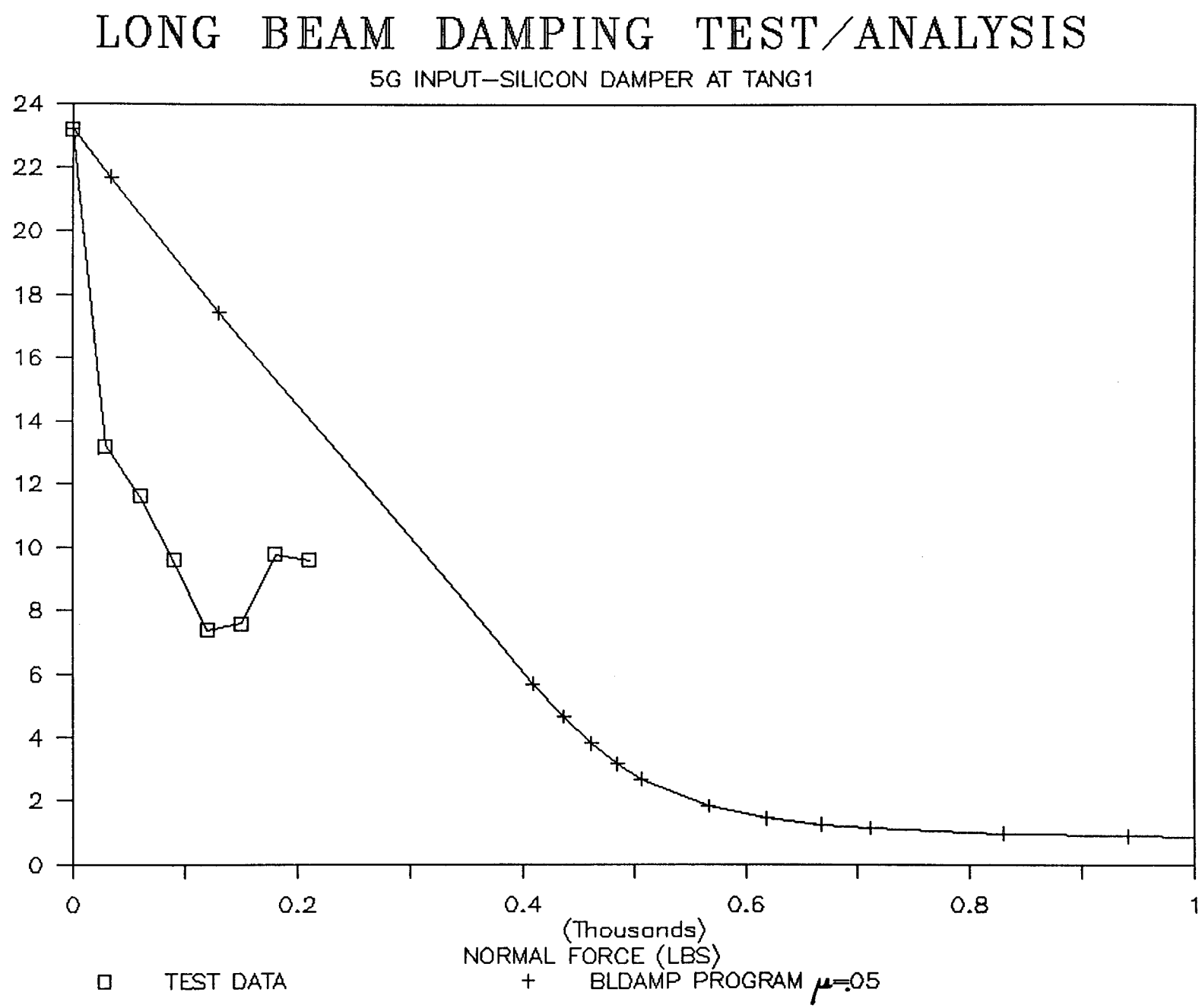

Figure 2.2-31 Low frequency beam optimum normal force curve

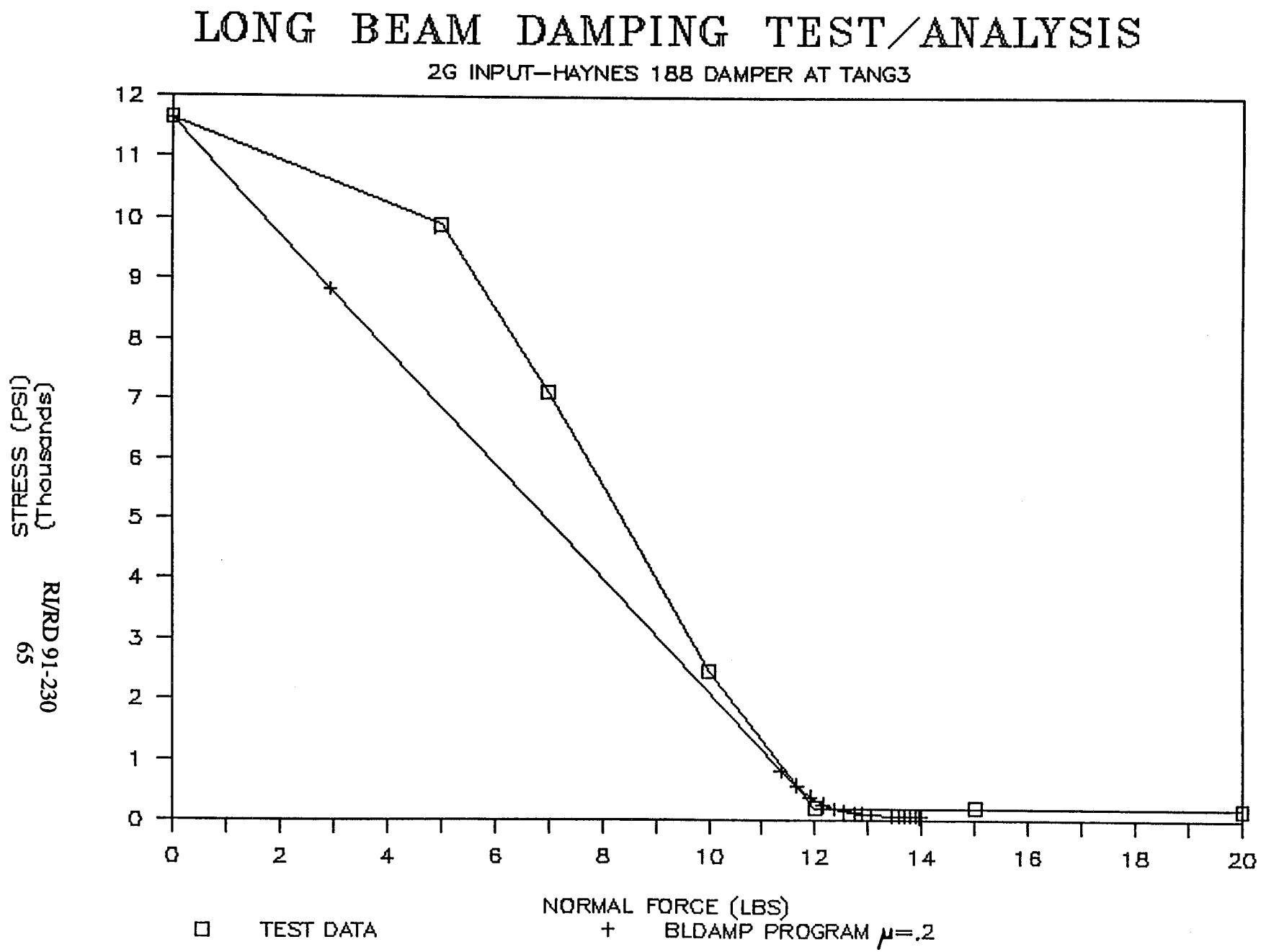

Figure 2.2-32 Low frequency beam optimum normal force curve for 2G input and Haynes 188 damper at tang 3

Figure 2.2-33 Low frequency beam optimum normal force curve

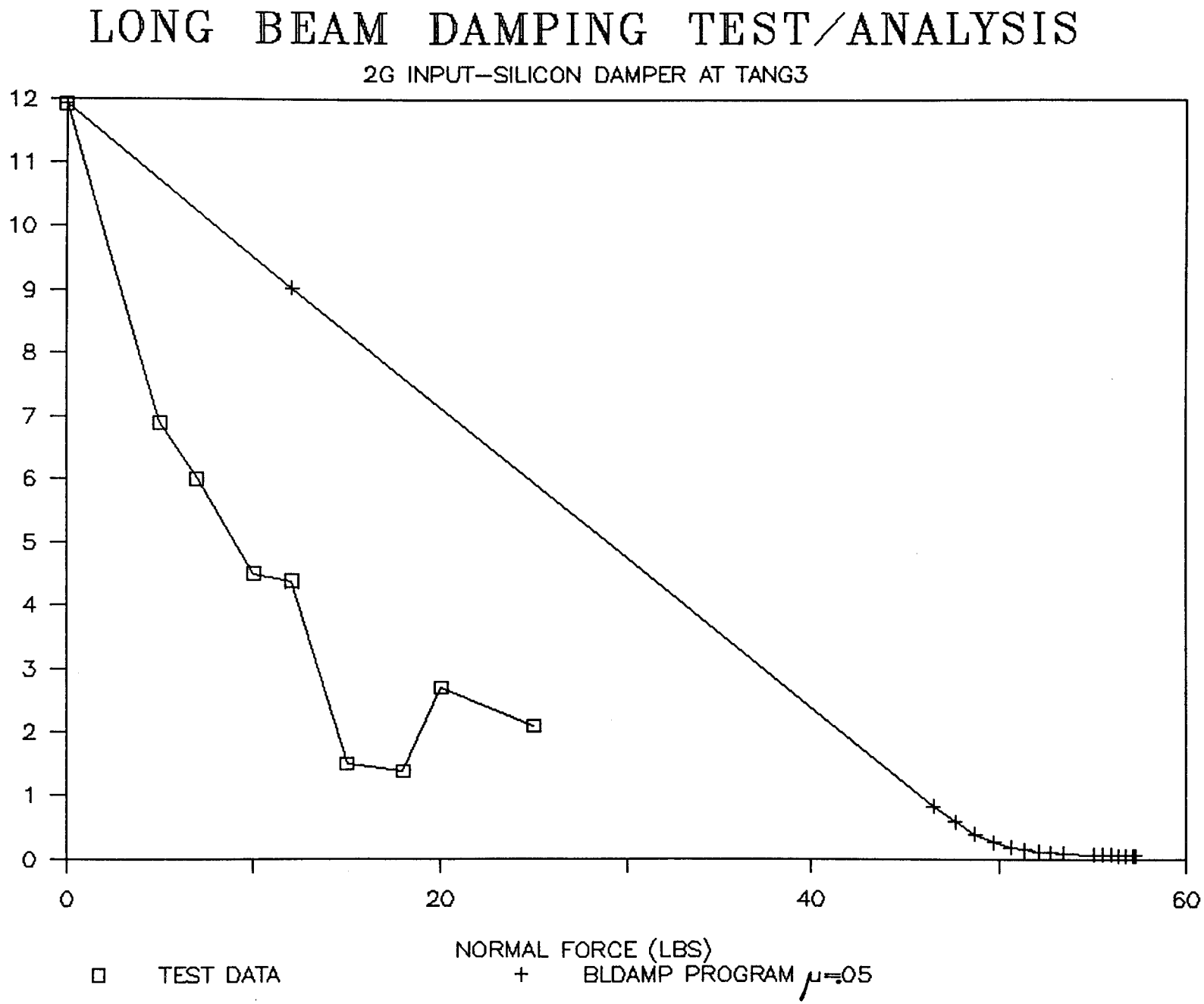

Figure 2.2-34 Low frequency beam optimum normal force curve for 2G input and Silicon Nitride damper at tang 3

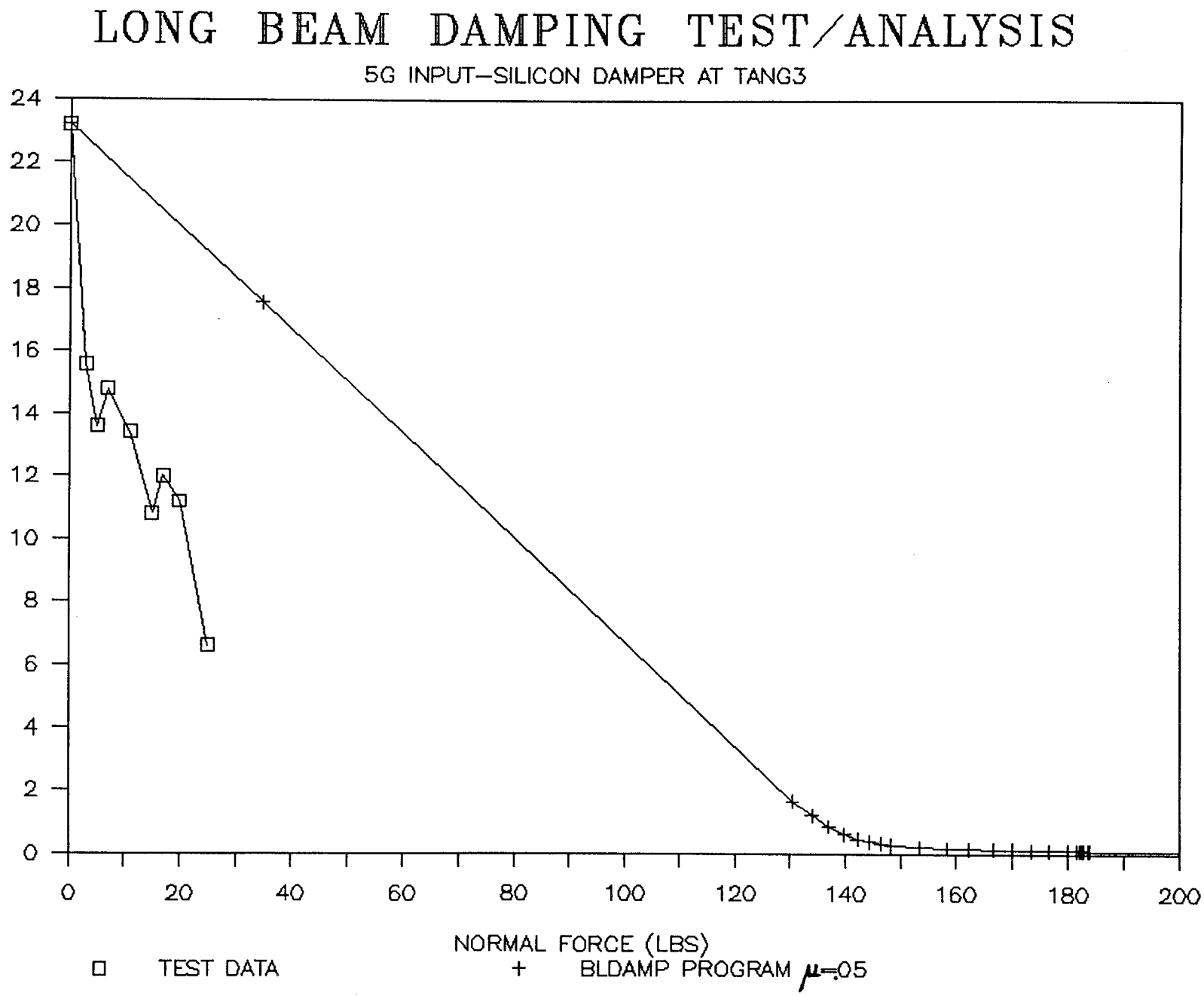

Figure 2.2-35 Low frequency beam optimum normal force curve for 5G input and Silicon Nitride damper at tang 3

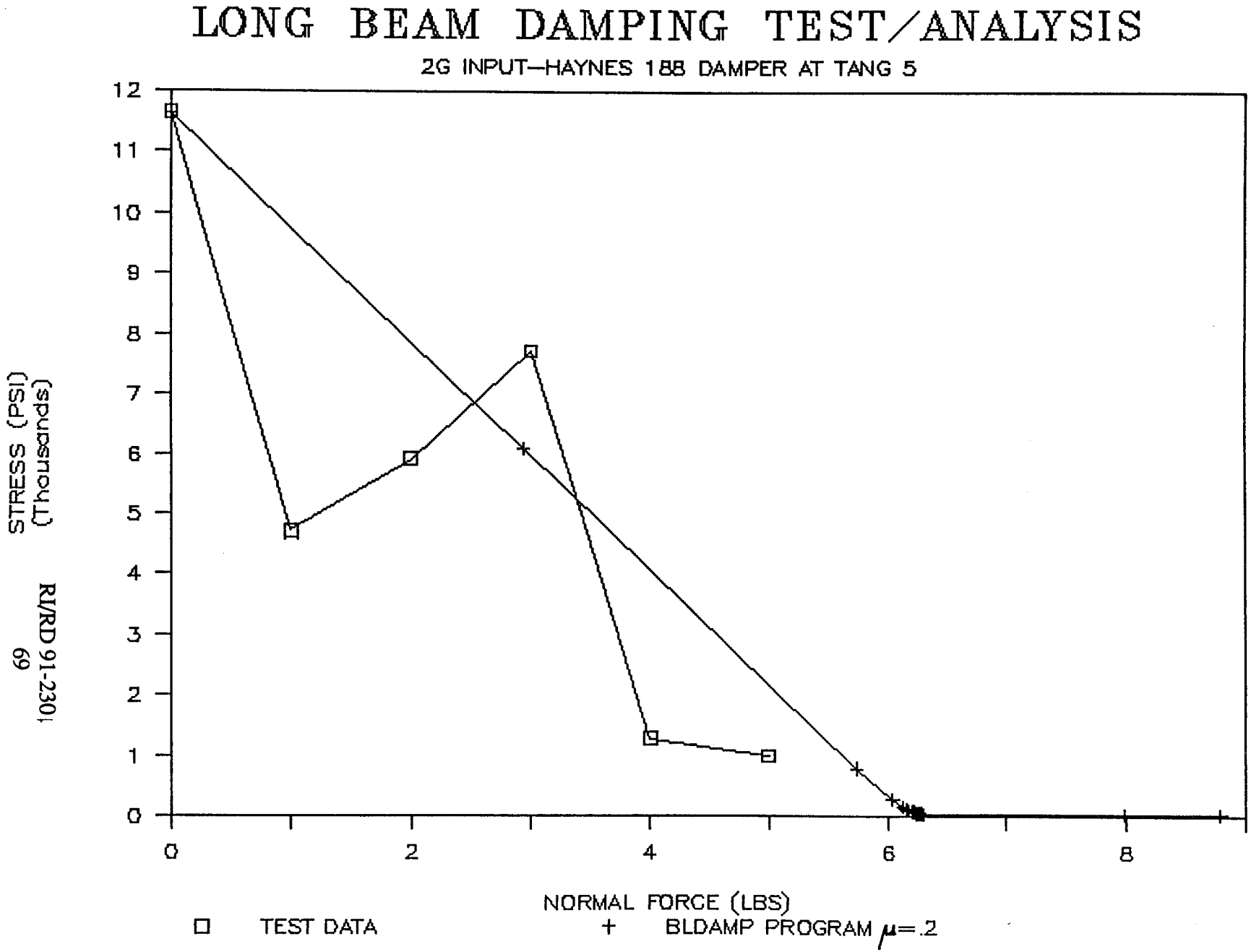

Figure 2.2-36 Low frequency beam optimum normal force curve for 2G input and Haynes 188 damper at tang 5

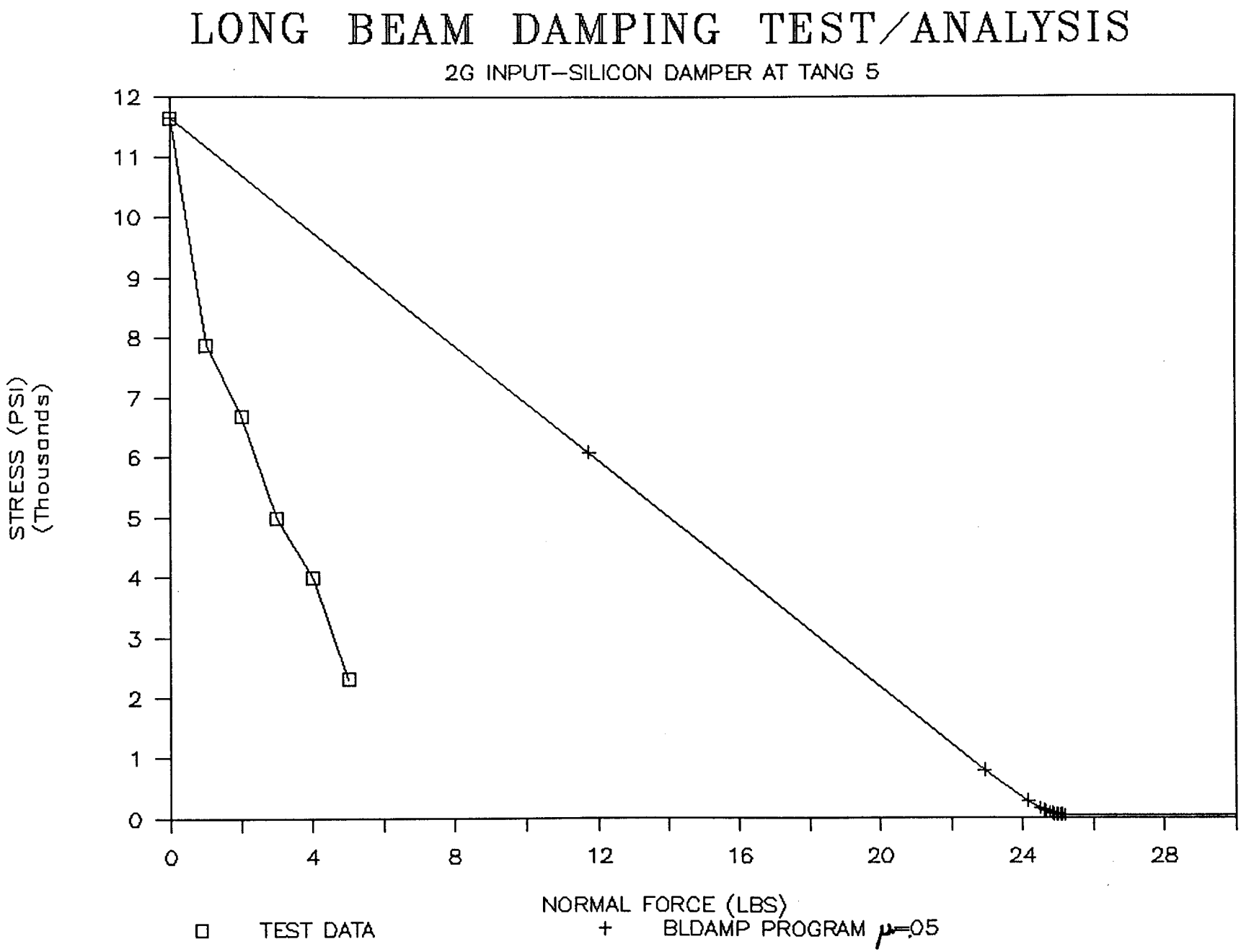

Figure 2.2-37 Low frequency beam optimum normal force curve

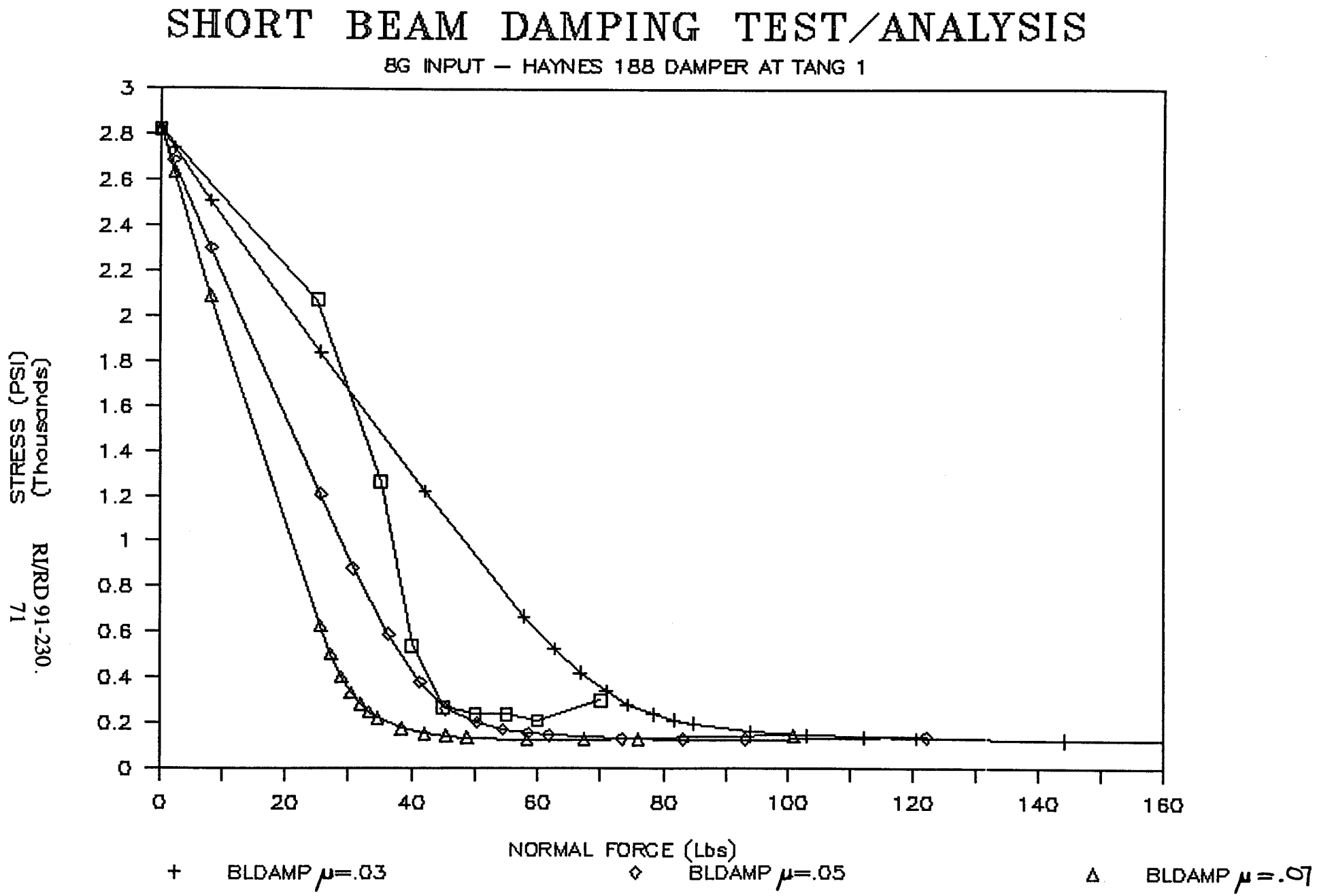

Figure 2.2-38 High frequency beam optimum normal force curve for 8G input and Haynes 188 damper at tang 1

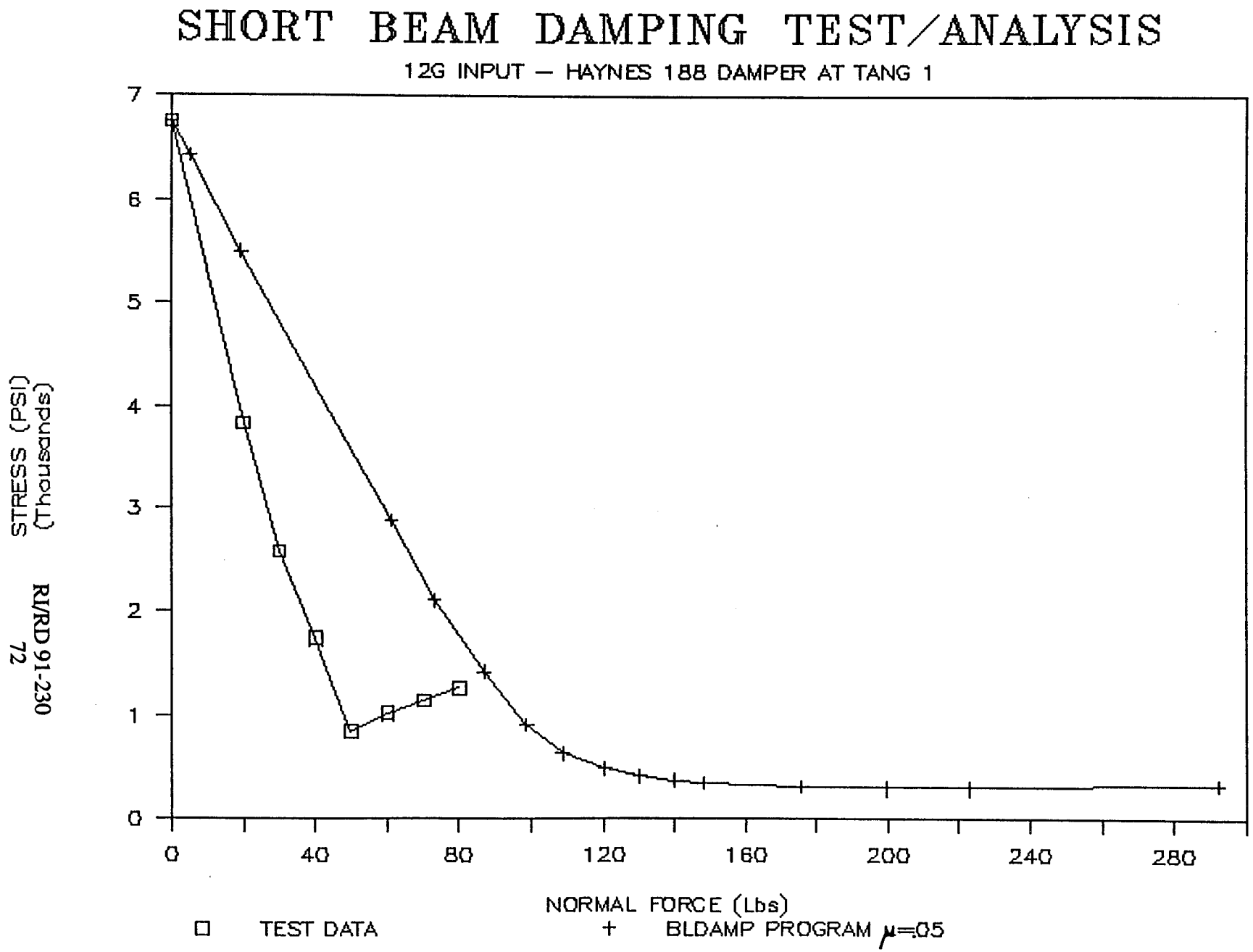

Figure 2.2-39 High frequency beam optimum normal force curve

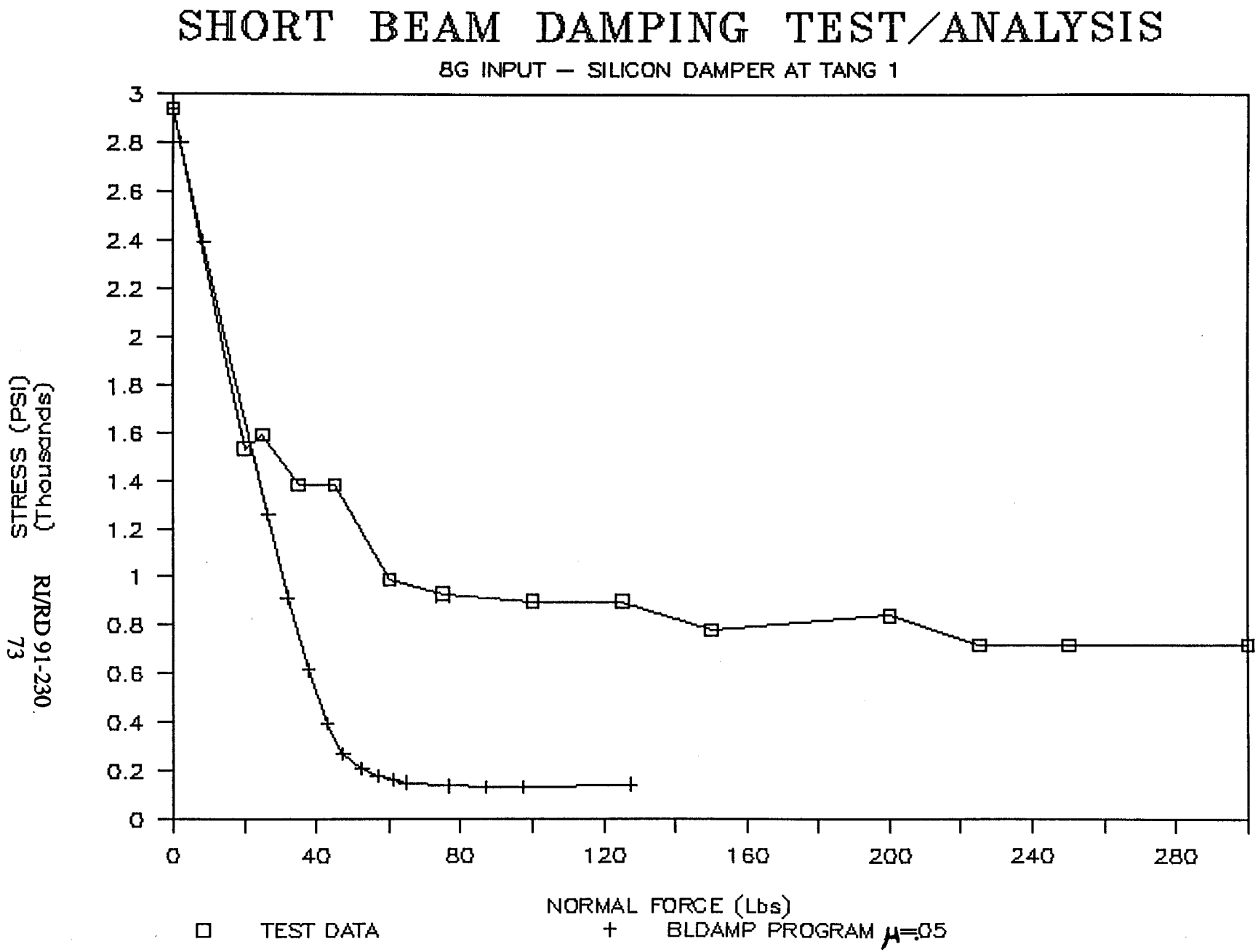

Figure 2.2-40 High frequency beam optimum normal force curve for 8G input and Silicon Nitride damper at tang 1

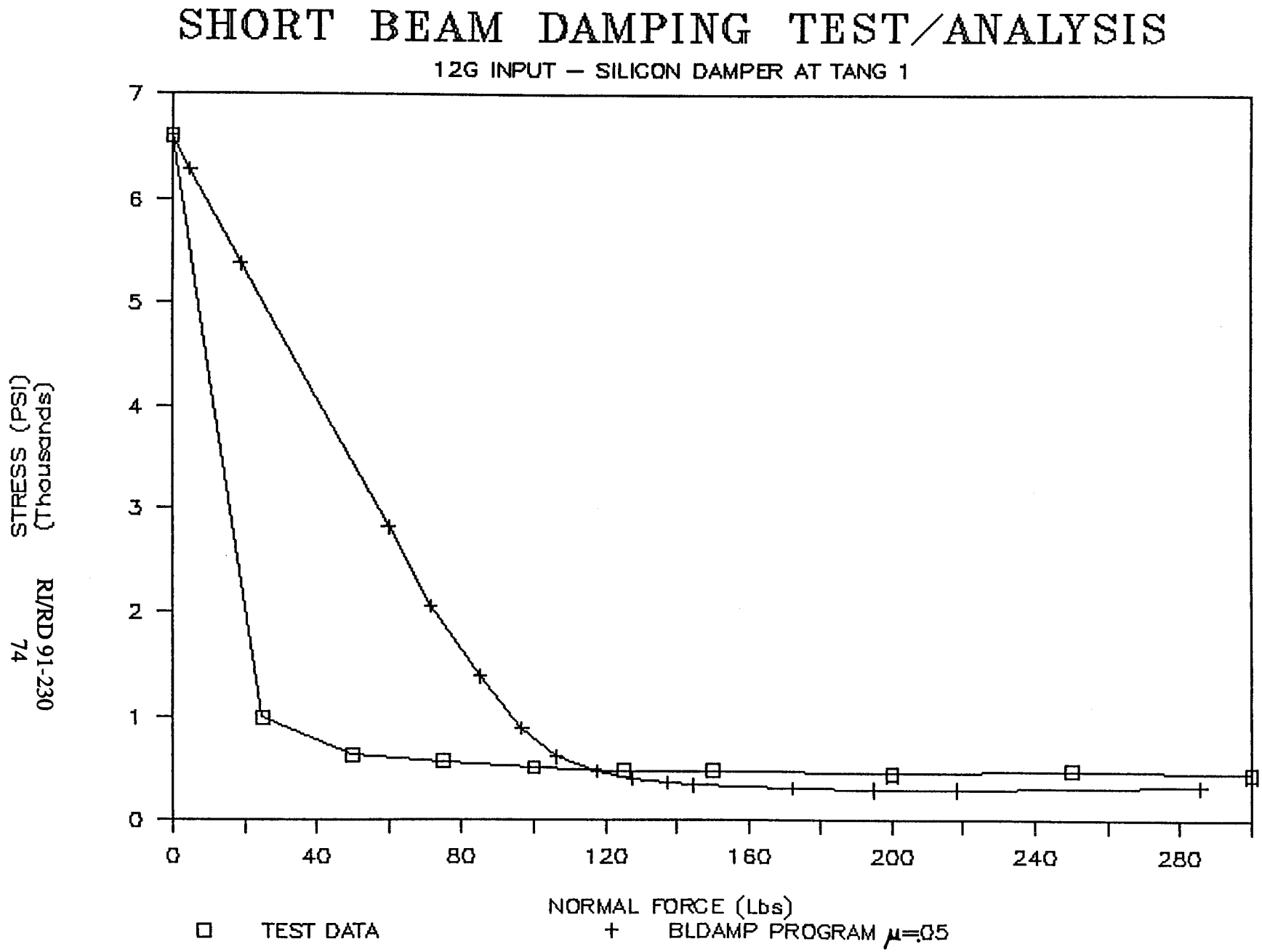

Figure 2.2-41 High frequency beam optimum normal force curve

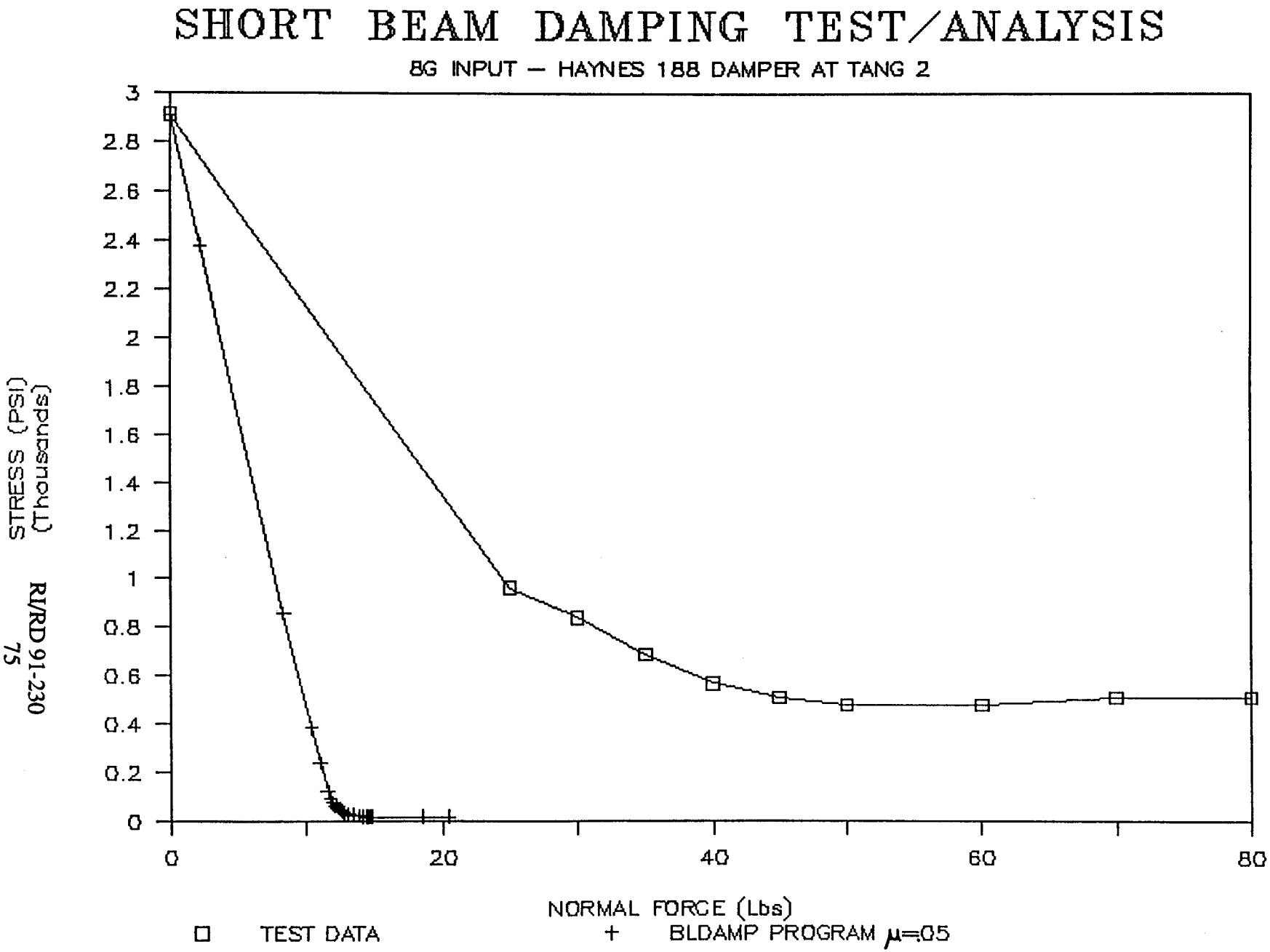

Figure 2.2-42 High frequency beam optimum normal force curve for 8G input and Haynes 188 damper at tang 2

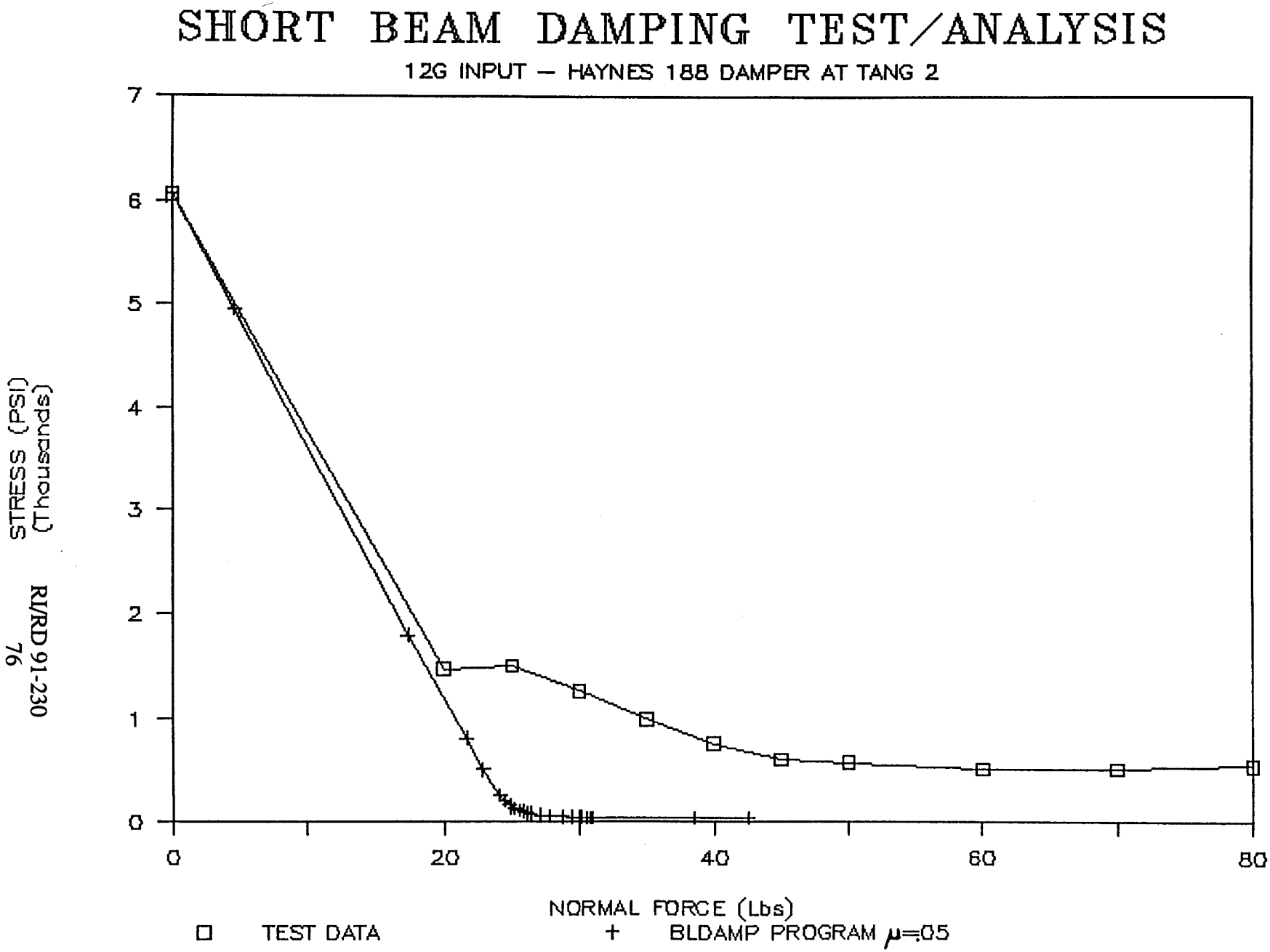

Figure 2.2-43 High frequency beam optimum normal force curve

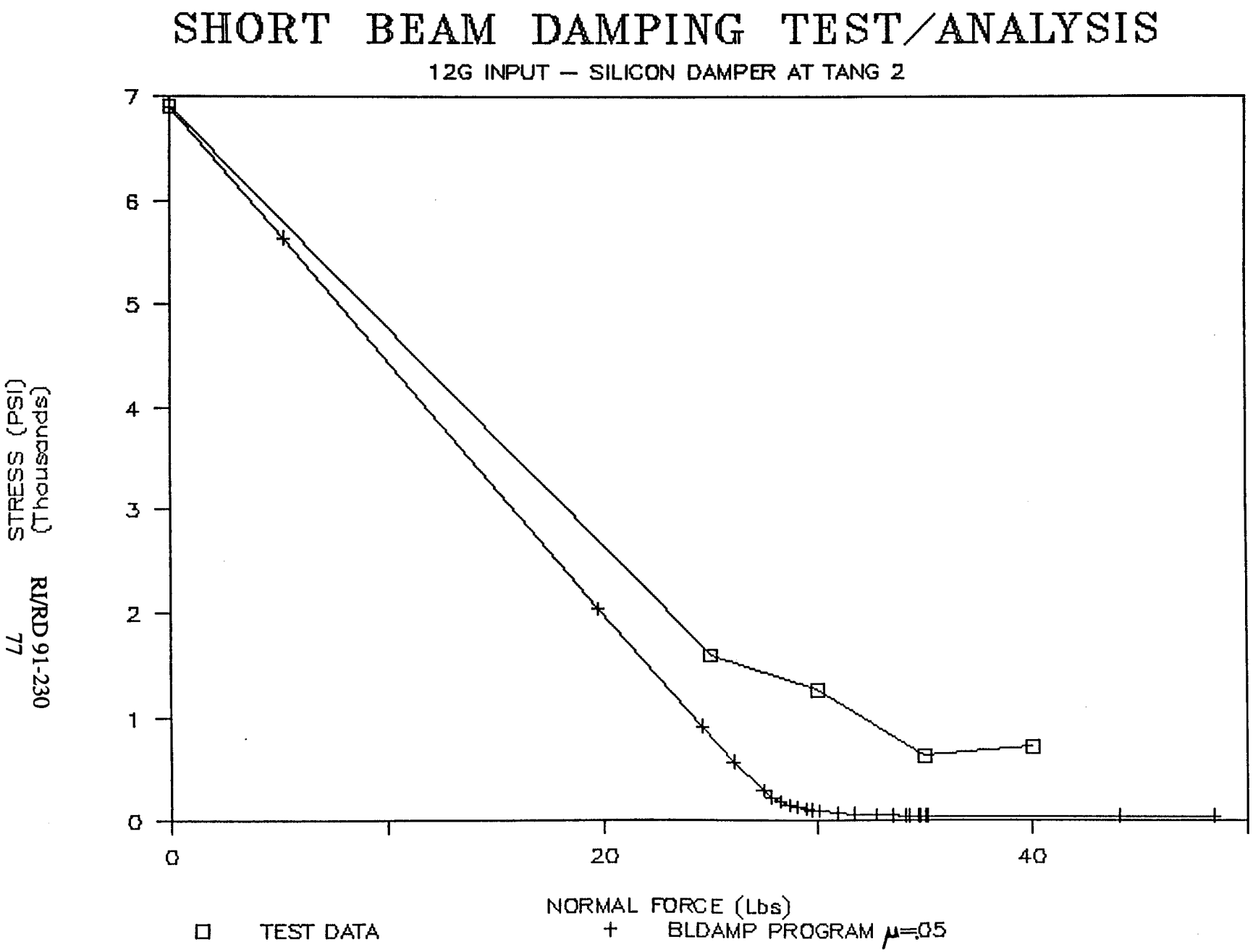

Figure 2.2-44 High frequency beam optimum normal force curve for 12G input and Silicon Nitride damper at tang 2

chatter and shaker control problems. As the damper transitioned from a locked state to a slipping state, a loud noise emanated from the damper area and the shaker could no longer be controlled. The damper would not remain centered in position and tended to drift off to one side. It was also found that the output signals from the strain gages and accelerometers were not sinusoidal during this period. The nonsinusoidal nature of the vibration is significant, because the BLDAMP program assumes sinusoidal excitation.

The surface finish on the test beams was originally machined smooth. However, after a short period of testing, rub marks were observed at the damper contact points. These rub marks were very similar to the marks observed on the HPOTP blade platforms after time in service. The contact surface for the Haynes 188 dampers, however, was worn in a much different manner than dampers that have been hot-fire tested on actual blades. The damper surface was extremely rough and pitted. A black powdery residue was observed on both the beam and damper after testing. The residue is believed to be coming from the damper, because most of the wear occurred there. The reason behind the abnormal wear patterns is most likely because of the dynamic response of the damper itself. As will be discussed later in this report, the damper was vibrating excessively during the period of time when the beam was passing through resonance. The silicon nitride damper contact surface did not show the wear that was present on the Haynes damper.

2.2.1.9 Problems. As can be seen from a comparison of the plots of Figures 2.2-23 and 2.2-25, the character of the vibration changed dramatically when friction dampers were installed. The plots of these figures represent RMS data and do not show the actual time histories of the signal. Although the time histories are not presented here, the intent was to keep the input to the shaker as sinusoidal as possible, during the entire sweep through the frequency range of interest. This proved quite difficult when friction dampers were installed, particularly in the high-frequency beam and also in the low-frequency beam at damper locations near the tip. During testing under these conditions, the beam response was not sinusoidal and feedback into the shaker table distorted the input, to a large degree. Since the analytical program BLDAMP assumes a constant magnitude sinusoidal input, it was impossible to correlate the analysis results to the tests, during which damper chatter occurred.

2.2.2 Follow-on Testing

2.2.2.1 Summary. Another test series was completed using the low-frequency beam, due to the problems encountered with the initial testing, as described in Section 2.2.1. Testing was performed at lower input levels, using a different shaker and control system, which helped prevent the nonsinusoidal oscillations observed with the previous setup. This testing did not alter the basic conclusions regarding friction dampers; but the quality of the test results was improved significantly. A large database was also acquired, which will aid in the development of future analytical methods of damper design. Furthermore, a set of design curves was generated, which will greatly aid in the selection of the correct damper design parameters for a given blade configuration.

2.2.2.2 Test Description. Testing was performed in an identical manner to that described in Section 2.2.1, with several exceptions. Most importantly, the input vibration levels were reduced from the previous testing. This was done because excess motion of the test beam at high vibration levels caused the damper to chatter. This behavior is probably not indicative of actual turbine damper behavior, because turbine damper blade motion is an order of magnitude smaller than what was used on the beam during the initial testing. Also, very large centrifugal forces, on the order of 150,000 Gs, are present in

typical turbines. These forces, which are impossible to duplicate in a nonrotating test setup, should keep the damper from chattering by holding it tightly against the blade surface. The second improvement to the test was the use of a LTV Model 275A vibration shaker, which was rated at 10,000 lb force. This shaker was coupled with an Unholtz Dickie SP-7 control system, which helped to reduce feedback and kept the shaker motion as sinusoidal as possible.

Data was obtained by first placing the damper at one of seven locations on the test beam and then slowly sweeping through the resonant point. Two series of tests were performed on the beam for each of the seven damper locations; one at a shaker input level of 0.5G peak and another at a level of 1.0G peak. The normal force on the damper was changed, after each test run, to obtain curves of response, as a function of normal force. Testing proceeded with both input levels and two damper types, until data were obtained at all seven damper locations. Over 100 test runs were completed during the course of the testing.

2.2.2.3 Test Results. Curves of peak beam response at the resonant point, as a function of damper normal load, are presented in Figures 2.2-45 through 2.2-72 for the Haynes 188 damper and in Figures 2.2-73 through 2.2-100 for the silicon nitride damper. Each of the curves shows the characteristic damper behavior. This behavior consists of an initial drop in beam motion, until an optimum normal load is reached; at which point the response flattens. Further increases in normal load fail to reduce the beam response and, in some cases, may even increase the response slightly.

Friction damping was shown to be extremely effective in reducing vibratory response, as was observed in the previous testing on this beam. Figures 2.2-101 through 2.2-106 summarize damper effectiveness, as a function of location on the beam. These data show that reductions of over 95 percent can be achieved with proper placement. These curves have been completely nondimensionalized, thereby providing a valuable design tool for determining the best position for a damper. These plots show the damper should be located at a blade span of at least 30 percent to be most effective. The results shown in these figures are also consistent with previous work; in that the damper performs better as it is moved toward the beam tip. Vibratory motion is larger toward the tip. Therefore, more energy dissipation will occur with the damper at that location. However, the curves are relatively flat, once the 30-40 percent span position is reached, which was an unexpected result from testing. This is an indication that a damper placed at 40 percent span is nearly as good as a tip damper. Tip dampers have been shown in spin testing to perform extremely well (see Reference 1).

The normal force required to attain minimum response is presented in Figure 2.2-107 for the first mode of the beam. This curve indicates that a lower value of force is needed, as the damper is moved closer to the tip. Values plotted in this figure have also been nondimensionalized, which will aid future designers in the selection of the optimum normal force for their application. Proper use of this curve involves specification of the turbine blade generalized force, which, in turn, requires knowledge of the flow field forcing function and the blade mode shape. Blade mode shapes different from those of a cantilever beam will invalidate the results. Nevertheless, the curve of Figure 2.2-107 yields a starting point for selection of the optimum damper weight. Also worth noting is the close overlay of the Haynes 188 and silicon nitride damper curves. This indicates the two damper materials have roughly the same friction coefficient. Friction coefficients of materials different from Haynes 188 or silicon nitride will result in different curves. However, most materials used for dampers will probably have about the same friction coefficient, indicating that the curves will still be useful.

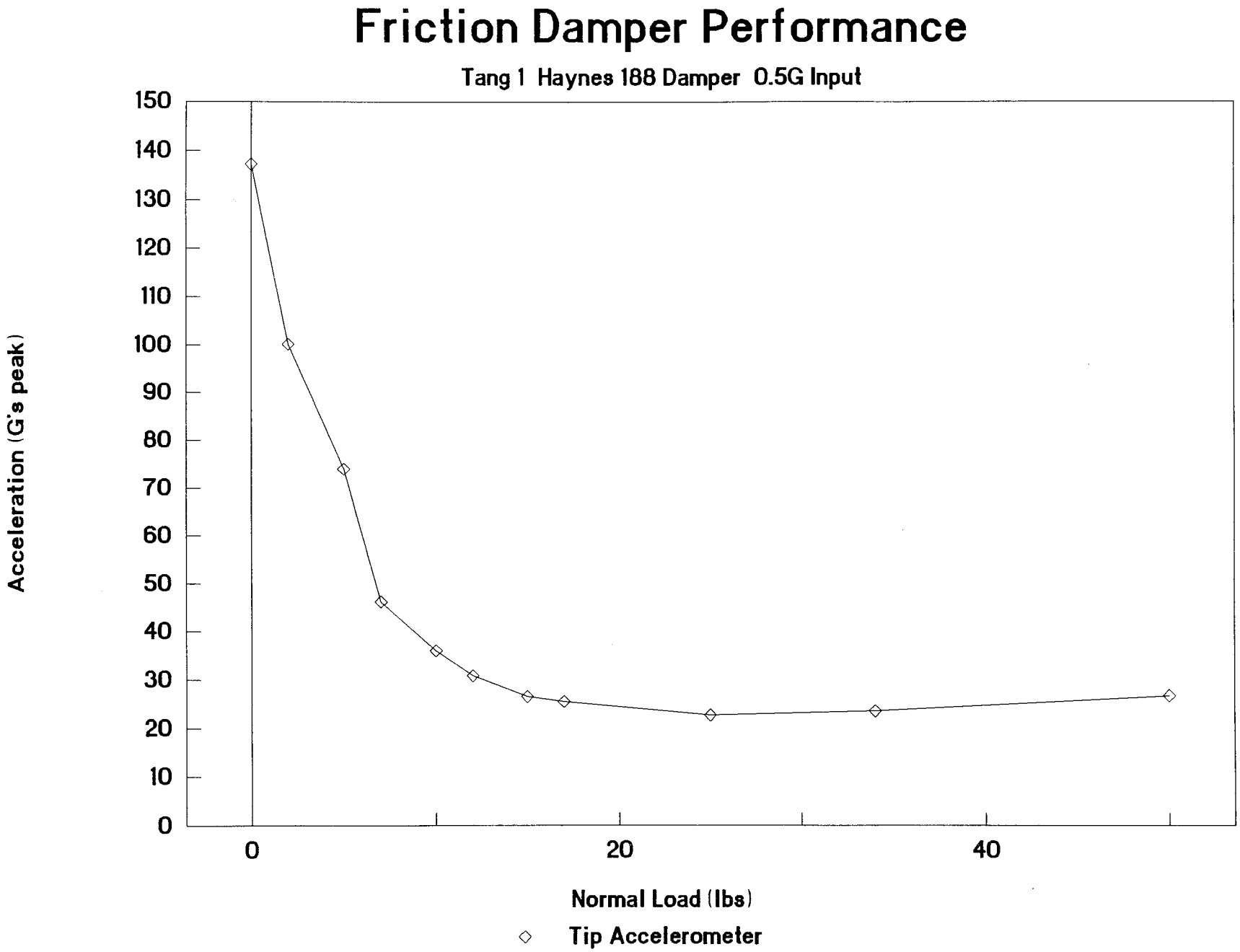

Figure 2.2-45 Low frequency beam optimization curve based on test data Haynes 188 damper at tang 1, 0.5G input

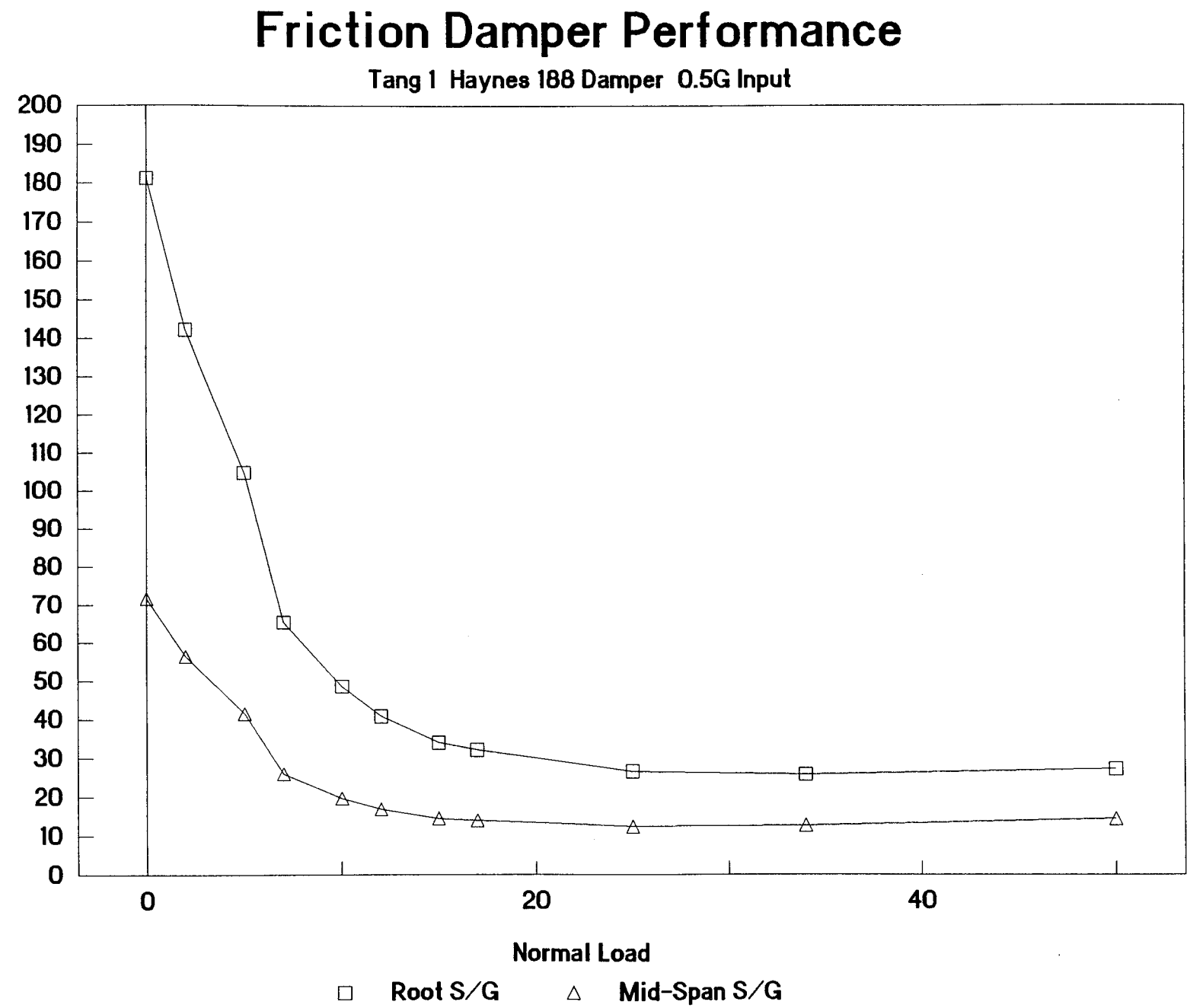

Figure 2.2-46 Low frequency beam optimization curve based on test data Haynes 188 damper at tang 1, 0.5G input

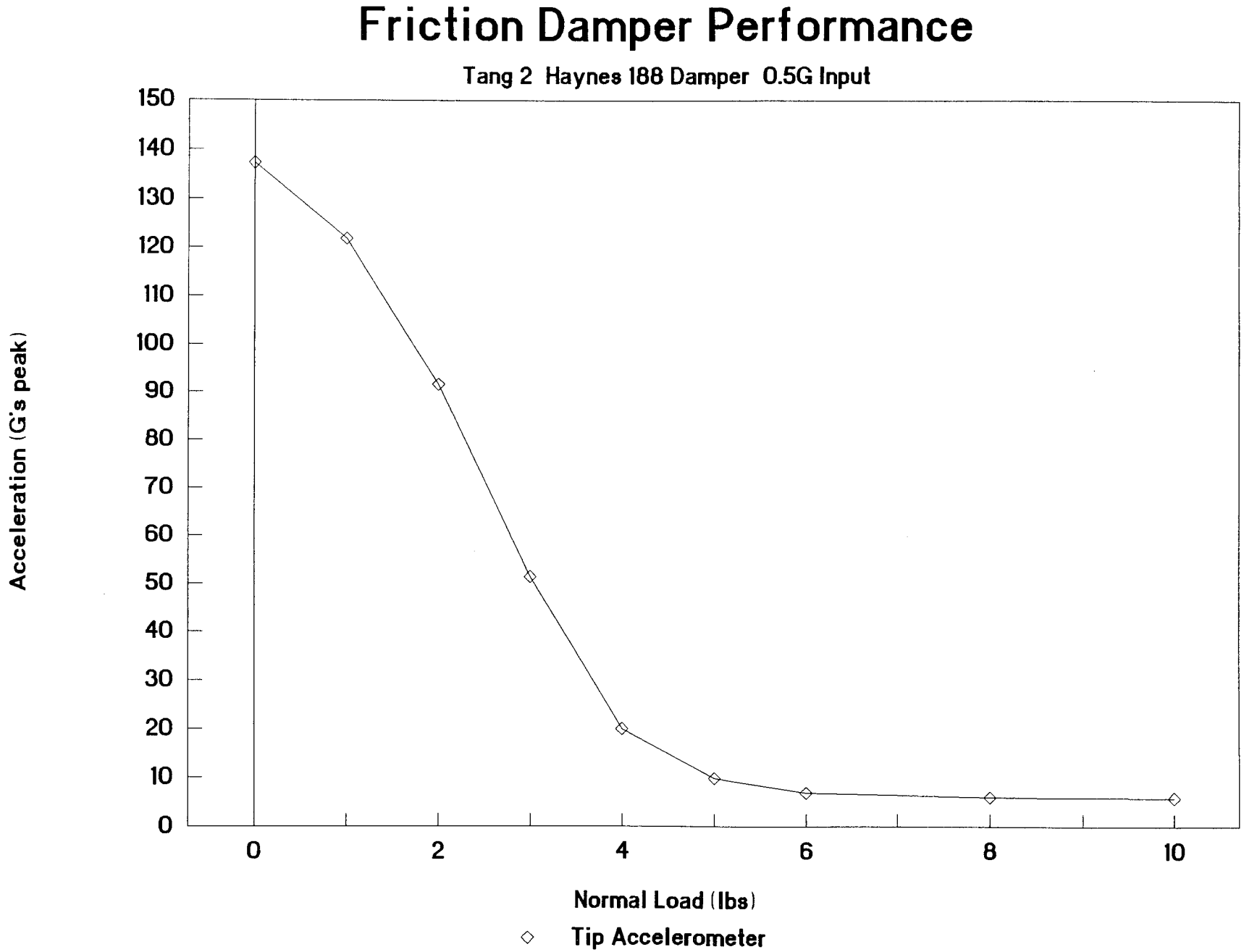

Figure 2.2-47 Low frequency beam optimization curve based on test data

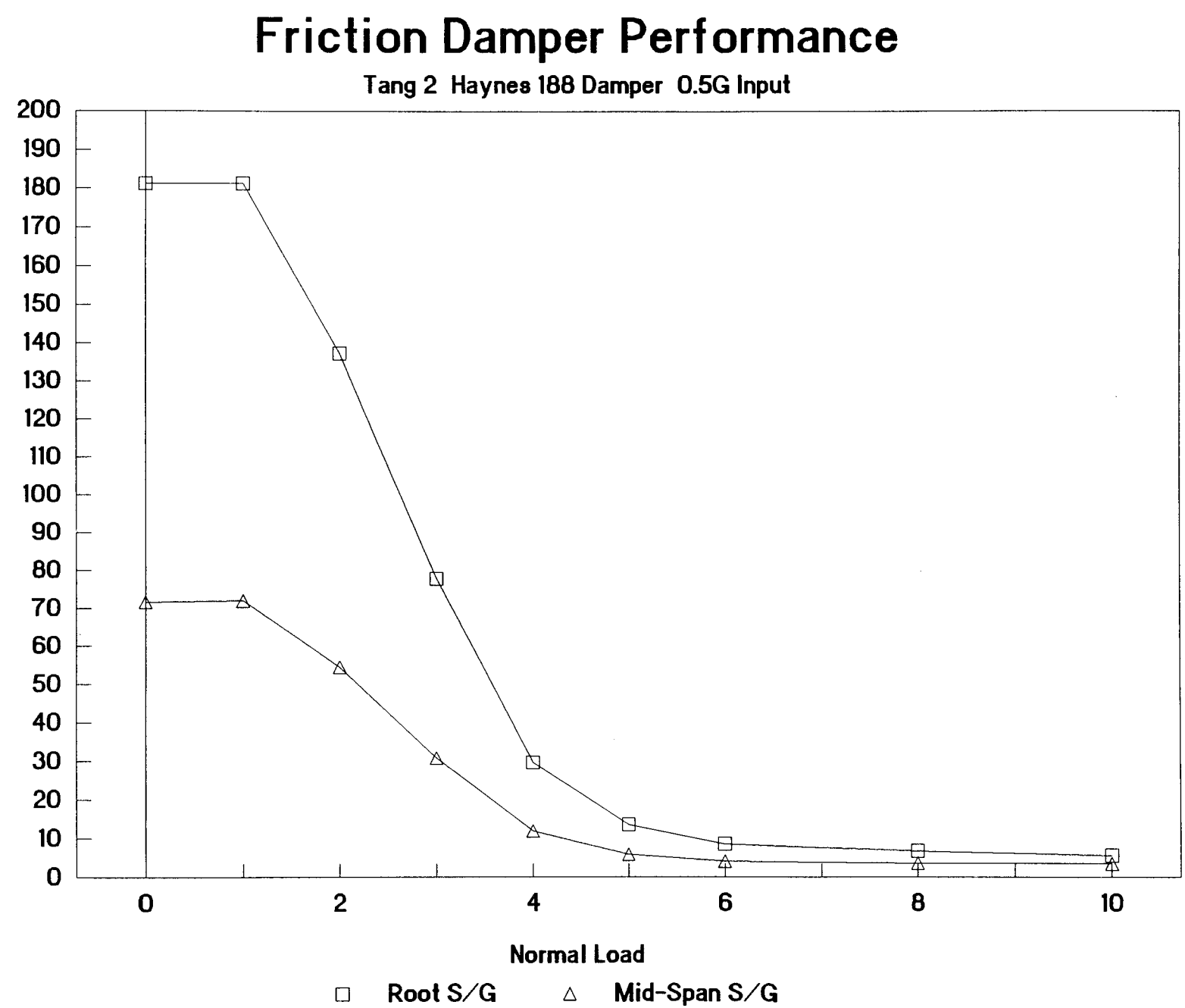

Figure 2.2-48 Low frequency beam optimization curve based on test data Haynes 188 damper at tang 2, 0.5G input

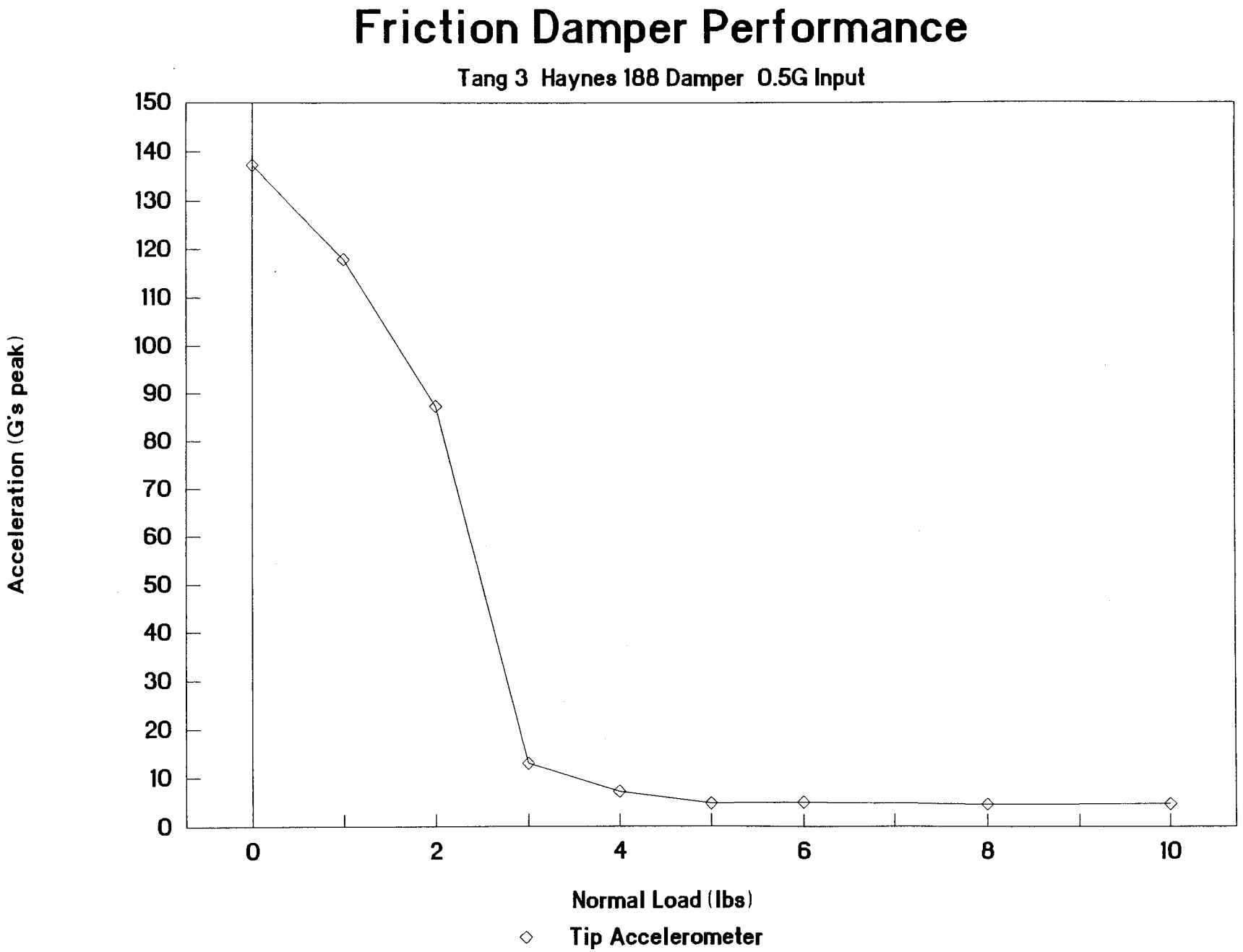

Figure 2.2-49 Low frequency beam optimization curve based on test data

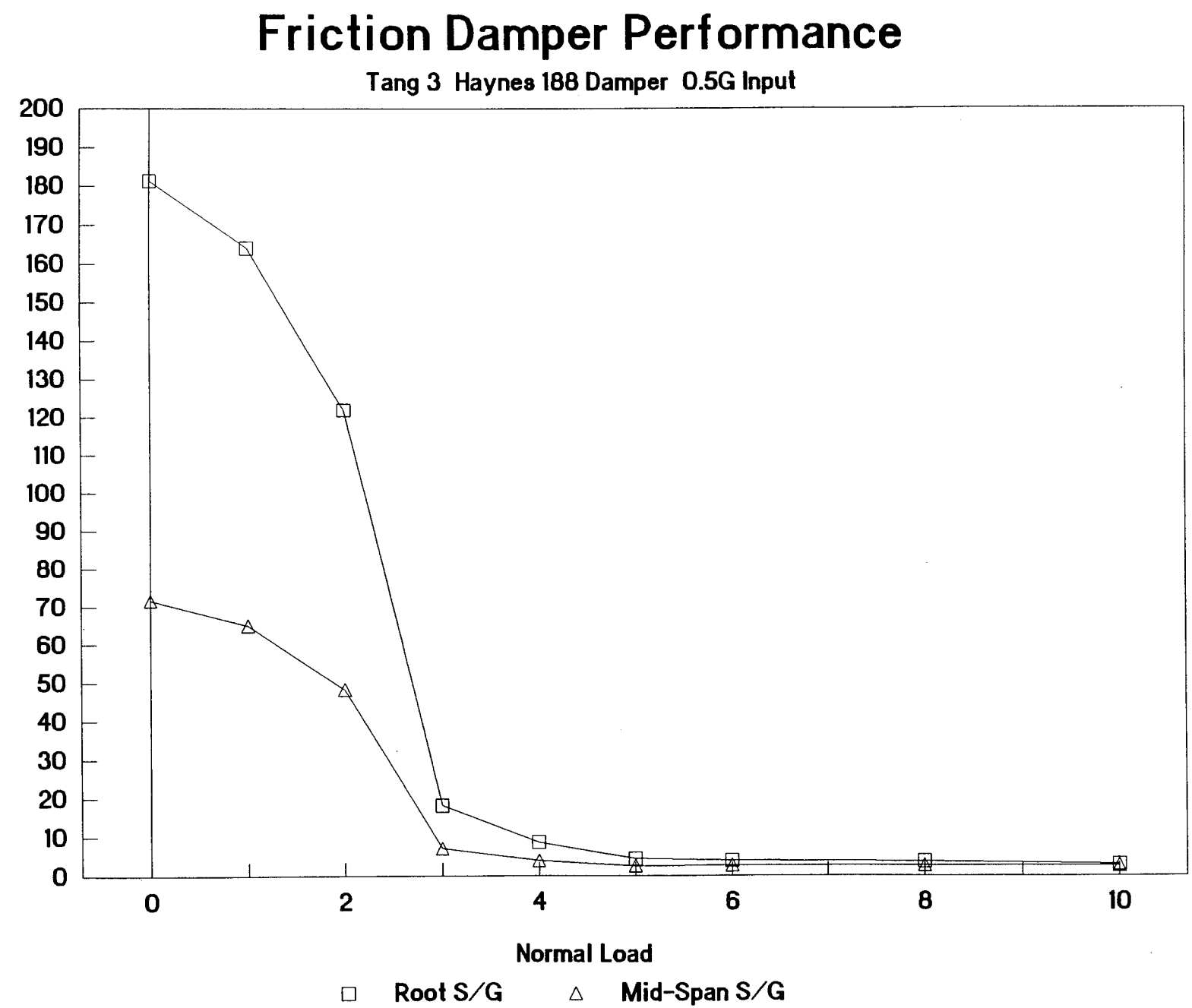

Figure 2.2-50 Low frequency beam optimization curve based on test data Haynes 188 damper at tang 3, 0.5G input

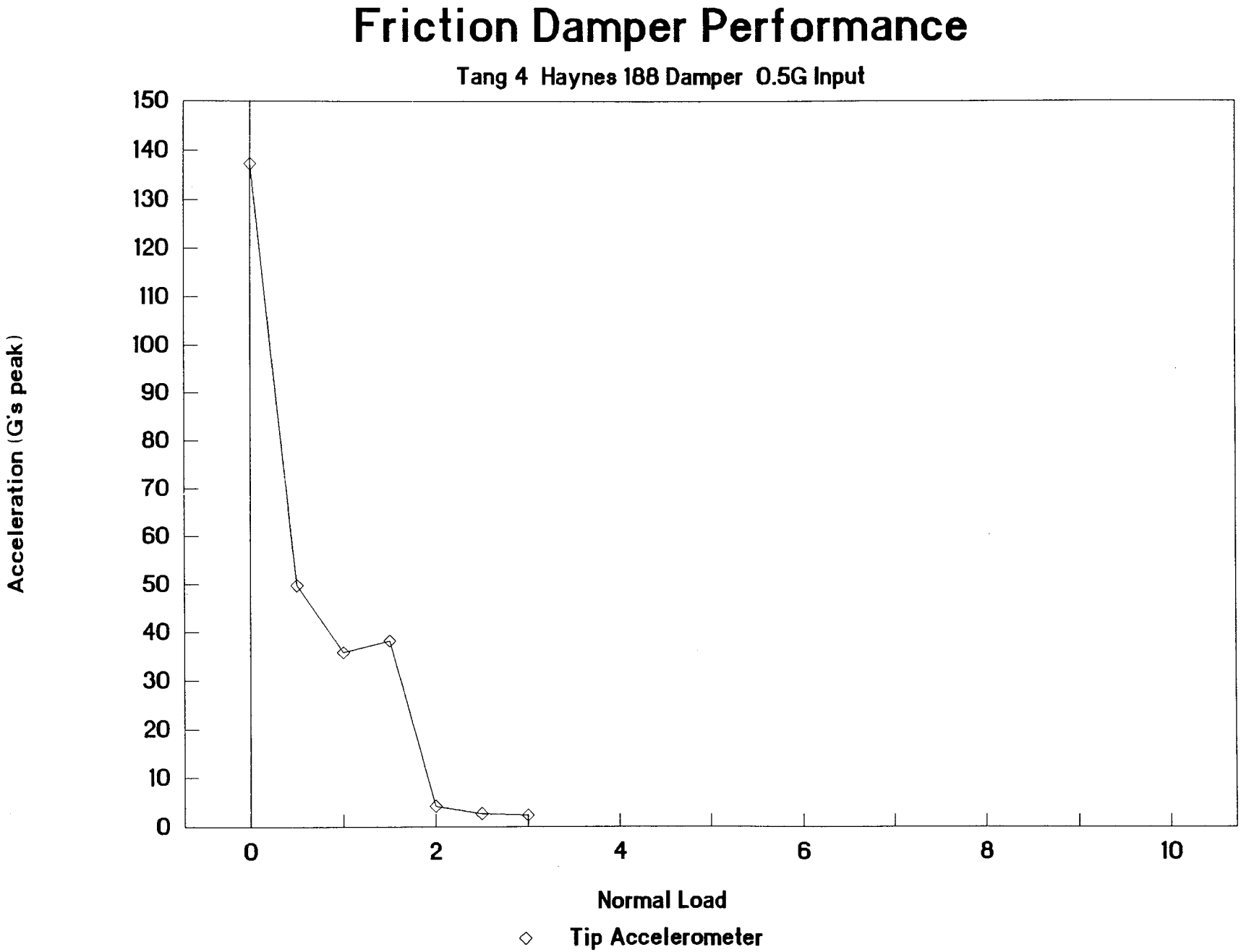

Figure 2.2-51 Low frequency beam optimization curve based on test data

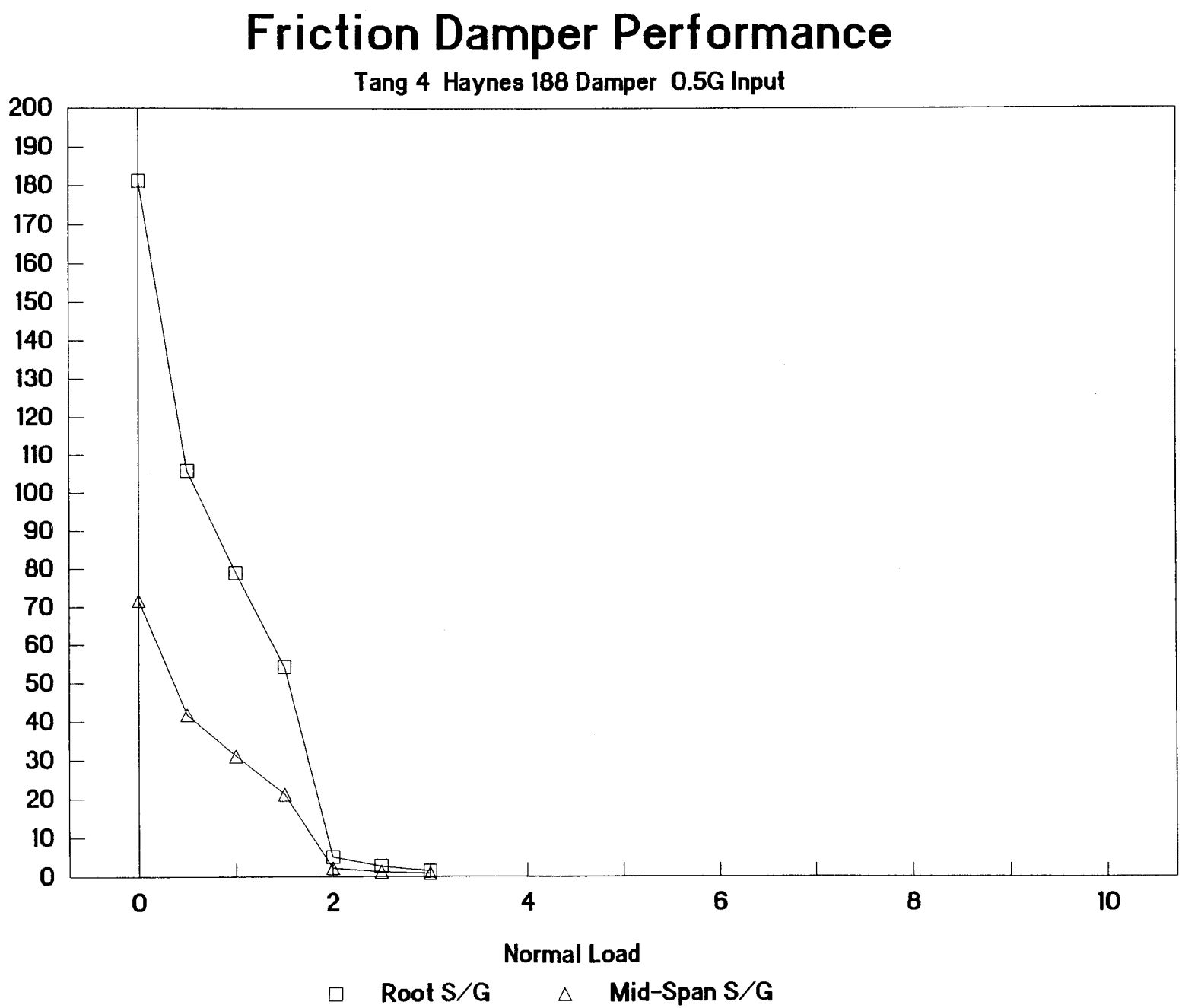

RI/RD 91-230
87

Figure 2.2-52 Low frequency beam optimization curve based on test data Haynes 188 damper at tang 4, 0.5G input

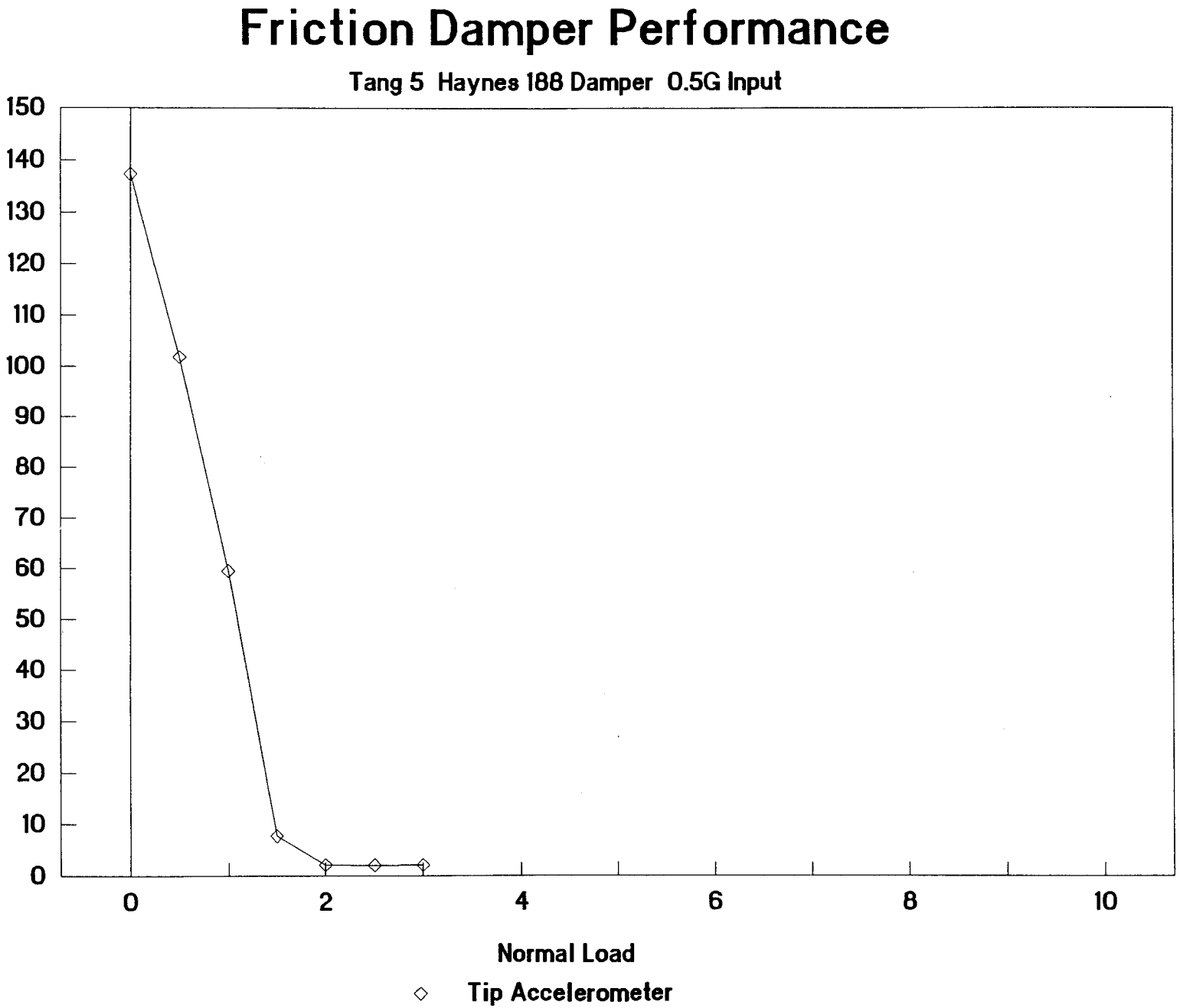

RI/RD 91-230

88

Figure 2.2-53 Low frequency beam optimization curve based on test data.

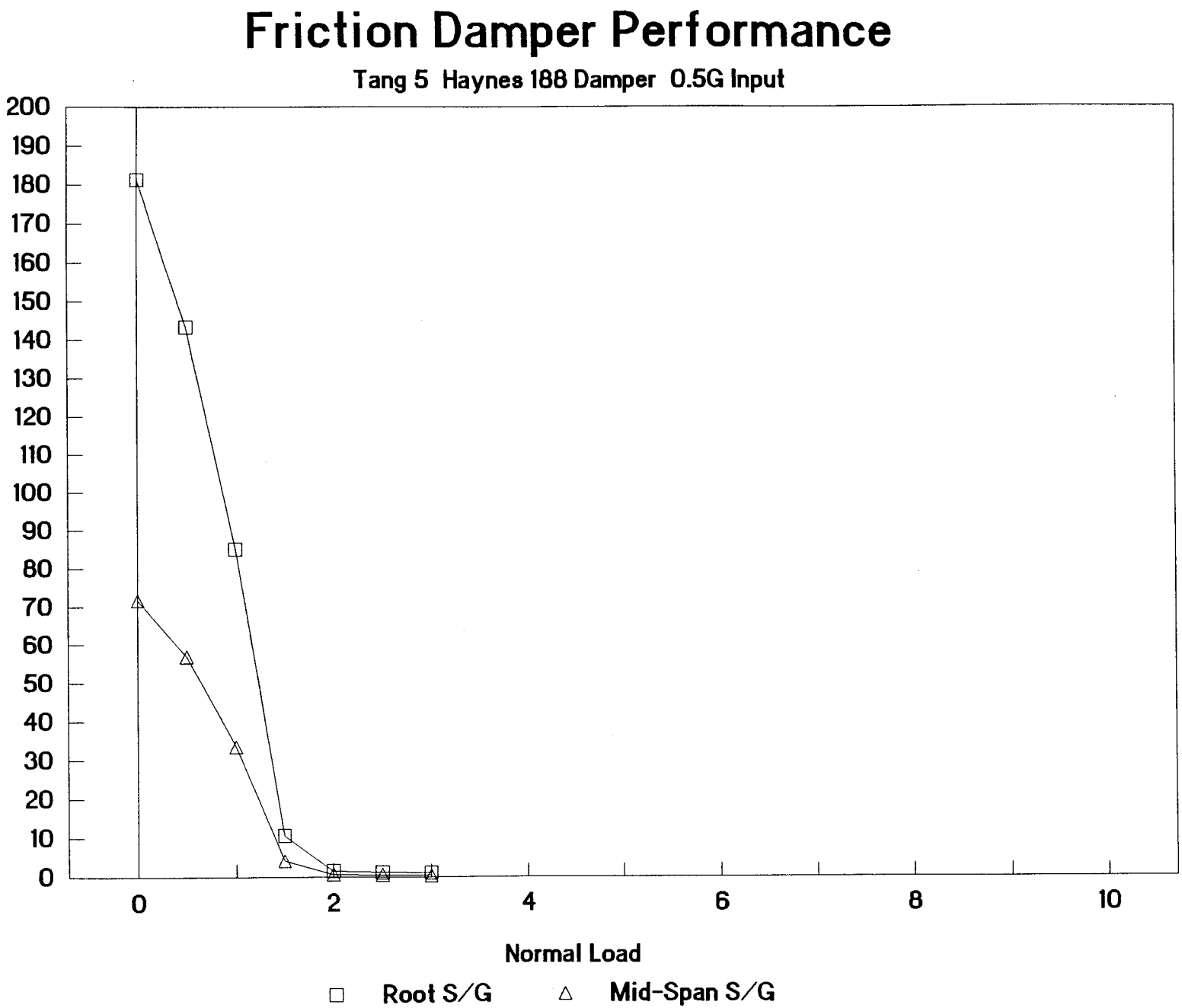

Figure 2.2-54 Low frequency beam optimization curve based on test data Haynes 188 damper at tang 5, 0.5G input

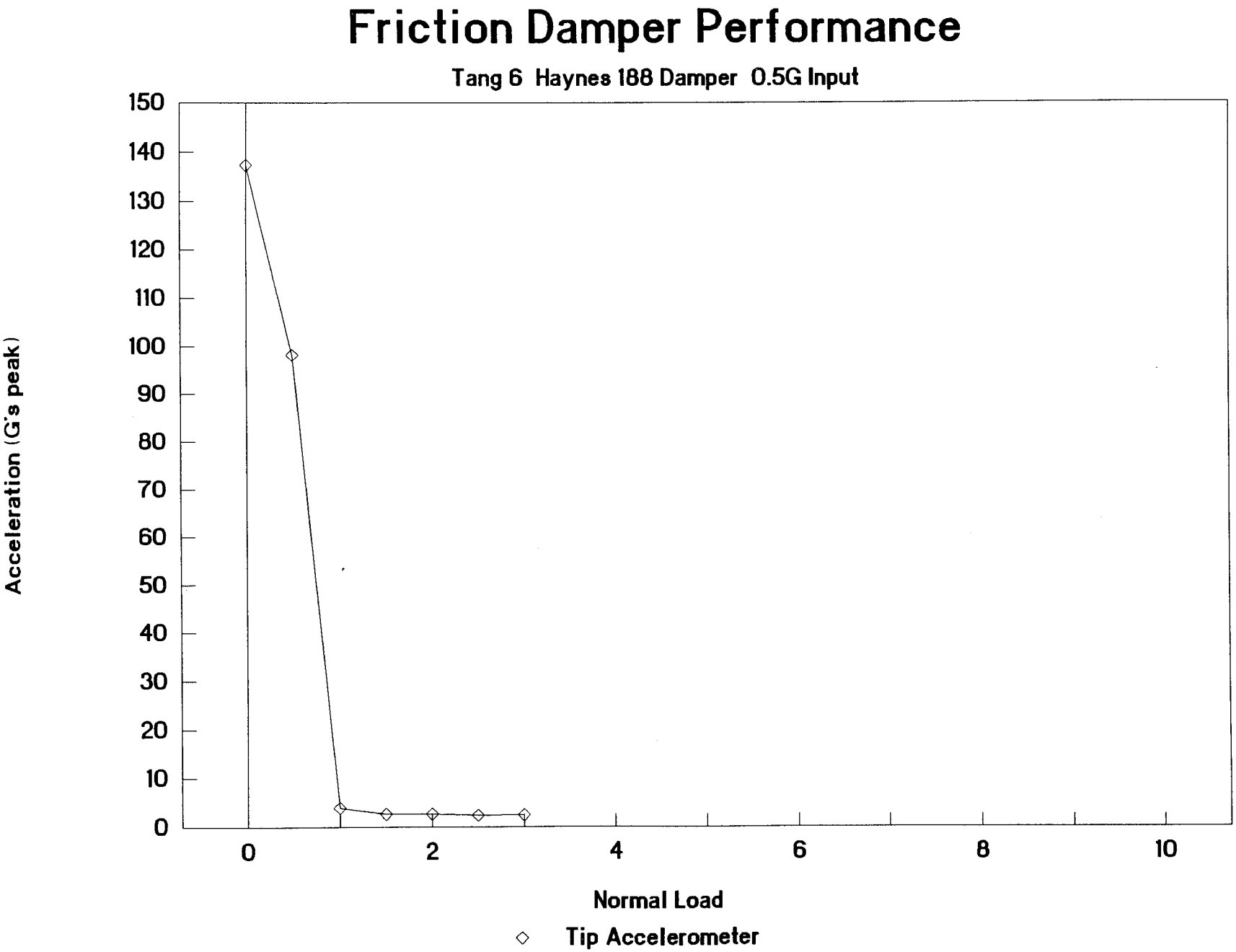

Figure 2.2-55 Low frequency beam optimization curve based on test data

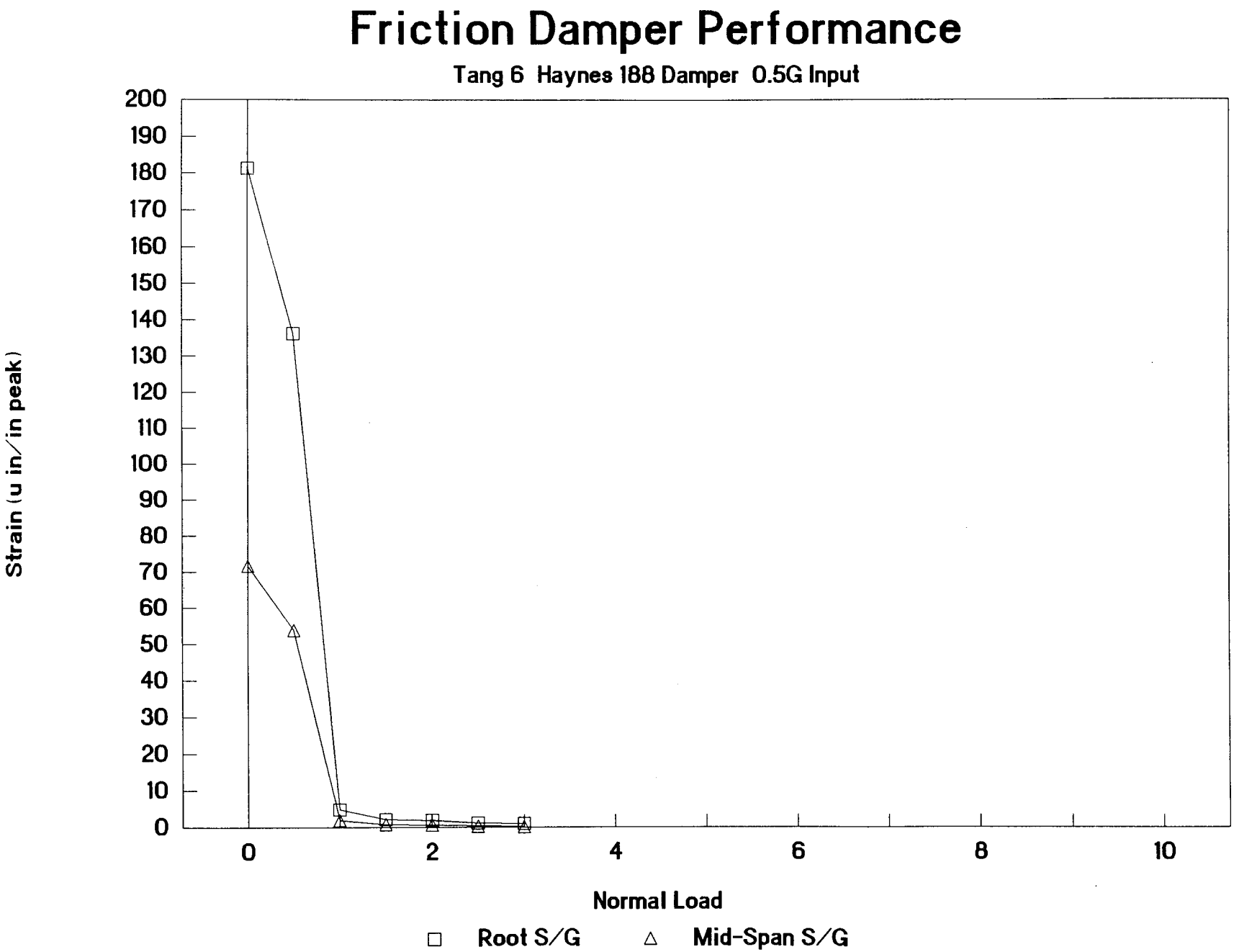

Figure 2.2-56 Low frequency beam optimization curve based on test data Haynes 188 damper at tang 6, 0.5G input

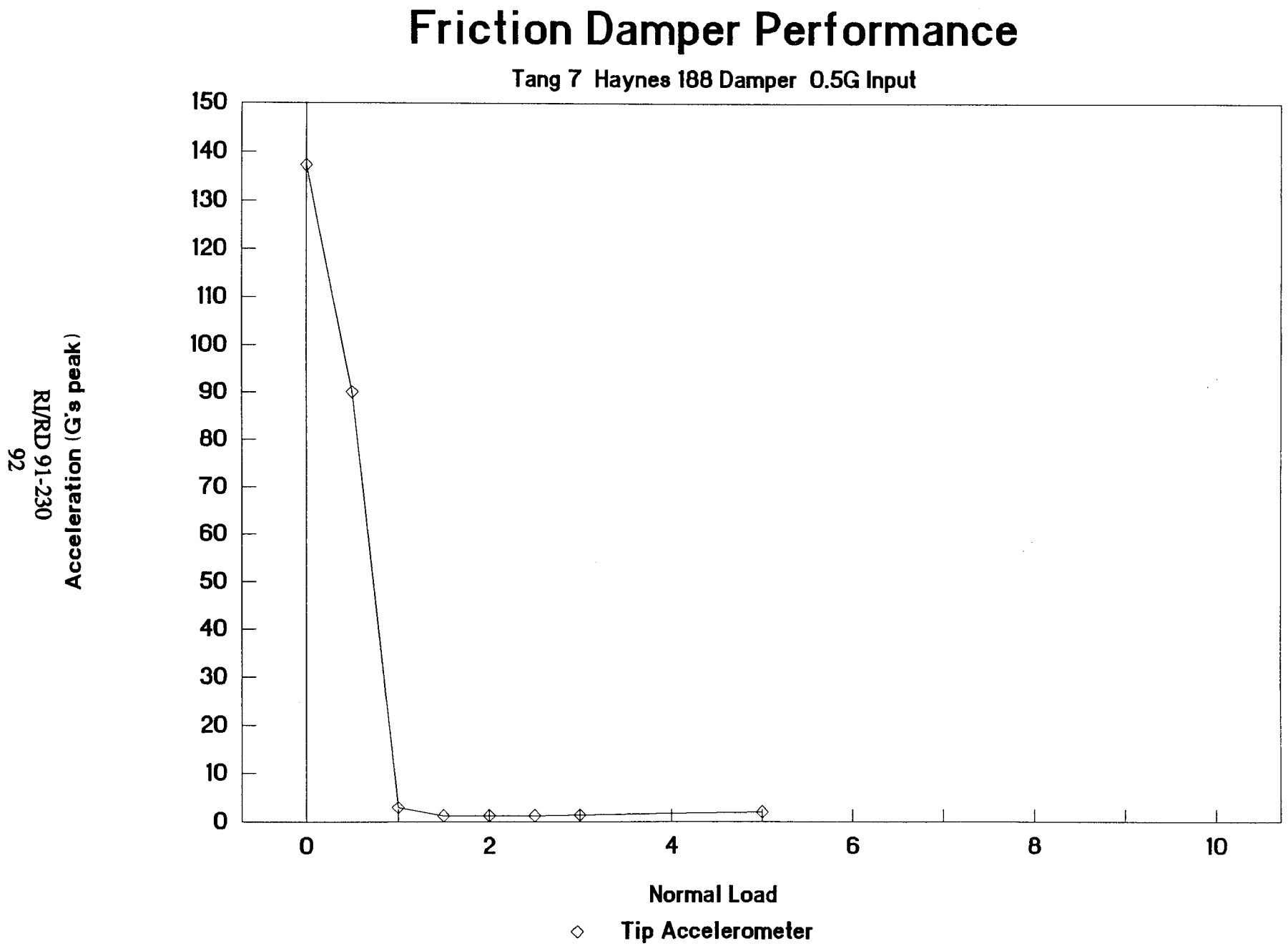

Figure 2.2-57 Low frequency beam optimization curve based on test data Haynes 188 damper at tang 7, 0.5G input

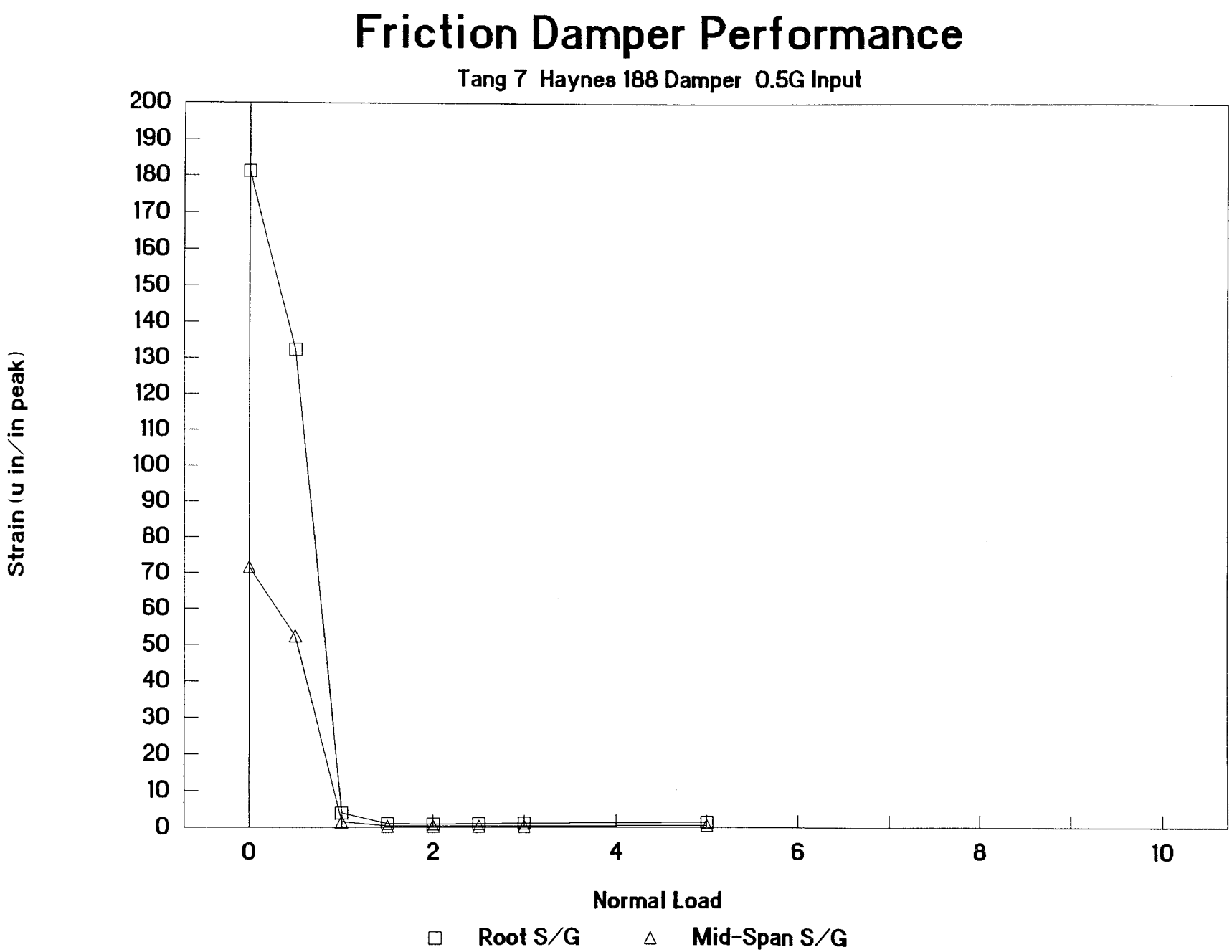

Figure 2.2-58 Low frequency beam optimization curve based on test data Haynes 188 damper at tang 7, 0.5G input

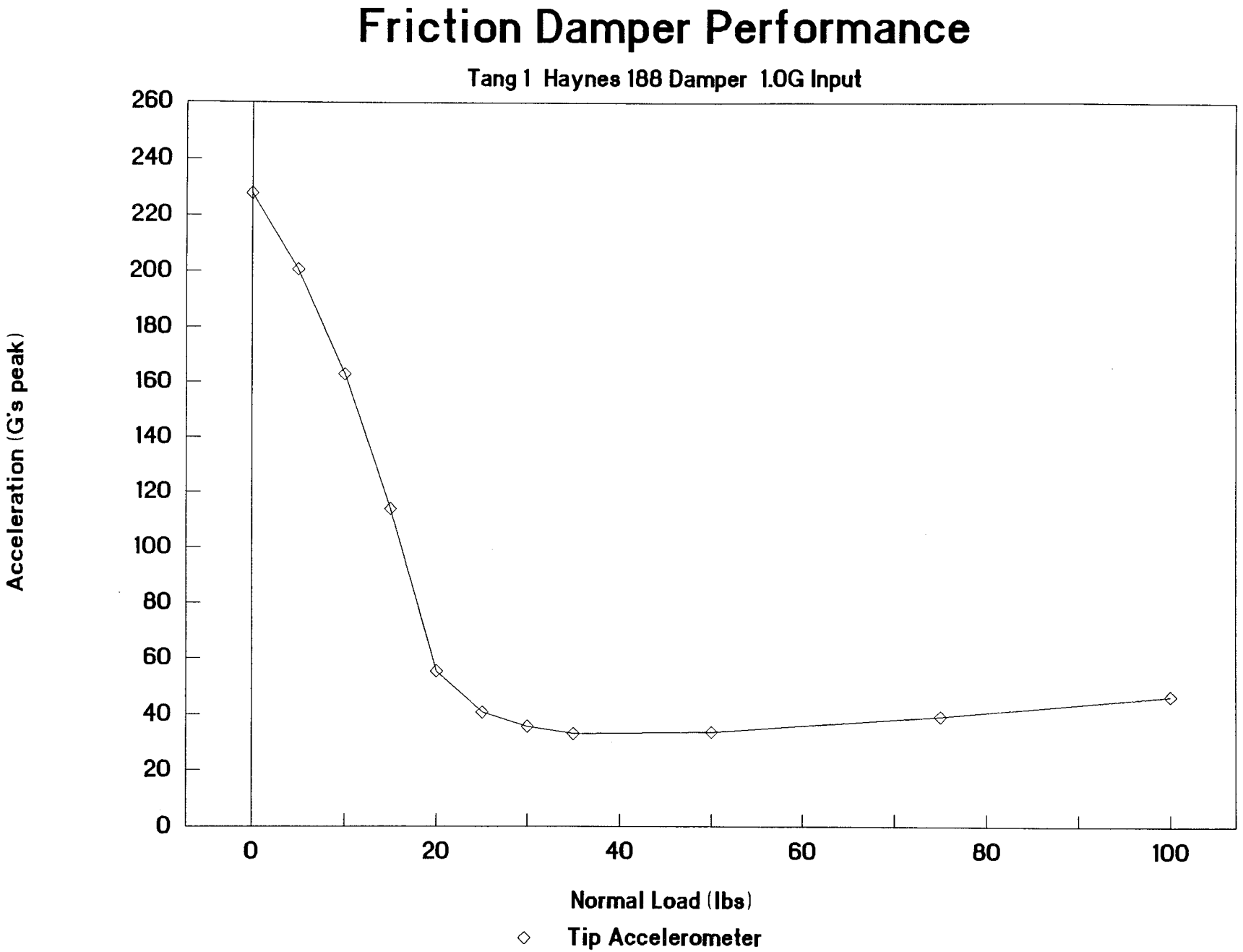

Figure 2.2-59 Low frequency beam optimization curve based on test data

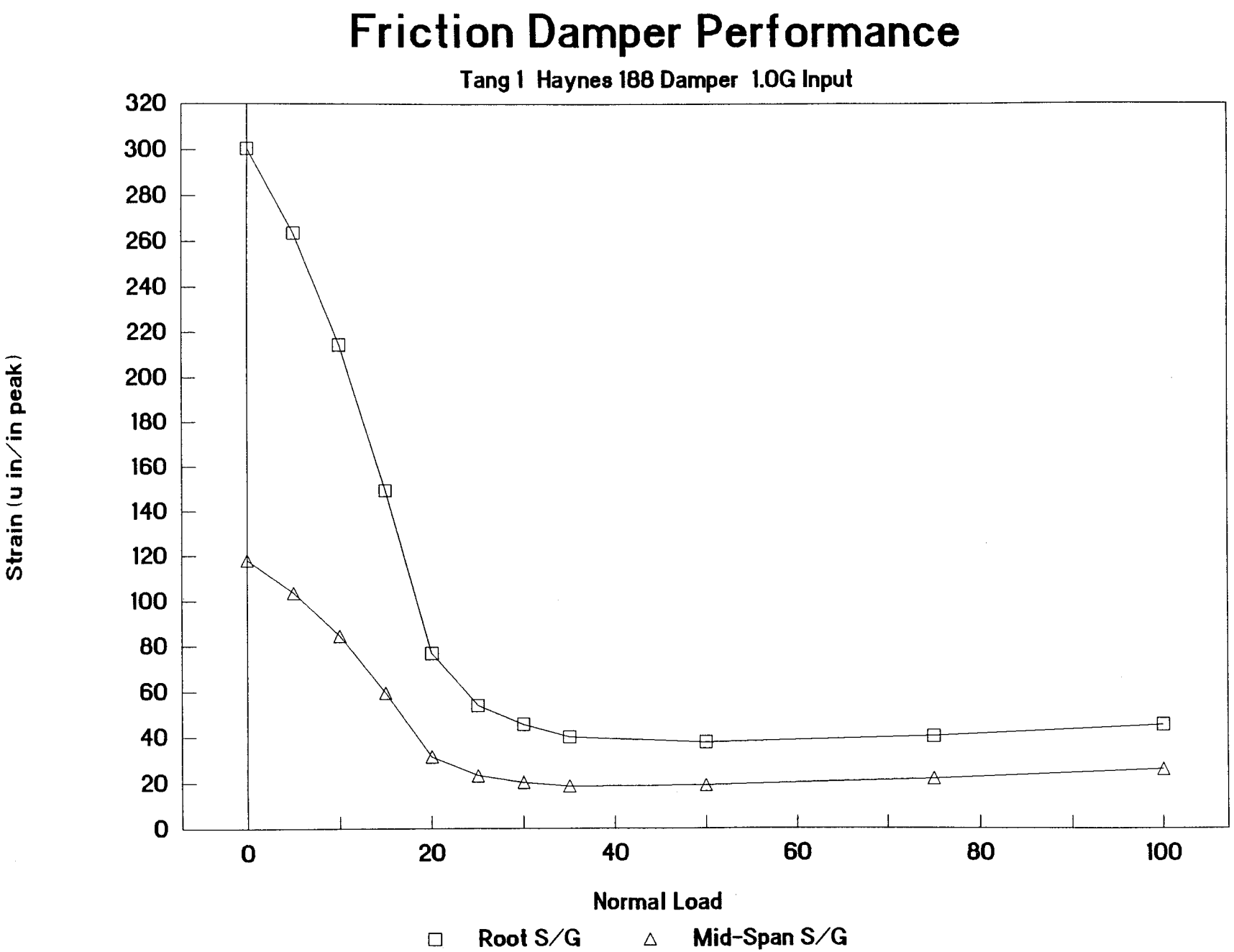

Figure 2.2-60 Low frequency beam optimization curve based on test data Haynes 188 damper at tang 1, 1.0G input

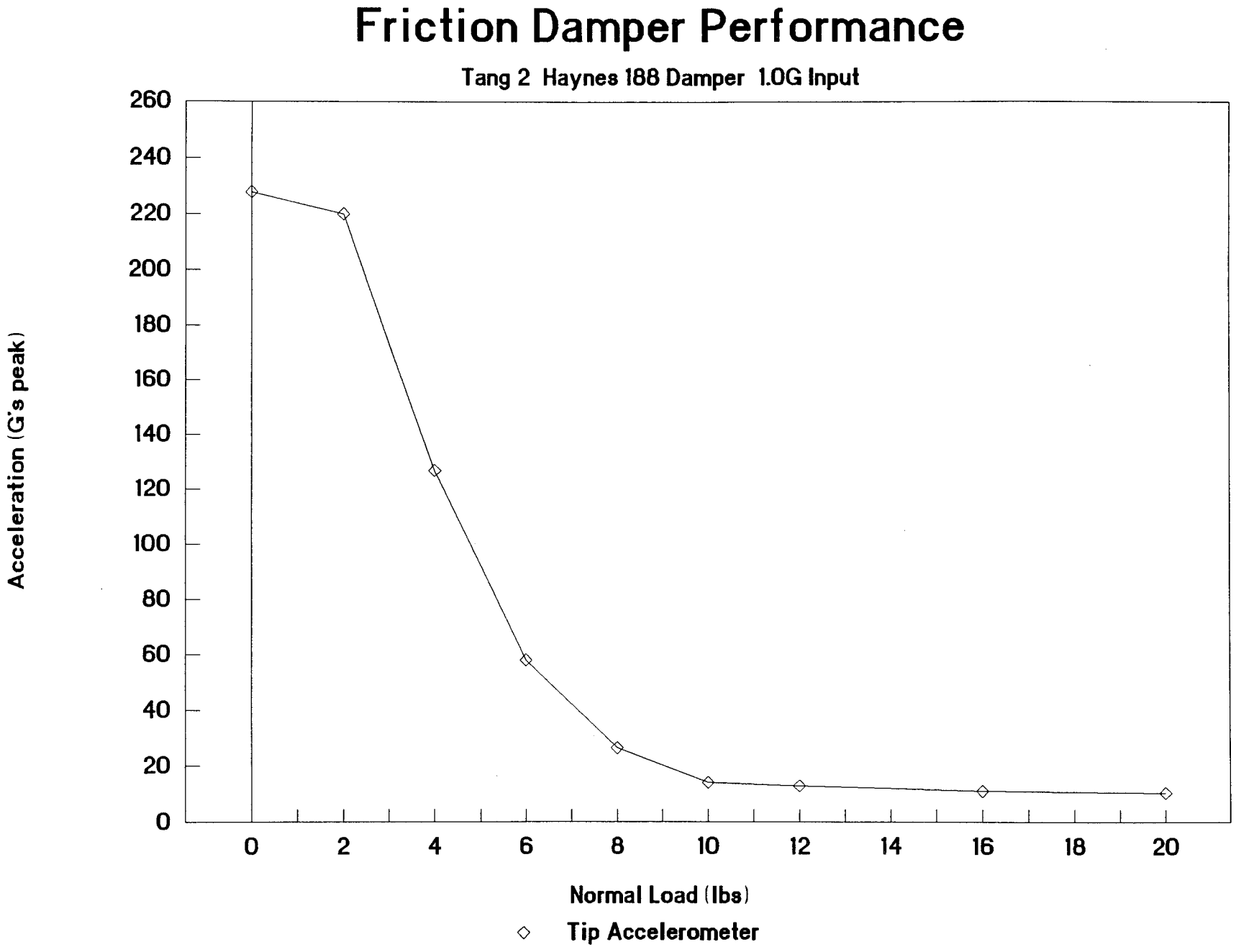

Figure 2.2-61 Low frequency beam optimization curve based on test data Haynes 188 damper at tang 2, 1.0G input

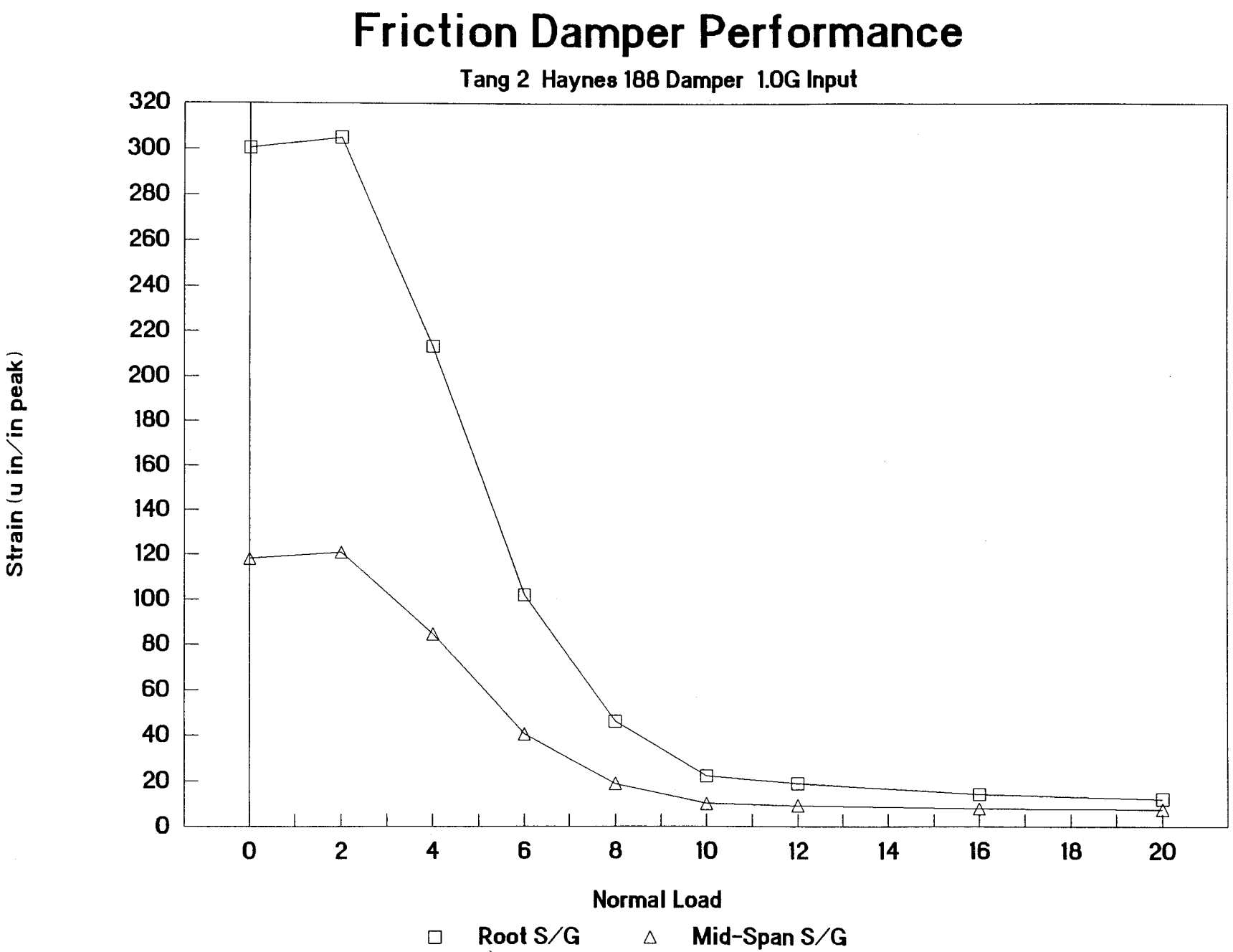

Figure 2.2-62 Low frequency beam optimization curve based on test data Haynes 188 damper at tang 2, 1.0G input

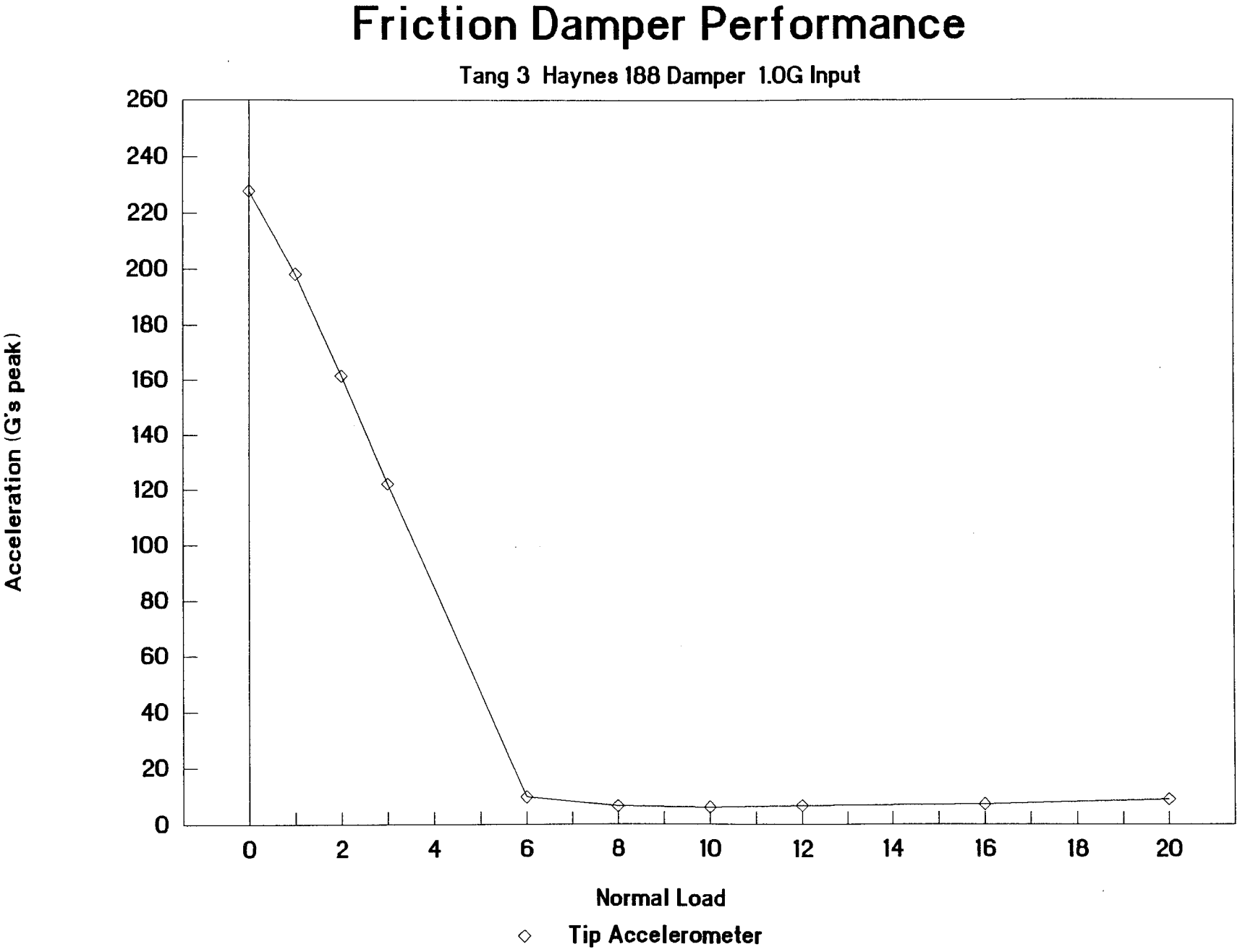

Figure 2.2-63 Low frequency beam optimization curve based on test data Haynes 188 damper at tang 3, 1.0G input

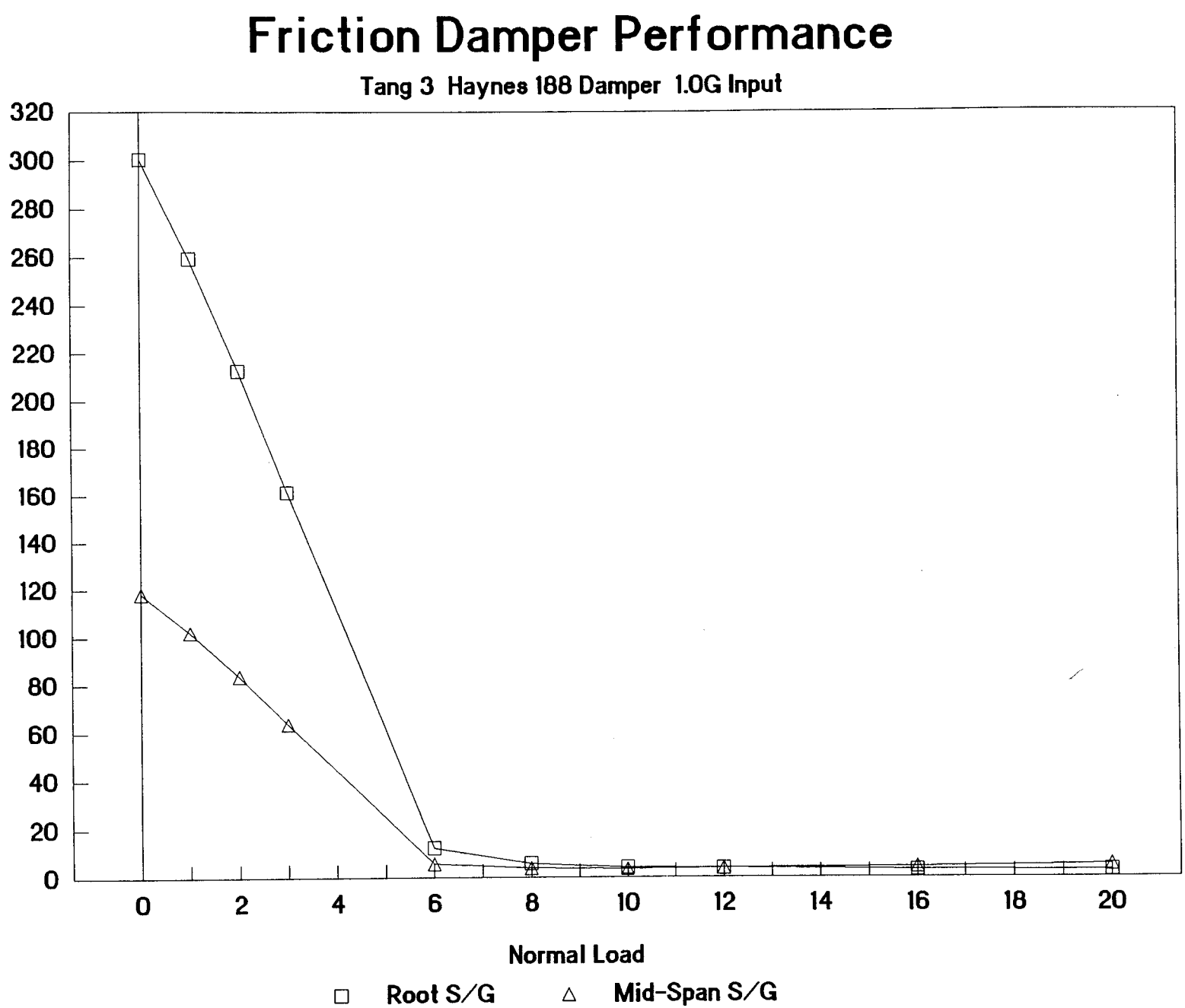

Figure 2.2-64 Low frequency beam optimization curve based on test data Haynes 188 damper at tang 3, 1.0G input

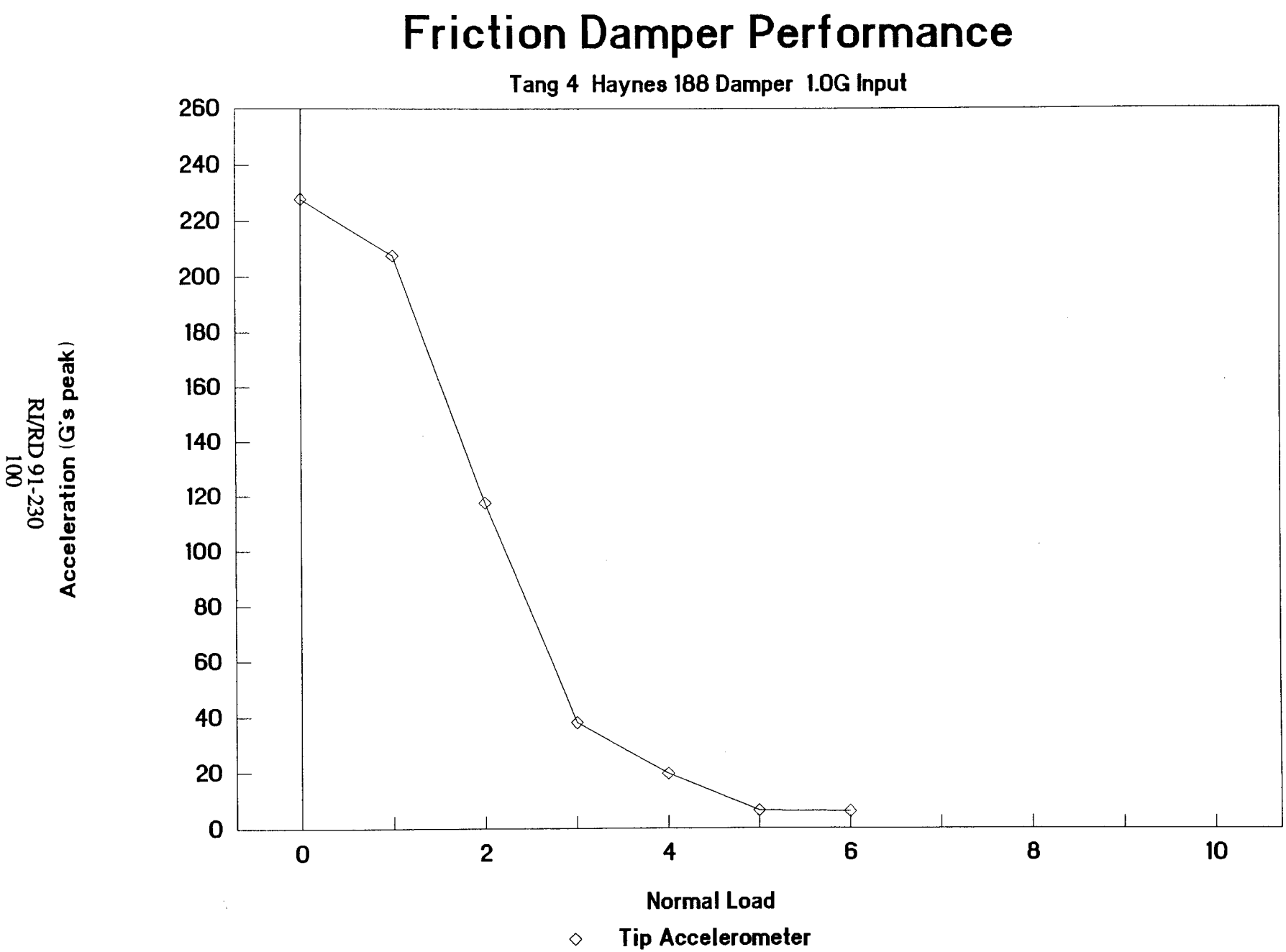

RI/RD 91-230
100

Figure 2.2-65 Low frequency beam optimization curve based on test data Haynes 188 damper at tang 4, 1.0G input

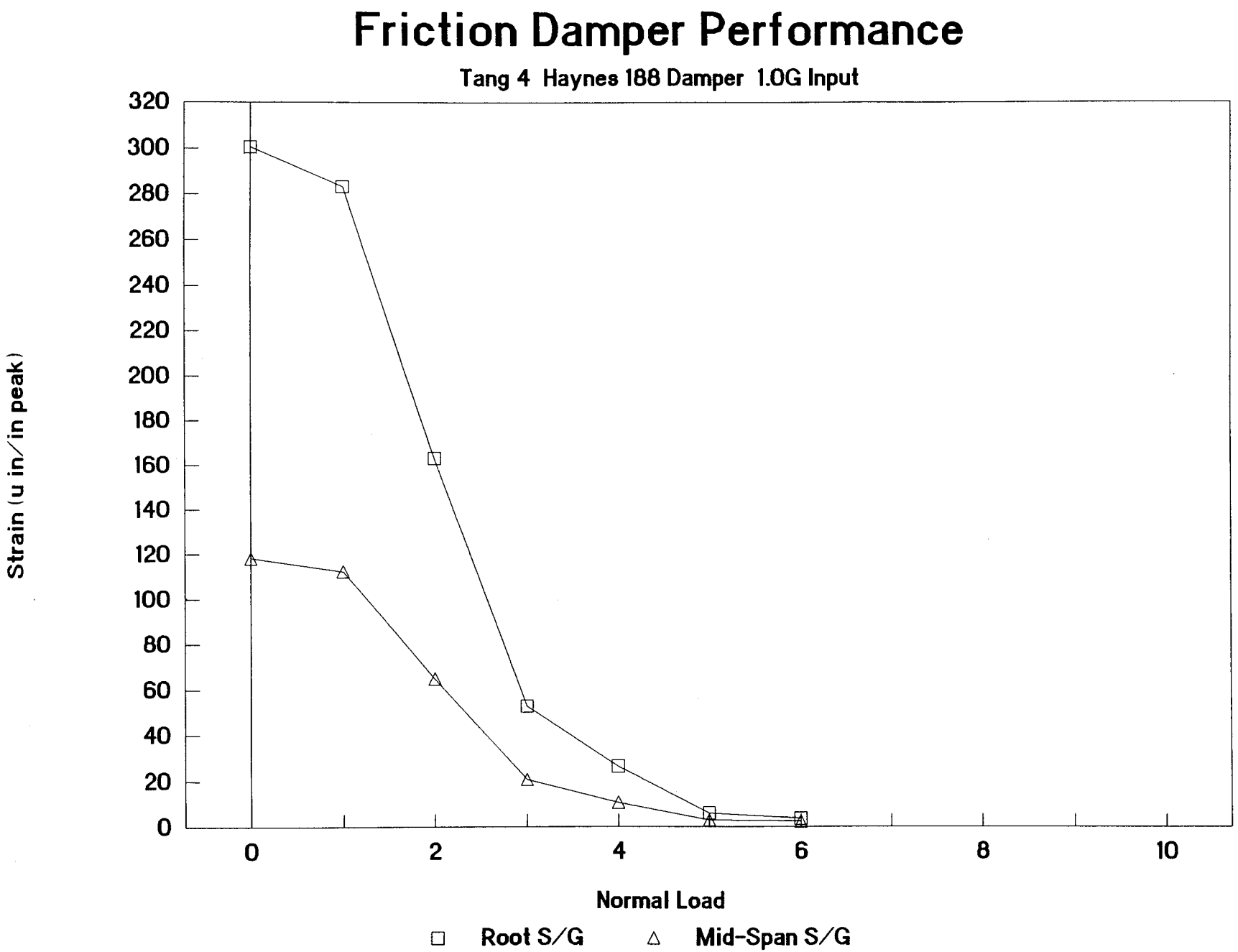

Figure 2.2-66 Low frequency beam optimization curve based on test data Haynes 188 damper at tang 4, 1.0G input

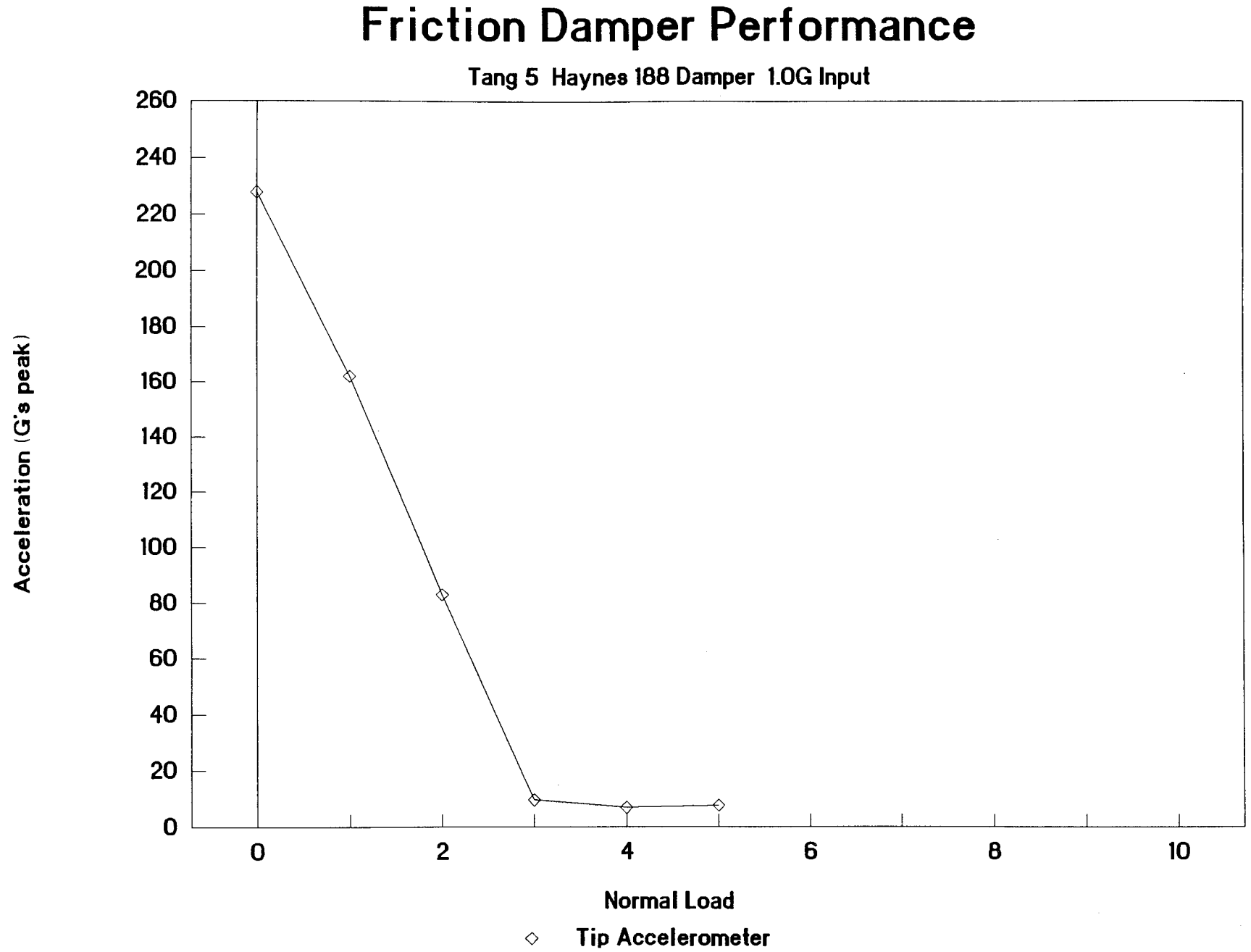

Figure 2.2-67 Low frequency beam optimization curve based on test data Haynes 188 damper at tang 5, 1.0G input

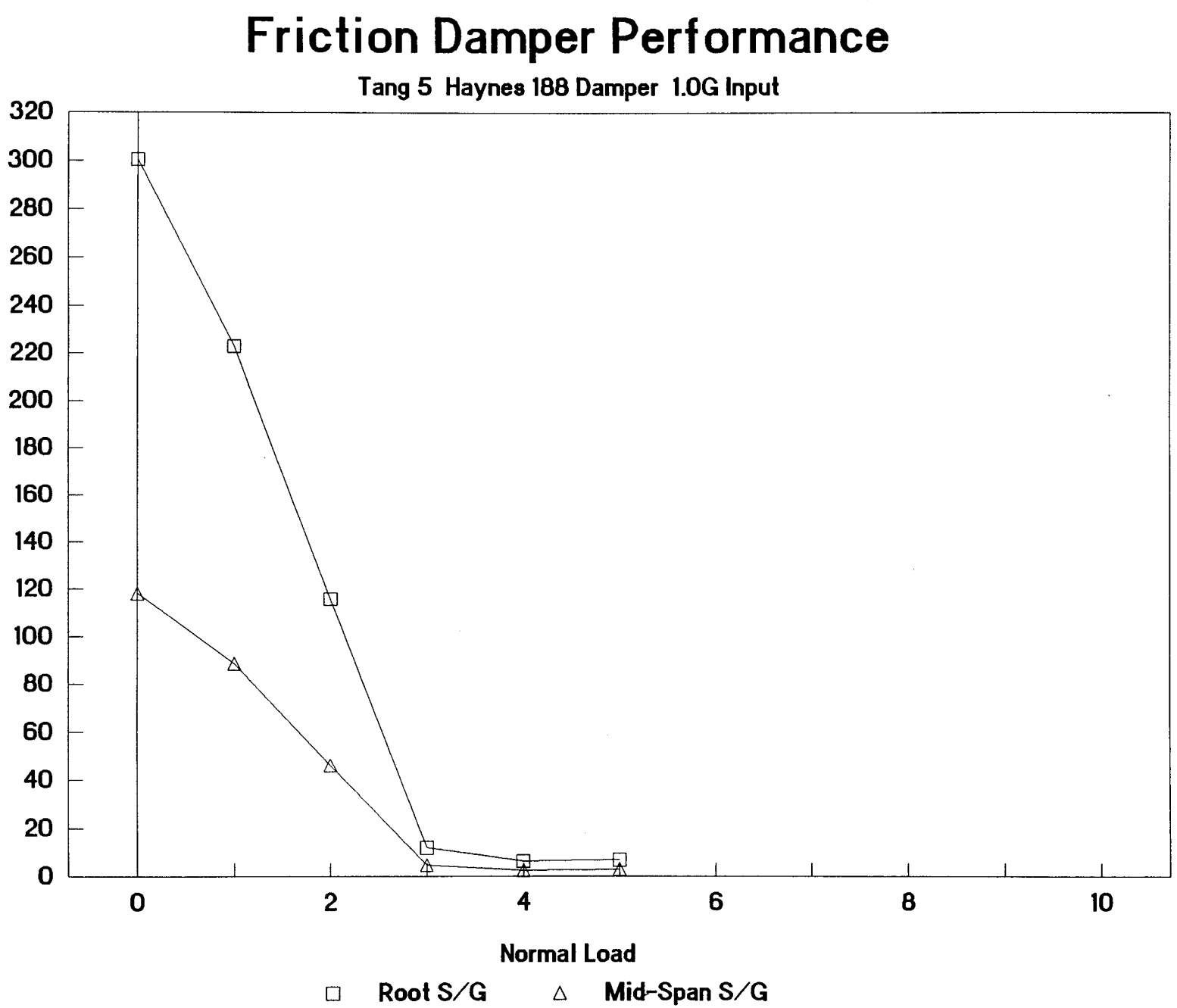

Figure 2.2-68 Low frequency beam optimization curve based on test data Haynes 188 damper at tang 5, 1.0G input

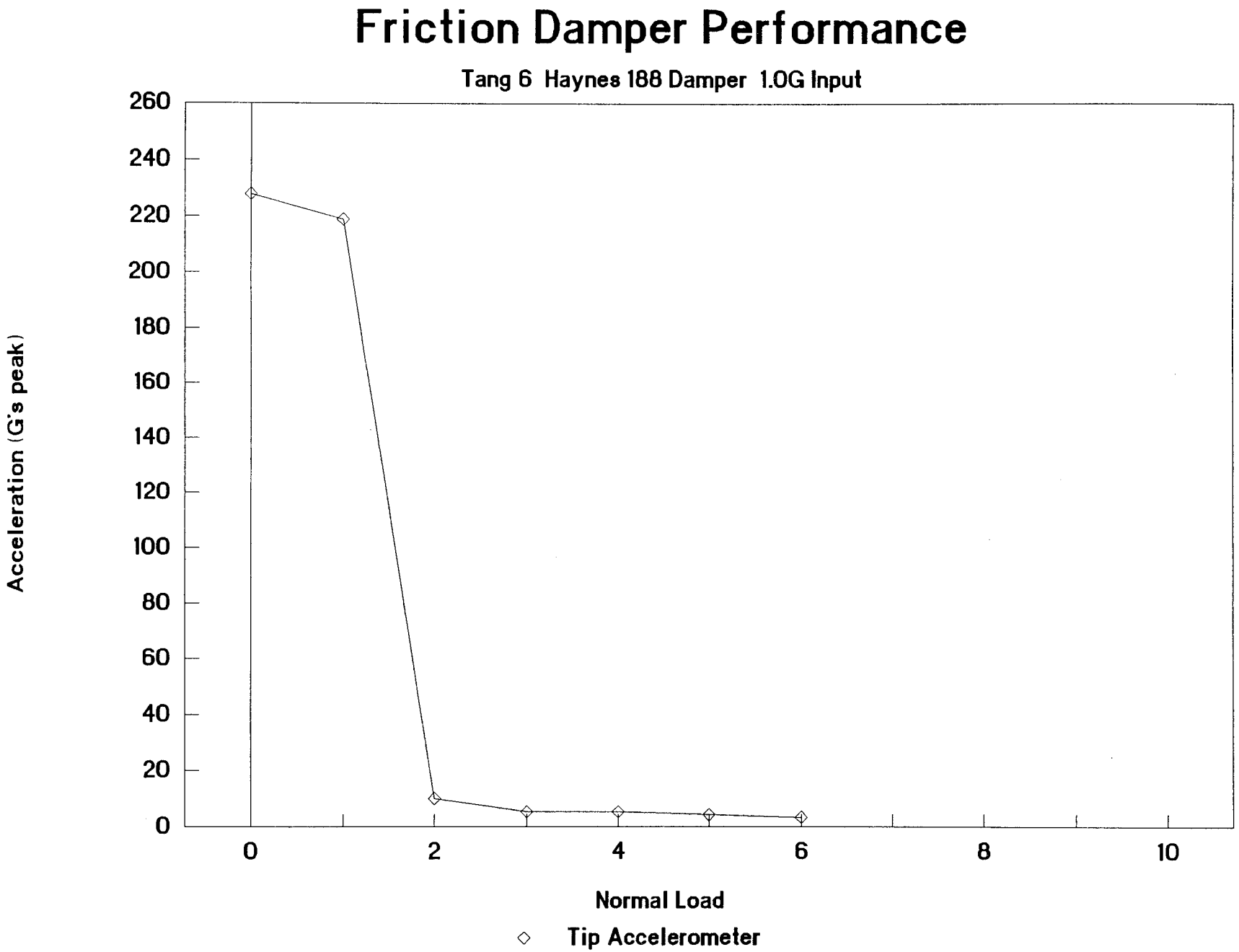

Figure 2.2-69 Low frequency beam optimization curve based on test data Haynes 188 damper at tang 6, 1.0G input

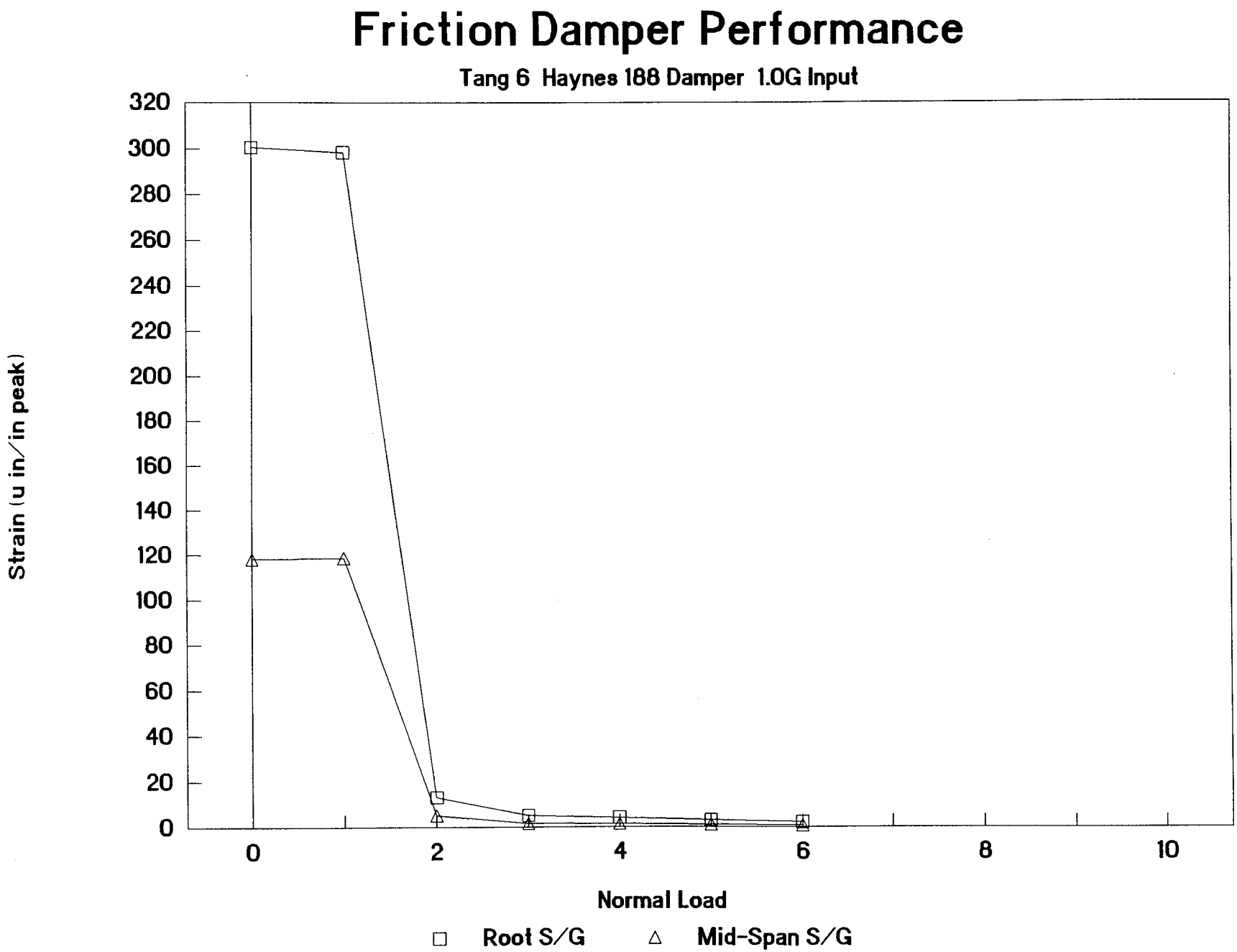

Figure 2.2-70 Low frequency beam optimization curve based on test data Haynes 188 damper at tang 6, 1.0G input

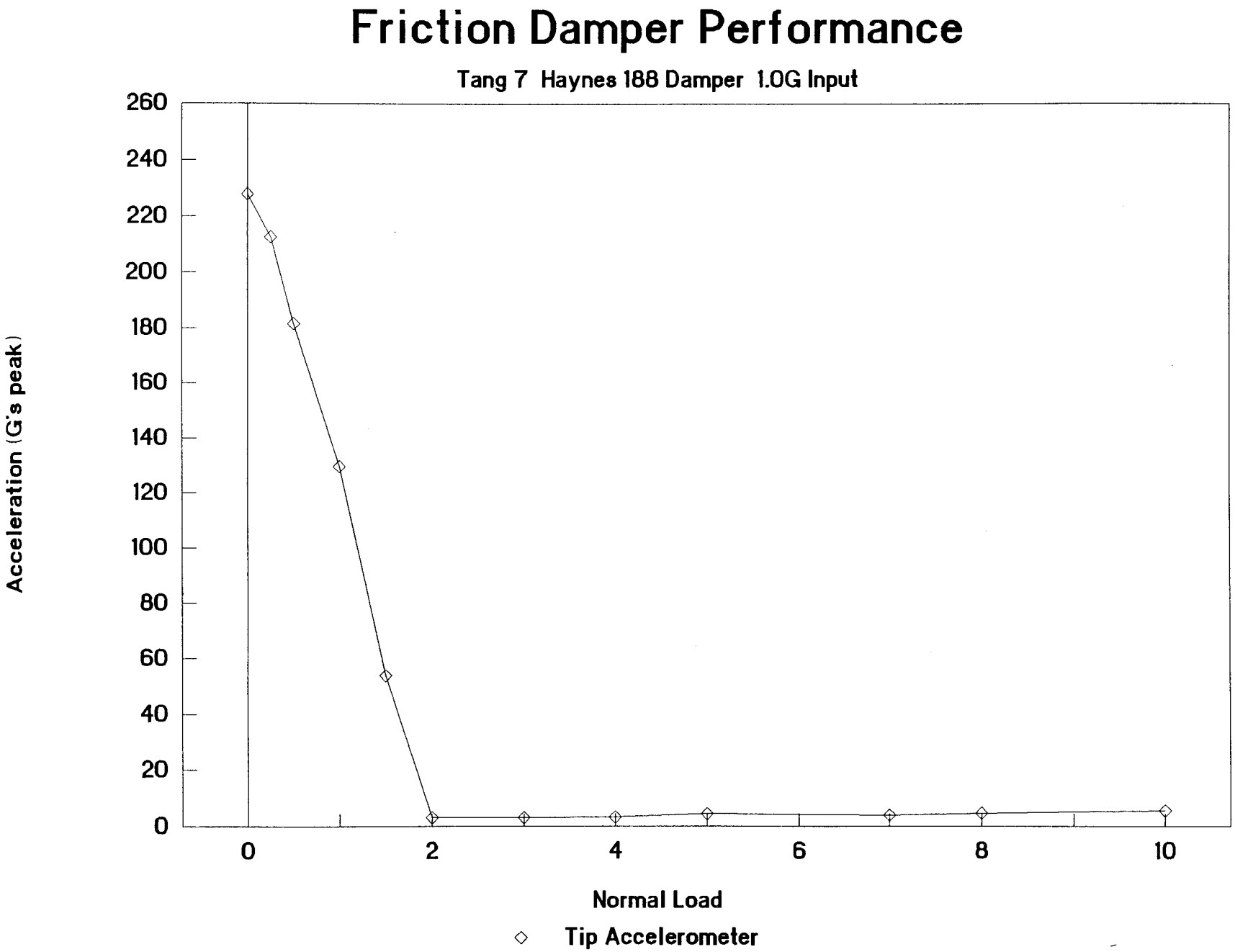

Figure 2.2-71 Low frequency beam optimization curve based on test data Haynes 188 damper at tang 7, 1.0G input

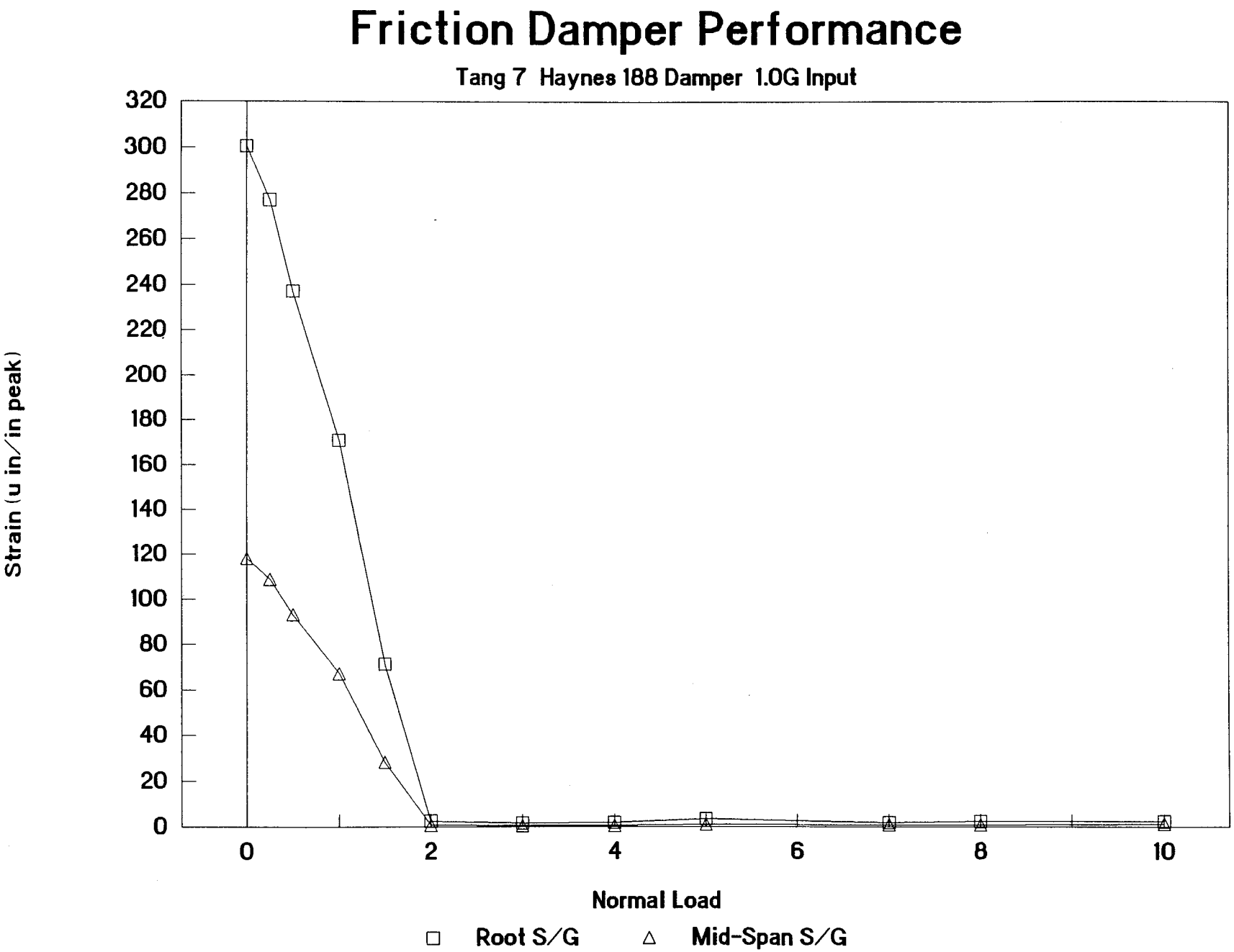

Figure 2.2-72 Low frequency beam optimization curve based on test data Haynes 188 damper at tang 7, 1.0G input

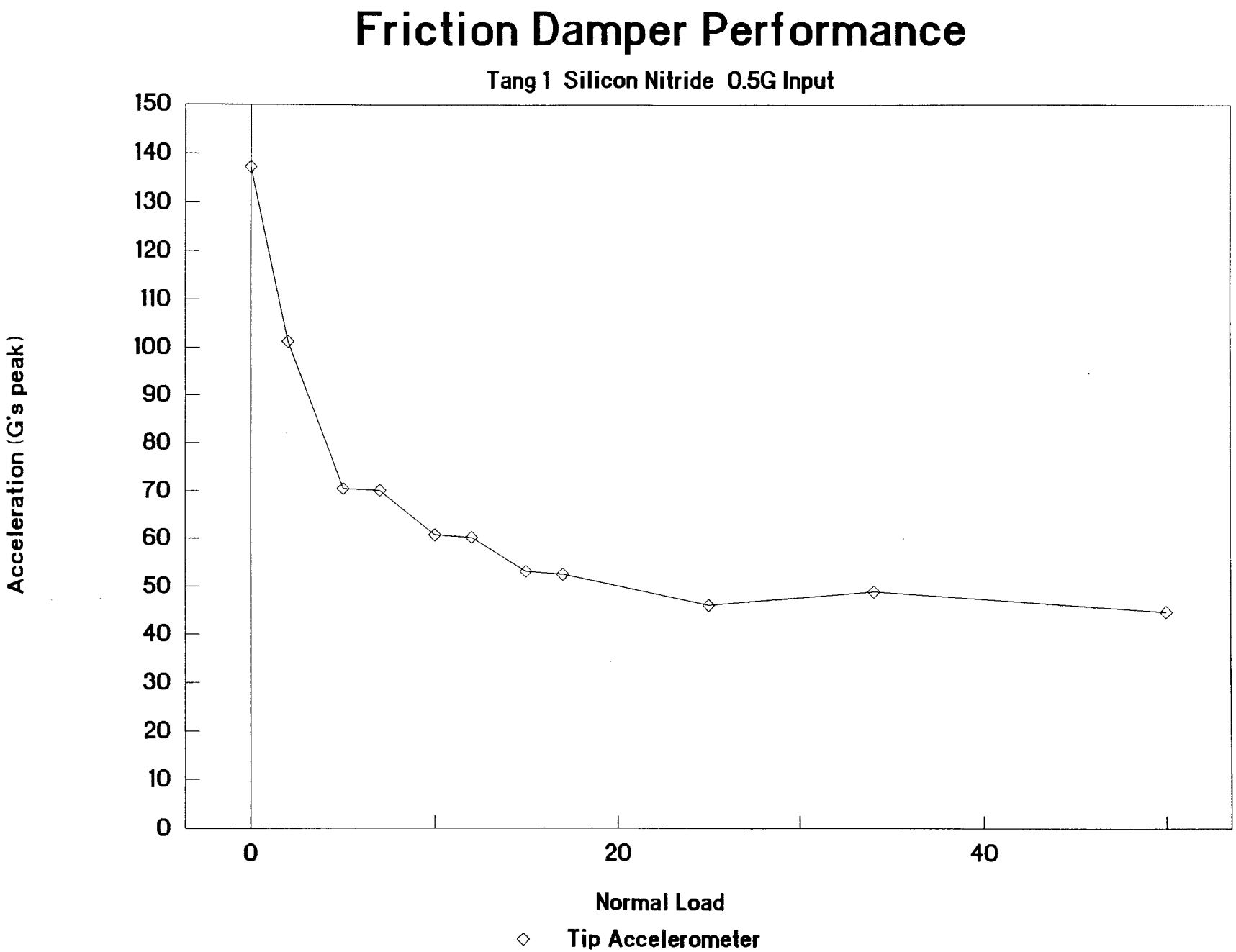

Figure 2.2-73 Low frequency beam optimization curve based on test data Silicon Nitride damper at tang 1, 0.5G input

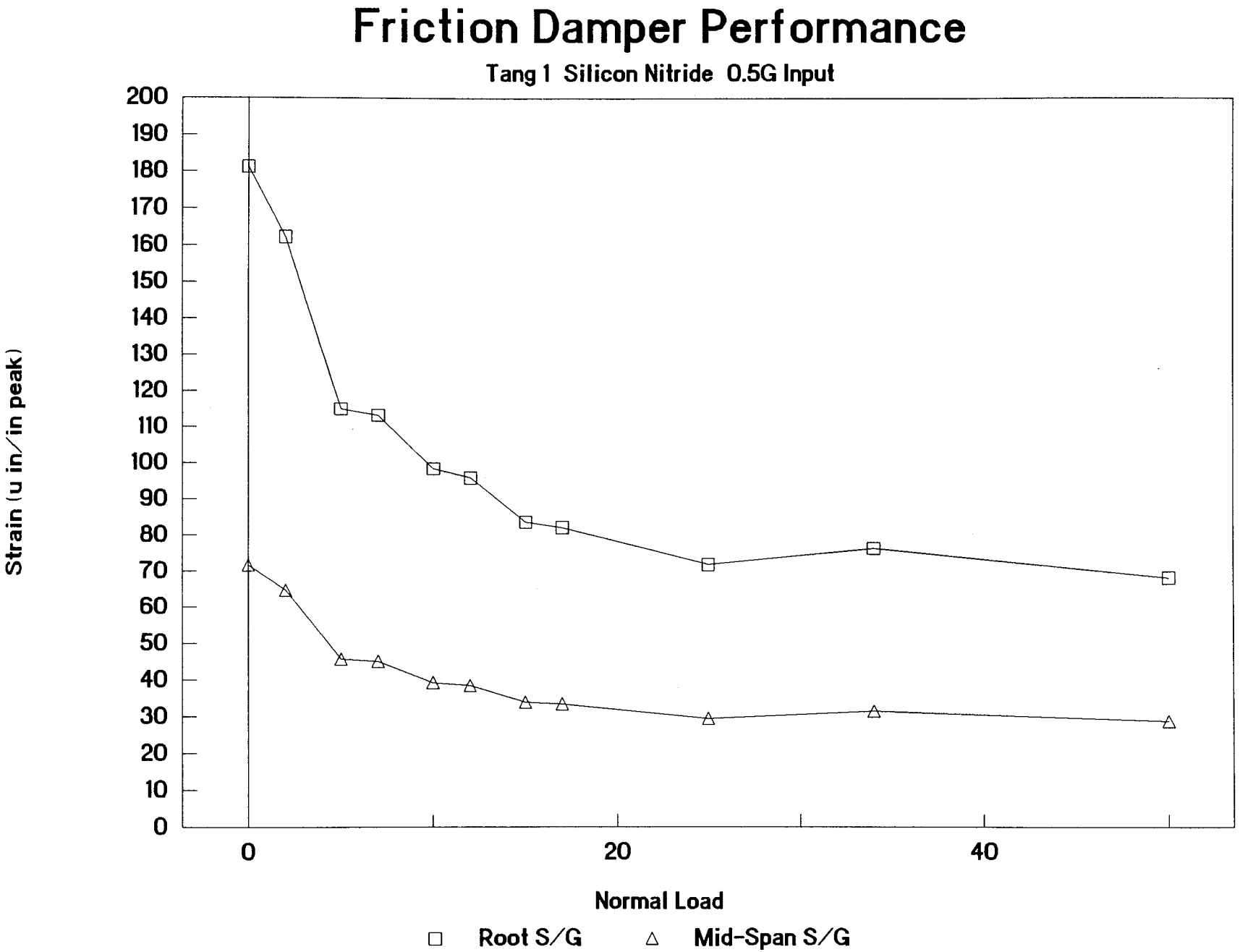

Figure 2.2-74 Low frequency beam optimization curve based on test data Silicon Nitride damper at tang 1, 0.5G input

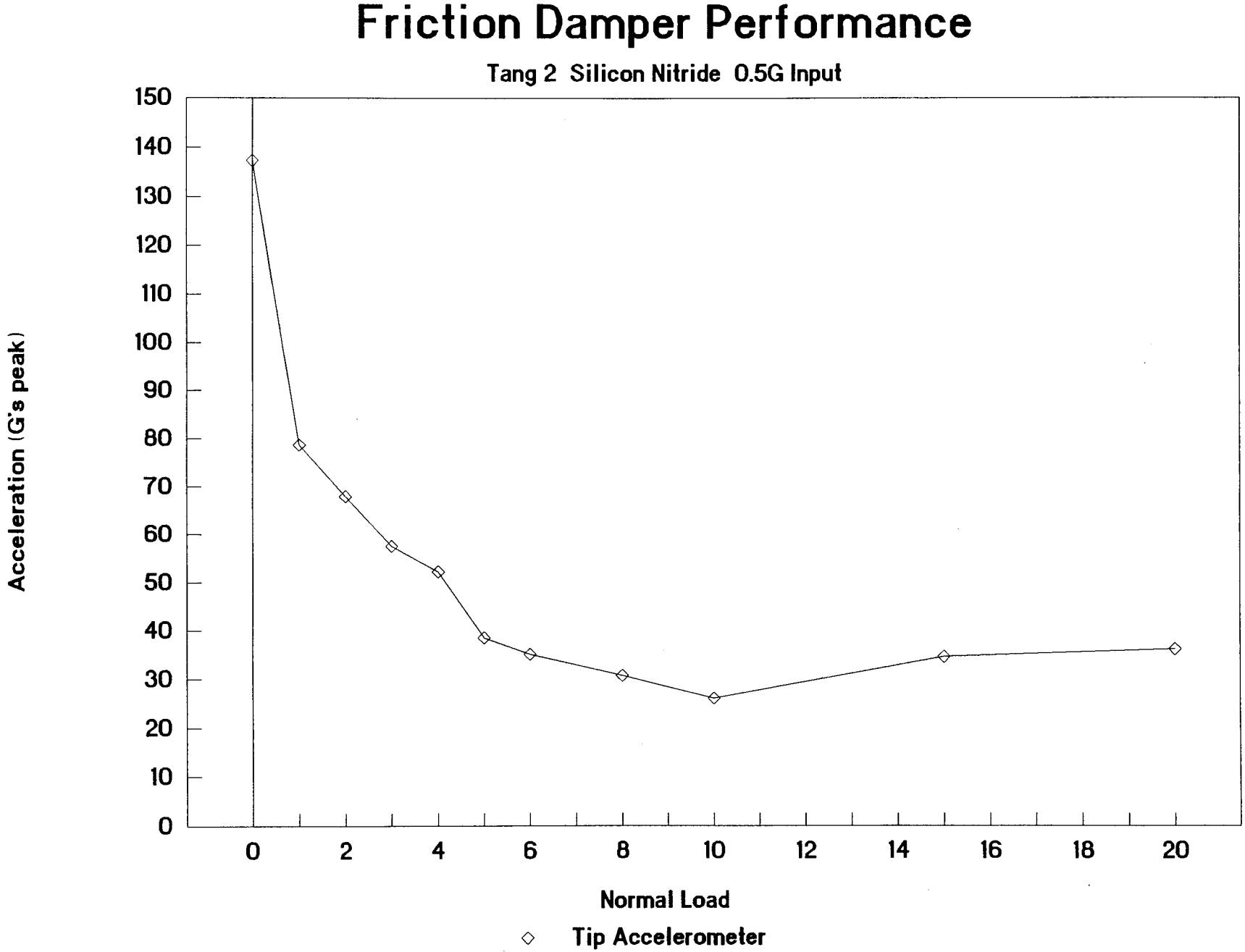

Figure 2.2-75 Low frequency beam optimization curve based on test data Silicon Nitride damper at tang 2, 0.5G input

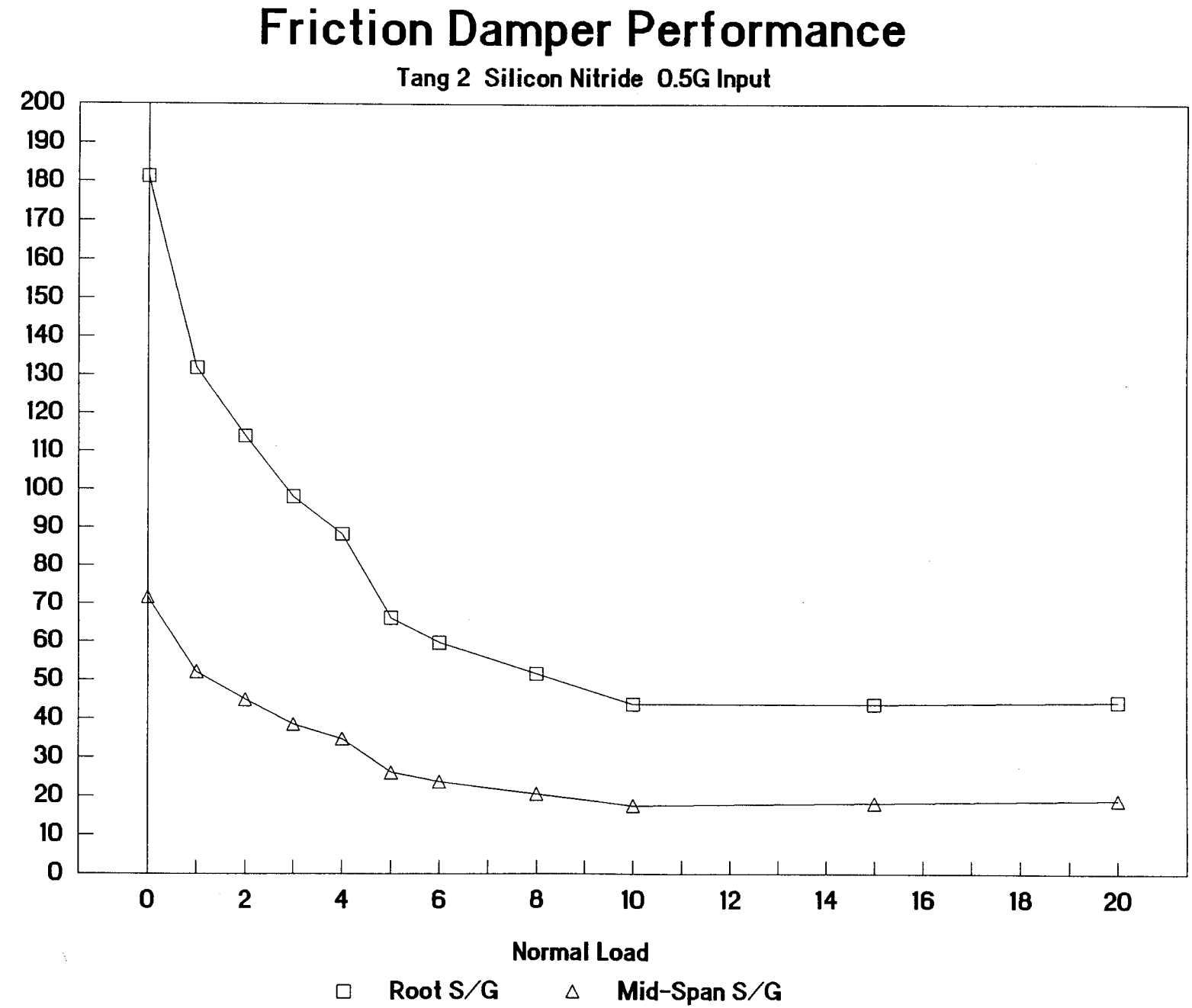

Figure 2.2-76 Low frequency beam optimization curve based on test data Silicon Nitride damper at tang 2, 0.5G input

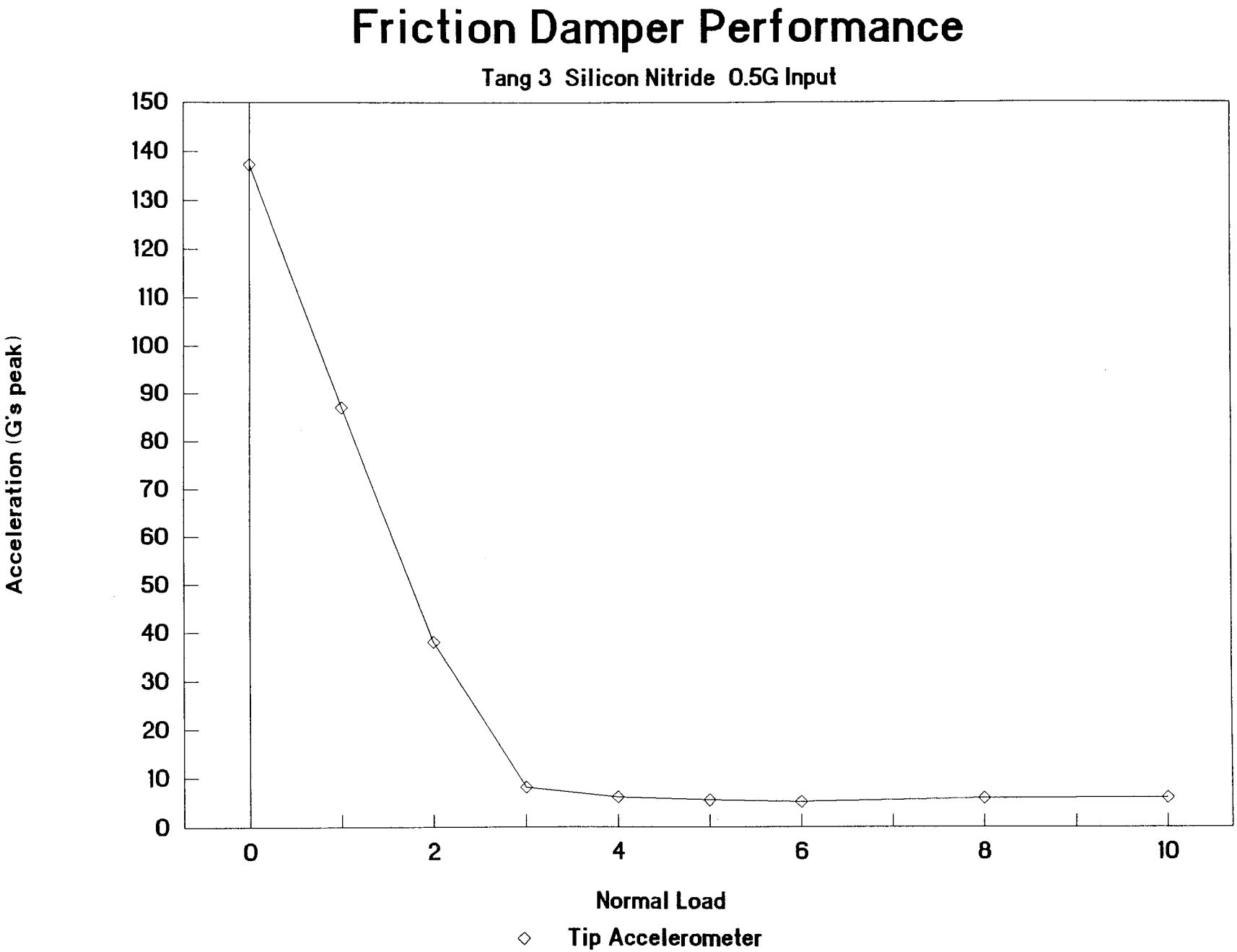

Figure 2.2-77 Low frequency beam optimization curve based on test data Silicon Nitride damper at tang 3, 0.5G input

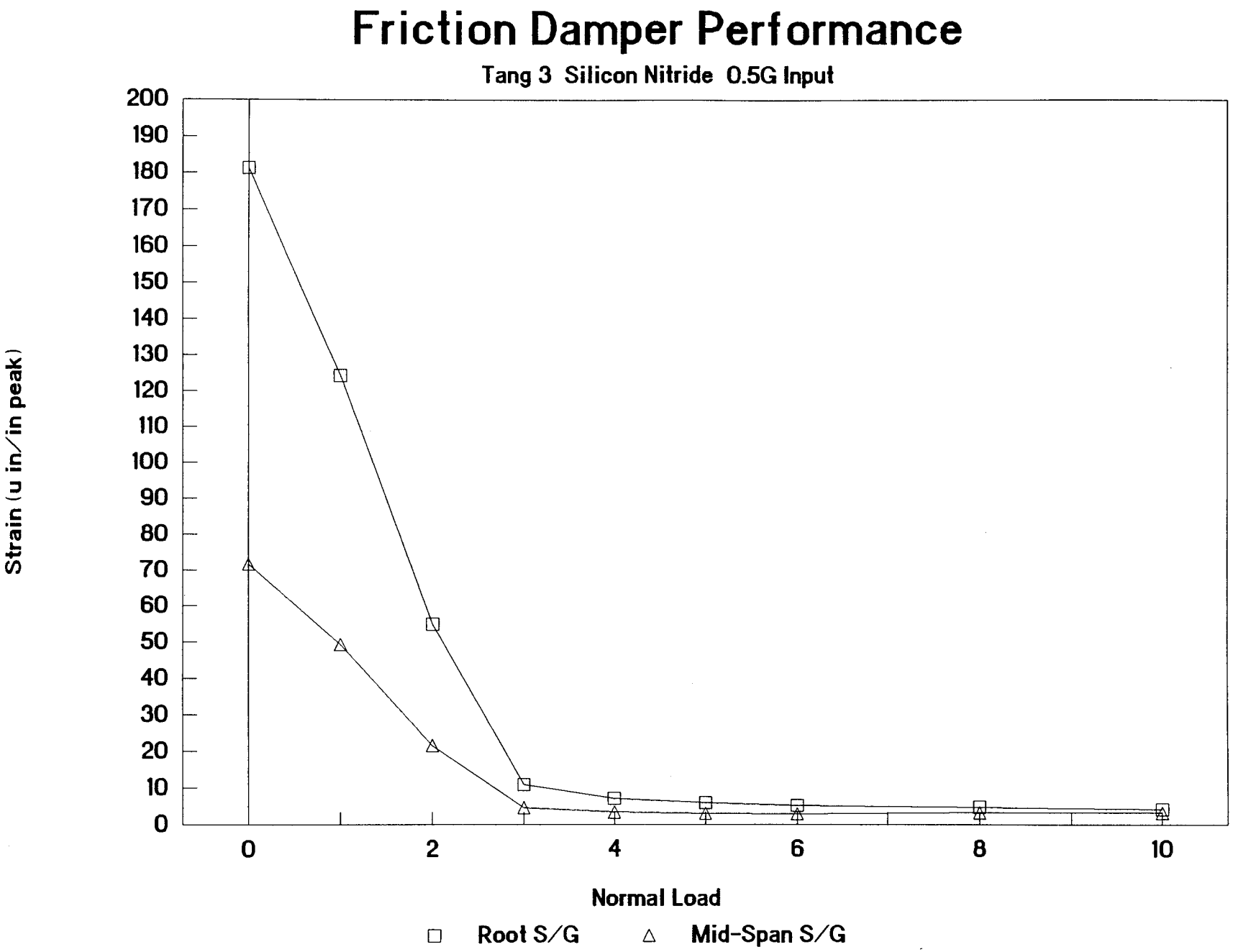

Figure 2.2-78 Low frequency beam optimization curve based on test data Silicon Nitride damper at tang 3, 0.5G input

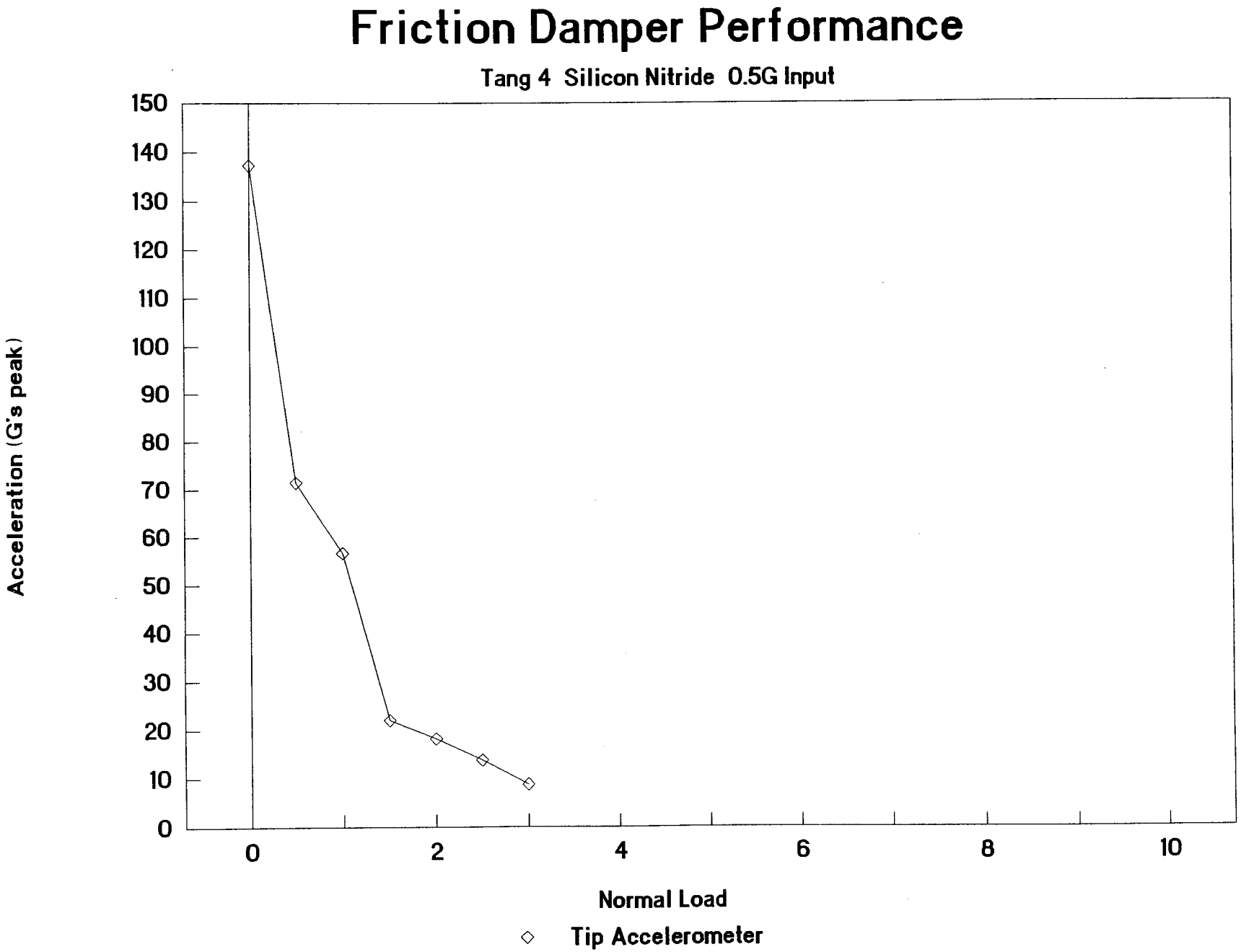

Figure 2.2-79 Low frequency beam optimization curve based on test data Silicon Nitride damper at tang 4, 0.5G Input

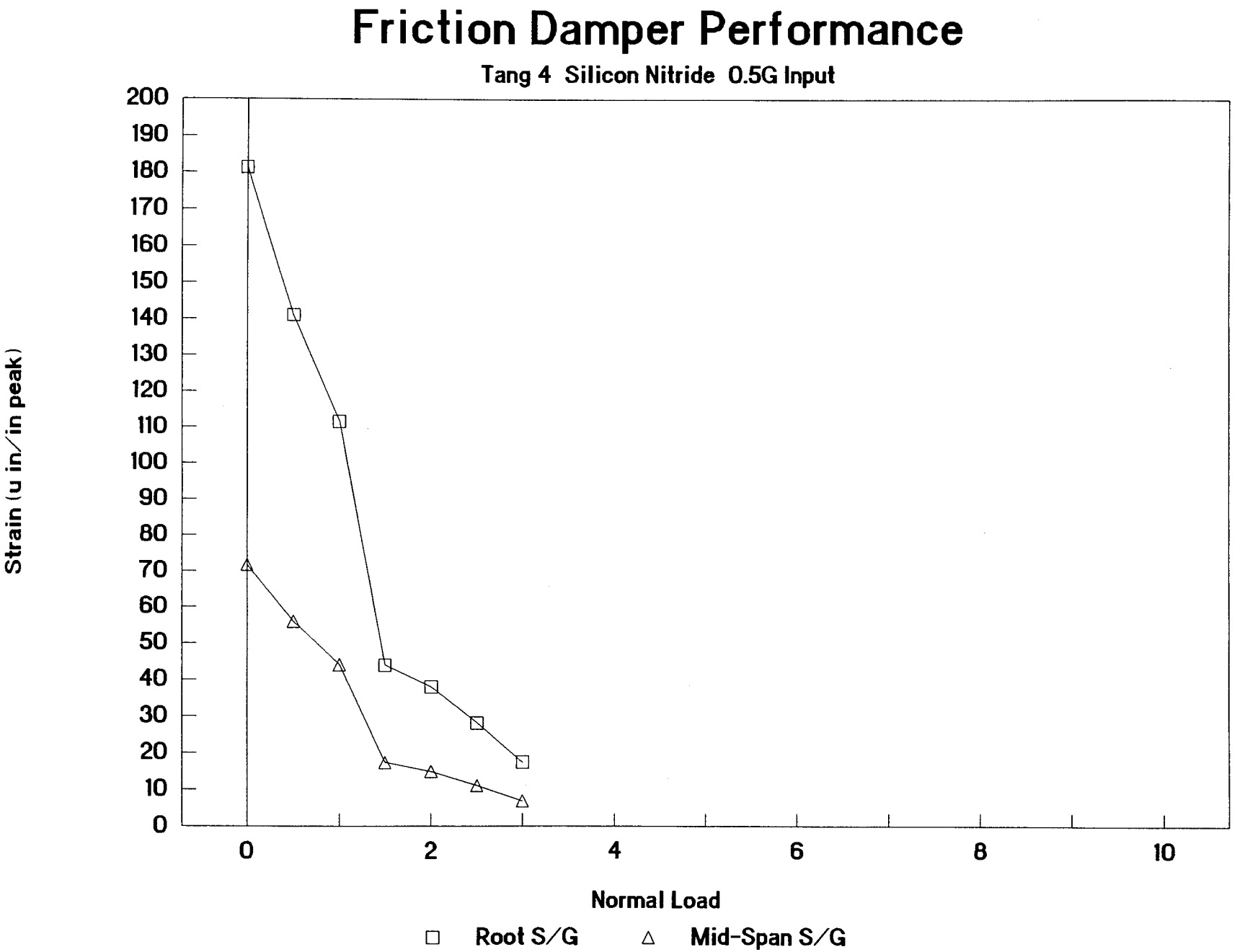

Figure 2.2-80 Low frequency beam optimization curve based on test data Silicon Nitride damper at tang 4, 0.5G input

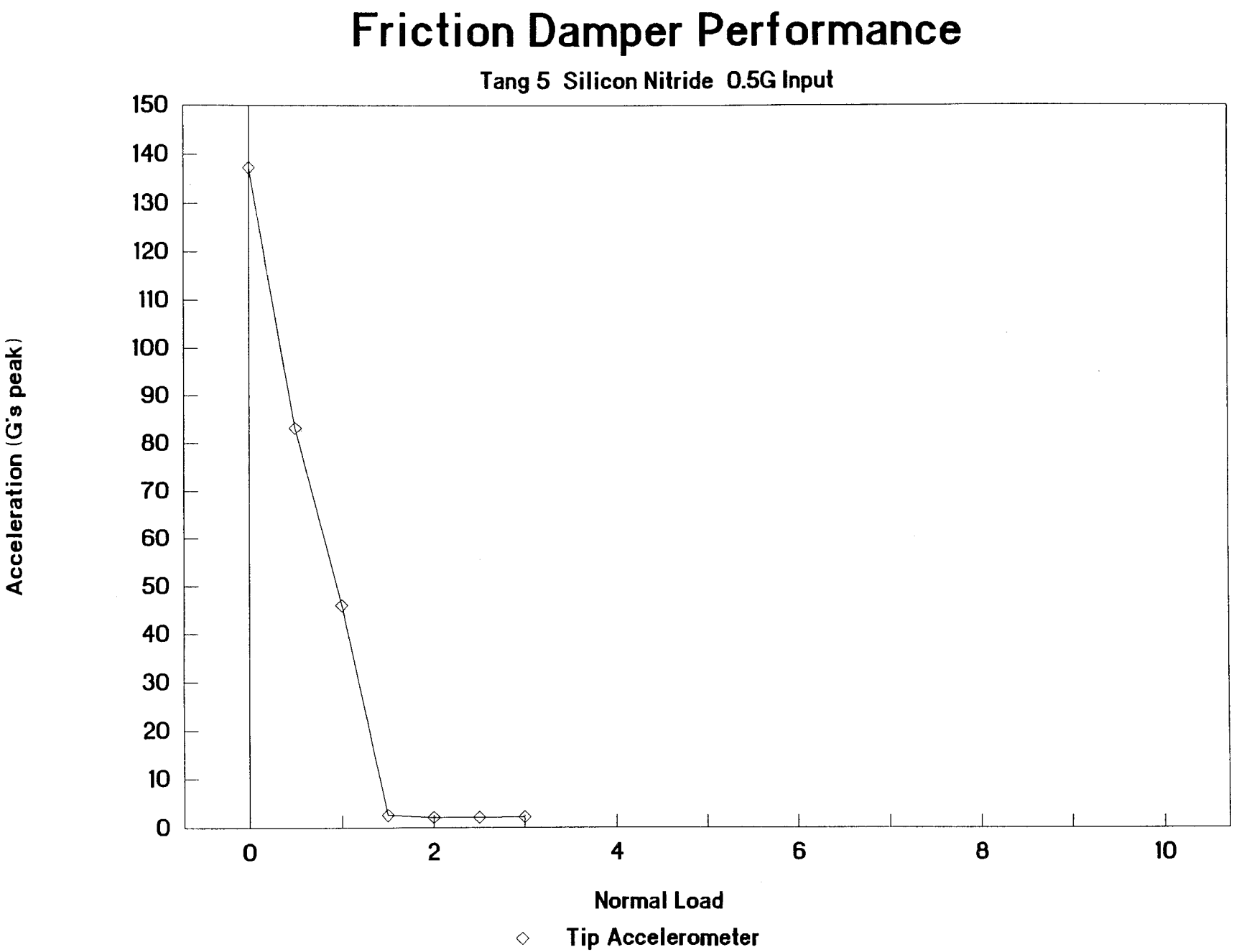

Figure 2.2-81 Low frequency beam optimization curve based on test data Silicon Nitride damper at tang 5, 0.5G input

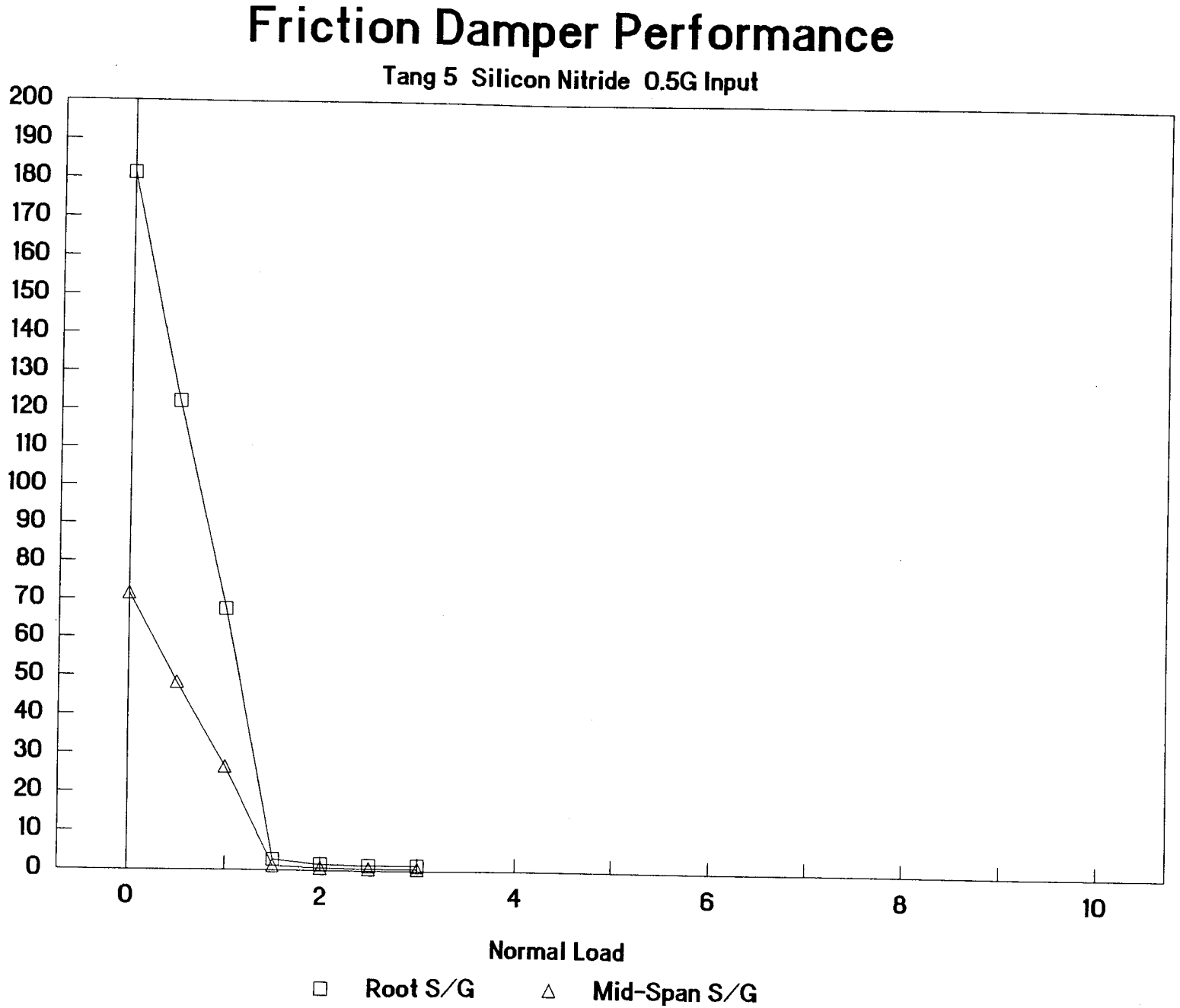

Figure 2.2-82 Low frequency beam optimization curve based on test data Silicon Nitride damper at tang 5, 0.5G input

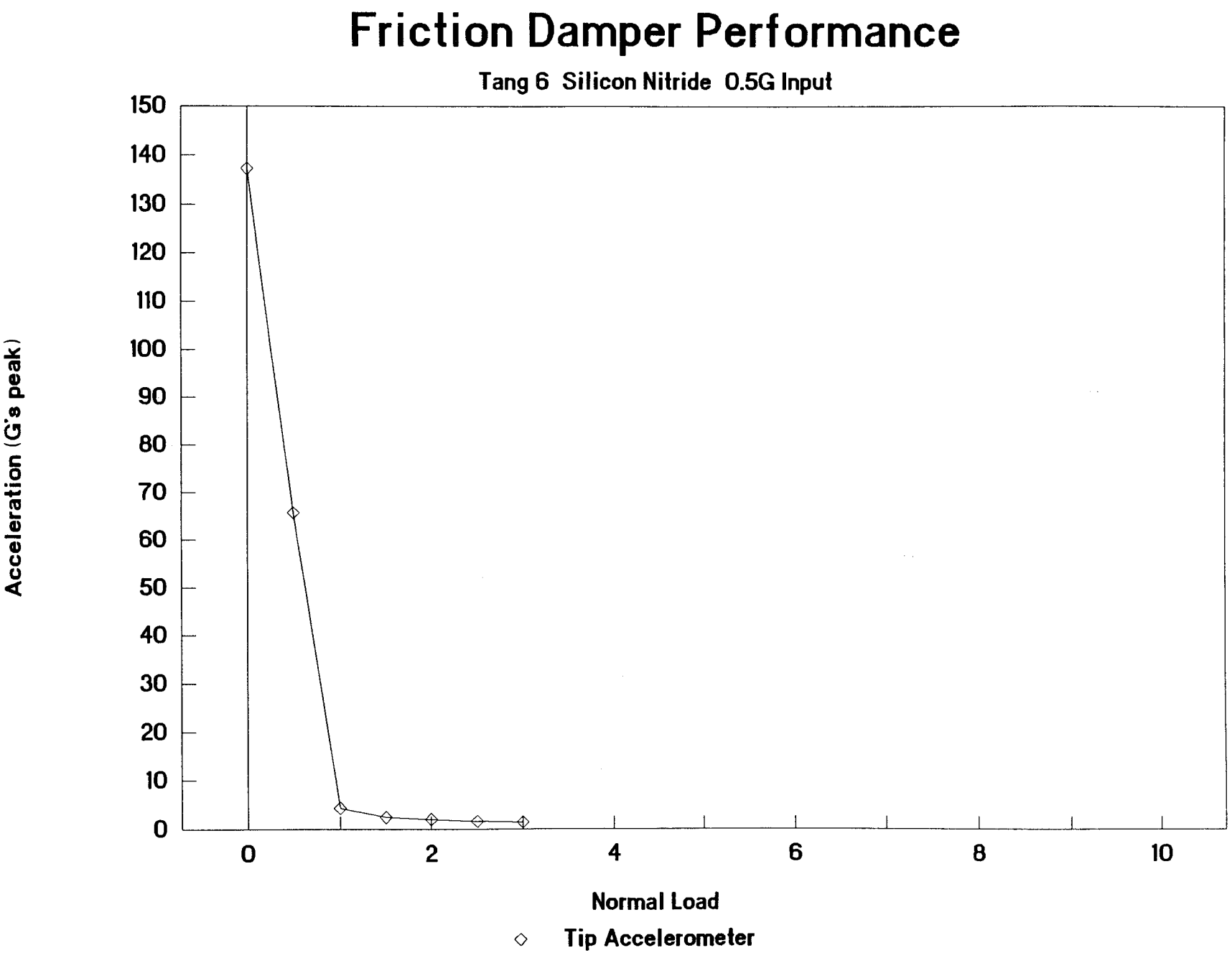

Figure 2.2-83 Low frequency beam optimization curve based on test data Silicon Nitride damper at tang 6, 0.5G input

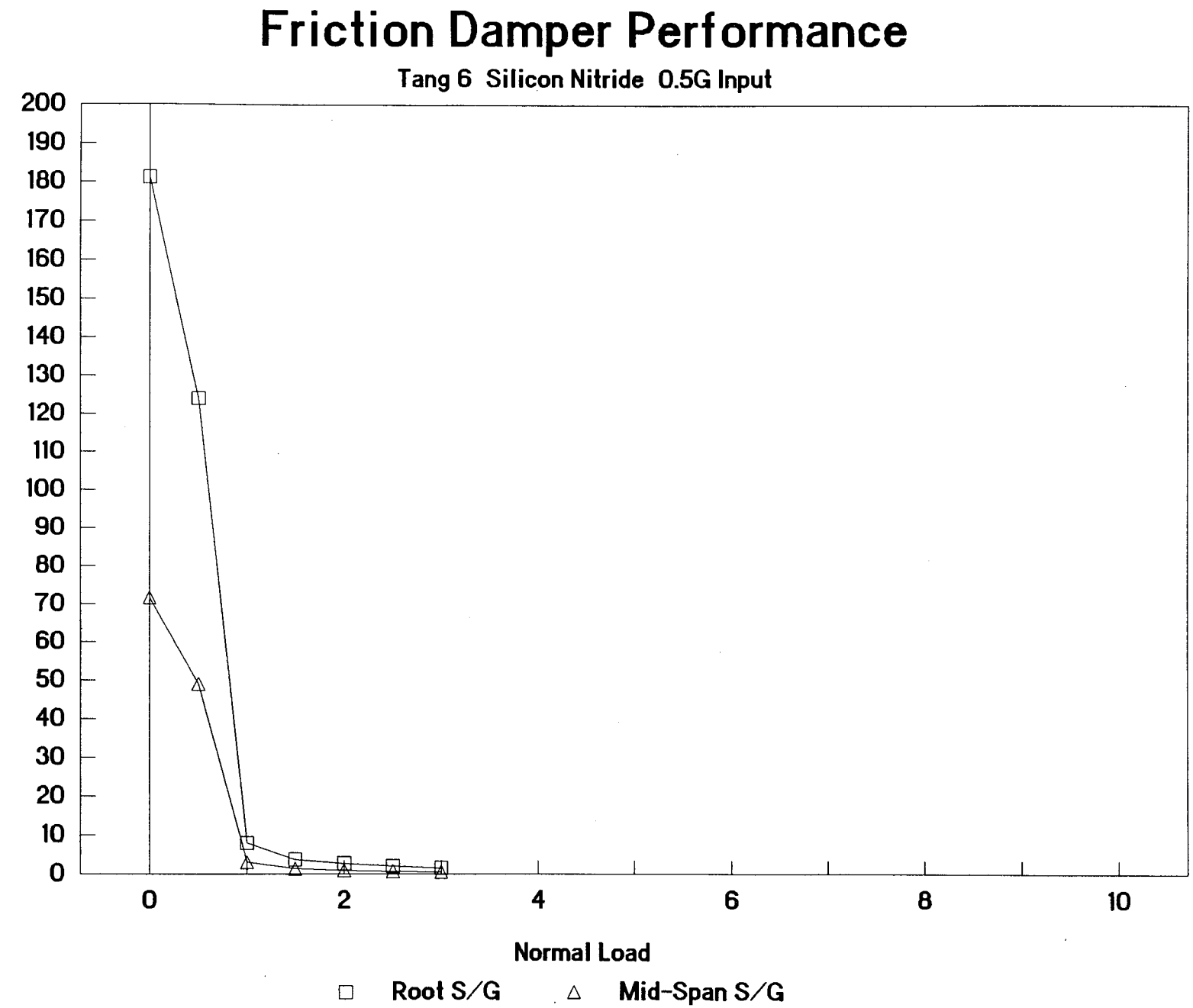

Figure 2.2-84 Low frequency beam optimization curve based on test data Silicon Nitride damper at tang 6, 0.5G input

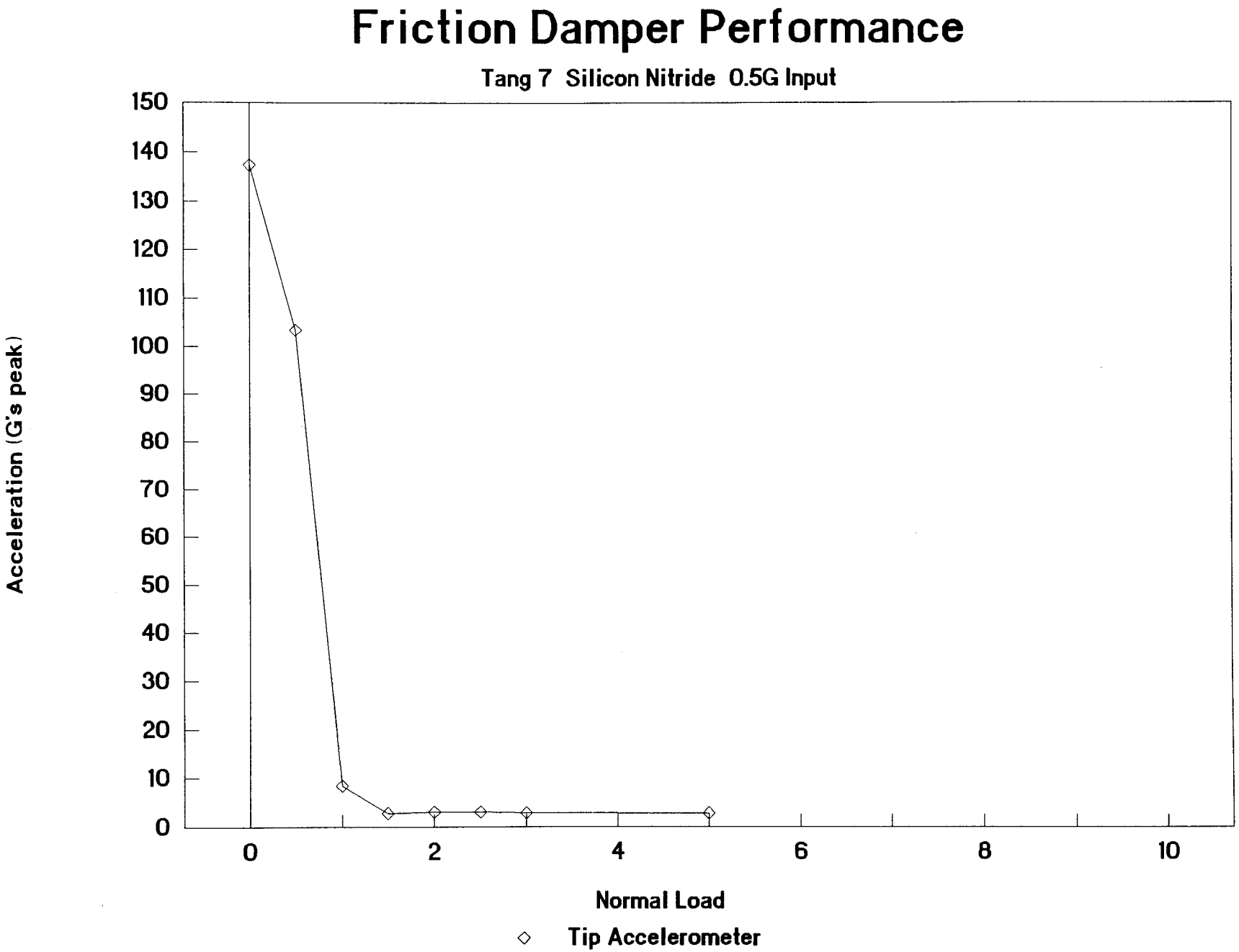

Figure 2.2-85 Low frequency beam optimization curve based on test data Silicon Nitride damper at tang 7, 0.5G input

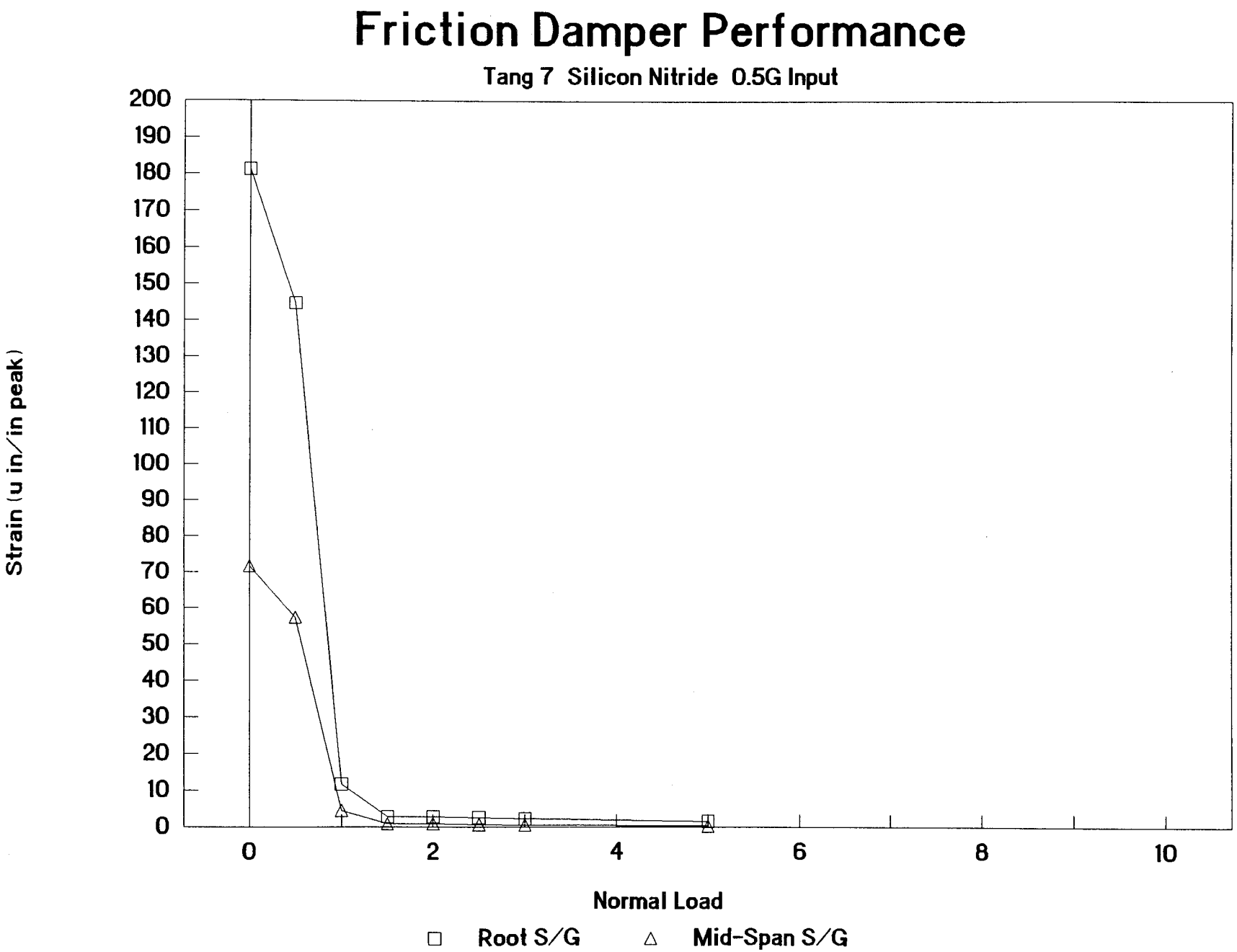

Figure 2.2-86 Low frequency beam optimization curve based on test data Silicon Nitride damper at tang 7, 0.5G input

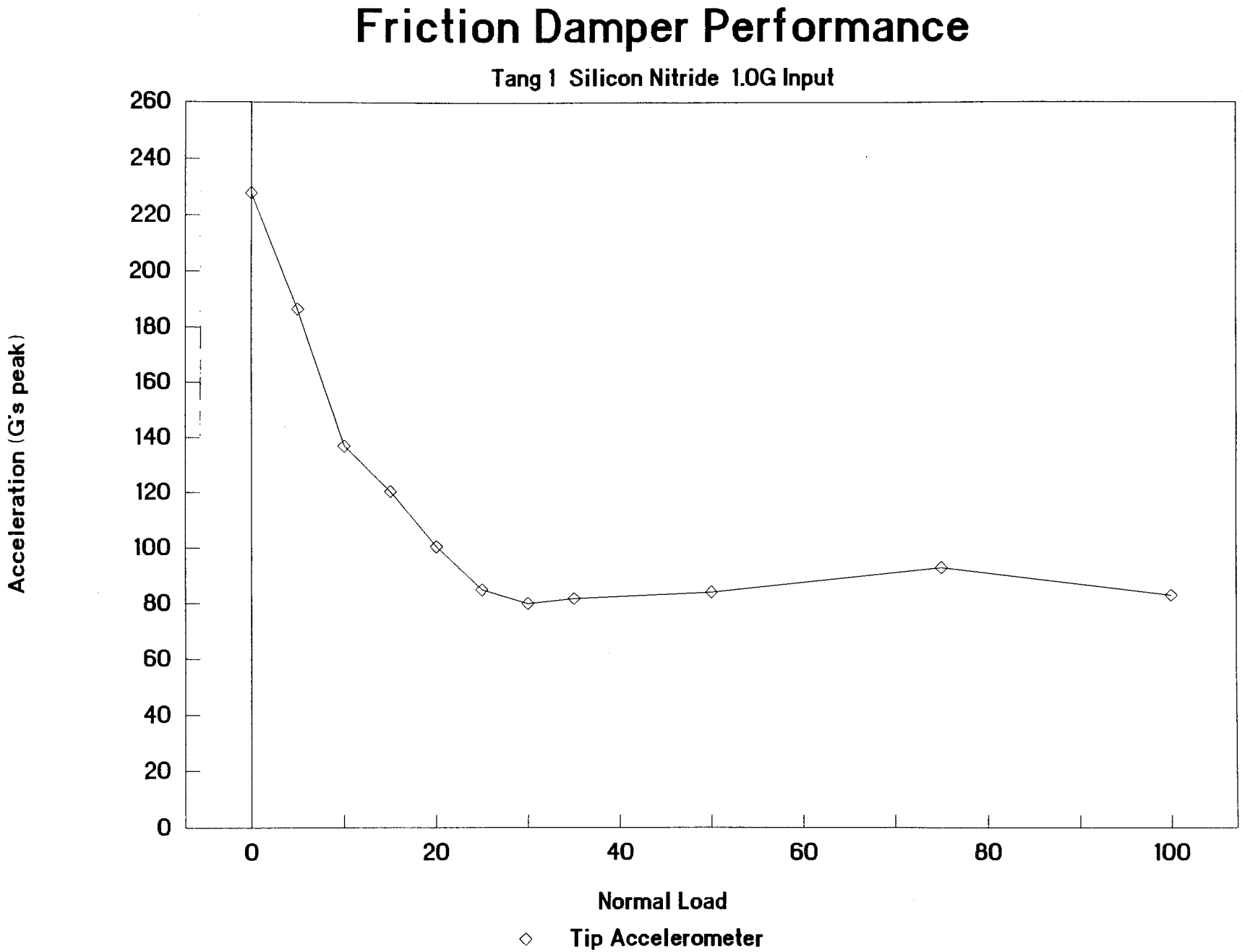

Figure 2.2-87 Low frequency beam optimization curve based on test data Silicon Nitride damper at tang 1, 1.0G input

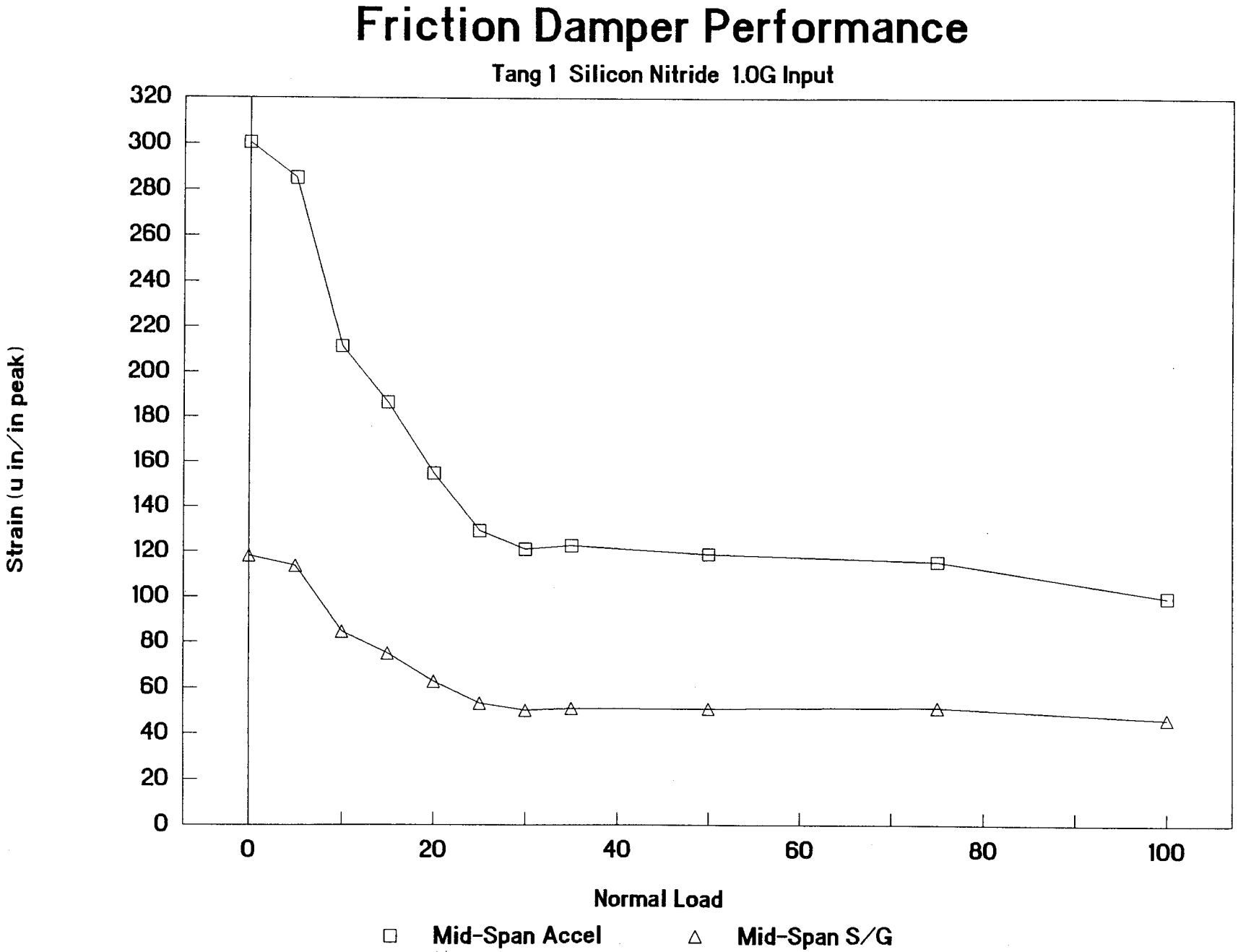

Figure 2.2-88 Low frequency beam optimization curve based on test data Silicon Nitride damper at tang 1, 1.0G input

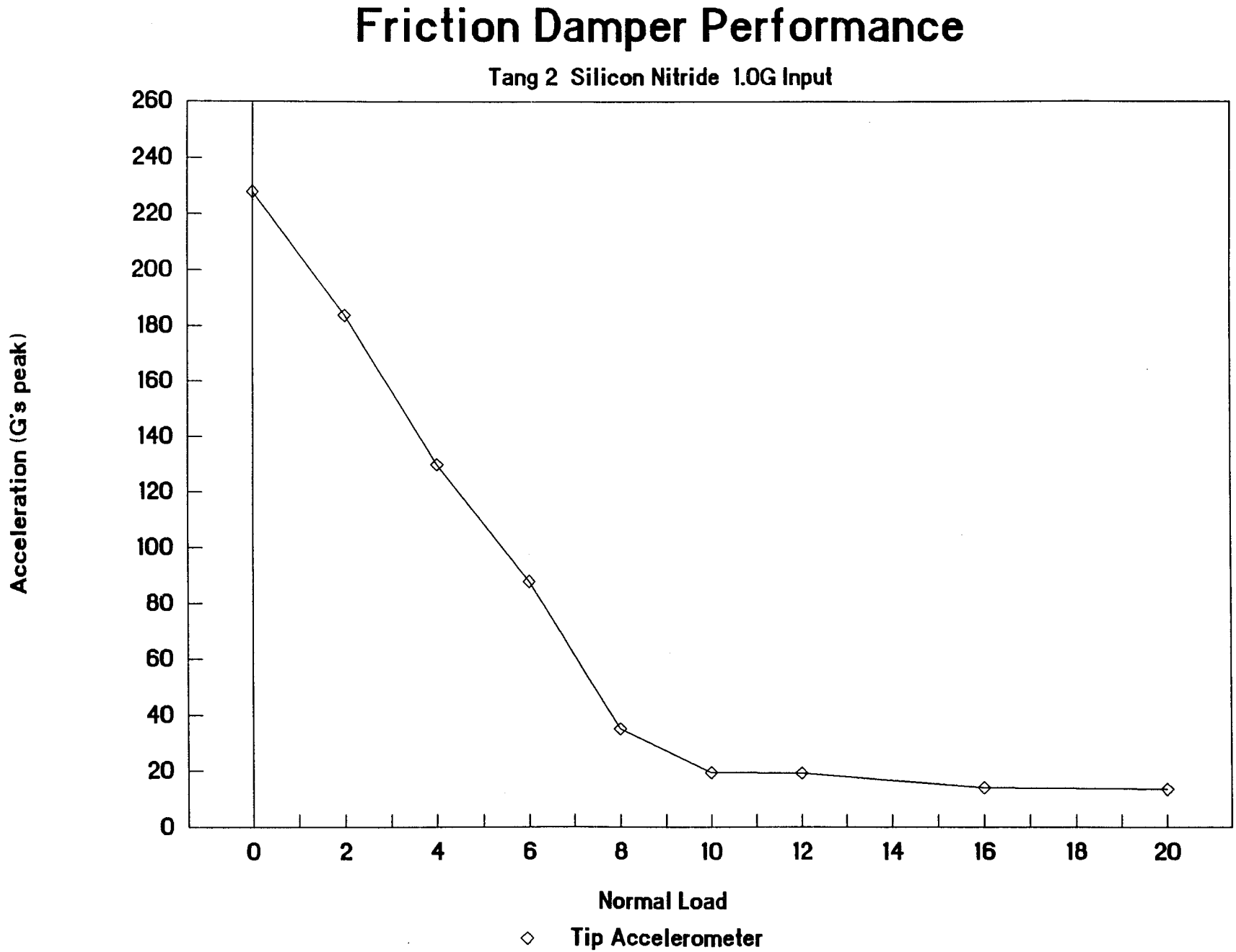

Figure 2.2-89 Low frequency beam optimization curve based on test data Silicon Nitride damper at tang 2, 1.0G input

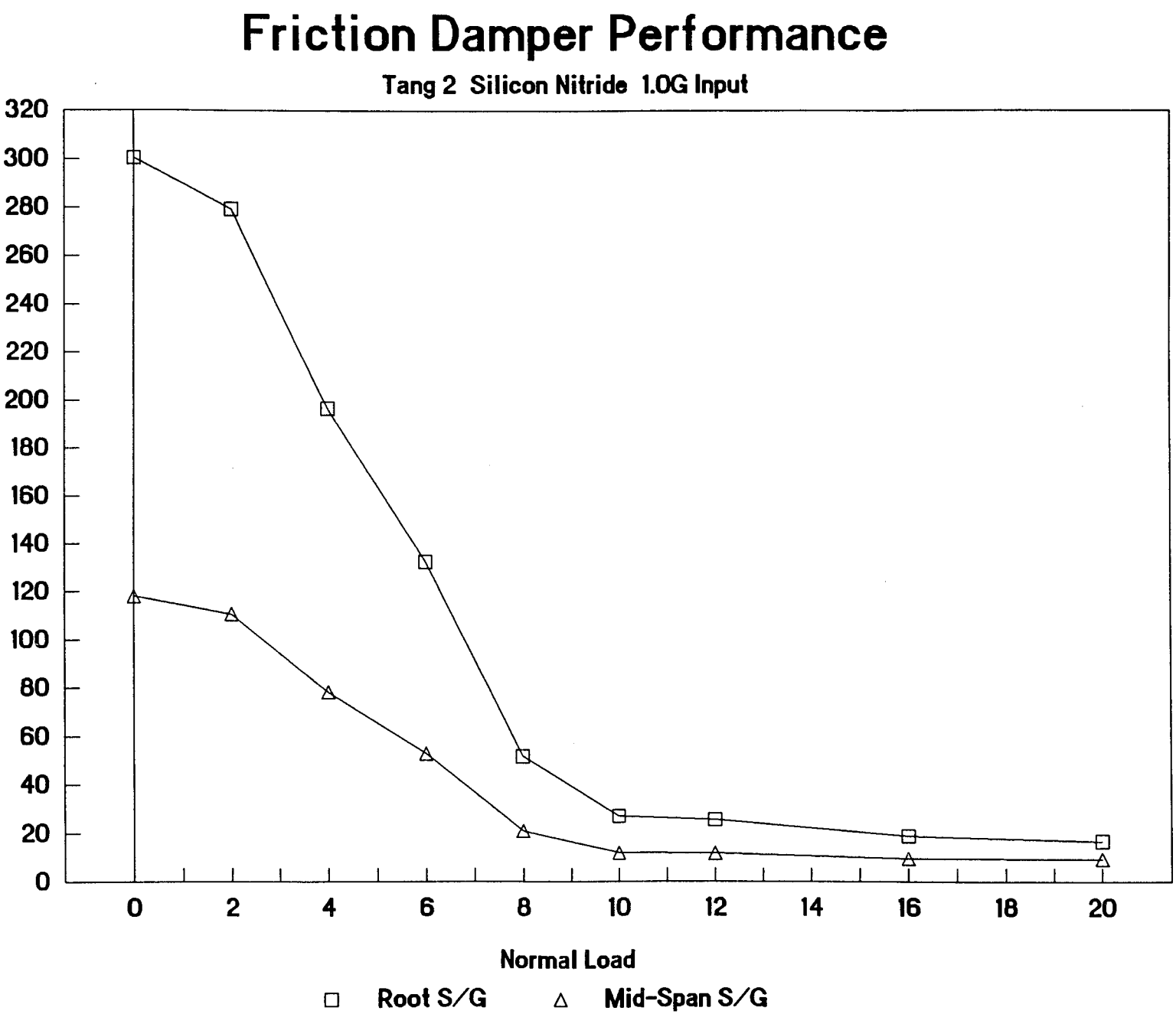

Figure 2.2-90 Low frequency beam optimization curve based on test data Silicon Nitride damper at tang 2, 1.0G input

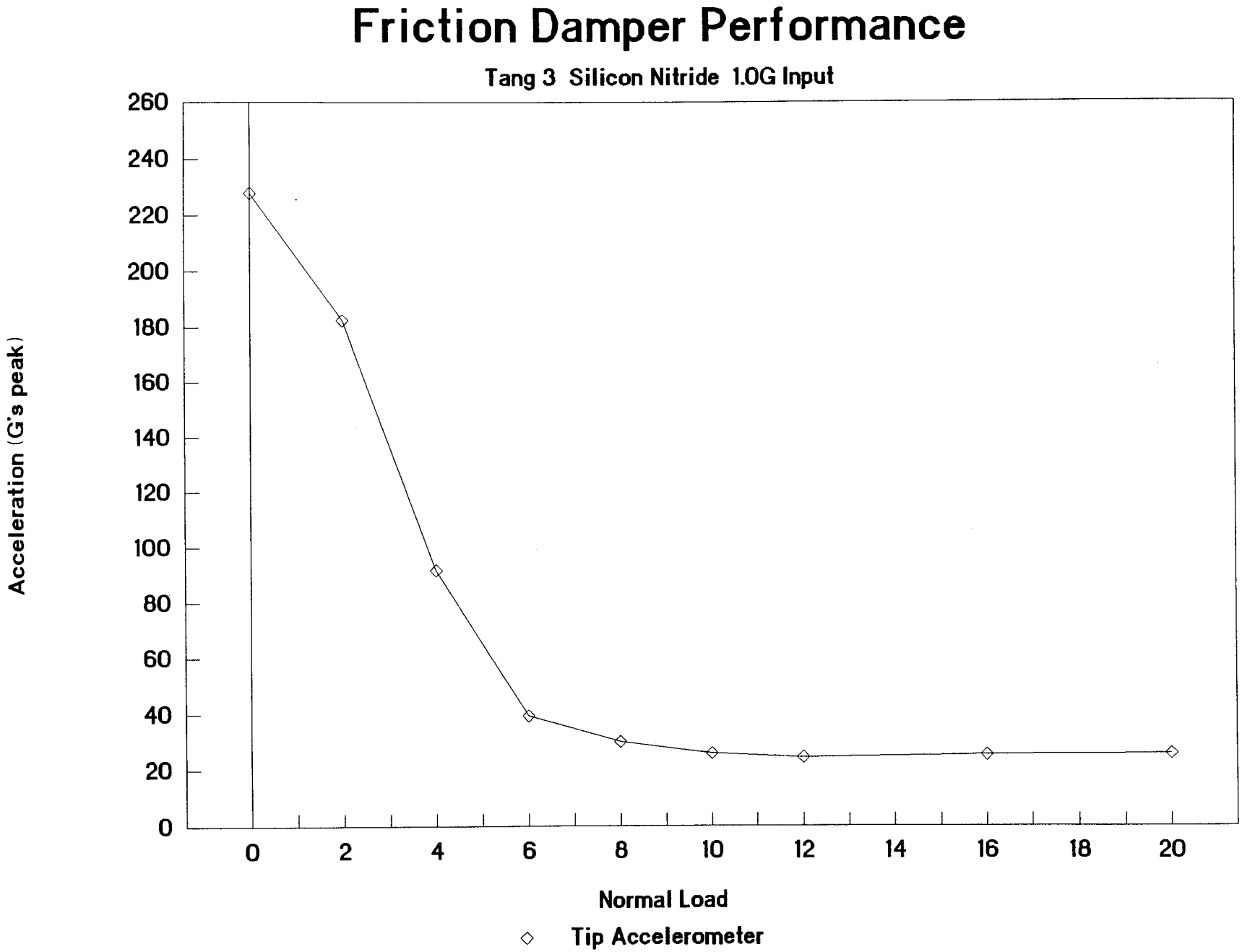

Figure 2.2-91 Low frequency beam optimization curve based on test data Silicon Nitride damper at tang 3, 1.0G input

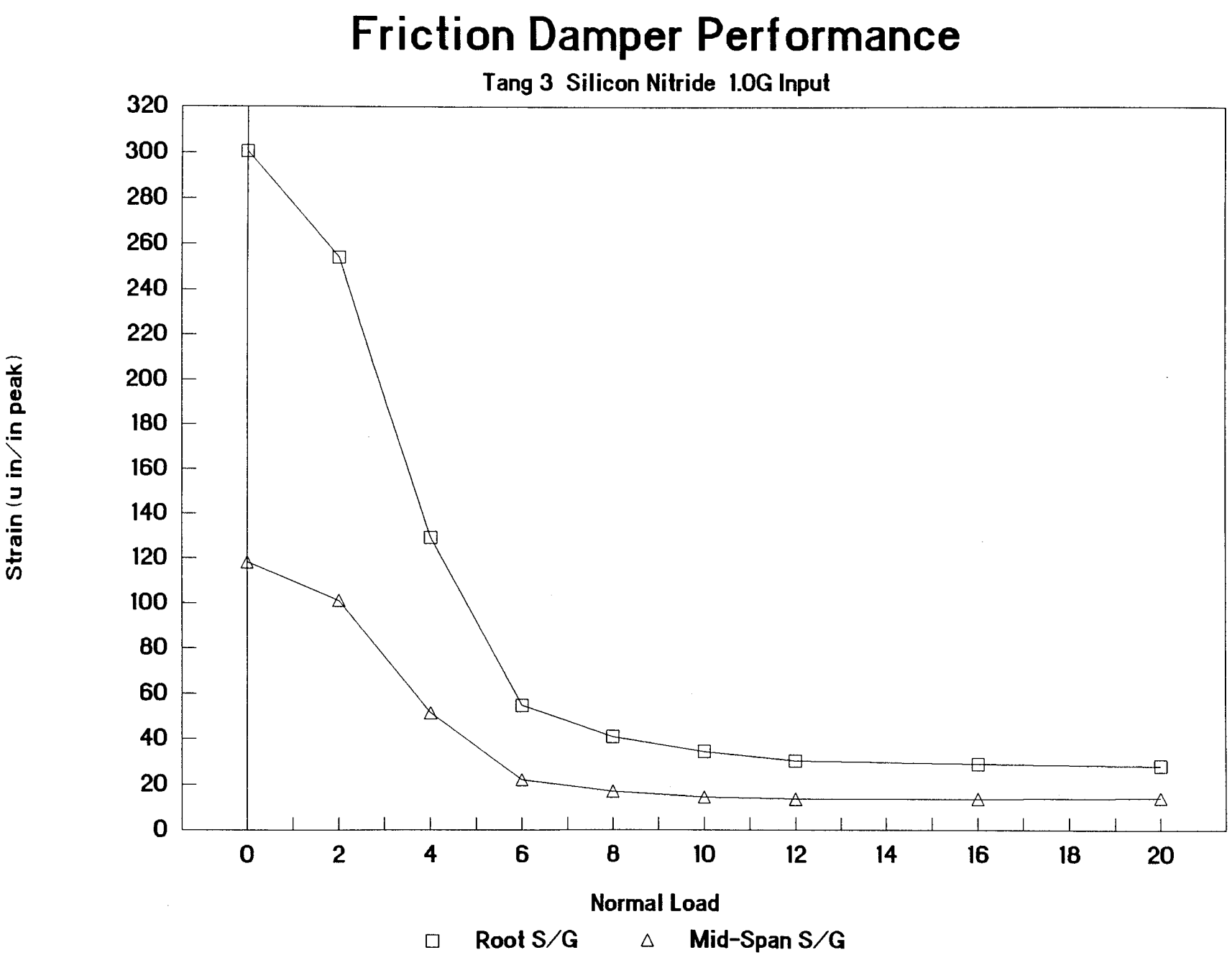

Figure 2.2-92 Low frequency beam optimization curve based on test data Silicon Nitride damper at tang 3, 1.0G input

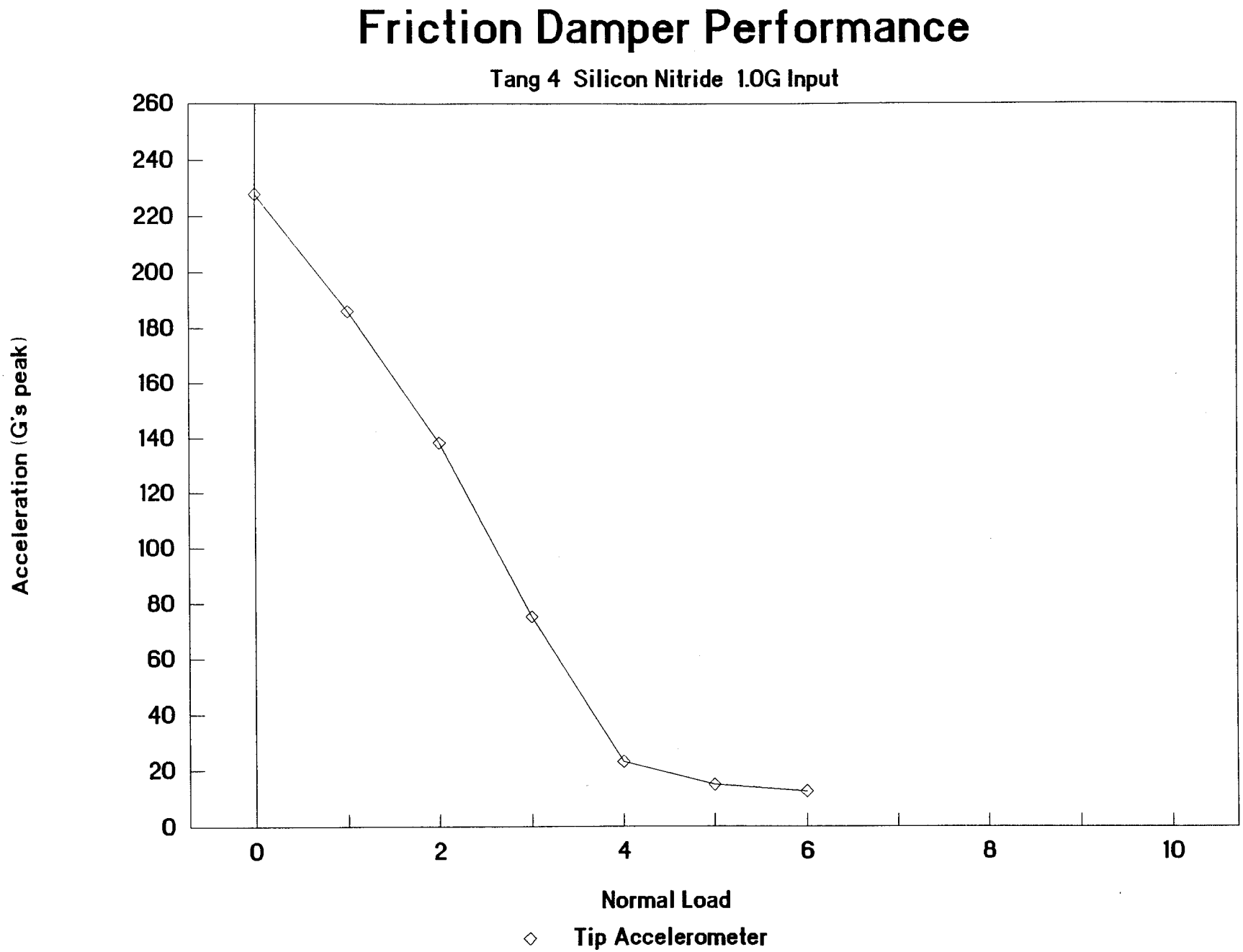

Figure 2.2-93 Low frequency beam optimization curve based on test data Silicon Nitride damper at tang 4, 1.0G input

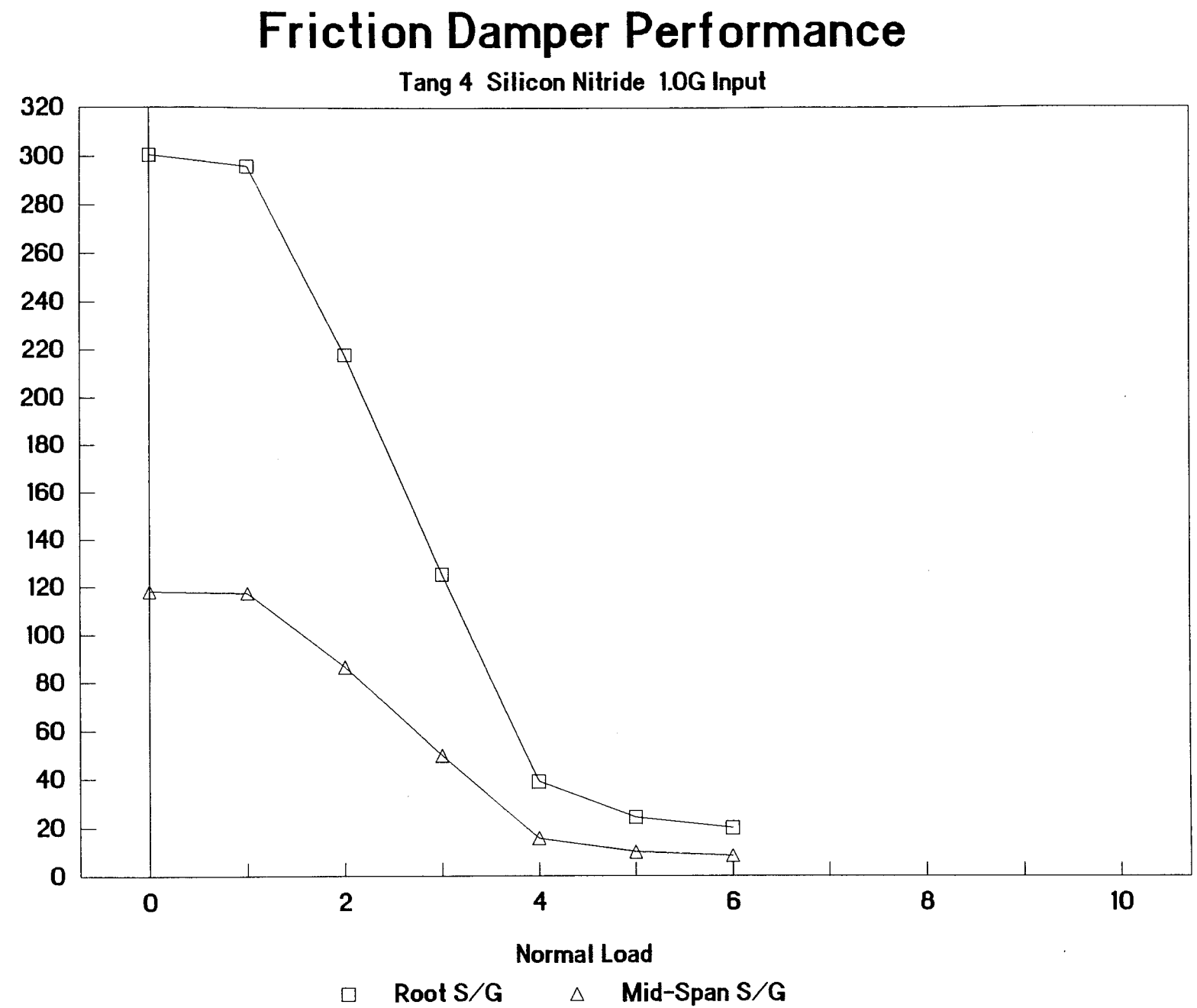

Figure 2.2-94 Low frequency beam optimization curve based on test data Silicon Nitride damper at tang 4, 1.0G input

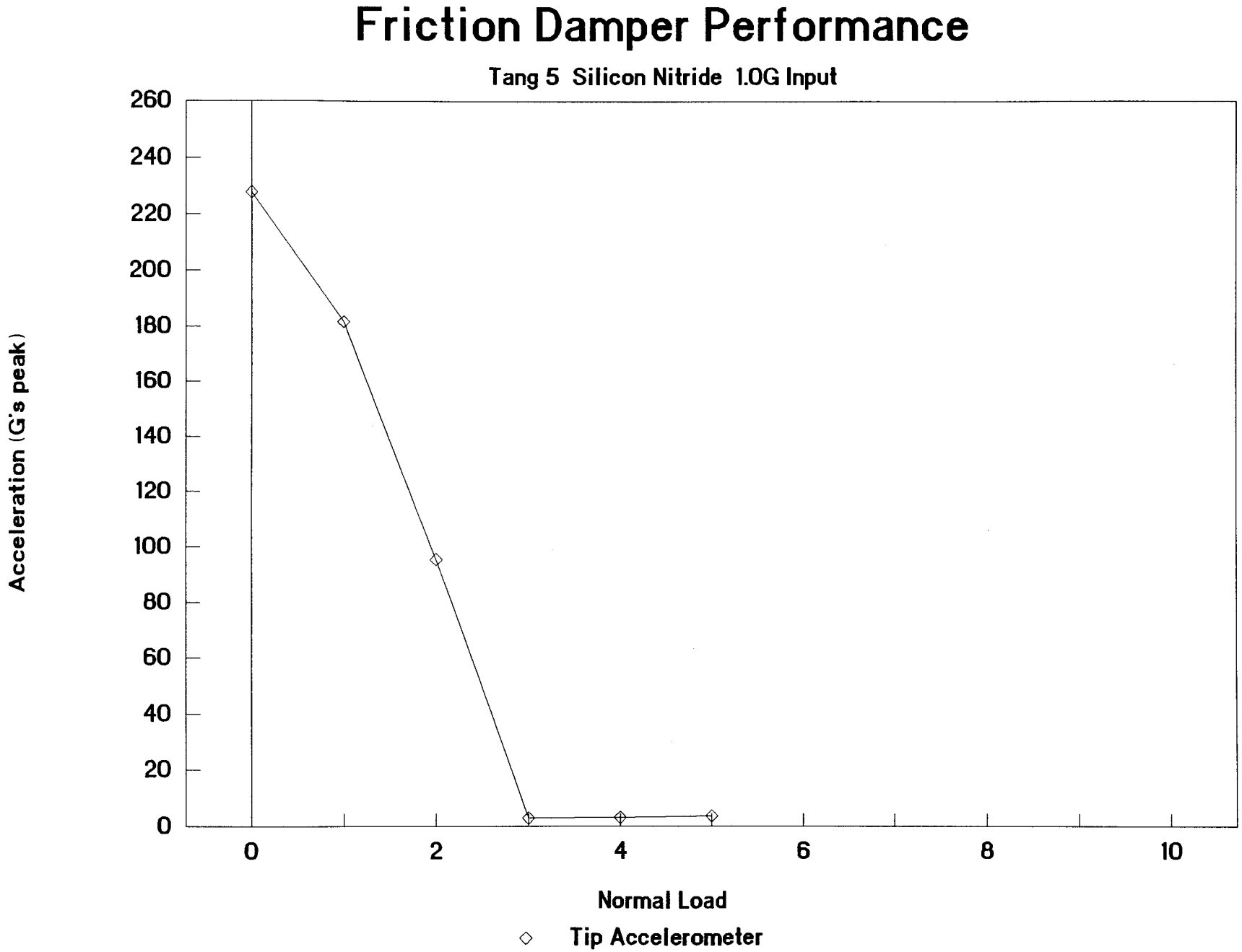

Figure 2.2-95 Low frequency beam optimization curve based on test data Silicon Nitride damper at tang 5, 1.0G input

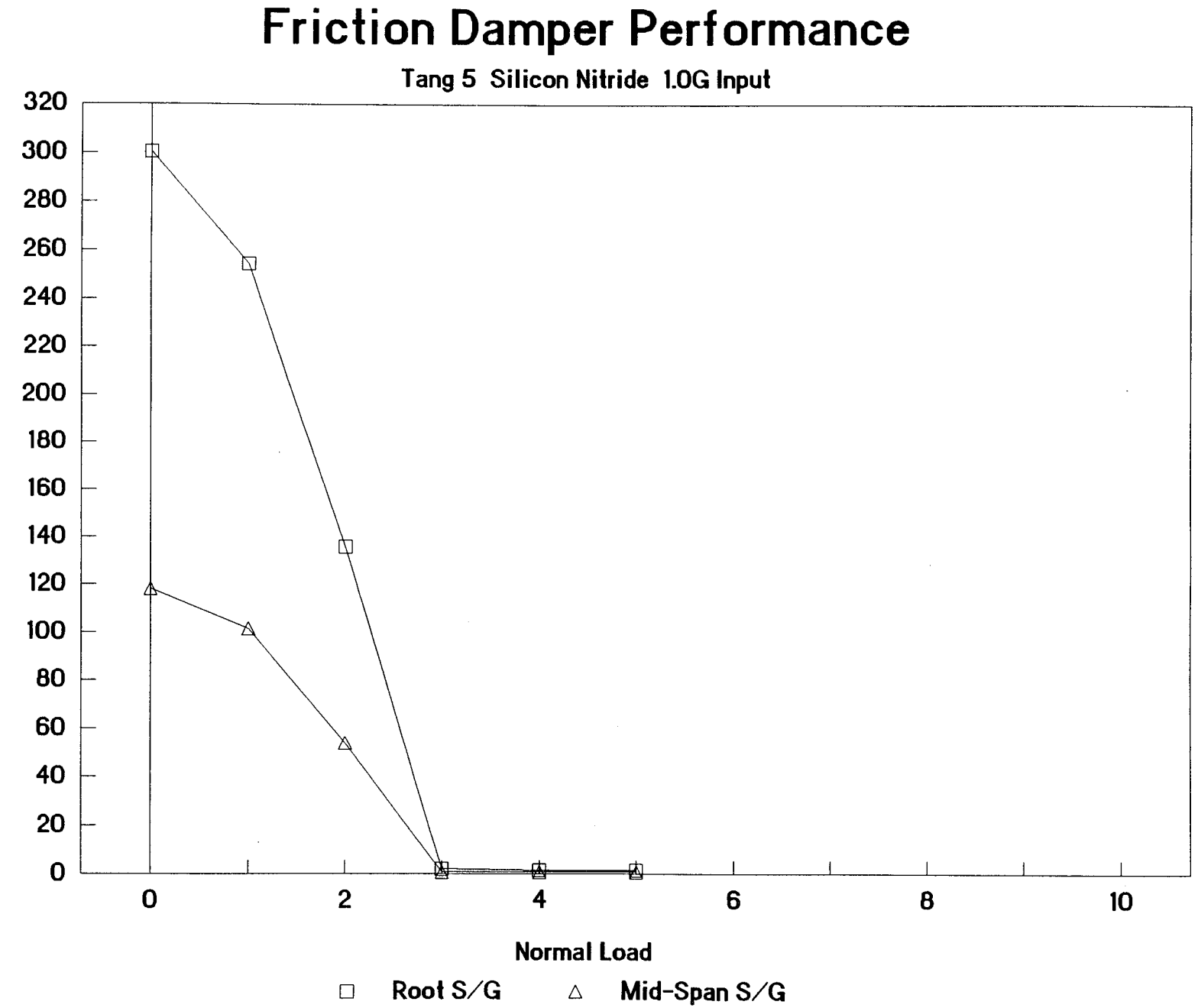

Figure 2.2-96 Low frequency beam optimization curve based on test data Silicon Nitride damper at tang 5, 1.0G input

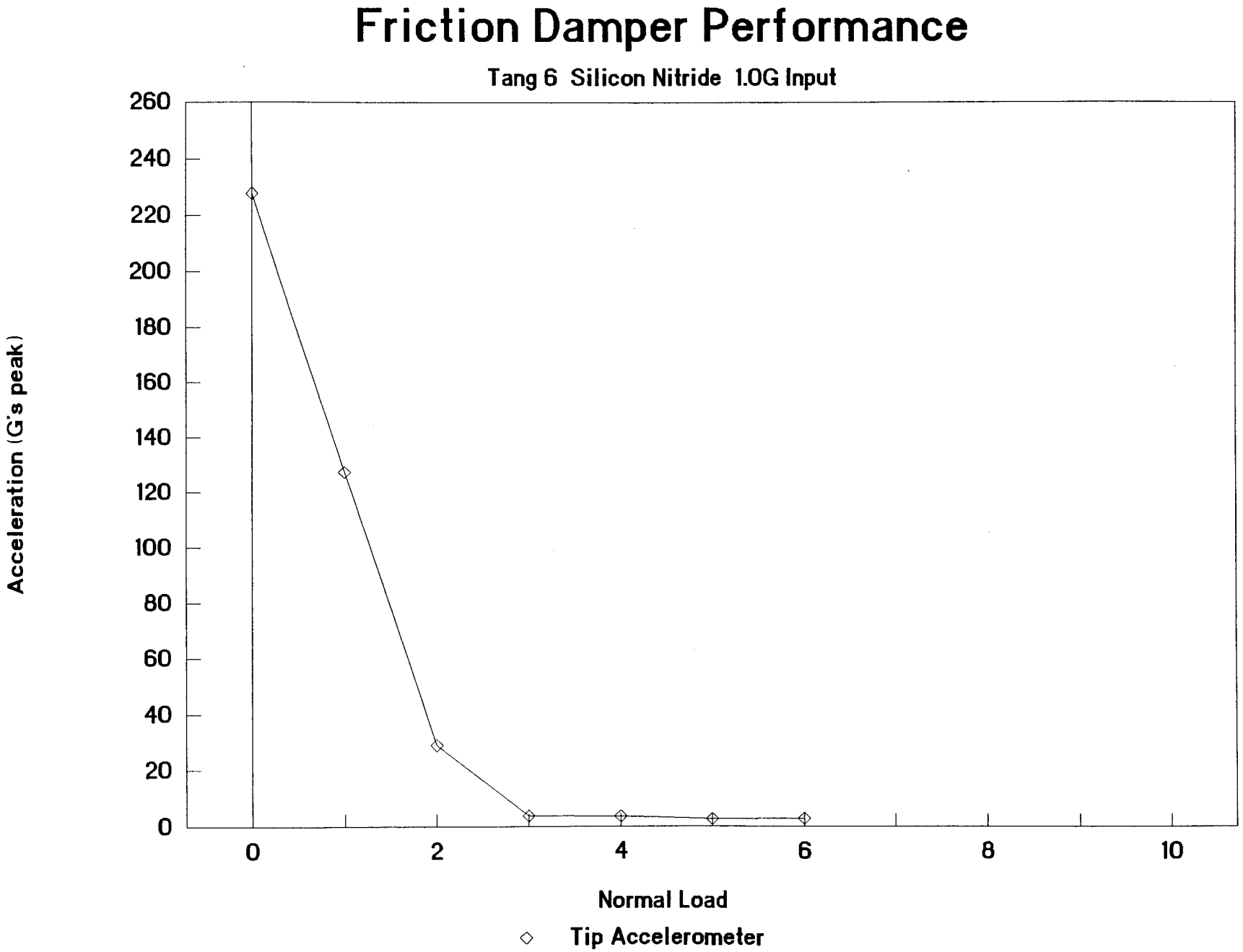

Figure 2.2-97 Low frequency beam optimization curve based on test data Silicon Nitride damper at tang 6, 1.0G input

FIGURE 11

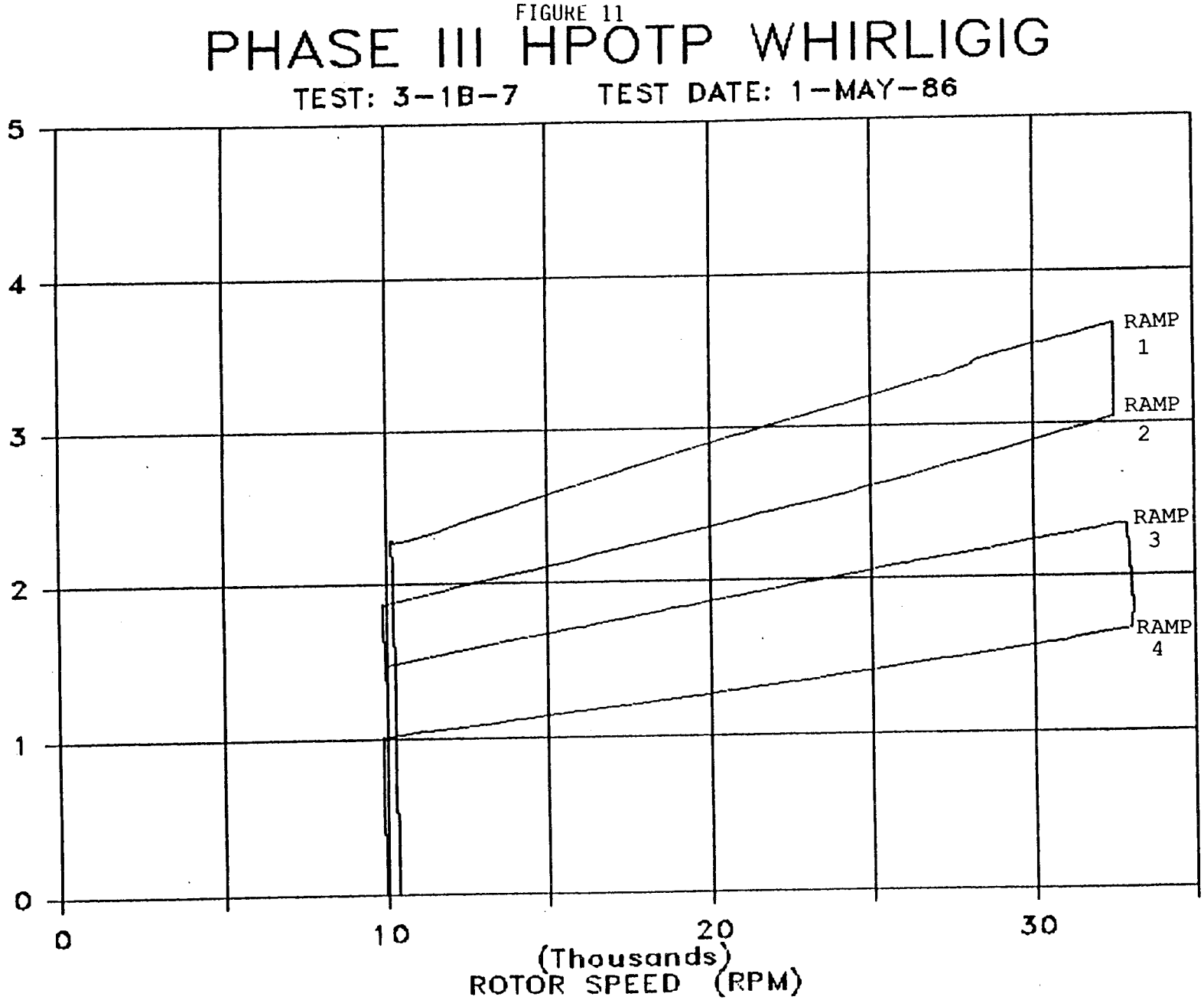

Figure 2.3-11 Peak blade jet force in spin test for 19N excitation, damped

FIGURE 14

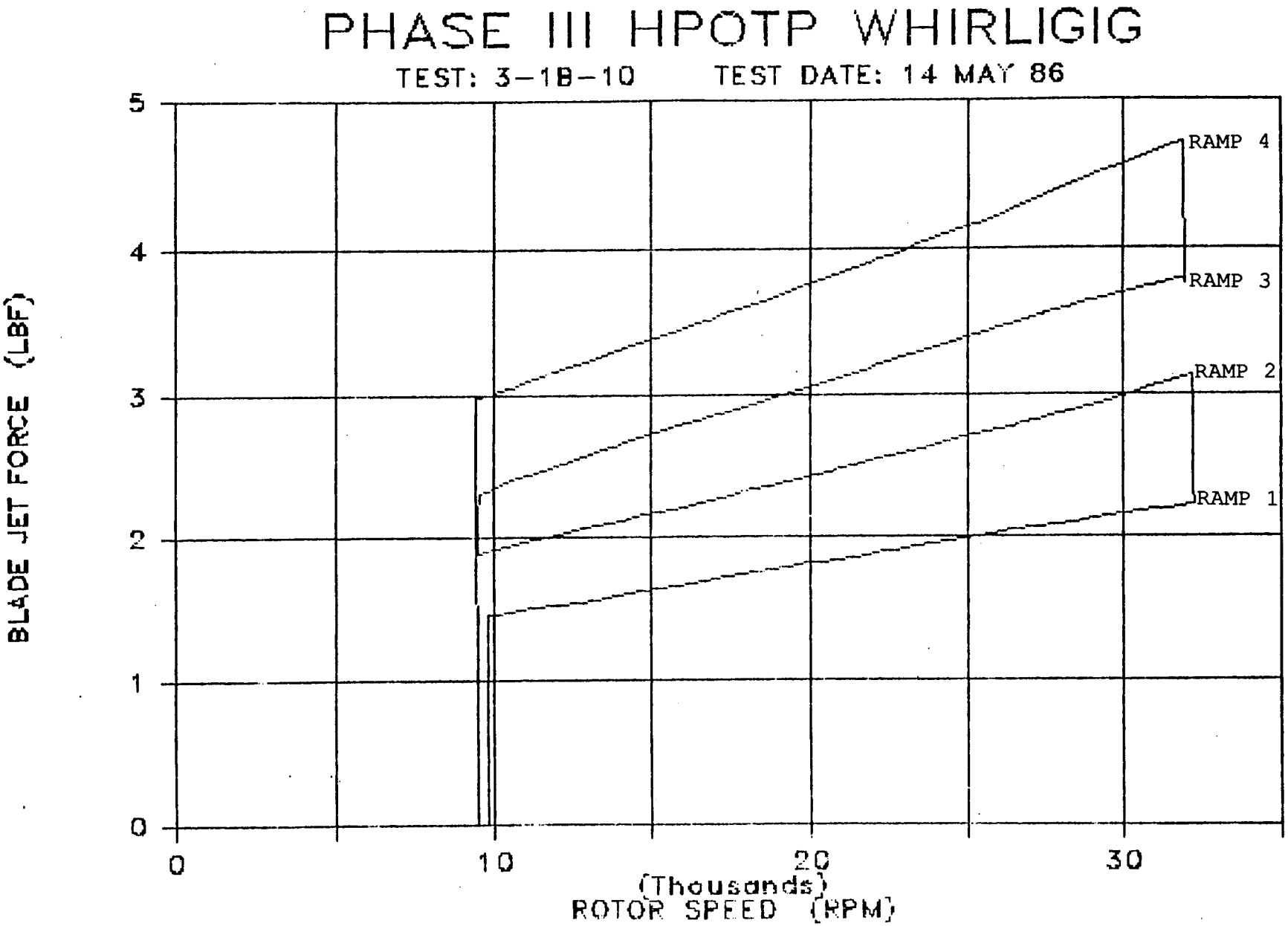

Figure 2.3-10 Peak blade jet force in spin test for 12N excitation, damped

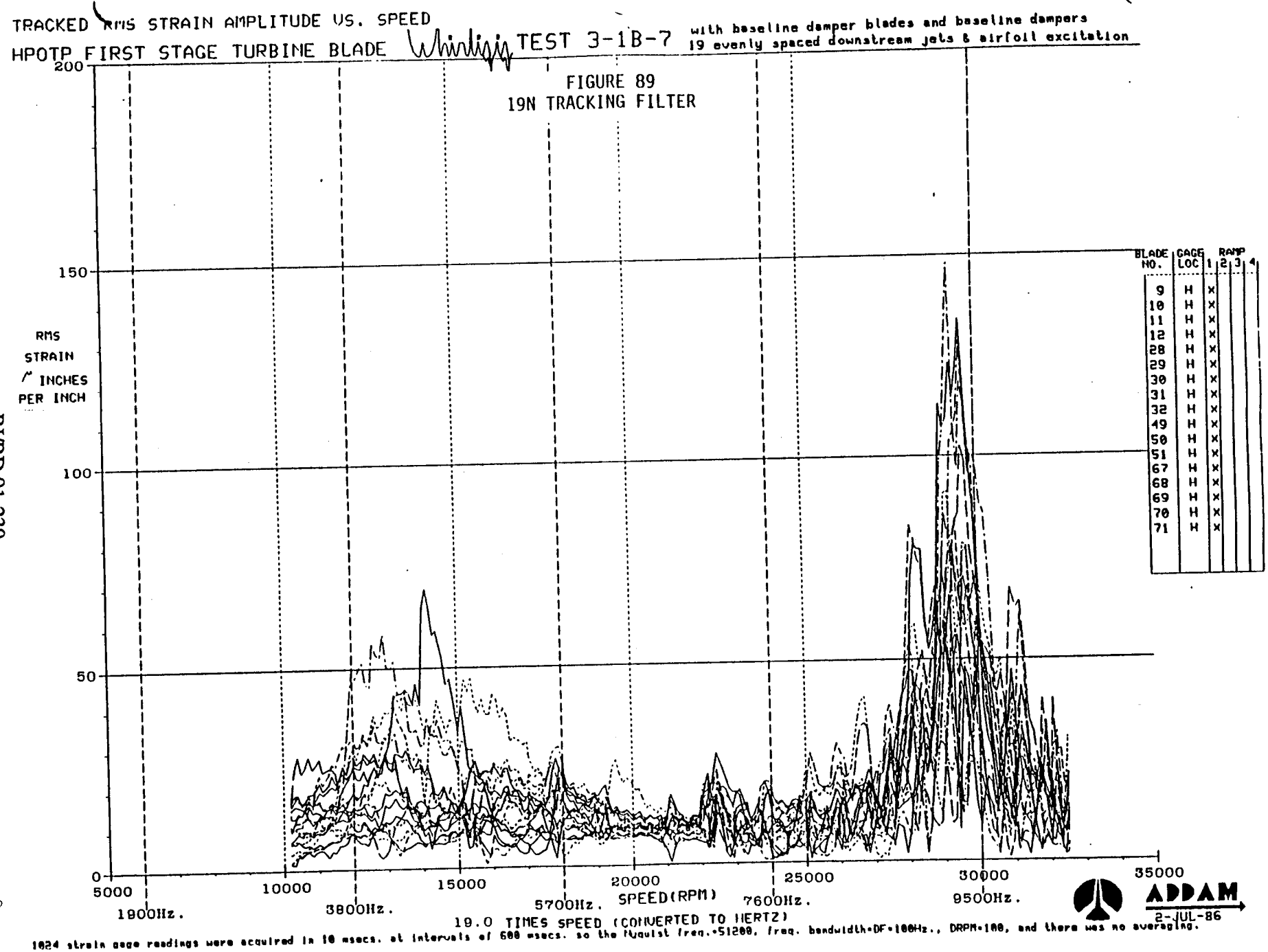

Figure 2.3-9 Spin test data for 19N excitation of mode #1 and mode #2, damped

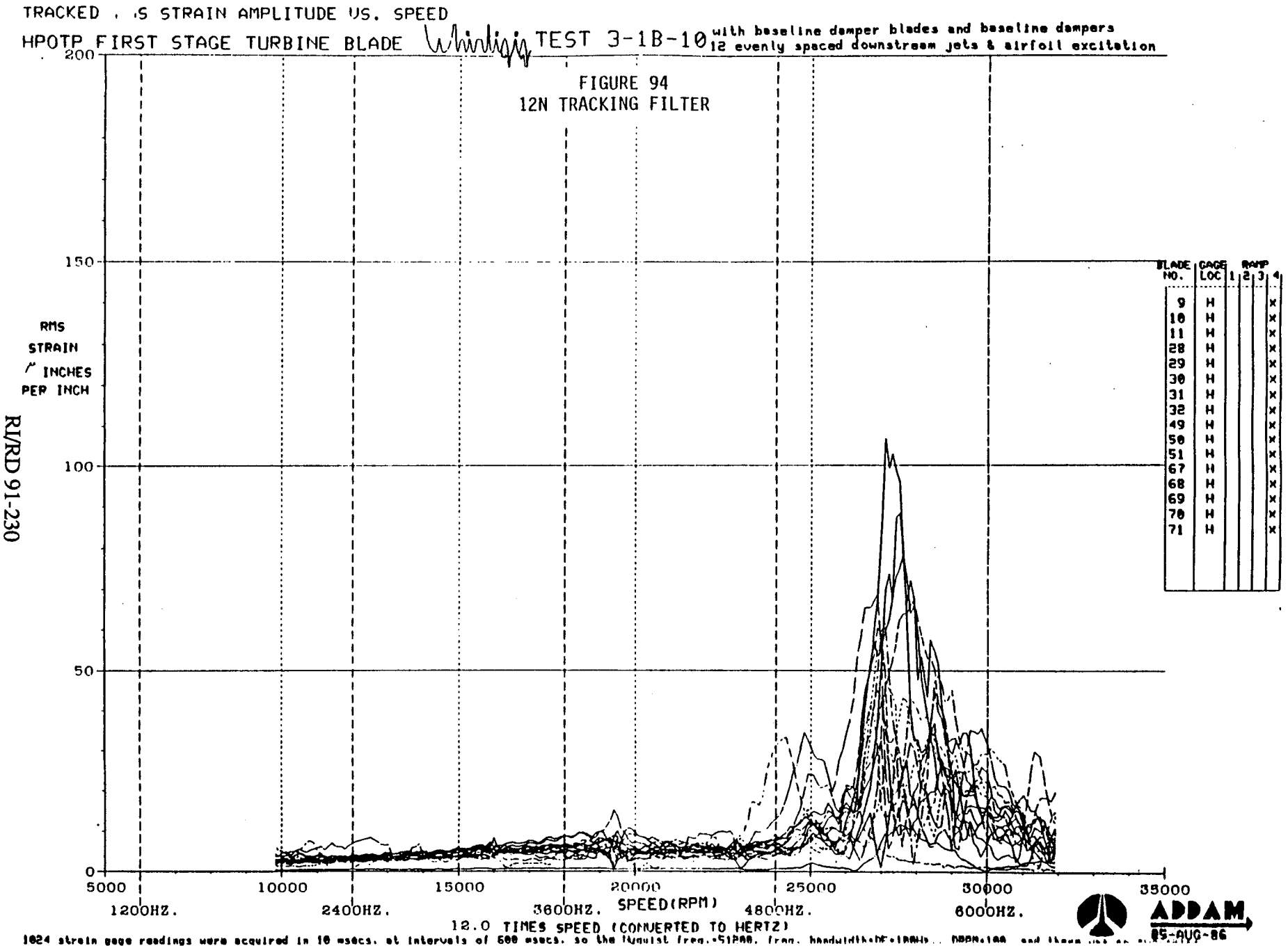

RJ/RD 91-230
153

Figure 2.3-8 Spin test data for 12N excitation of mode #1, damped

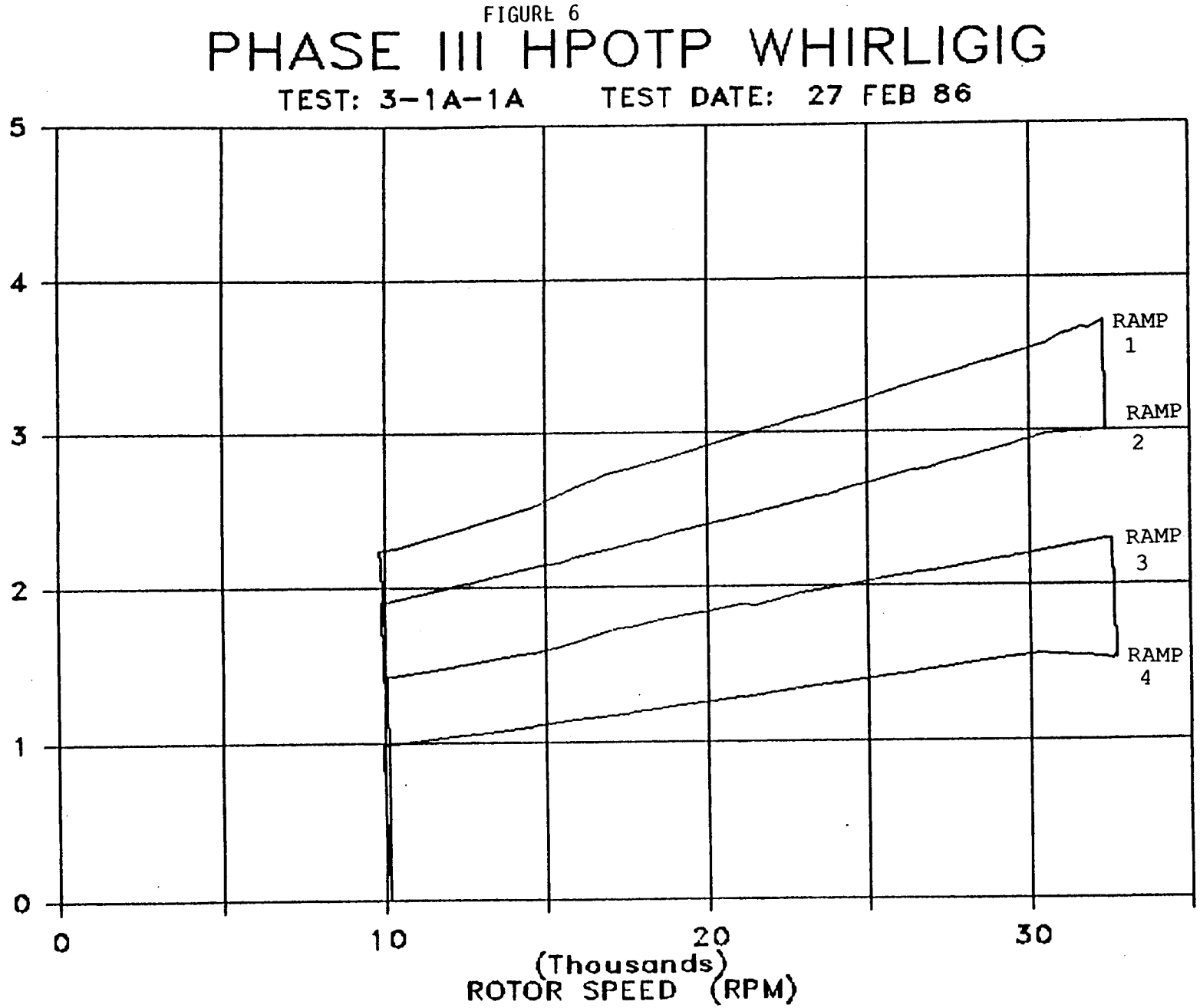

Figure 2.3-7 Peak blade jet force in spin test for 19N excitation, undamped

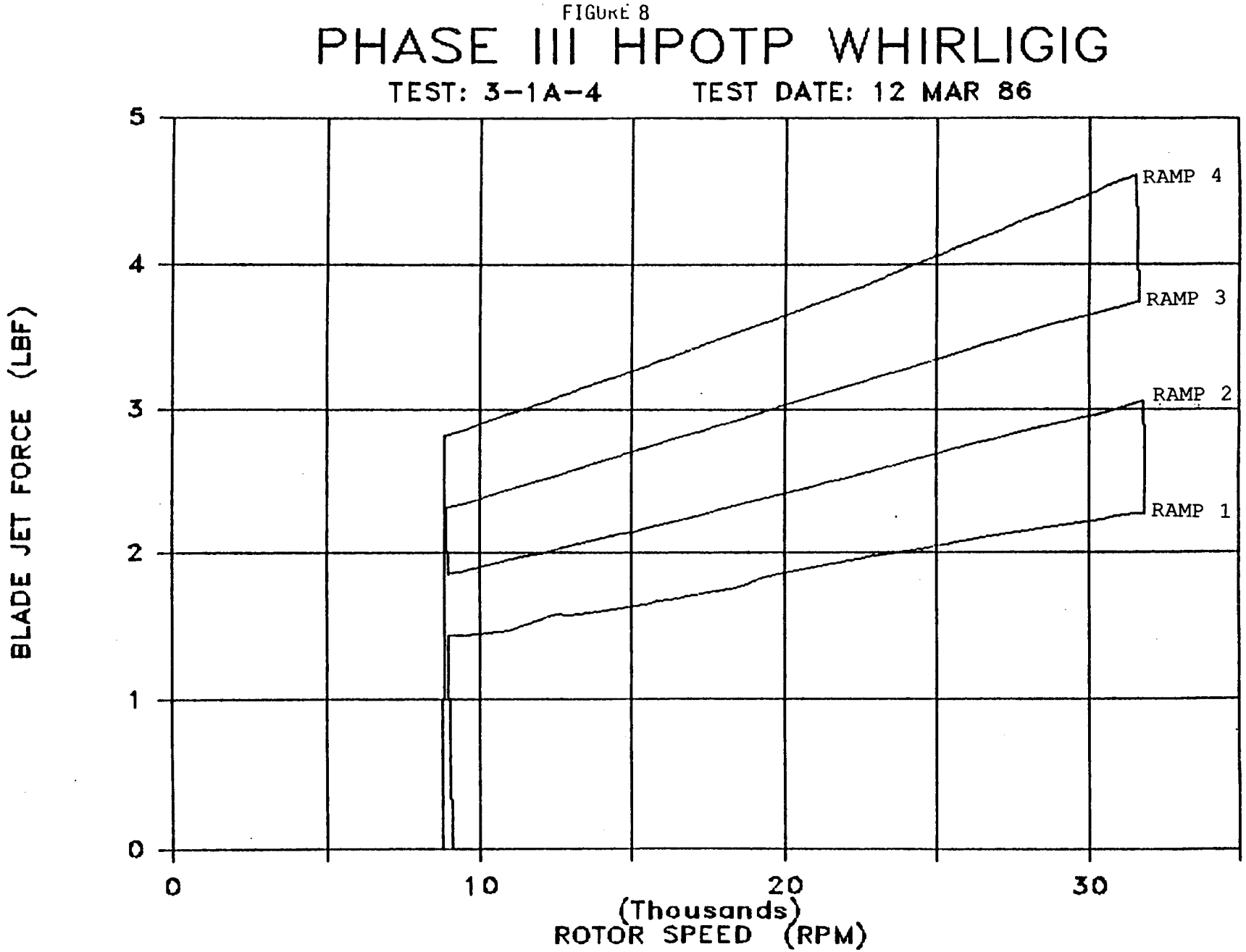

Figure 2.3-6 Peak blade jet force in spin test for 12N excitation, undamped

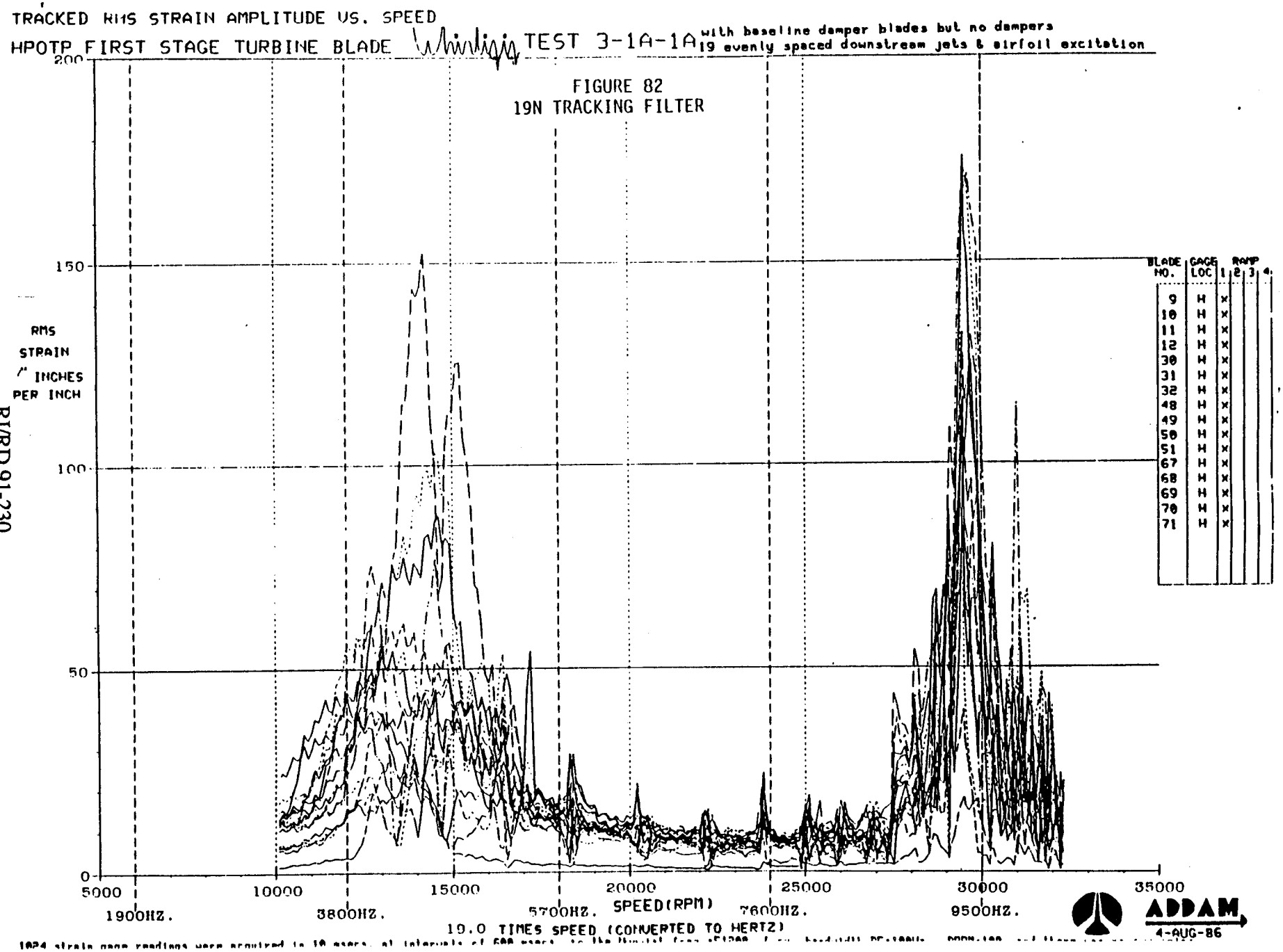

RI/RD 91-230
150

6

Figure 2.3-5 Spin test data for 19N excitation of mode #1

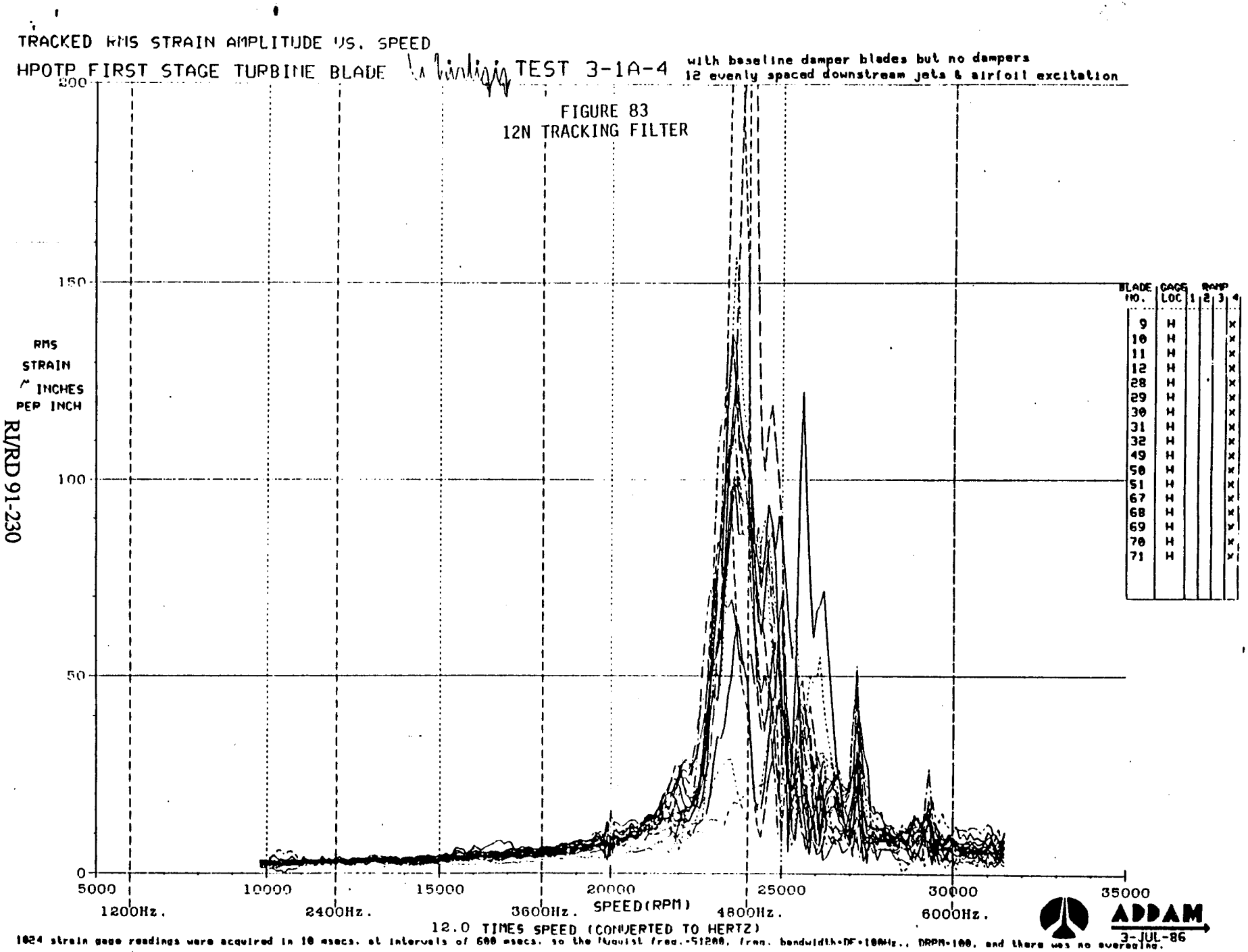

Figure 2.3-4 Spin test data for 12N excitation of mode #1, undamped

Figure 2.3-3 HPOTP blade and baseline damper

type. A coefficient of friction of 0.2 was used, based on the test/analysis comparison of Section 2.3-1. This coefficient is consistent with the material and surface finish of the blades and dampers.

The damper for the HPOTP first-stage blade is shown in Figure 2.3-3. It is a first-generation-type damper that stands vertically between the blades underneath the platforms. The damper is forced against the platforms of neighboring blades, with a total force of 38 lbs, and provides damping by frictional means during operation.

The primary modes of interest are the first two modes of the blade; the tangential mode and the axial mode. The natural frequency of the tangential mode, as measured in the spin test, is approximately 4,800 Hz. The natural frequency of the axial mode is approximately 9,500 Hz. This compares with the tangential and axial modes of the model, which are 5,089 Hz and 11,345 Hz, respectively. The first mode can be excited by the 12N excitation at approximately 24,000 rpm or by the 19N excitation at approximately 14,000 rpm. The second mode can be excited by the 19N excitation at approximately 30,000 rpm. Spin test data for the HPOTP first-stage blades without dampers is shown in Figures 2.3-4 and 2.3-5. The corresponding peak jet forces are shown in Figures 2.3-6 and 2.3-7. Data from ramp number 4 (test 3-1A-4, 12N excitation, undamped) and ramp number 1 (test 3-1A-1A, 19N excitation, undamped case) were used for the comparison. The corresponding friction-damped test data are shown in Figures 2.3-8 through 2.3-11.

An initial run of the program BLDAMP was made to find the generalized force scaling factor, due to the estimation of the peak jet forces. This was done so that analysis results would match test data for the undamped case. The case of 19N excitation of the axial mode was used as the scaling point. A generalized force scaling factor of 3.02 was calculated for this case. This factor was then used for the remaining cases. A parametric study was then performed using various damper stiffnesses, once the generalized forces were fixed. The case of 12N excitation of the tangential mode was used to determine this parameter. Results are shown in Figure 2.3-13. The graph shows that the undamped data point (damper force = 0.0) agrees very well with test data. Also, the parametric data shows that a damper stiffness of 20,000 lb/in agrees very well with the friction-damped test data. The response curve in Figure 2.3-13 can be compared to the test data in Figure 2.3-8. This again shows the friction-damped amplitudes to be very close. The program BLDAMP predicted a shift in frequency of resonant response of approximately 4 percent for this case. The test data shows a shift of approximately 12 percent.

The case of 19N excitation of the axial mode is shown in Figure 2.3-14. The undamped test data matches the analysis exactly, because the generalized force was scaled from this case. The friction-damped case also agrees quite well with the test data. The response curve in Figure 2.3-15 can be compared to the test data in Figure 2.3-9. The program BLDAMP predicted a shift in frequency of resonant response of approximately one percent for this case. The test data also shows a negligible shift in frequency.

The case of 19N excitation of the tangential mode is show in Figure 2.3-16. The graph shows that the undamped data point is somewhat higher than test data. This could be caused by the equivalent viscous damping in the blade being higher than the one percent used in the analysis. This data point is taken at a much lower speed. The equivalent viscous damping could be higher, because the blade is not fully locked in the fir-tree area. However, the friction-damped response agrees well with the test data. To get a more realistic comparison, the case could be rerun with the generalized force adjusted, so that the undamped case matches test data. The response curve in Figure 2.3-17 can be compared to the test data in figure 2.3-9. The program BLDAMP predicted a shift in frequency of

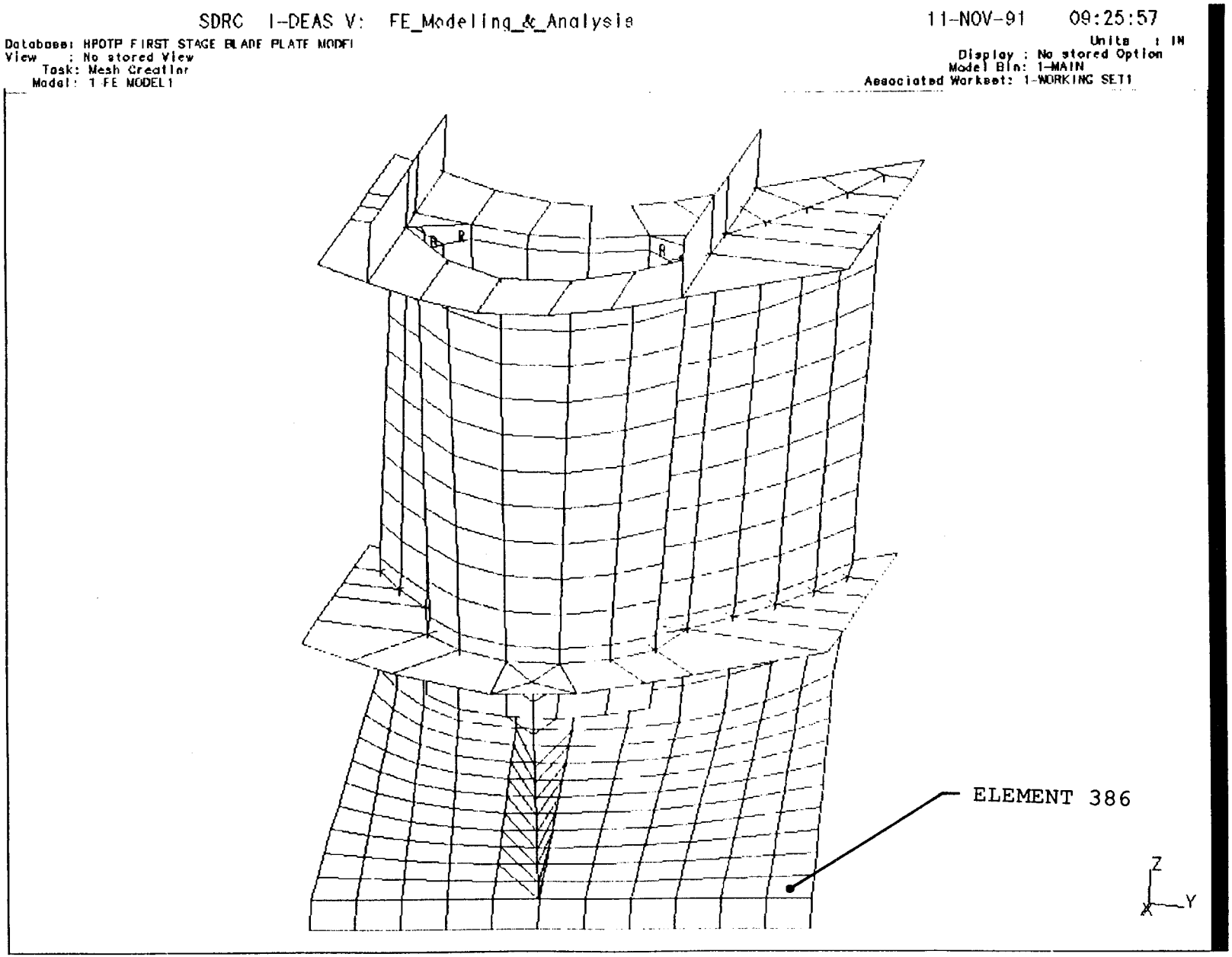

Figure 2.3-2 HPOTP finite element model used for modal data

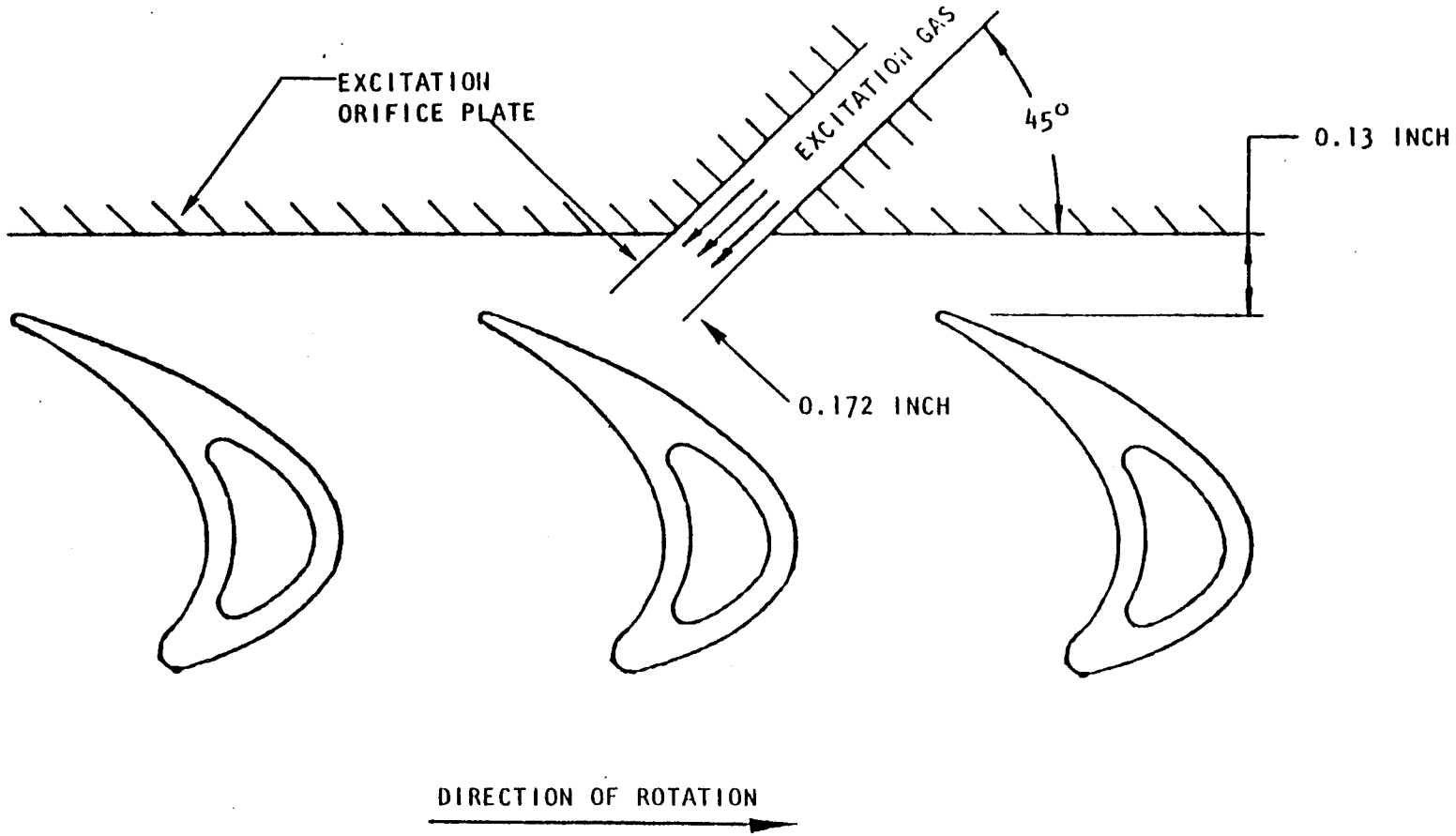

Figure 2.3-1 Spin test jet excitation geometry

Figures 2.2-40, 2.2-41, and 2.2-44 for the high-frequency beam. Results show the silicon nitride damper required a higher value of friction force to achieve the same reduction in vibration amplitude as the Haynes 188 damper. This indicates that silicon nitride has a lower coefficient of friction. The test/analysis match for the low-frequency beam, with the damper at tang 1, gives a friction coefficient of $\mu = 0.05$ (see Figure 2.2-30). This value is approximately four times less than the Haynes 188 friction coefficient, under the same test conditions. This is in disagreement with the results predicted in Section 2.2.2.3, which are based on data of a better quality than that used here.

2.3.2 Spin Test Comparison

The test results from a Rocketdyne High-pressure Oxidizer Turbopump (HPOTP) first-stage blade (P/N RS007707) spin test (see Reference 1) were compared to predictions from the program BLDAMP. The comparison showed good agreement between test and analysis results. However, the analytical predictions were highly dependent on damper stiffness. Since the HPOTP first-stage blade damper stiffness was not readily available, this parameter was used to tune the analytical model to match test data for one condition. Two other conditions, utilizing the same damper stiffness as in the first condition, also matched data very well. In addition, this comparison shows the degree to which the damper has been optimized.

The Rocketdyne spin pit accomodates a turbomachinery shaft, disk, and turbine blades. This assembly is spun up to operational speeds in a vacuum by an electric motor. Various fluid forces can be placed on the blades by means of nitrogen gas jets. In one test series, 12 evenly spaced jets of gas were directed onto the trailing edges of the HPOTP first-stage turbine blades. A schematic of the jet configuration is shown in Figure 2.3-1. In another test series, 19 evenly spaced jets were directed onto the blades. The blade response is measured by strain gages placed on the blades. The strain gage wires are attached to a slip ring, that allows the signal to be sent from the rotating blades to the stationary test equipment.

The program BLDAMP and a HPOTP first-stage blade finite-element model were used to analytically predict the friction-damped response. The finite-element model is a STARDYNE plate model (shown in Figure 2.3-2). The turbine blade model is fixed at the root. Modal data from the model were used as input to the BLDAMP program. Modal stresses were obtained from the trailing-edge root, pressure side location (element number 386 shown in Figure 2.3-2). This location matches the strain gage location in the spin test data.

Generalized forces for each mode are also needed as input to the BLDAMP program. Because the blade will have peak responses only when it is being forced at one of its natural frequencies, only the harmonic components of force that match the natural frequencies of the blade need to be input to BLDAMP. First, the peak jet-pulse force on a blade was estimated, using hydrodynamic principles. Then, because the harmonic components of a pulse are dependent on jet spacing, a Fourier series decomposition was performed for the 12 jets and 19 jets, individually. The first harmonic of the 12 jets was found to be 0.09163 for a unit pressure pulse, while the first harmonic for 19 jets was 0.14383. The peak jet force is multiplied by the harmonic factor to give the harmonic force. The generalized forces were obtained by first matrix-multiplying the modal vectors with a unit vector, in the direction of the jet force, and then multiplying that resulting vector by the harmonic force.

Equivalent viscous damping of 1 percent was used in the analysis to represent damping due to fir-tree motion and losses in the blade material. This value is typical for hardware of this

2.3 COMPARISON OF ANALYSIS AND TEST RESULTS

2.3.1 Nonrotating Beam Comparison

The friction damping test results of Section 2.2.1 were compared with analytical predictions made using the the computer program BLDAMP, described in Section 2.1. This comparison showed good agreement between test and analytical results. However, the analytical predictions were highly dependent on friction coefficient. Since friction coefficients were not readily available for the materials used in the test program, this parameter was used to tune the results to match test data.

Validation of the computer code was accomplished by creating finite-element models of the two beams, analytically simulating their response, and comparing analytical results to test data. Modal parameters of the two test beams and stiffness properties of the damper were input to BLDAMP to obtain the damper performance curves, which are presented in Figures 2.2-28 through 2.2-44. These figures also contain plots of the test data, as was discussed previously. A sensitivity study was performed, with friction coefficient as the variable parameter, to obtain a good analytical match with the test data. This parameter was adjusted until the results from BLDAMP closely matched test results, since friction coefficients are not well known. This match is clearly shown in Figure 2.2-28, where the test and analytical results from the low-frequency beam with the Haynes 188 damper are compared, for three different values of friction coefficient. This figure indicates the best match was found by choosing $\mu = 0.2$ as the friction coefficient. The test was then repeated at a higher G level, since friction damping is a nonlinear phenomenon. The test/analysis comparison was then made, using the same friction coefficient found in the previous lower-level test. This comparison is presented in Figure 2.2-29. The comparison shows a good match between test and analysis results. A similar procedure was performed for the high-frequency beam with the Haynes 188 damper, the results of which are shown in Figure 2.2-38. Here, the friction coefficient necessary for a good test/analysis match was $\mu = 0.05$, which is unrealistically low and does not agree with the value obtained in the low-frequency beam tests. Subsequent testing of the same configuration at a higher vibration level gave the results shown in Figure 2.2-39. The coefficient of friction used in this figure is the same as was obtained from the low-level testing and yields a poor comparison with the test data. The poor comparison observed is probably due to damper chatter and nonsinusoidal motion of the shaker, which was prevalent on this beam. Therefore, for this reason, the test data for the high-frequency beam should be regarded as indicative of general trends only and these test data should not be used for detailed comparison with analytical results.

A possible explanation, for the abnormally low friction coefficient found for the short beam (Figure 2.2-38), is that the damper may not have been in contact with the beam, during the entire cycle of vibration. As mentioned previously, when the beam passed through the resonant frequency, a loud noise emanated from the damper area and the damper tended to wander in a direction parallel to the damper knife-edge slot. It was difficult to keep the damper centered in the slot. Subsequent inspection of the dampers indicated considerable wear at the damper/test beam interface. The wear pattern observed on the dampers was not indicative of tangential sliding motion, as would be expected. The pattern suggested the damper was beating against the beam in a direction normal to the contact surface. It is believed the damper was not in contact with the beam, during the entire vibration cycle. Since the analysis assumes damper contact at all times, a lower coefficient of friction would be required to match the test data, which was taken with only partial contact.

A comparison of the silicon nitride damper test data with analytical results is shown in Figures 2.2-30, 2.2-31, 2.2-34, 2.2-35, and 2.2-37 for the low-frequency beam and in

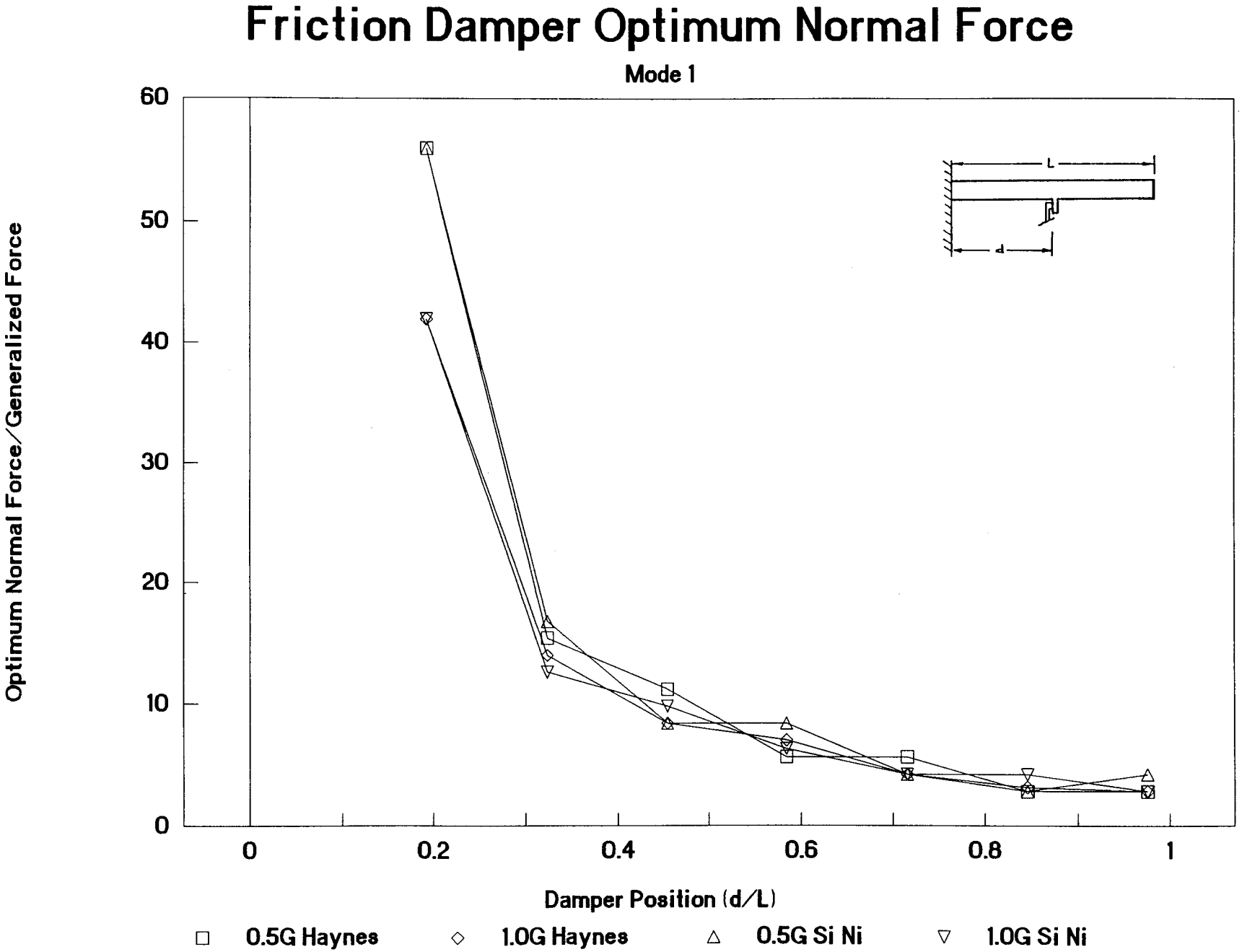

Figure 2.2-107 Optimum normal force as a function of damper position

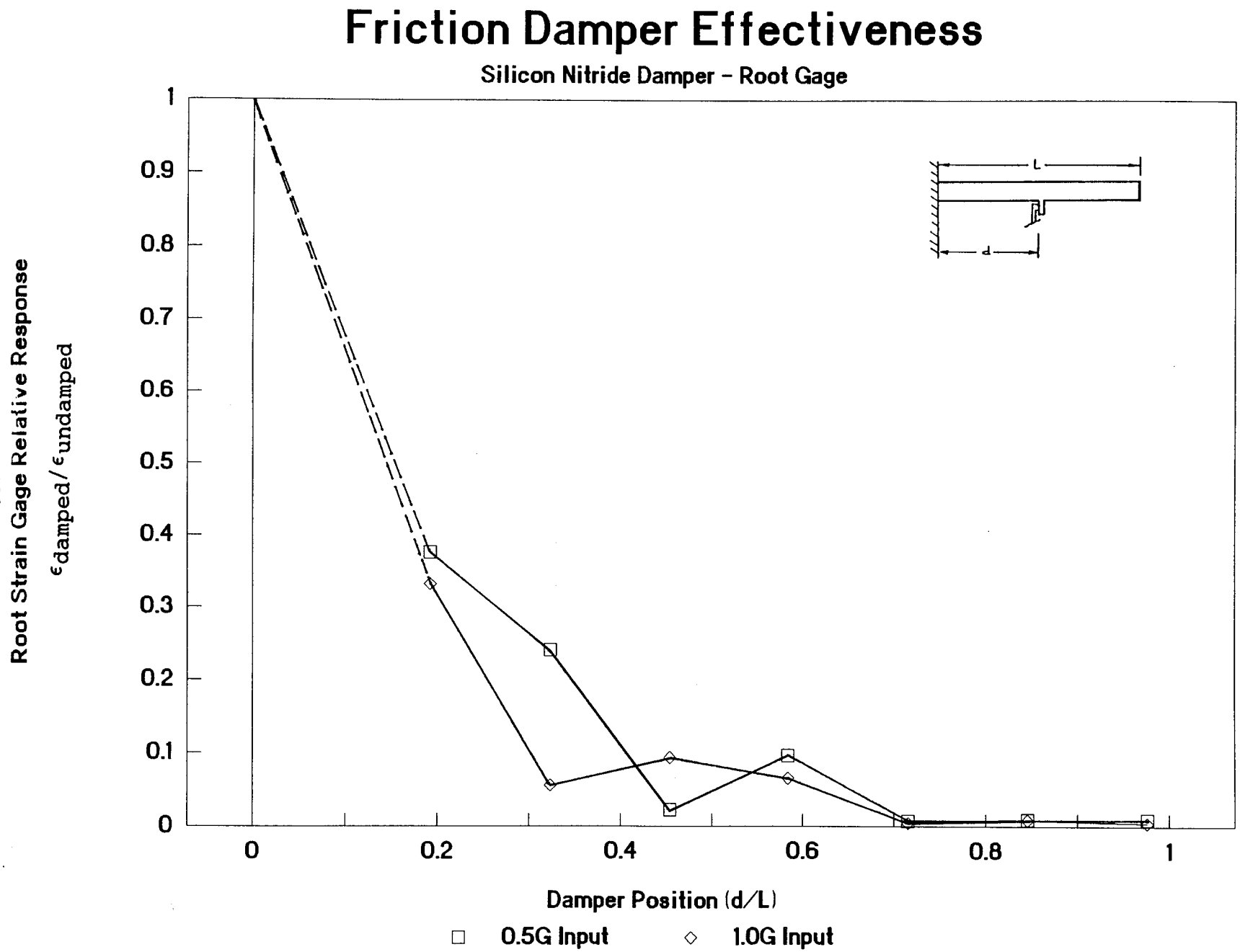

Figure 2.2-106 Relative response of beam as measured by the root strain gage for Silicon Nitride damper

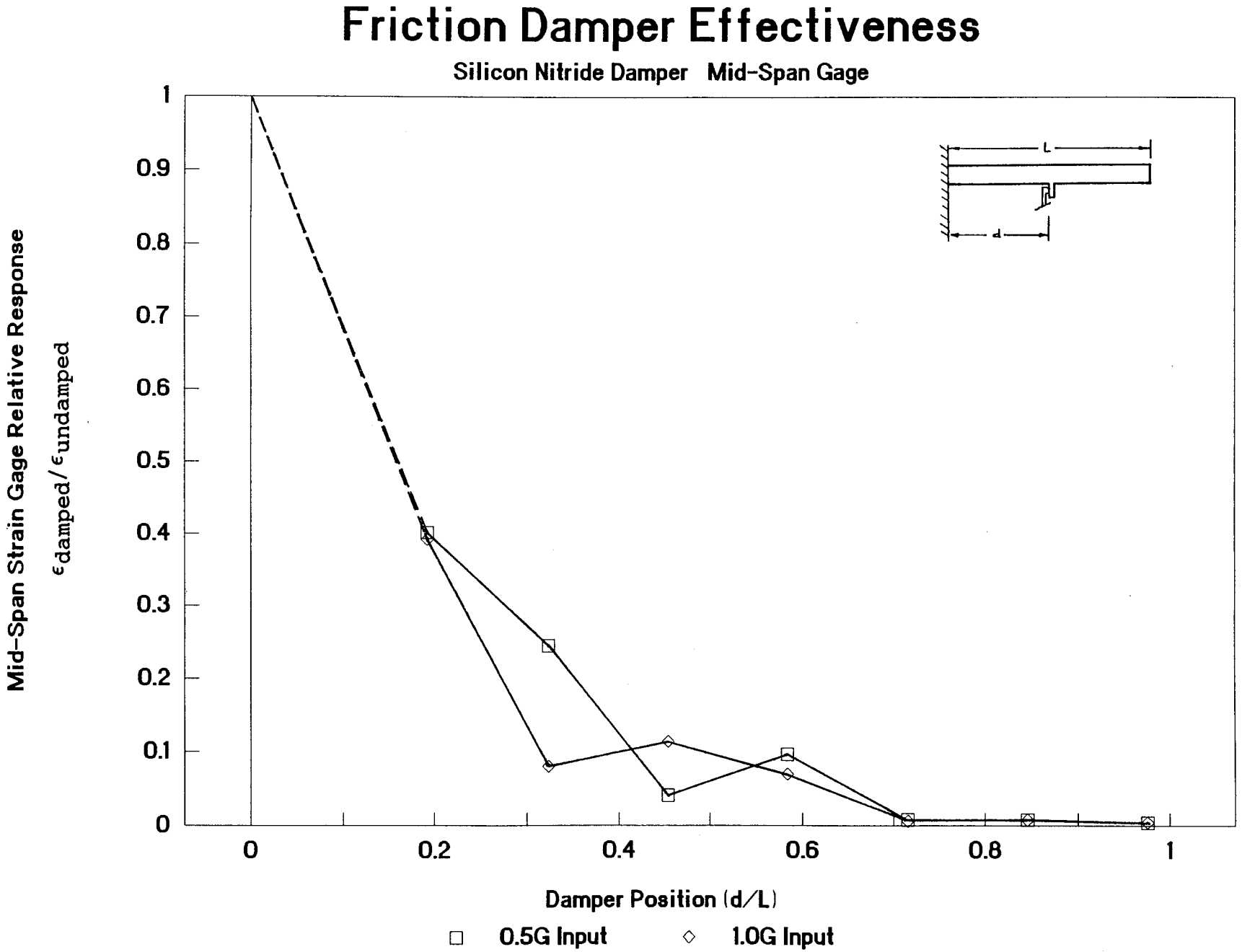

Figure 2.2-105 Relative response of beam as measured by the mid-span strain gage for Silicon Nitride damper

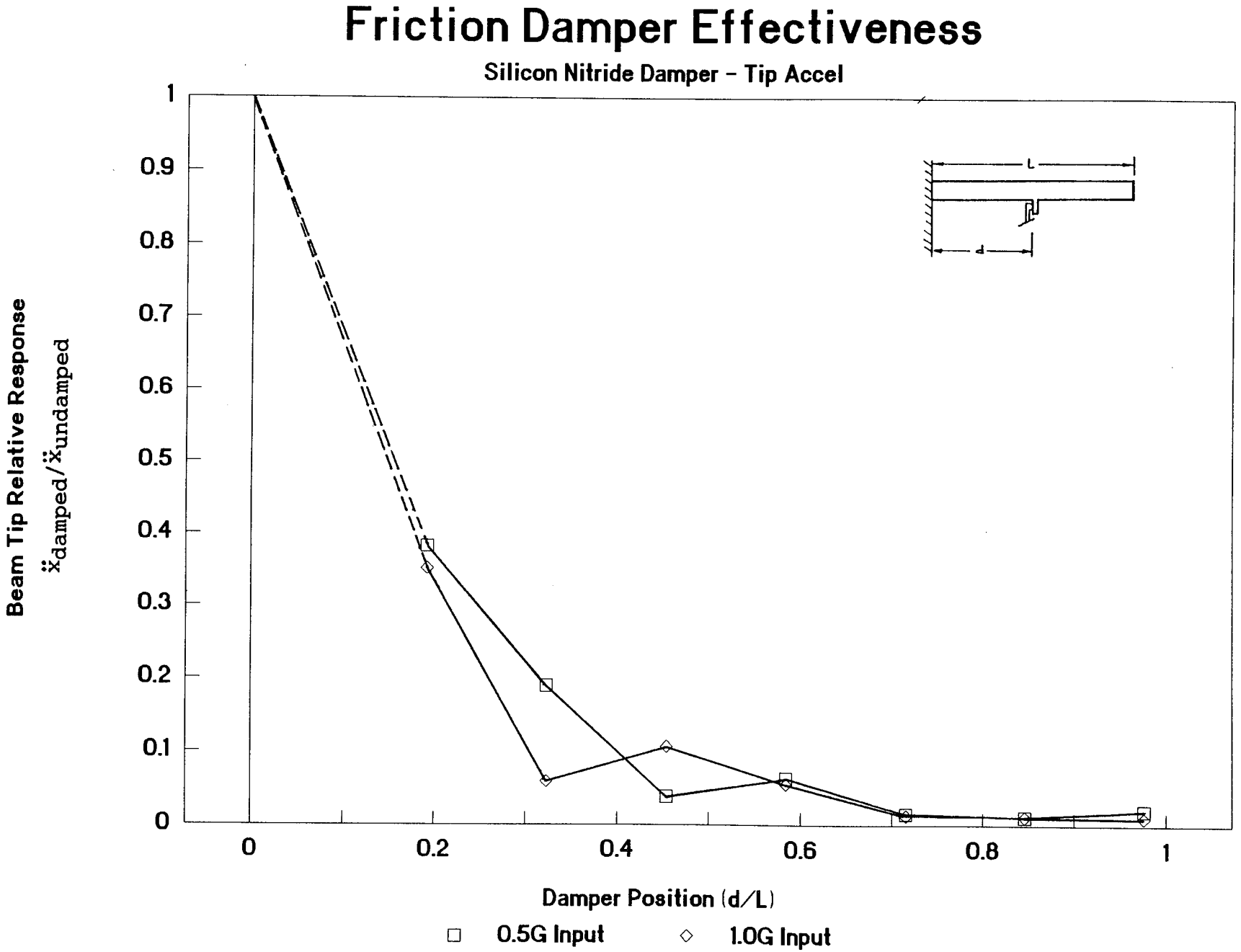

Figure 2.2-104 Relative response of beam tip as a function of damper position for Silicon Nitride damper

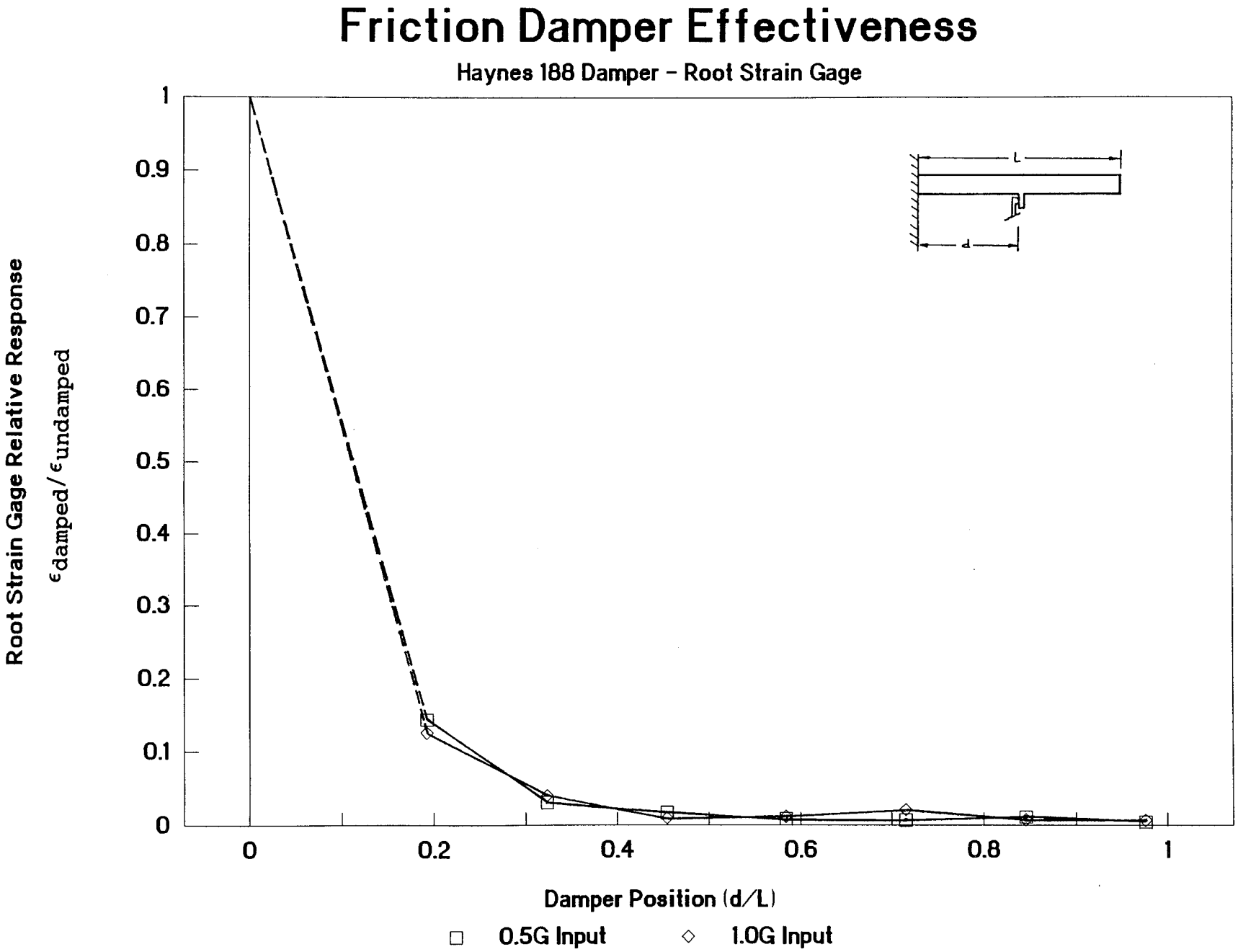

Figure 2.2-103 Relative response of beam as measured by the root strain gage for Haynes 188 damper

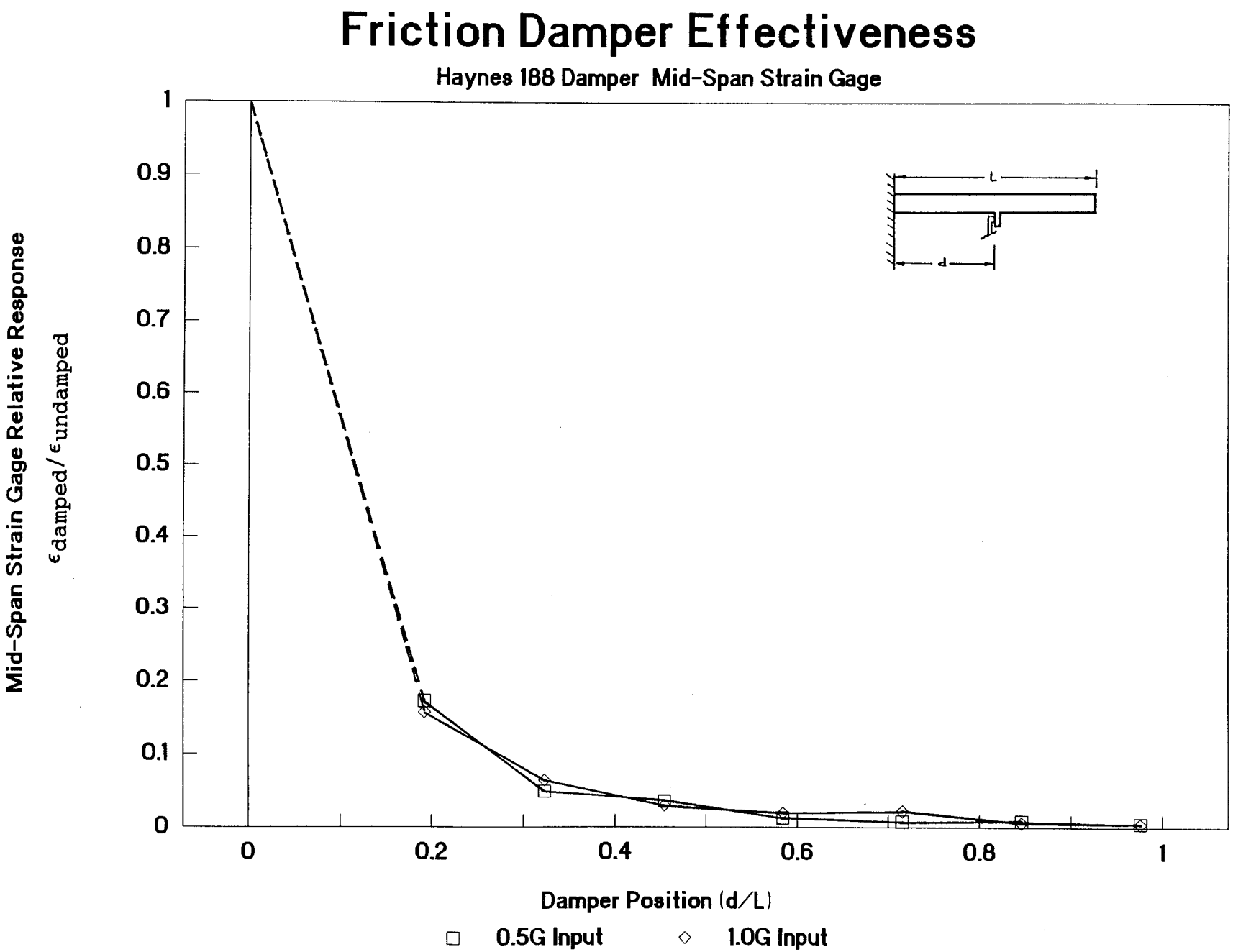

Figure 2.2-102 Relative response of beam as measured by the mid-span strain gage for Haynes 188 damper

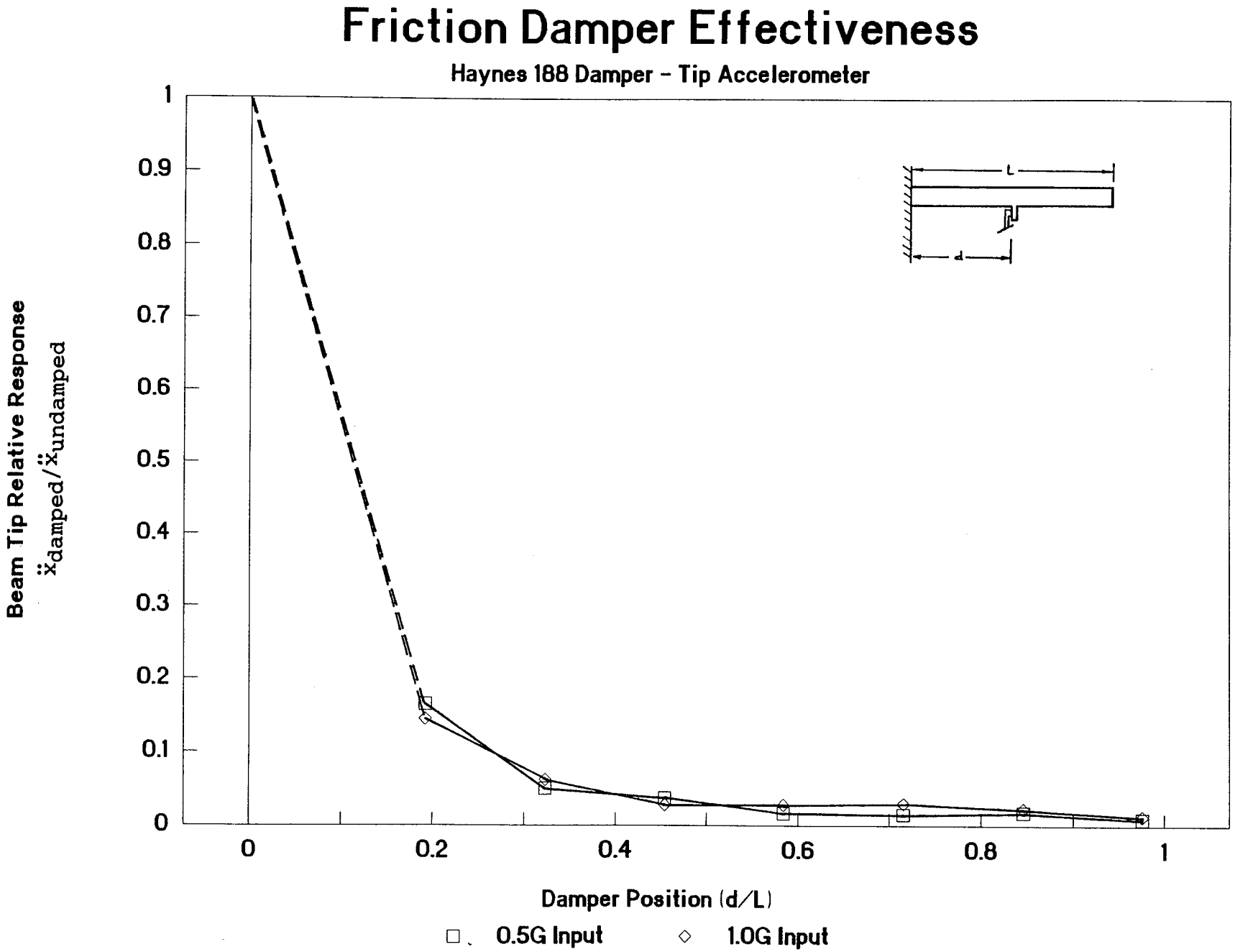

Figure 2.2-101 Relative response of beam tip as a function of damper position for Haynes 188 damper

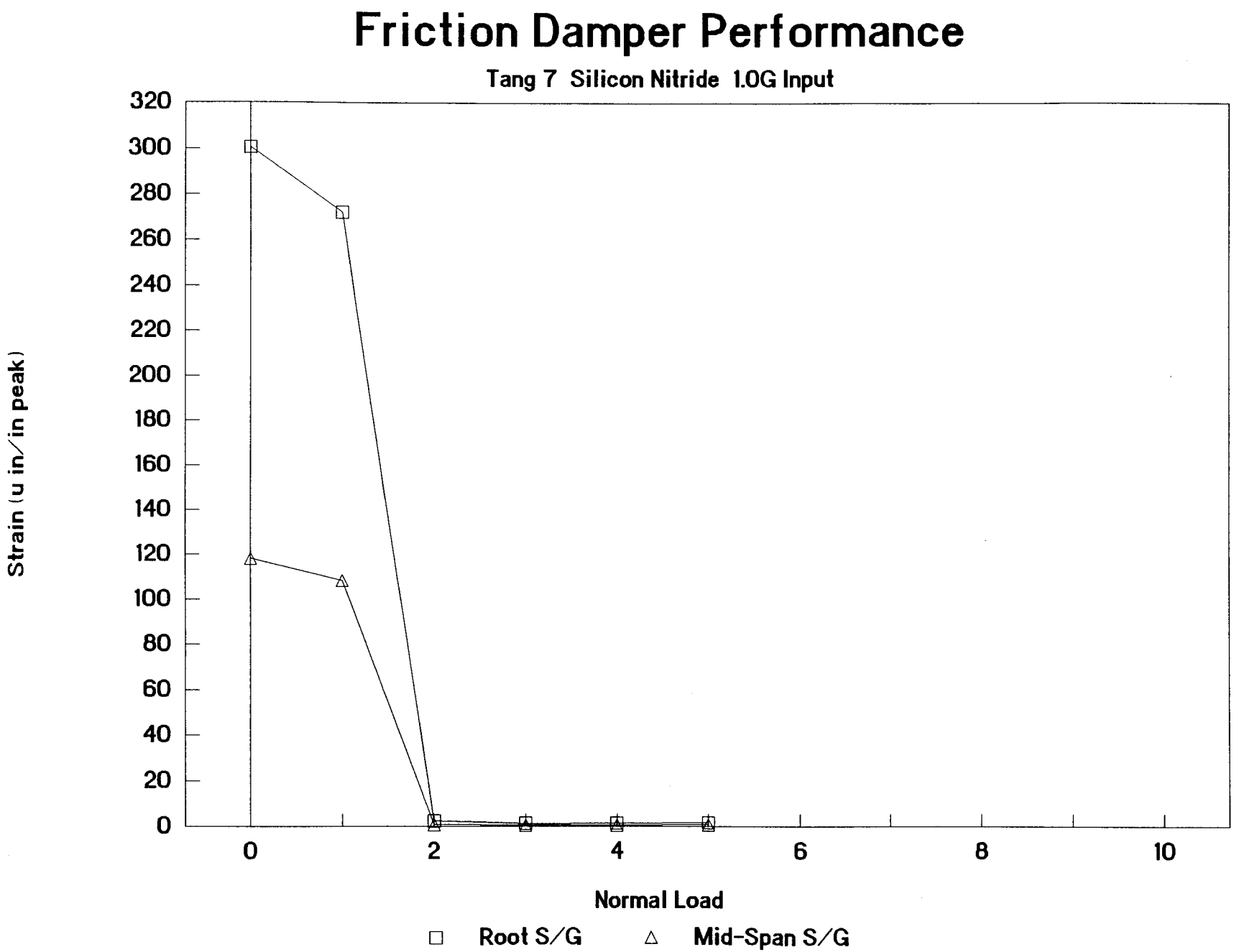

Figure 2.2-100 Low frequency beam optimization curve based on test data Silicon Nitride damper at tang 7, 1.0G input

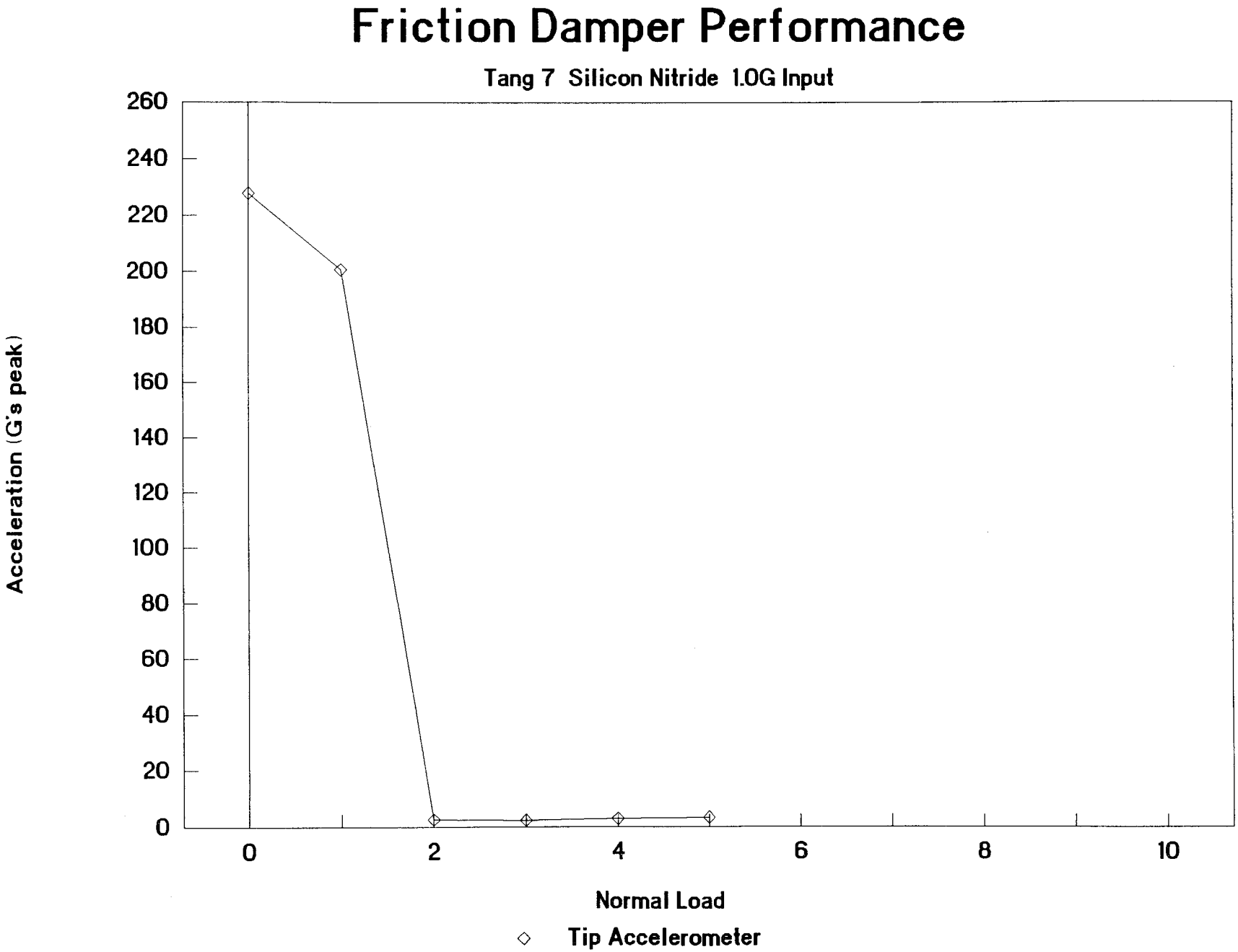

Figure 2.2-99 Low frequency beam optimization curve based on test data Silicon Nitride damper at tang 7, 1.0G input

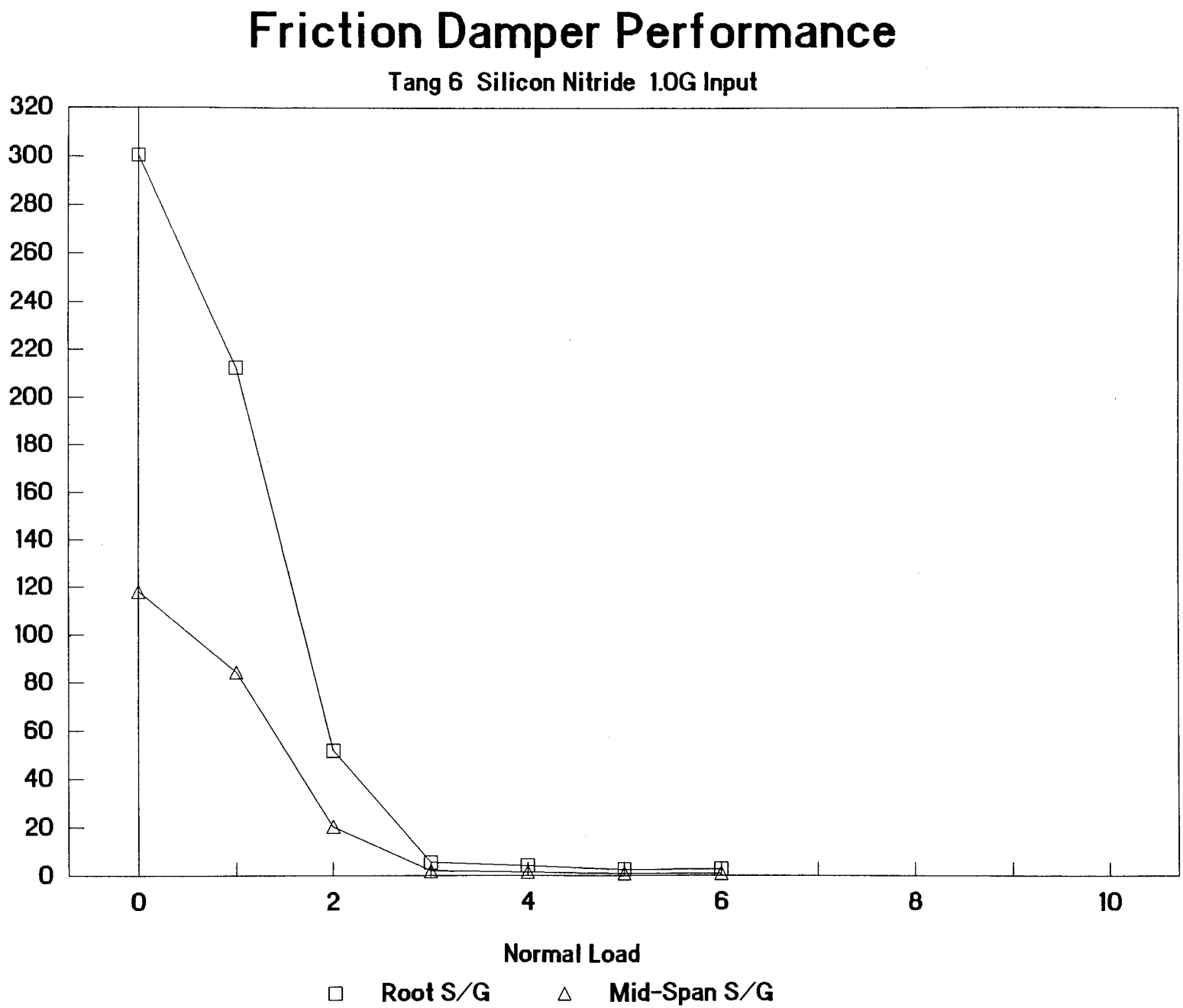

Figure 2.2-98 Low frequency beam optimization curve based on test data Silicon Nitride damper at tang 6, 1.0G input

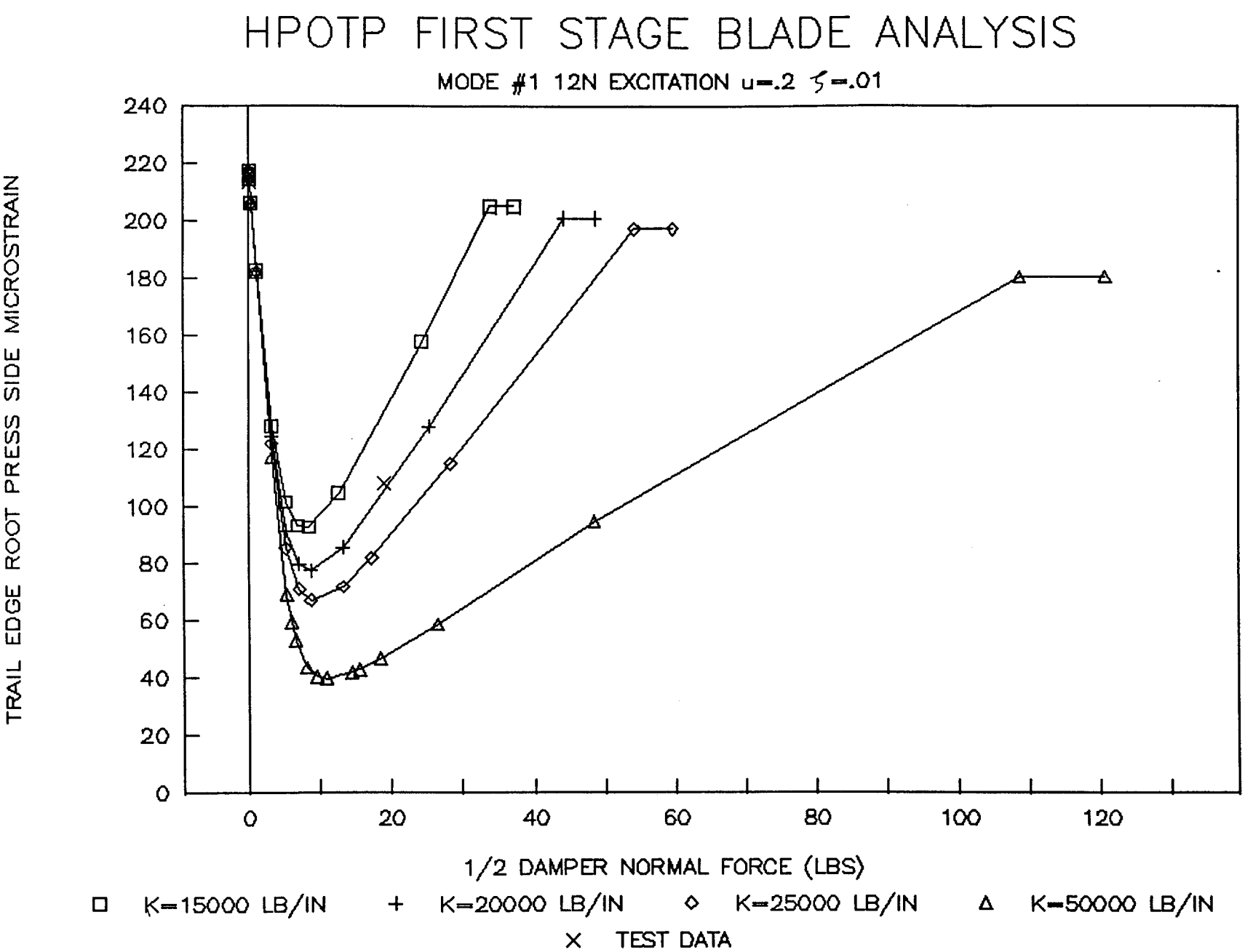

Figure 2.3-12 Optimization curve from BLDAMP, mode #1, 12N excitation

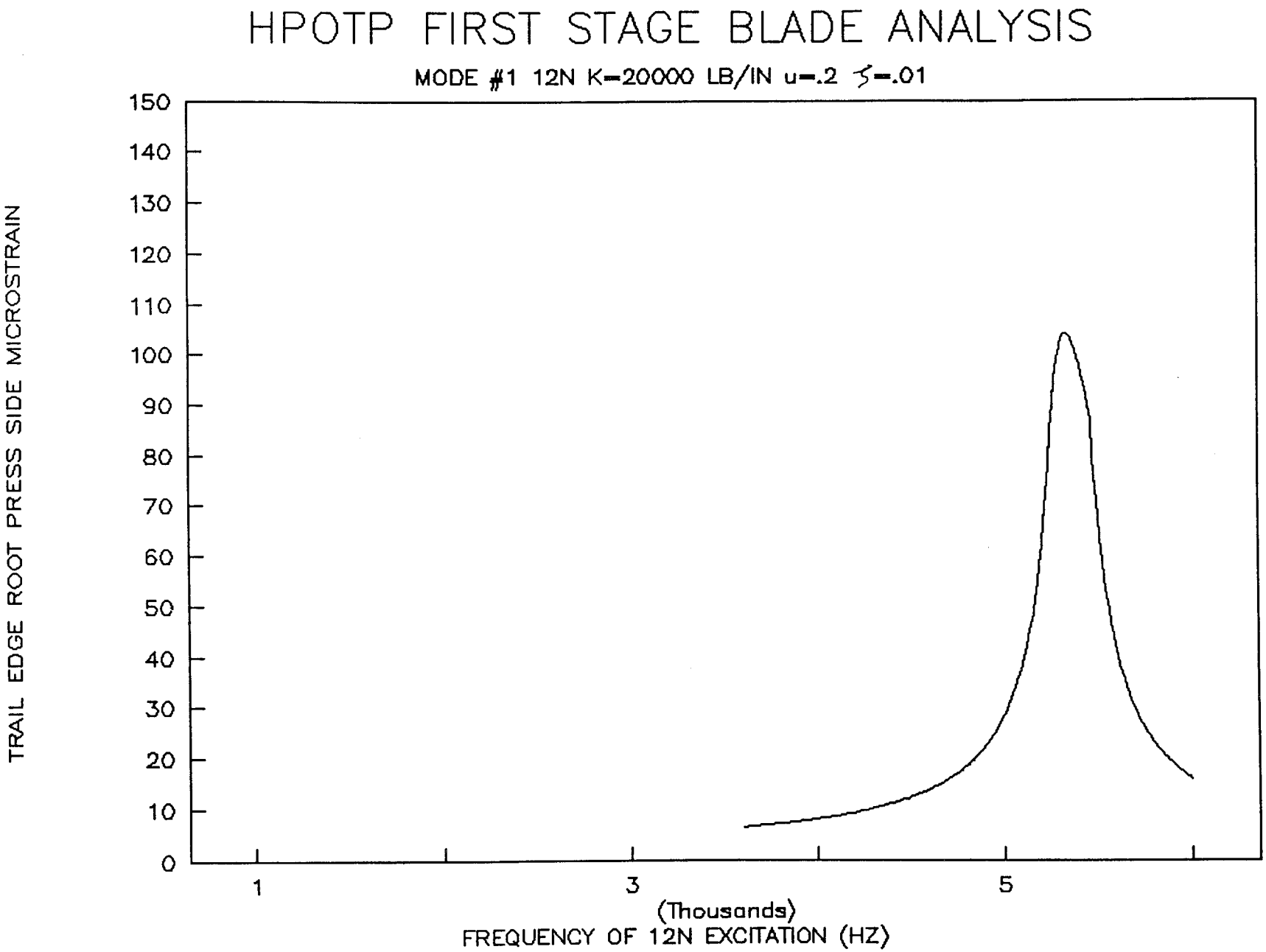

Figure 2.3-13 Response curve from BLDAMP, mode #1, 12N excitation

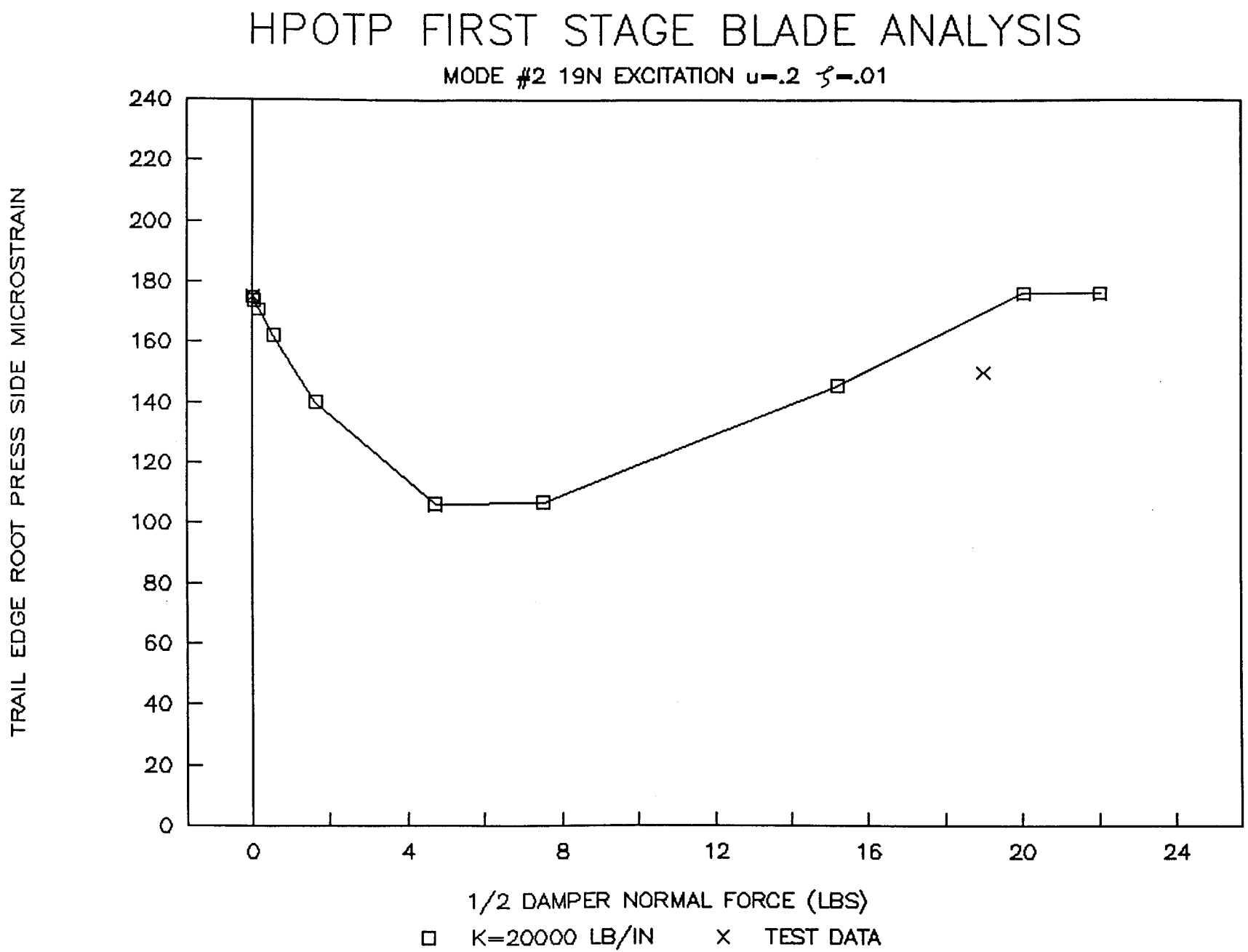

Figure 2.3-14 Optimization curve from BLDAMP, mode #2, 19N excitation

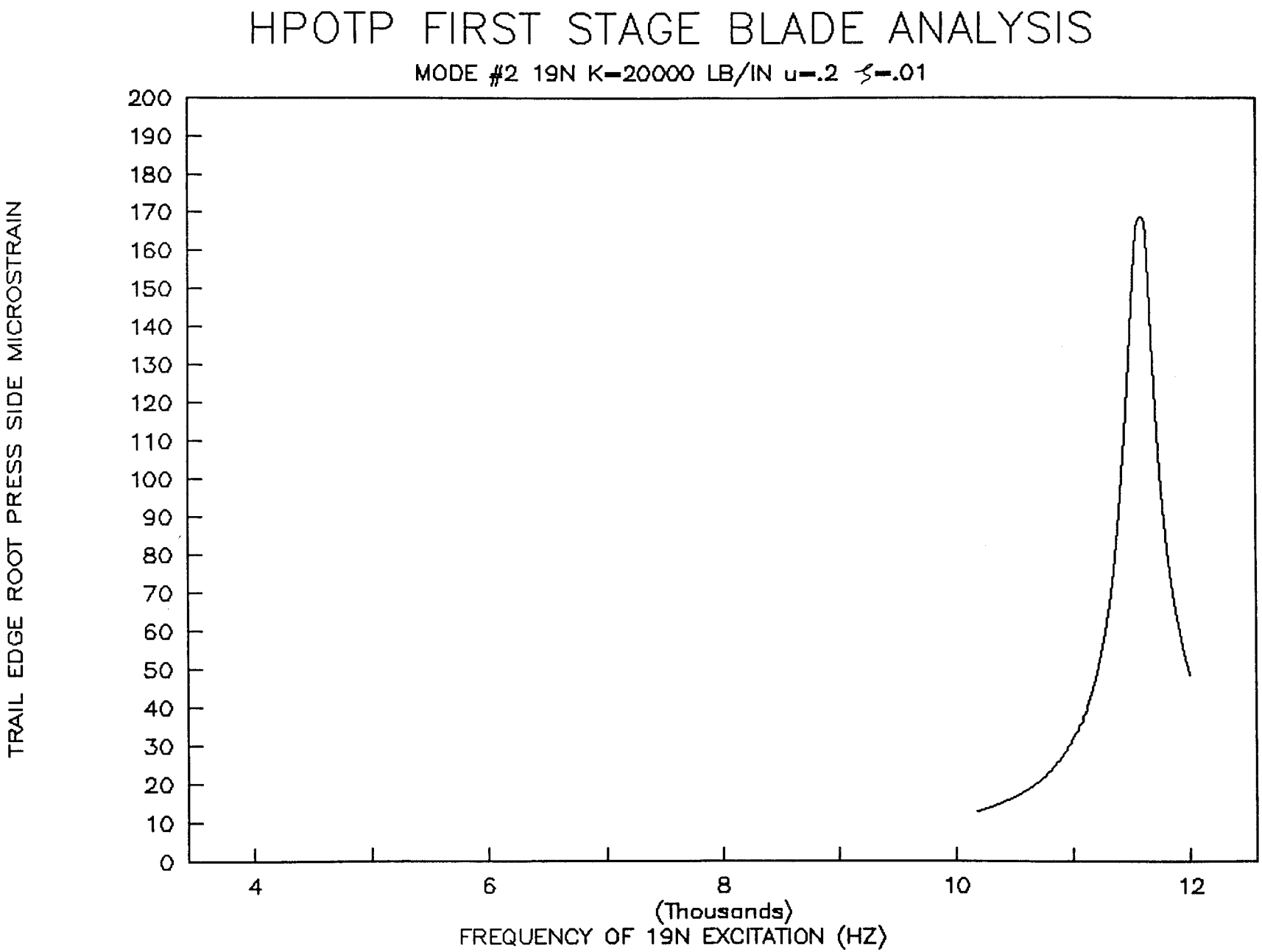

Figure 2.3-15 Response curve from BLDAMP, mode #2, 19N excitation

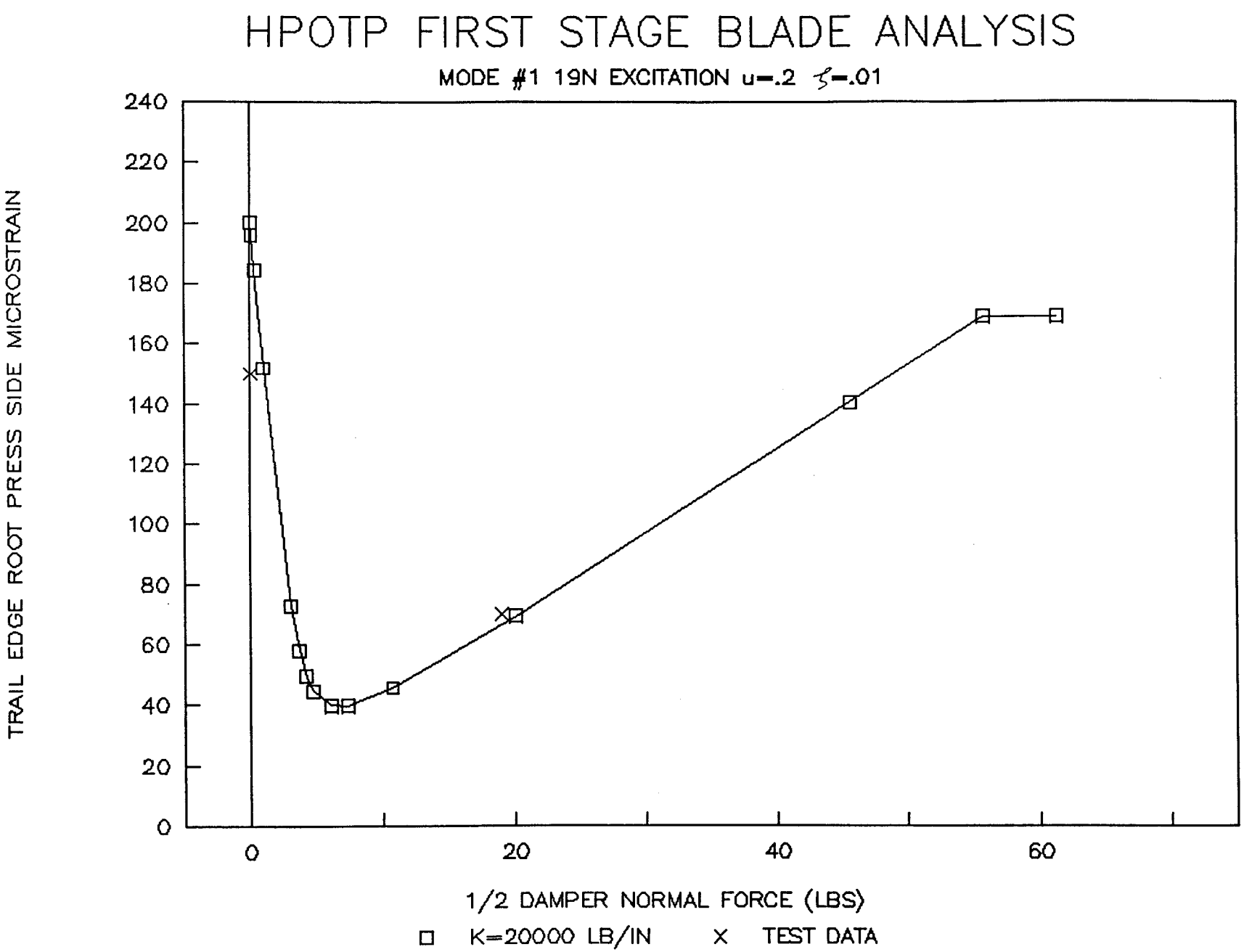

Figure 2.3-16 Optimization curve from BLDAMP, mode #1, 19N excitation

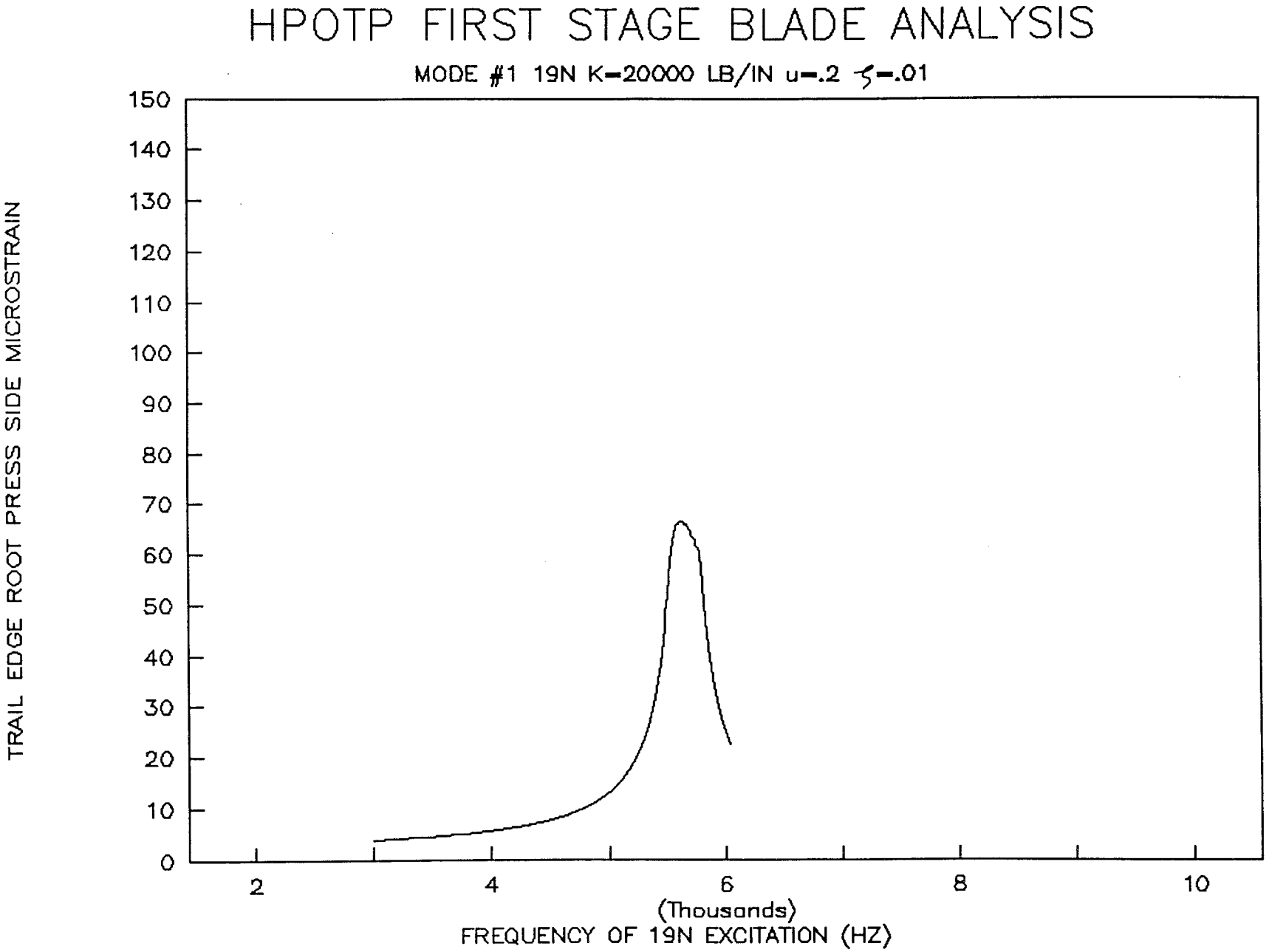

Figure 2.3-17 Response curve from BLDAMP, mode #1, 19N excitation

resonant response of approximately 8 percent for this case, while the test data show a negligible shift in frequency.

The optimization curves in Figures 2.3-12, 2.3-14, and 2.3-16 indicate that the damper is, for its stiffness, about twice as heavy as it should be for optimal damping of the first two modes. Also, the figures indicate that a stiffer damper could further reduce resonant response and decrease the optimum normal force sensitivity.

Overall, the test and analysis correlated very well, although there are a few key parameters that need to be accurately predicted before the program BLDAMP can be truly useful as a design tool. The damper stiffness, forcing function, and coefficient of friction are very important in predicting friction-damped response. Comparisons of test data with analysis, such as the one described here, are helpful in the determination of these key parameters for future design work.

3.0 CONCLUSIONS

A state-of-the-art computer code has been developed for the analysis of friction dampers, as a result of this program . The new code represents a significant improvement over existing analytical tools; in that multiple modes of the structure are accounted for, without the use of expensive time integration techniques. This allows the accurate representation of turbine blades, using the mode shapes generated from high-fidelity, finite-element models. Previous analytical methods considered only single modes of simple one degree of freedom systems.

The new computer code, BLDAMP, was modified to improve input and output formats. Sample cases have been run, which exactly match those provided by the code developer, Griffin Consulting. In addition, more realistic cases have been run using the HPFTP first-stage turbine blade as a test case. Results of the study show that the program is easy to use and provides answers which appear to be reasonable.

Further comparison of BLDAMP results, against test data from nonrotating test beams and spin pit data from instrumented turbine blades, has provided a good validation of the code. Results from the test/analysis comparison show that the normal force that causes the lowest response was highly dependent on the friction coefficient between the damper and beam surfaces. This makes prediction of damper performance very difficult, unless friction characteristics are known for the materials at hand. It was found, however, that once the friction coefficient was known, damper performance can be reliably predicted using the BLDAMP computer code.

It can be concluded, from the results of the extensive testing presented in this report, that friction damping is an effective way to reduce the response of vibrating structures. Response reductions of over 95 percent, from the undamped configuration, were observed in the test beam. It was also found that the most effective position to locate the dampers is at a beam span of 30 percent, or more. The effectiveness of the friction damper remained relatively constant for damper locations between 30 and 100 percent span. This is a significant observation, because it was previously thought tip dampers were the only way to obtain response reductions of the magnitude observed in the testing.

The test data were plotted in nondimensional form and a set of design curves was generated, which will greatly aid in the selection of damper parameters for future applications. On an equal level with the development of the BLDAMP computer code, these design curves are one of the major accomplishments of this program. They provide a much needed base from which to understand damper behavior.

4.0 RECOMMENDATIONS FOR FURTHER WORK

The main problem encountered, in the initial friction damper testing reported herein, was the lack of good signal quality and repeatability from test to test. These problems were solved, for the most part, in the second test series, where the vibration amplitude was reduced and a more sophisticated test controller and shaker were used. The testing was still not as repeatable as desired and improvements could be made to improve the data quality. The problem centers on the method of applying the excitation to the beam, which was by use of base motion of the entire test apparatus. Thus, the beam was excited by inertial forces, which were dependent on the motion of the base. This development necessitated very accurate control of the shaker. As an improvement, it is suggested that further testing be done, using an exciter that applies an easily controllable force directly to the beam, without using base excitation. A magnetic excitation device may be the solution, because it can be commanded to provide a sinusoidal force and it would not involve any feedback, due to the response of the beam.

All the test data gathered in this program was from nonrotating beam specimens. Although the data should be applicable to blades in a rotating environment, there is one major difference that may alter the results. The rotating environment differs from the nonrotating test in the method of application of the normal force. Centrifugal accelerations in typical turbines can be on the order of 150,000 Gs. These accelerations provide normal forces of the same magnitude as were used in the nonrotating test. However, the ratio of damper mass to normal force is many orders of magnitude smaller in the rotating test. The small mass/force ratio in the rotating environment makes it almost impossible for damper chatter to occur, while in the nonrotating test setup chatter was observed. A logical extension to the testing already completed would be to perform similar tests using the Rocketdyne whirligig spin facility.

Another improvement, which would increase the quality of the data, involves damper wear as the test progresses. In the initial testing, a large amount of damper wear was observed which was attributed to damper chatter. A black residue formed on the damper contact surfaces, which undoubtedly affected the results by changing the frictional characteristics of the interface. Damper chatter was not observed, to any great extent, in the second phase of testing. However, a small amount of the residue appeared on the damper and beam during testing. An attempt was made to clean the residue as it appeared, but the cleaning process was not continuous. It is not known if the residue changed the results. Damper wear will occur in an actual turbine, but any residue will be removed immediately by the hot-gas stream. Therefore, an improvement to the testing would incorporate an air jet directed at the damper to remove the residue as it is produced.

An extension to the testing, which may enhance knowledge of how friction dampers function, would involve instrumentation of the damper, as well as the beam. Currently, very simple models are used, which idealize the damper as a massless spring. This may not be adequate, as the damper may have a dynamic response of its own. For example, a strain gage mounted on the damper could measure the stretch that occurs before slipping. It may even determine if slip occurs instantaneously or over a period of time.

The test data was obtained on a uniform cantilever beam test specimen, vibrating in the first mode, only. A valuable extension to this work would be to repeat the testing for beam vibration in higher modes.

Although some turbine blades have mode shapes that are similar to those of cantilever beams, there are many other instances where the lower modes consist of localized motion of the airfoil, with little or no motion of the blade as a whole. A test program could be developed that would generate a set of design curves for complex mode shapes, which are commonly found in turbine blades. An example, of this type of program, would explore the capability of friction dampers to eliminate trailing-edge flap modes, which exist in many applications.

5.0 REFERENCES

1. Davis, G. A. and McCormick, C. L., "HPOTP First-stage Turbine Blade Whirligig Spin Test Results - Test Series 1A and 1B", Rocketdyne Internal Letter 7128-0040, February 1987.

2. Shinguchi, B. H., "Airfoil Vibration Damper Program Interim Report", Rocketdyne Report RI/RD 88-197, July 1988.

3. Davis, G. A., "Airfoil Vibration Damper Computer Code Implementation and Checkout", Rocketdyne Internal Letter 8127-30-058, September 1988.

4. Davis, G. A., "Airfoil Vibration Damper Nonrotating Vibration Test Plan", Rocketdyne Internal Letter 7127-30-014, February 1988.

5. Dominic, R. S., "Parametric Study of Turbine Blade Platform Damper Friction Damping Using the Lumped Parameter Analysis", ASME Paper 84-GT-109, 1984.

6. Sinha, A. and Griffin, J. H., "Effects of Static Friction on the Forced Response of Frictionally-damped Turbine Blades", ASME Paper 83-GT-155, July 1983.

7. Menq, C-H. and Griffin, J. H., "BLDAMP Manual", Griffin Consulting, January 1988.

8. Griffin, J. H., "HPOTP Damper Study", Griffin Consulting, January 1988.

6.0 APPENDIX

6.1 THEORETICAL DEVELOPMENT

GRIFFIN CONSULTING

1. INTRODUCTION

The objective of this report is to summarize the underlying physical assumptions and mathematics that provide the basis for a computer code, **BLDAMP**, that may be used to calculate the forced response of frictionally damped turbine blades and optimize the design of friction dampers. BLDAMP will be especially suited for studying SSME turbo-pump vibration in that it will have the following unique capabilities:

(1). It will simulate mode shape changes induced by the friction constraints, thus it can be used to analyze dampers located at the tips of the blades.

(2). It will automatically analyze the damping of torsional modes, i.e. blade rotations will also dissipate energy.

(3). Stiff-wise blade motion as well as ease-wise motion will be included in the formulation, thus the code can be used to analyze stiffwise bending as in the 2nd mode of the HPOTP blade.

These capabilities are not currently available in any existing computer code. As a result, the proposed computer code will significantly advance the state-of-the-art in friction damping analyses. The reasons that BLDAMP can analyze these types of problems is because a more general mathematical formulation is used that incorporates more physical features of the blade-damper system. Specifically, mode shape changes can be taken into account because the problem is formulated in terms of receptances rather than a specific mode of response. Torsional modes may be analyzed because friction contact is assumed to occur at four points on each blade and since the points do not lie on the center of rotation the frictional forces produce a resisting moment which damps torsional modes. Stiff-wise blade motion is included in the formulation by considering that the blade may move in two independent directions at the damper contact point. The mathematical basis of each of these features is presented in this report.

An important point to note is that the analysis of non-linear vibration problems is difficult. The more degrees-of-freedom or complexity that is introduced in modelling a problem the more computer time is required to solve it, and, in fact since you ultimately must solve systems of non-linear

algebraic equations, the algorithm may have difficulty converging if the system of equations is too large. As a result, developing a useful code involves making trade-offs between either having a tractable problem or including more complex physical features of the system. For this reason, it is important to initially model the problem as simply as possible and develop a code that works in an efficient manner. Once the baseline code is developed and tested then additional features can be incorporated if they are needed.

This report first summarizes the mathematical formulation of the problem, gives the input requirements of the code and a flow chart, discusses potential enhancements to the code that may be incorporated at a later time, and then provides some concluding remarks.

2. FORMULATION

2.1 RECEPTANCE FORMULATION OF BLADE RESPONSE

Initially, we consider the response on an individual blade. The aerodynamic forces that act on the blade are assumed to be harmonic (refer to Fig. 1), i.e.

$$\mathbf{f}^E(x,t) = f_0 \, \mathbf{F}(x) \, e^{i\omega t} \tag{1}$$

where bold letters indicate vectors or matrices. The friction forces are given by

$$\mathbf{f}_i^F(t) = \mathbf{f}_i \, e^{i\omega t} \tag{2}$$

In both expressions the phase of the quantities are included by considering **F** and $\mathbf{f}_i$ complex quanitities (physically the solution corresponds to the real parts of each of the quantities of interest).

The response of the blade is given by the displacement vector

$$\mathbf{u}_i(t) = \mathbf{U}_i \, e^{i\omega t} \tag{3}$$

and by the stress vector

$$\sigma_i(t) = \mathbf{s}_i \, e^{i\omega t} \tag{4}$$

where i takes on integer values that correspond to points of interest on the blade. In particular, i equals 1 through 4 corresponds to the damper contact points as indicated in Fig. 1 and i = 5 is a typical reference point at which we wish to know the vibratory stress.

The receptances are defined in terms of the response at a point of interest due to a sinusoidal excitation at a given point. In particular, the displacement at the ith point due to the external excitation is

$$\mathbf{u}_i^E = f_0 \mathbf{r}_i^E \, e^{i\omega t} \tag{5}$$

and the displacement at the ith point due to an unit excitation at the jth point is

$$u_i^j = R_{ij} f_j e^{i\omega t} \tag{6}$$

Then since the blade is linear, from (3) and (5) the displacement coefficients are given by

$$U_i = f_0 r_i^E + \sum_{j=1}^{4} R_{ij} f_j \tag{7}$$

and analogously the stress coefficients by

$$s_i = f_0 s_i^E + \sum_{j=1}^{4} S_{ij} f_j \tag{8}$$

2.2 CALCULATING RECEPTANCES

Many engineers are more familar with real receptances. In this approach if the excitation on a simple spring/mass oscillator is given by

$$f(t) = (1) \cos \omega t \tag{9}$$

then the displacement would be given by

$$u(t) = r_c \cos \omega t + r_s \sin \omega t \tag{10}$$

where r_C and r_S are referred to as the *real receptances*. Real receptances are readily related to complex receptances. For example, alternatively we could write (9) as

$$f(t) = \text{Real}(e^{i\omega t}) \tag{11}$$

and (10) as

$$u(t) = \text{Real}\ \{\ (r_c - i r_s)\, e^{i\omega t}\ \} \tag{12}$$

thus the complex receptance, r_c-ir_s, is just a linear combination of the real receptances.

Receptances can be calculated from modal information in the following manner. Suppose **u** satisfies the equation of motion

$$\mathbf{M}\frac{d^2\mathbf{u}}{dt^2} + \mathbf{C}\frac{d\mathbf{u}}{dt} + \mathbf{K}\mathbf{u} = \mathbf{F}e^{i\omega t} \tag{13}$$

where **M**, **C** and **K** are matrices derived from finite element analyses of the blade and **F** is a force acting on the blade (it could correspond to a unit excitation at the jth node, for example). Let ϕ_j be the modal displacement vector associated with the jth undamped mode, i.e. let ϕ_j satisfy

$$\mathbf{K}\phi_j = \omega_j^2\, \mathbf{M}\ \phi_j \tag{14}$$

where ω_j is the jth resonant frequency of the blade. Then from linear algebra we know that the modal displacement vectors are orthogonal with respect to **M**, i.e.

$$\phi_n^T\, \mathbf{M}\ \phi_j = 0 \quad \text{when } n = j \tag{15}$$

Let $\mathbf{C} = \alpha\,\mathbf{M} + \beta\,\mathbf{K}$. Then if the response **u** is

$$\mathbf{u} = \mathbf{U}e^{i\omega t} \tag{16}$$

it may be shown (using (14) and (15)) that the coefficients **U** are given by

$$\mathbf{U} = \sum_j \frac{\phi_j^T\, \mathbf{F}}{k_j + i\,\omega\, c_j - m_j\omega^2} \tag{17}$$

where

$$m_j = \phi_j^T M \phi_j \tag{18a}$$

$$k_j = m_j \omega_j^2 \tag{18b}$$

and

$$c_j = \alpha m_j + \beta k_j \tag{18c}$$

Thus, the receptances of equation (7), $R_{ij,}$ can be found from (17) provided we let **F** be a unit excitation at the jth node and calculate the components of **U** that correspond to the ith node.

2.3 TUNED SYSTEM THEORY

The goal of this section is to rewrite the equation that governs blade motion, equation (7), in terms of the relative motion between blades. This does two things for us. The first is that it becomes clear that for a *tuned* bladed disk all blades respond with the same amplitude (phases differ by a fixed amount) and, consequently, the problem can be formulated in terms of a single blade or in terms of the motion between a pair of blades. In this section we will derive the governing equations in terms of the relative motion between blades, since it is these motions that act on the friction dampers and that will be related in a later section to the damper forces, f_j.

The tuned system assumption is that all the blades are identical and consequently have exactly the same frequencies of vibration (thus, they are *tuned*). It is also assumed that the blades see exactly the same excitation except for the phase of the excitation which differs by a fixed amount, φ, from blade to blade, where

$$\varphi = \frac{2\pi n_{nd}}{n_b} \tag{19}$$

and where n_{nd} equals the number of nodal diameters of the response (also

equals the engine order of the excitation) and where n_b is the number of blades on the disk.

Consider Fig. 2, a schematic of a section of the bladed disk assembly. In this schematic we are looking down on a typical blade in the center and two blades on either side. The numbered nodal points are the damper contact points. Each nodal point has displacements and forces in the x and y directions as indicated in Fig. 3. Because of the phase difference of (19) the displacements and forces in the neighboring blades are (quantities with (') refer to the blade on the right, those with (") refer to the blade on the left and quantities with no (') refer to the center blade)

$$\mathbf{U}_i' = \mathbf{U}_i e^{i\varphi} \tag{20a}$$

$$\mathbf{F}_i' = \mathbf{F}_i e^{i\varphi} \tag{20b}$$

Thus, equation (17) can be written in terms of the motions that act on the damper between the center and right hand blades, i.e in terms of $\mathbf{U}_1$, $\mathbf{U}_2$, $\mathbf{U}_3'$, and $\mathbf{U}_4'$ and in terms of the forces that act on the damper, $\mathbf{F}_1$, $\mathbf{F}_2$, $\mathbf{F}_3'$, and $\mathbf{F}_4'$. From (17) and (20) we can write

$$\mathbf{U}_i = f_0 r_i^E + R_{i1} f_1 + R_{i2} f_2 + e^{-i\varphi} [\, R_{i3} f_3' + R_{i4} f_4' \,] \tag{21}$$

We can use (21) for i = 1,2. From (20) (a) and (21)

$$\mathbf{U}_i' = e^{i\varphi} [\, f_0 r_i^E + R_{i1} f_1 + R_{i2} f_2 \,] + R_{i3} f_3' + R_{i4} f_4' \tag{22}$$

which we can use when i equals 3 or 4. Thus, at this point in the formulation we have four equations and eight unknowns (4 displacements and 4 forces that act on the damper). The goal of the next sections will be to relate the damper forces and displacements and to complete the formulation.

2.4 DAMPER THEORY

The objective of this section is to simplify the formulation and reduce the number of unknowns. The blades and a simplified damper configuration are depicted in Fig. 4. Note that in order to simplify the formulation it is

assumed that dampers act independently on the upper and lower pairs of contact points. It is also assumed that the dampers' inertia are negligible (i.e. they behave as springs). Thus, from equilibrium there are two independent force vectors since

$$\dot{U}_i = e^{i\varphi}[f_0 r_i^E + R_{i1} f_1 + R_{i2} f_2] + R_{i3} \dot{f}_3 + R_{i4} \dot{f}_4 \tag{23}$$

The damper force can be related to the relative motion across the damper, thus the independent displacement quantities of interest are

$$w_1 = U_1 - U_4' \tag{24a}$$

$$w_2 = U_2 - U_3' \tag{24b}$$

from (21) and (22) we can write

$$w_1 = f_0[r_1^E - e^{i\varphi} r_4^E] + [R_{11} + R_{44} - e^{-i\varphi} R_{14} - e^{i\varphi} R_{41}] f_1 + [R_{12} + R_{43} - e^{-i\varphi} R_{13} - e^{i\varphi} R_{42}] f_2 \tag{25}$$

and

$$w_2 = f_0[r_2^E - e^{i\varphi} r_3^E] + [R_{21} + R_{34} - e^{-i\varphi} R_{24} - e^{i\varphi} R_{31}] f_1 + [R_{22} + R_{33} - e^{-i\varphi} R_{23} - e^{i\varphi} R_{32}] f_2 \tag{26}$$

or

$$w = [w_1, w_2]^T = f_0 r^{*E} + R^* F^* \tag{27}$$

where

$$F^* = [f_1, f_2]^T$$

and r^{*E} and R^* are defined to be consistent with (25) and (26).

2.5 DAMPER FORCES: $F^* = F^*(w)$ FOR TWO DIMENSIONAL MOTIONS

2.5.1 *Differences Between One and Two Dimensional Motion: A Special Case of Circular Motion*

Consider the case of damper element depicted in Fig. 5 (a) in which the motion is only in one direction. The force-displacement relationship is depicted in Fig. 5 (b). Note that the damper slips during part of the cycle no matter how large the displacement amplitude becomes. Now consider the case of a damper element in which the input displacement **w** is a vector that can move in two directions. If the input motion (i.e. the relative motion between the blades) is circular then **w** can be given as

$$\mathbf{w} = w_0 [\cos \omega t , \sin \omega t]^T \tag{28}$$

and if the damper spring is isotropic, i.e. the damper stiffness matrix is of the form

$$\mathbf{f} = \mathbf{K}\,\mathbf{z} \quad \text{and} \quad \mathbf{K} = k_d \mathbf{I} \text{ where } \mathbf{I} \text{ is the unit matrix} \tag{29}$$

then the motion of the damper will be circular, but may lag the input by an angle, δ. Mathematically,

$$\mathbf{z} = \frac{\mu N}{k_d} [\cos(\omega t - \delta) , \sin (\omega t - \delta)]^T \tag{30}$$

where

$$\delta = \cos^{-1}\left(\frac{\mu N}{w_o k_d}\right)$$

where μN is the magnitude of the force required for slip. Note that slip only occurs if $w_0 > \mu N/k_d$ and that when slip does occur the damper never sticks. This is a fundamental difference between friction contact in one and two dimensions, i.e. for large motions if the motion is two dimensional the damper slips all of the time.

2.5.2 *Establishing the Principal and Minor Axes of a Vector Following an Elliptical Orbit*

For two dimensional motions, the displacement and friction forces at contacting points can be represented as two component vectors. In the use of receptance formulation, each component of the vector is assumed to be sinusoid with an arbitrary phase. In this section it will be shown that such vectors follow an elliptical path and that as a consequence the magnitude of the vector has a maximum equal to the length of the principal axis of the ellipse and has a minimum equal to the length of the minor axis. This section summarizes the mathematics necessary to determine the characteristics of the ellipse. This information is important in that it provides a basis for establishing whether or not the force in a node is large enough to cause slip.

Considering a periodically varying vector of the form

$$f(t) = F\begin{bmatrix}\cos\omega t \\ \sin\omega t\end{bmatrix} \tag{31}$$

where

$$F = \begin{bmatrix} f_{xc} & f_{xs} \\ f_{yc} & f_{ys}\end{bmatrix}$$

Figure 6 shows that such vector follows an elliptical path whose principal direction is at an angle ϕ_z with respect to the x direction

Using a singular value decomposition of the matrix F, one may write

$$F = [z_1, z_2]\begin{bmatrix}\lambda_1 & 0 \\ 0 & \lambda_1\end{bmatrix}\begin{bmatrix}s_1^T \\ s_2^T\end{bmatrix} \tag{32}$$

where

$$[z_1, z_2] = \begin{bmatrix}\cos\phi_z & -\sin\phi_z \\ \sin\phi_z & \cos\phi_z\end{bmatrix}$$

and

$$[s_1,s_2] = \begin{bmatrix} \cos\phi_s & -\sin\phi_s \\ \sin\phi_s & \cos\phi_s \end{bmatrix}$$

From (31) and (32), one can get

$$f(t) = \lambda_1 \cos(\omega t - \phi_s) z_1 + \lambda_2 \sin(\omega t - \phi_s) z_2 \tag{33}$$

where

$$\lambda_1 = \frac{1}{2}\left\{\sqrt{(f_{xc} + f_{ys})^2 + (f_{yc} - f_{xs})^2} + \sqrt{(f_{xc} - f_{ys})^2 + (f_{xs} + f_{yc})^2}\right\}$$

$$\lambda_2 = \frac{1}{2}\left\{\sqrt{(f_{xc} + f_{ys})^2 + (f_{yc} - f_{xs})^2} + \sqrt{(f_{xc} - f_{ys})^2 + (f_{xs} + f_{yc})^2}\right\}$$

$$\phi_z = \frac{1}{2}\left\{\tan^{-1}\left[\frac{f_{xs} + f_{yc}}{f_{xc} - f_{ys}}\right] + \tan^{-1}\left[\frac{f_{yc} + f_{xs}}{f_{xc} + f_{ys}}\right]\right\}$$

$$\phi_s = \frac{1}{2}\left\{\tan^{-1}\left[\frac{f_{xs} + f_{yc}}{f_{xc} - f_{ys}}\right] - \tan^{-1}\left[\frac{f_{yc} - f_{xs}}{f_{xc} + f_{ys}}\right]\right\} \tag{34}$$

It is clear that z_1 is a unit vector pointing in the direction of the principal axis of the ellipse, λ_1 is the length of the principal axis, λ_2 is the length of the minor axis, and ϕ_s is the phase lag of the motion.

2.5.3 *Elliptical Motion When Slip at Contact Point Does Not Occur*

Consider the case when the contacting point does not slip. Then

$$\mathbf{Z} = \mathbf{W} \tag{35}$$

where **w** is the motion between blades and **z** is the motion of the damper.

If **w** is assumed to be sinusoid, then **w** can be expressed as the following.

$$w = \begin{bmatrix} w_{xc} & w_{xs} \\ w_{yc} & w_{ys} \end{bmatrix} \begin{bmatrix} \cos\omega t \\ \sin\omega t \end{bmatrix} \tag{36}$$

and the friction force becomes

$$f(t) = \begin{bmatrix} k_{11} & k_{12} \\ k_{21} & k_{22} \end{bmatrix} \begin{bmatrix} w_{xc} & w_{xs} \\ w_{yc} & w_{ys} \end{bmatrix} \begin{bmatrix} \cos\omega t \\ \sin\omega t \end{bmatrix} \tag{37}$$

Then, using equation (33), it is seen that slip does not occur when $\lambda_1 \leq \mu N$.

2.5.4 *Elliptical Motion at a Fully Slipping Node*

As the periodical motion becomes larger ($\lambda_1 > \mu N$), slip at the interface occurs. The problem of analyzing slip-stick motion for the two-dimensional case is very complex. However, if the motion is large enough, one can assume that the interface slips all the time. Since **w** is large, the motion across the contact point is given by

$$V = W - Z \simeq W \tag{38}$$

By using equation (33) and rotate the coordinate frame to align with the principal axes, **v** can be expressed as

$$v = \begin{bmatrix} a\cos\theta \\ b\sin\theta \end{bmatrix} \tag{39}$$

where $\theta = \omega t - \phi_s$ and the friction force

$$f = -\mu N\, \dot{v}/|\dot{v}|$$

becomes

$$f(t) = -\mu N \begin{bmatrix} \dfrac{-a\sin\theta}{\sqrt{a^2\sin^2\theta + b^2\cos^2\theta}} \\ \dfrac{+b\cos\theta}{\sqrt{a^2\sin^2\theta + b^2\cos^2\theta}} \end{bmatrix} \tag{40}$$

It is seen that f is not a sinusoid. For first order approximation, f may be expanded in a Fourier series to obtain its fundamental harmonic components. As a result, f can be expressed as

$$f(t) = \mu N \begin{bmatrix} F_x^c(a,b) & F_x^s(a,b) \\ F_y^c(a,b) & F_y^s(a,b) \end{bmatrix} \begin{bmatrix} \cos\theta \\ \sin\theta \end{bmatrix} \tag{41}$$

where

$$F_x^c = \frac{1}{T_1}\int_0^{2T_1} \frac{a\sin\theta\cos\theta}{\sqrt{a^2\sin^2\theta + b^2\cos^2\theta}}\,d\theta$$

$$F_x^s = \frac{1}{T_1}\int_0^{2T_1} \frac{a\sin\theta\sin\theta}{\sqrt{a^2\sin^2\theta + b^2\cos^2\theta}}\,d\theta$$

$$F_y^c = \frac{1}{T_1}\int_0^{2T_1} \frac{-b\cos\theta\cos\theta}{\sqrt{a^2\sin^2\theta + b^2\cos^2\theta}}\,d\theta$$

$$F_y^s = \frac{1}{T_1}\int_0^{2T_1} \frac{-b\cos\theta\sin\theta}{\sqrt{a^2\sin^2\theta + b^2\cos^2\theta}}\,d\theta$$

It may be shown that $F_x{}^c$ and $F_y{}^s$ are zero and $F_x{}^s$ and $F_y{}^c$ can be found explicitly in terms of elliptic integrals.

2.5.5 *Interpolation Method for Estimating Friction Force*

The problem of analyzing slip-stick motion for the two-dimensional case is very complex. Since we know the force displacement relationship for the damper when the damper is stuck (equation (37)) and when the interface is fully slipping (equation (41)), we can set up an interpolation method for estimating the harmonic coefficients of the friction force for intermediate values of displacement.

When the motions are small, the friction force in (37) is pure spring force which may be expressed as $f_s(w)$. When the motions are large, the friction force in (41) is pure damping force which may be expressed as $f_d(w)$. Then a general formulation of interpolation for estimating the friction force can be expressed as

$$f = s(\lambda_1,\lambda_2)\, f_s(w) + D(\lambda_1,\lambda_2)\, f_d(w) \tag{42}$$

where λ_1 and λ_2 are singular values of the matrix KW and $s(\lambda_1,\lambda_2)$ and $D(\lambda_1,\lambda_2)$ should meet the following boundary conditions.

$$\lambda_1 \le \mu N \begin{cases} S(\lambda_1,\lambda_2) = 1 \\ D(\lambda_1,\lambda_2) = 0 \end{cases} \tag{43a}$$

$$\lambda_1 >> \mu N \begin{cases} S(\lambda_1,\lambda_2) = 0 \\ D(\lambda_1,\lambda_2) = 1 \end{cases} \tag{43b}$$

To the present time, the selection of these two interpolation functions is not clear. The interpolation functions used in BLDAMP are adapted from the solution for one-dimensional motion. They are

$$S(\lambda_1,\lambda_2) = \begin{cases} 1 & \lambda_1 \le \mu N \\ \frac{1}{\pi}[\theta^* - 0.5 \sin(2\theta^*)] & \lambda_1 > \mu N \end{cases} \tag{44}$$

$$D(\lambda_1,\lambda_2) = \begin{cases} 0 & \lambda_1 \le \mu N \\ (1 - \frac{\mu N}{\lambda_1}) & \lambda_1 > \mu N \end{cases} \quad (45)$$

where $\theta^* = \cos^{-1}[1 - 2\mu N/\lambda_1]$.

3. CODE INPUT AND PROGRAM FLOW CHART

The input requirements for the code are:

A. Blade Information:

- n_b the number of blades.
- E_o engine order of excitation = (# of nodal diameters).
- N_m number of modes (all modes correspond to E_o nodal diameter disk modes).
- ω_i resonant frequency of each mode, i = 1,....., N_m.
- ϕ_i modal displacements for each mode.
- N_r number of reference points
- s_i modal stress vector for reference points.
- m_i modal mass for each mode.
- ζ_i modal damping for each mode.

B. Damper Properties:

$K_{di}^{(1)}$, $N_i^{(1)}$ and $K_{di}^{(2)}$, $N_i^{(2)}$ ..... damper stiffness matrices for 2 slip loads i = 1,2

μ_i coefficients of friction for upper and lower dampers.

α, N^* $N_1 = \alpha N^*$ and $N_2 = (1-\alpha) N^*$

C. Excitation Options

1. Simulate a tracking plot, i.e. find stress versus frequency of excitation for a given input (refer to Fig. 7(a)).

2. For a given level of input excitation find the peak stress as a function of N^* (refer to Fig. 7(b)).

3. For a given damper normal load find the peak stress with the damper in place as a function of what the stress would be without the damper (refer to Fig. 7(c)).

The user will be able to select what type of analysis he would like to run.

The code will call a subroutine to calculate the undamped response of the blade and establish the blade's receptance to the external excitation. There will be a default version of the subroutine which only requires the user to identify which mode is of interest and the magnitudes of the peak modal stresses that would occur if the damper is not present. Calculations will then proceed automatically tracing the response of the mode of interest. The code will be written so that the function of this subroutine can be replaced with a user written version. Thus, the user will be able to specify his own excitation model as required.

The flow chart for the code is indicated in Fig. 8.

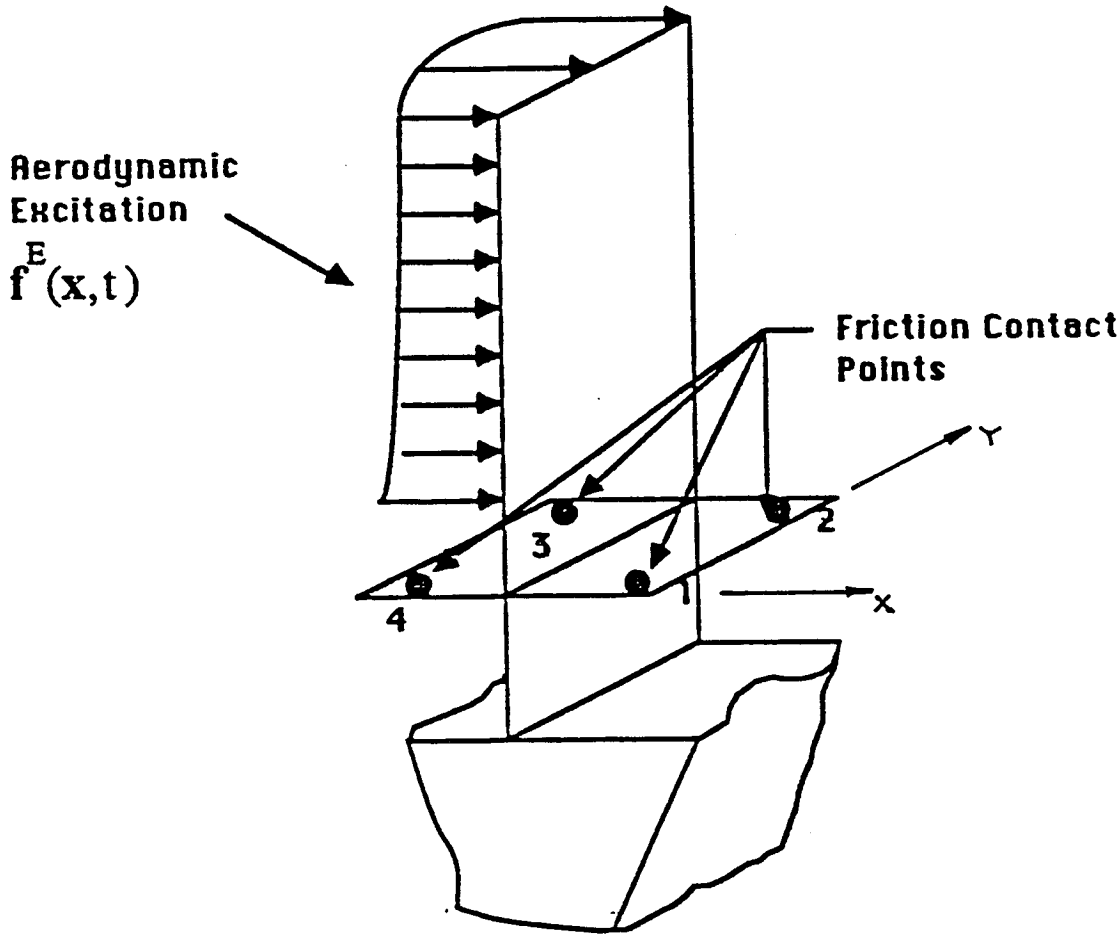

FIGURE 1. BLADE SCHEMATIC

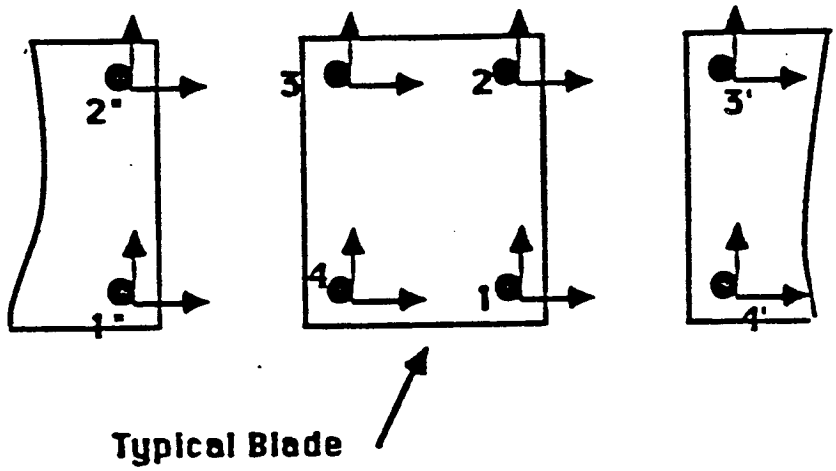

FIGURE 2. SCHEMATIC OF BLADE ASSEMBLY

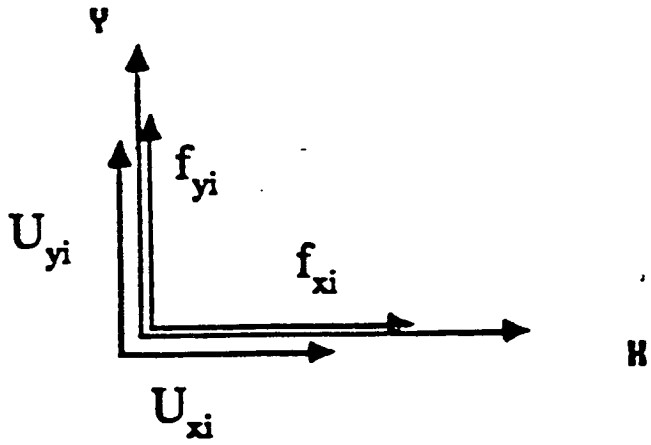

FIGURE 3. NODAL FORCES AND DISPLACEMENTS

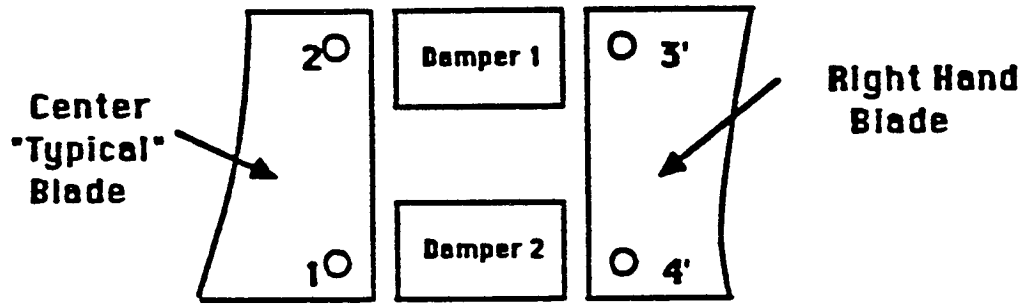

FIGURE 4. DAMPER CONFIGURATION

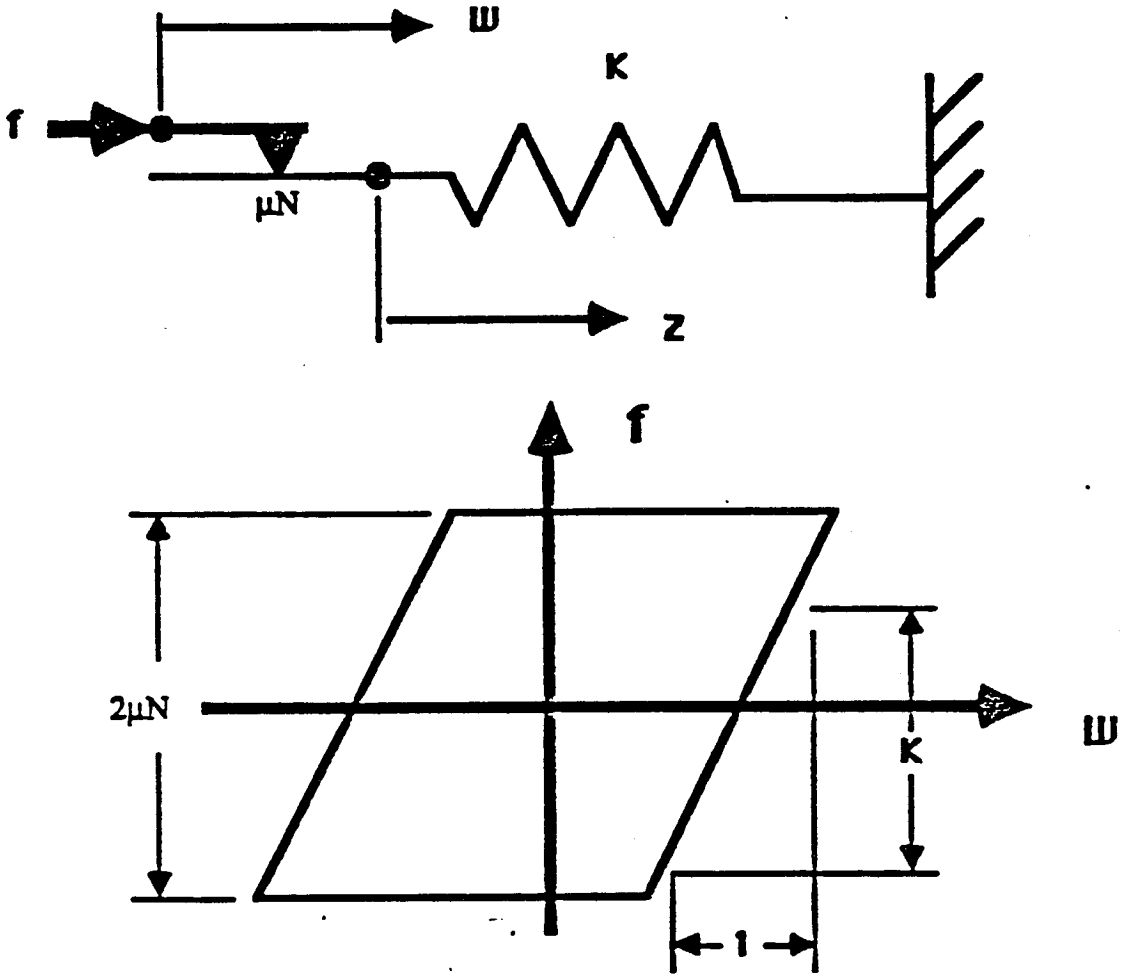

FIGURE 5 ONE DIMENSIONAL FRICTION ELEMENT

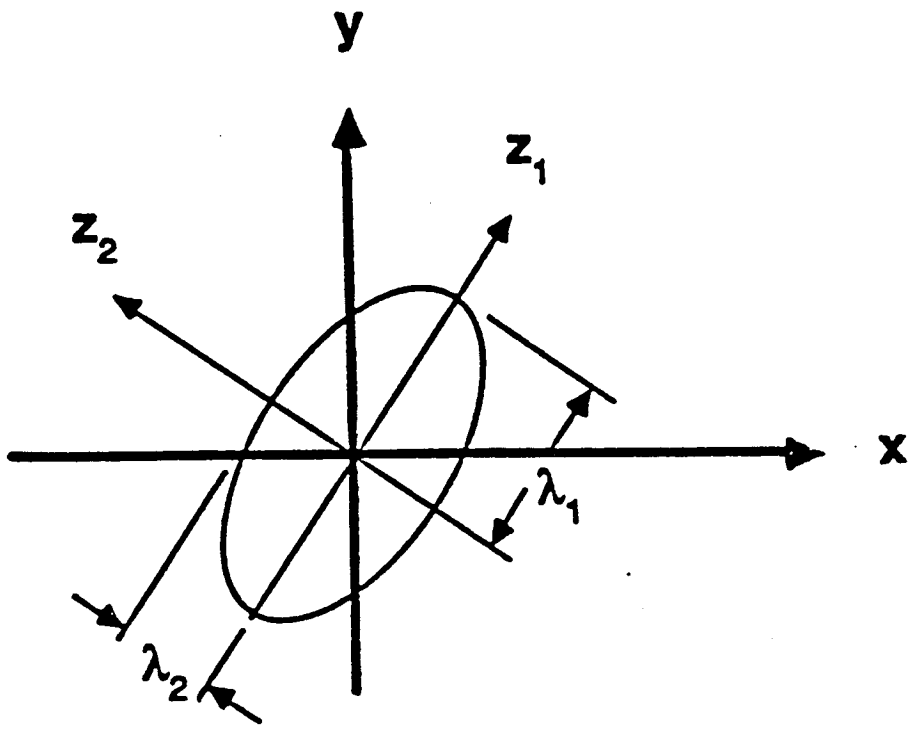

FIGURE 6. ROTATION OF AXES YIELDS PRINCIPAL DIRECTIONS OF ELLIPSE

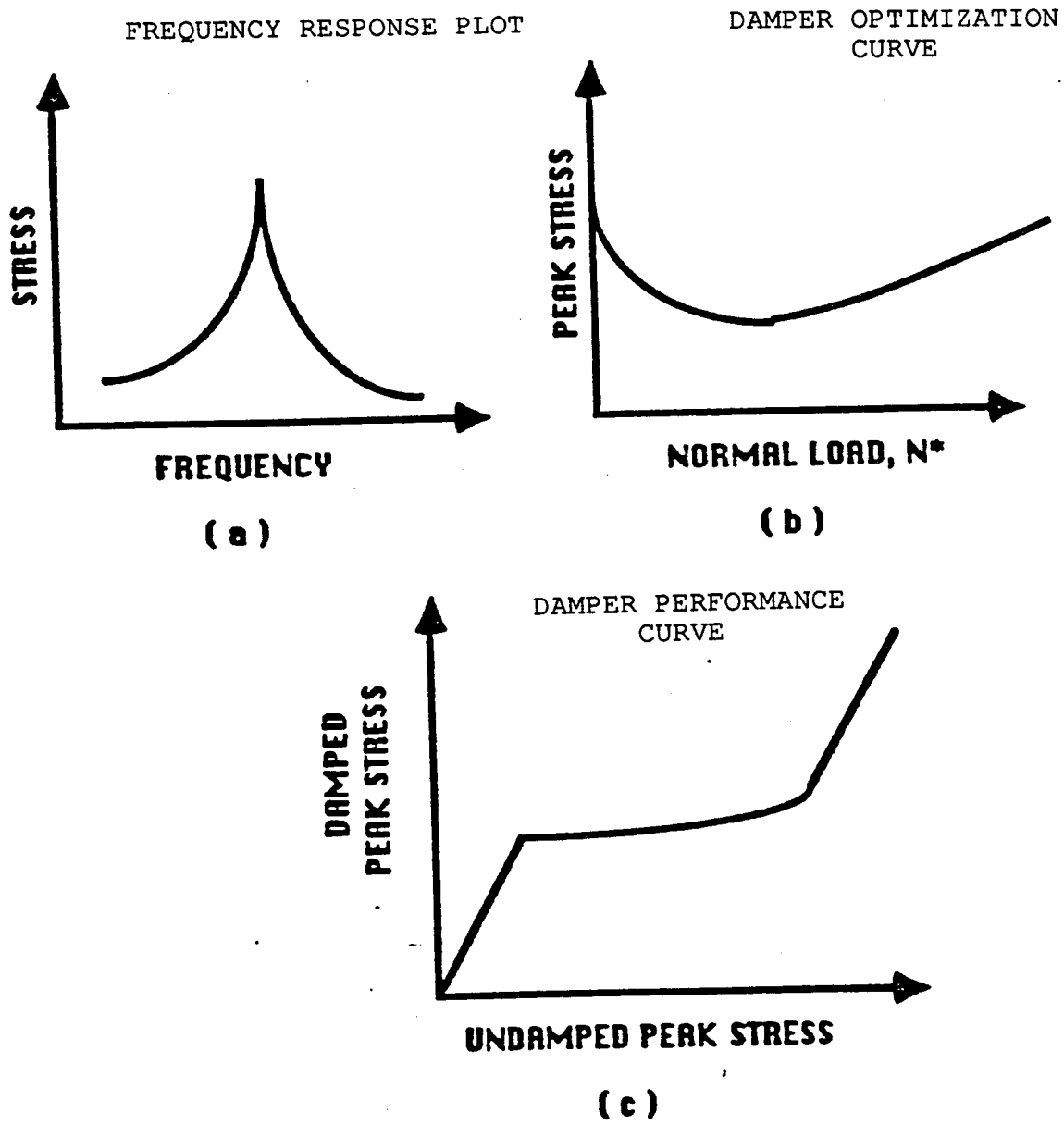

FIGURE 7 OPTIONAL TYPES OF ANALYSES

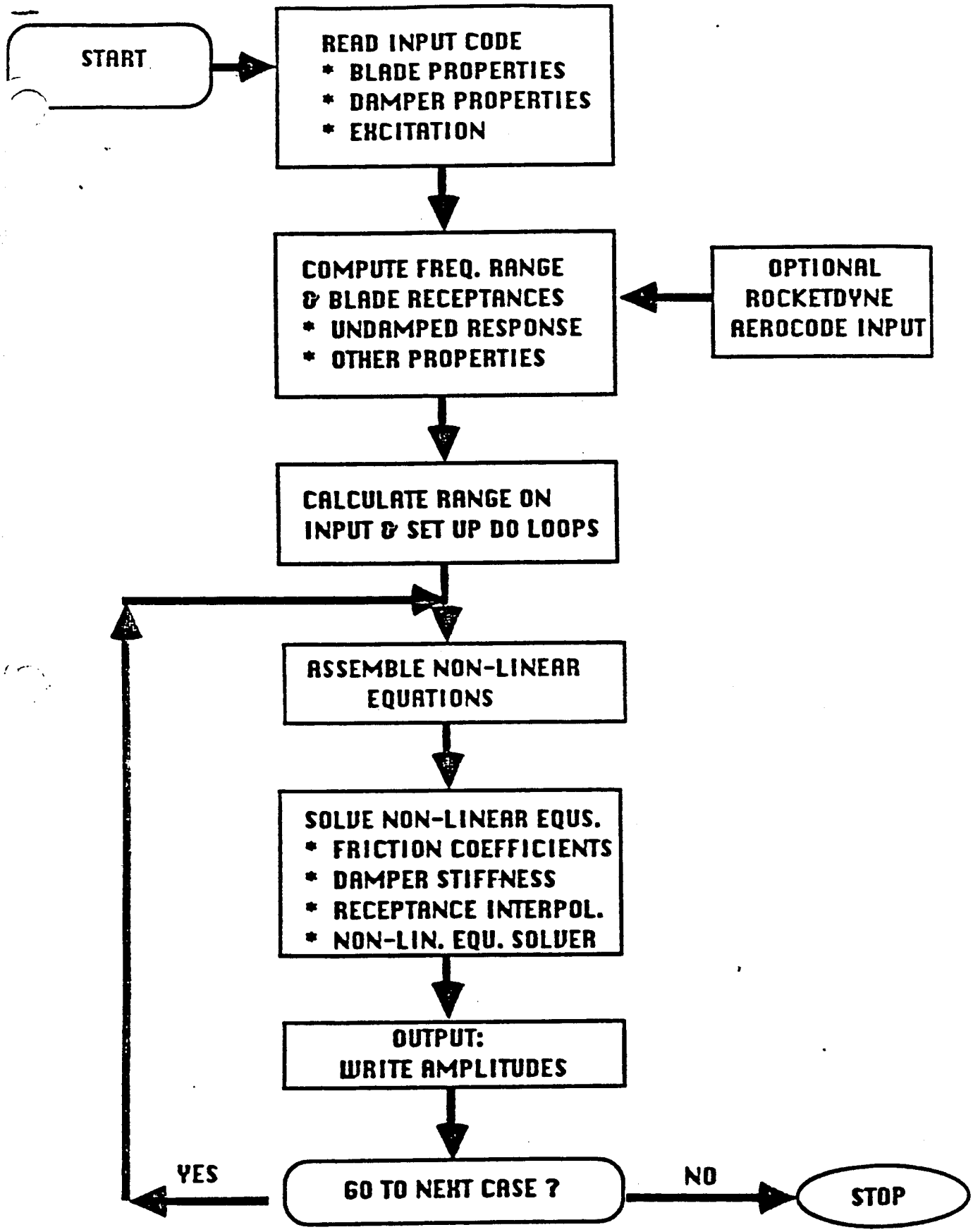

FIGURE 8 FLOW CHART

6.0 APPENDIX

6.2 BLDAMP REQUIRED INPUT DATA AND CODE LISTING

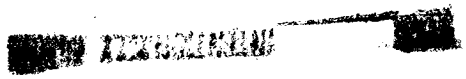

BLDAMP INPUT DATA

TITLE - 72 Character Title

ITYPE
- 1 = Frequency Response Plot
- 2 = Stress vs. Normal Force Optimum Curve
- 3 = Performance Curve

NBLADE,NEODER,NMODES - Number of blades, Engine order of excitation, Number of modes

EMASS,WMODAL,DAM - Generalized mass, Modal frequency, Viscous modal damping ratio

.
.
.

(Repeat NMODES times)

U(1,1), U(1,2), U(1,3), ... , U(1,NMODES) - x direction modal displacement of damper contact point one

U(2,1), U(2,2), U(2,3), ... , U(2,NMODES) - y direction modal displacement of damper contact point one

.
.
.
.

U(8,1), U(8,2), U(8,3), ... , U(8,NMODES)

NRS,NCO - Number of reference stresses, Number of components for each reference stress

SR(1,1), SR(1,2), ... , SR(1,NMODES) - Modal stresses
SR(2,1), SR(2,2), ... , SR(2,NMODES)

.
.
.

SR(NRS*NCO,1), SR(NRS*NCO,2), ... , SR(NRS*NCO,NMODES)

FNM11 - Lower normal load for contact point 1
K11, K12, K21, K22 - Damper stiffness matrix

FNM12 - Upper normal load for contact point 2
K11, K12, K21, K22 - Damper stiffness matrix

FNM21 - Lower normal load for contact point 1
K11, K12, K21, K22 - Damper stiffness matrix

FNM22 - Upper normal load for contact point 2
K11, K12, K21, K22 - Damper stiffness matrix

FNMC11,FCOE11 - Lower normal load, friction coefficient
FNMC12,FCOE12 - Upper normal load, friction coefficient
FNMC21,FCOE21 - Lower normal load, friction coefficient
FNMC22,FCOE22 - Upper normal load, friction coefficient

ALPHA - Fraction of normal load at contact point 1

IA1 - Type of input excitation data

If IA1 = 1 Then,
PSTRESS(1), SVRM(1) - Max undamped stress, modal stress (mode 1)
PSTRESS(2), SVRM(2)
.
.
.
PSTRESS(NMODES), SVRM(NMODES)

If IA1 = 2 Then,
GF(1) - Generalized force for mode 1
GF(2) - Generalized force for mode 2
.
.
.
GF(NMODES)

If ITYPE = 1 : Frequency Response Analysis
WMIN, WMAX, DW - Minimum excitation frequency, maximum excitation frequency, frequency increment
FN - Damper normal load (lbs)

If ITYPE = 2 : Optimum N Curve Analysis
NP, NC, NONMOD - Stress reference point, component number for optimum curve, nonlinear mode number

If ITYPE = 3 : Performance Curve Analysis
FN - Damper normal load
NP, NC, NONMOD - Stress reference point, component number for performance curve, Nonlinear mode number

```
      PROGRAM BLDAMP
C
C        BLDAMP CALCULATES THE FORCED RESPONSE OF FRICTIONALLY
C        CONSTRAINED TURBINE BLADES AND CAN BE USED TO OPTIMIZE
C        THE DESIGN OF FRICTION DAMPERS
C        TAPE7=INPUT,TAPE6=OUTPUT
C
C        AUTHOR - CHIA-HSIANG MENQ
C
      IMPLICIT DOUBLE PRECISION (A-H,O-Z)
      COMMON/NUMB/NBLADE,NEODER,NMODES,NRS,NCO
      COMMON/MAIN/PHASE
      COMMON/BLADE/U(8,10),SR(15,10),EMASS(10),WMODAL(10),
     1  DAM(10)
      COMMON/DAMPER/SMTX11(2,2),SMTX12(2,2),SMTX21(2,2),SMTX22(2,2),
     1  S1(2,2),S2(2,2),FCOE11,FCOE12,FCOE21,FCOE22,FNM11,FNM12,
     2  FNM21,FNM22,FNMC11,FNMC12,FNMC21,FNMC22,COE1,COE2
      COMMON/NLOAD/FN1,FN2,ALPHA
      COMMON/CONVE/CEPSI
      CHARACTER TITLE*72,FINAME*20,FONAME*20
C
C
      WRITE(*,5)
    5 FORMAT(//,2X,'ENTER INPUT FILE NAME',//)
      READ(*,7) FINAME
    7 FORMAT(A20)
      WRITE(*,8)
    8 FORMAT(//,2X,'ENTER OUTPUT FILE NAME',//)
      READ(*,7) FONAME
C
C
      OPEN(7,FILE=FINAME,STATUS='OLD')
      OPEN(6,FILE=FONAME,STATUS='NEW')
C
C
C        READ ANALYSIS TYPE
C
C        ITYPE=1  FREQUENCY RESPONSE PLOT
C        ITYPE=2  OPTIMUM CURVE (STRESS VS. NORMAL FORCE)
C        ITYPE=3  PERFORMANCE CURVE (DAMPED VS. UNDAMPED STRESSES)
C
      READ(7,10) TITLE
   10 FORMAT(A72)
      READ(7,*) ITYPE
C
C        READ MODAL INFORMATION AND DAMPER PROPERTIES
C
      CALL READMD
C
C        PRINT INPUT PARAMETERS
C
      CALL PRINT(TITLE)
C
      IF(ITYPE .EQ. 1) THEN
C
C        CALCULATE FREQUENCY RESPONSE PLOT
C
      CALL IO1
C
      ELSE IF (ITYPE .EQ. 2) THEN
```

```
C
C        CALCULATE OPTIMUM CURVE
C
      CALL IO2
C
      ELSE IF (ITYPE .EQ. 3) THEN
C
C        CALCULATE PERFORMANCE CURVE
C
      CALL IO3
      END IF
      END
C
      SUBROUTINE READMD
C
C        READMD READS BLADE AND DAMPER INFORMATION
C
C        NBLADE - THE NUMBER OF BLADES
C        NEODER - ENGINE ODER OF EXCITATION
C        NMODES - THE NUMBER OF MODES; UP TO 10 MODES
C        EMASS - MODAL MASS
C        WMODAL - MODAL FREQ.
C        DAM - MODAL DAMPING RATIO
C        U - MODAL DISP. AT CONTACT POINTS
C        NRS - THE NUMBER OF REFERENCE STRESS POINTS (5 MAX)
C        NCO - THE NUMBER OF MODAL STRESS COMPONENTS (3 MAX)
C        SR - MODAL STRESS AT REFERENCE POINTS
C        SMTX11 - DAMPER STIFFNESS MATRIX AT CONTACT POINT #1
C                 AT LOWER BOUND OF THE NORMAL LOAD
C        SMTX12 - AT THE UPPER BOUND OF THE NORMAL LOAD
C        SMTX21 - DAMPER STIFFNESS MATRIX AT CONTACT POINT #2
C                 AT LOWER BOUND OF THE NORMAL LOAD
C        SMTX22 - AT THE UPPER BOUND OF THE NORMAL LOAD
C        FNM11 - LOWER BOUND OF THE NORMAL LOAD AT POINT #1
C        FNM12 - UPPER BOUND OF THE NORMAL LOAD AT POINT #1
C        FNM21 - LOWER BOUND OF THE NORMAL LOAD AT POINT #2
C        FNM22 - UPPER BOUND OF THE NORMAL LOAD AT POINT #2
C        FCOE11 - FRICTION COEFFICIENT AT CONTACT POINT #1
C                 AT LOWER BOUND OF THE NORMAL LOAD
C        FCOE12 - AT THE UPPER BOUND OF THE NORMAL LOAD
C        FCOE21 - FRICTION COEFFICIENT AT CONTACT POINT #2
C                 AT LOWER BOUND OF THE NORMAL LOAD
C        FCOE22 - AT THE UPPER BOUND OF THE NORMAL LOAD
C        FNMC11 - LOWER BOUND OF THE NORMAL LOAD AT POINT #1
C        FNMC12 - UPPER BOUND OF THE NORMAL LOAD AT POINT #1
C        FNMC21 - LOWER BOUND OF THE NORMAL LOAD AT POINT #2
C        FNMC22 - UPPER BOUND OF THE NORMAL LOAD AT POINT #2
C        ALPHA = FRACTION OF NORMAL LOAD AT CONTACT POINT 1
C        CEPSI = MAX ALLOWABLE ERROR FOR CONVERGENCE
C
      IMPLICIT DOUBLE PRECISION (A-H,O-Z)
      COMMON/NUMB/NBLADE,NEODER,NMODES,NRS,NCO
      COMMON/MAIN/PHASE
      COMMON/BLADE/U(8,10),SR(15,10),EMASS(10),WMODAL(10),
     1  DAM(10)
      COMMON/DAMPER/SMTX11(2,2),SMTX12(2,2),SMTX21(2,2),SMTX22(2,2),
     1  S1(2,2),S2(2,2),FCOE11,FCOE12,FCOE21,FCOE22,FNM11,FNM12,
     2  FNM21,FNM22,FNMC11,FNMC12,FNMC21,FNMC22,COE1,COE2
      COMMON/NLOAD/FN1,FN2,ALPHA
      COMMON/CONVE/CEPSI
```

```
C
      CEPSI=1.0D-09
C
      READ(7,*) NBLADE,NEODER,NMODES
      PHASE = 2.0*3.1415927*NEODER/NBLADE
      DO 10 I=1,NMODES
   10 READ(7,*) EMASS(I),WMODAL(I),DAM(I)
      DO 20 I=1,8
   20 READ(7,*) (U(I,J),J=1,NMODES)
      READ(7,*) NRS,NCO
      NN=NRS*NCO
      DO 40 I=1,NN
   40 READ(7,*) (SR(I,J),J=1,NMODES)
      READ(7,*) FNM11
      READ(7,*) SMTX11(1,1),SMTX11(1,2),SMTX11(2,1),SMTX11(2,2)
      READ(7,*) FNM12
      READ(7,*) SMTX12(1,1),SMTX12(1,2),SMTX12(2,1),SMTX12(2,2)
      READ(7,*) FNM21
      READ(7,*) SMTX21(1,1),SMTX21(1,2),SMTX21(2,1),SMTX21(2,2)
      READ(7,*) FNM22
      READ(7,*) SMTX22(1,1),SMTX22(1,2),SMTX22(2,1),SMTX22(2,2)
      READ(7,*) FNMC11,FCOE11
      READ(7,*) FNMC12,FCOE12
      READ(7,*) FNMC21,FCOE21
      READ(7,*) FNMC22,FCOE22
      READ(7,*) ALPHA
      RETURN
      END
C
      SUBROUTINE PRINT(TITLE)
C
C        PRINTS PROBLEM INPUT DATA
C
      IMPLICIT DOUBLE PRECISION (A-H,O-Z)
      COMMON/NUMB/NBLADE,NEODER,NMODES,NRS,NCO
      COMMON/MAIN/PHASE
      COMMON/BLADE/U(8,10),SR(15,10),EMASS(10),WMODAL(10),
     1  DAM(10)
      COMMON/DAMPER/SMTX11(2,2),SMTX12(2,2),SMTX21(2,2),SMTX22(2,2),
     1  S1(2,2),S2(2,2),FCOE11,FCOE12,FCOE21,FCOE22,FNM11,FNM12,
     2  FNM21,FNM22,FNMC11,FNMC12,FNMC21,FNMC22,COE1,COE2
      COMMON/NLOAD/FN1,FN2,ALPHA
      COMMON/CONVE/CEPSI
      CHARACTER MD*4,TITLE*72
      DATA MD/'MODE'/
C
      WRITE(6,10)
   10 FORMAT(/,3X,'-- BLDAMP V1.1 DECEMBER 5,1987 --')
      WRITE(6,20)
   20 FORMAT(/,3X,'WRITTEN BY C-H. MENQ,GRIFFIN CONSULTING,1987',
     1  /,3X,'WARNINGS: 1. THESE CALCULATIONS ARE BASED ON',
     2  /,15X,' APPROXIMATIONS THAT MAY LEAD TO SIGNIFICANT',
     3  /,15X,' ERRORS IN CERTAIN CASES--REFER TO USER MANUAL.',/,
     4  /,13X,'2. THE SOLUTION ALGORITHM IS ITERATIVE & MAY NOT',
     5  /,16X,'CONVERGE. THIS MAY LEAD TO EXCESSIVE COMPUTER USAGE.')
      WRITE(6,30)
   30 FORMAT(1H1,2X,'******* PROBLEM DESCRIPTION *******')
      WRITE(6,40) TITLE,NBLADE
   40 FORMAT(/,2X,A72,//,3X,'NUMBER OF BLADES',26X,'=',I4)
      WRITE(6,50) NEODER
```

```
 50 FORMAT(3X,'ENGINE ORDER OF EXCITATION',16X,'=',I4)
    WRITE(6,60) NMODES
 60 FORMAT(3X,'NUMBER OF MODES',27X,'=',I4)
    WRITE(6,90) NRS
 90 FORMAT(3X,'NUMBER OF STRESS REFERENCE POINTS',9X,'=',I4)
    WRITE(6,110)
110 FORMAT(///,3X,'******* MODAL INPUT DATA *******',//,5X,'MODE',
   1 5X,'FREQUENCY (HZ)',5X,'GENERALIZED MASS',5X,'DAMPING RATIO',/)
    WRITE(6,120) (I,WMODAL(I),EMASS(I),DAM(I),I=1,NMODES)
120 FORMAT(/,5X,I3,6X,1PE12.5,8X,1PE12.5,7X,0PF10.4)
    WRITE(6,130)
130 FORMAT(//,3X,'MODAL DISPLACEMENTS AT DAMPER CONTACT POINTS',/)
    WRITE(6,140) (MD,I=1,NMODES)
140 FORMAT(3X,'CONTACT',6X,8(A4,11X))
    WRITE(6,145) (I,I=1,NMODES)
145 FORMAT(4X,'POINT',7X,8(I3,12X))
    DO 170 I=1,4
    K=2*I-1
    KK=2*I
    WRITE(6,150) I,(U(K,J),J=1,NMODES)
150 FORMAT(/,4X,I3,4X,8(1PE12.5,3X))
    WRITE(6,160) (U(KK,J),J=1,NMODES)
160 FORMAT(11X,8(1PE12.5,3X))
170 CONTINUE
    IF(NRS .EQ. 0) GO TO 235
    WRITE(6,180)
180 FORMAT(//,3X,'MODAL STRESSES AT STRESS REFERENCE POINTS',/)
    WRITE(6,190) (MD,I=1,NMODES)
190 FORMAT(2X,'REFERENCE',5X,8(A4,11X))
    WRITE(6,145) (I,I=1,NMODES)
    NN=NCO*NRS
    DO 230 I=1,NN
230 WRITE(6,150) I,(SR(I,J),J=1,NMODES)
235 CONTINUE
    WRITE(6,300)
300 FORMAT(1H1,1X,'******* DAMPER PROPERTIES *******',//)
    WRITE(6,310)
310 FORMAT(/,3X,'DAMPER CONTACT POINT 1:')
    WRITE(6,320) FNM11
320 FORMAT(/,5X,'LOWER NORMAL LOAD       =',F14.4)
    WRITE(6,330)
330 FORMAT(/,5X,'DAMPER STIFFNESS MATRIX:')
    WRITE(6,340)SMTX11(1,1),SMTX11(1,2)
    WRITE(6,350)SMTX11(2,1),SMTX11(2,2)
340 FORMAT(7X,'KXX,KXY = ',2(2X,F14.4))
350 FORMAT(7X,'KYX,KYY = ',2(2X,F14.4))
    WRITE(6,360) FNM12
360 FORMAT(/,5X,'UPPER NORMAL LOAD       =',F14.4)
    WRITE(6,330)
    WRITE(6,340)SMTX12(1,1),SMTX12(1,2)
    WRITE(6,350)SMTX12(2,1),SMTX12(2,2)
    WRITE(6,370)
370 FORMAT(//,3X,'DAMPER CONTACT POINT 2:')
    WRITE(6,320) FNM21
    WRITE(6,330)
    WRITE(6,340)SMTX21(1,1),SMTX21(1,2)
    WRITE(6,350)SMTX21(2,1),SMTX21(2,2)
    WRITE(6,360) FNM22
    WRITE(6,330)
    WRITE(6,340) SMTX22(1,1),SMTX22(1,2)
```

```
      WRITE(6,350) SMTX22(2,1),SMTX22(2,2)
      WRITE(6,380)
  380 FORMAT(//,10X,'-- COEFFICIENT OF FRICTION --')
      WRITE(6,310)
      WRITE(6,320) FNMC11
      WRITE(6,390) FCOE11
  390 FORMAT(/,5X,'COEFFICIENT OF FRICTION =',F12.5)
      WRITE(6,360) FNMC12
      WRITE(6,390) FCOE12
      WRITE(6,370)
      WRITE(6,320) FNMC21
      WRITE(6,390) FCOE21
      WRITE(6,360) FNMC22
      WRITE(6,390) FCOE22
      WRITE(6,400) ALPHA
  400 FORMAT(/,5X,'ALPHA = ',1X,F5.2)
      WRITE(6,410) CEPSI
  410 FORMAT(/,5X,'CEPSI = ',1PE12.5)
      RETURN
      END
C
      SUBROUTINE IO1
C
C        IO1 - PERFORM TRACKING PLOT
C
      IMPLICIT DOUBLE PRECISION (A-H,O-Z)
      COMMON/EXCIT/GF(10),MODE
C
      WRITE(6,10)
   10 FORMAT(1H1,3X,'ANALYSIS TYPE SELECTED: FREQUENCY RESPONSE PLOT')
C
C        READ GENERALIZED FORCES FROM STRESS?
C        IA1=1 YES
C        IA1=2 NO
C
      READ(7,*) IA1
      IF(IA1 .EQ. 1) THEN
      CALL READS
      ELSE
      CALL READGF
      END IF
C
C        READ FREQUENCY RANGE
C
      READ(7,*) WMIN,WMAX,DW
      WRITE(6,15)
   15 FORMAT(/,4X,'FREQUENCY RANGE:',/)
      WRITE(6,20) WMIN,WMAX,DW
   20 FORMAT(7X,'MINIMUM FREQUENCY =',F10.3,/,
     1       7X,'MAXIMUM FREQUENCY =',F10.3,/,
     2       7X,'FREQ. INCREMENT   =',F10.3,/)
C
C        READ TOTAL DAMPER LOAD
C
      READ(7,*) FN
      WRITE(6,30) FN
   30 FORMAT(4X,'TOTAL DAMPER LOAD =',F10.3)
      CALL FREQRP(WMIN,WMAX,DW,FN)
      RETURN
      END
```

```
C
      SUBROUTINE IO2
C
C        IO2 - CALCULATE OPTIMUM CURVE
C
      IMPLICIT DOUBLE PRECISION (A-H,O-Z)
      COMMON/BLADE/U(8,10),SR(15,10),EMASS(10),WMODAL(10),
     1  DAM(10)
      COMMON/MSTRESS/PSTRESS,SVRM
      COMMON/EXCIT/GF(10),MODE
      COMMON/STICK/IS,SFN,SW
      COMMON/OPTIMUM/NP,NC
      WRITE(6,10)
   10 FORMAT(1H1,2X,'ANALYSIS TYPE SELECTED: OPTIMUM N CURVE')
      WRITE(6,20)
   20 FORMAT(/,3X,'INPUT DATA:')
C
C        READ GENERALIZED FORCES FROM STRESS?
C        A1=1 YES
C        A1=2 NO
C
      READ(7,*) A1
      IF(A1 .EQ. 1.) THEN
      CALL READS
      ELSE
      CALL READGF
      ENDIF
C
C        READ REFERENCE STRESS, COMPONENT NUMBER, AND MODE
C
      READ(7,*) NP,NC,NONMOD
      WRITE(6,30) NP,NC,NONMOD
   30 FORMAT(/,3X,'PEAK RESPONSE IS BASED ON:',//,
     1          5X,'STRESS NUMBER    =',I3,/,
     2          5X,'COMPONENT NUMBER =',I3,/,
     3          5X,'MODE NUMBER      =',I3)
C
      CALL OPTIM(NONMOD)
      RETURN
      END
C
      SUBROUTINE IO3
C
C        IO3 - CALCULATE PERFORMANCE CURVE
C
      IMPLICIT DOUBLE PRECISION (A-H,O-Z)
      COMMON/EXCIT/GF(10),MODE
      COMMON/STICK/IS,SFN,SW
      COMMON/OPTIMUM/NP,NC
      WRITE(6,10)
   10 FORMAT(1H1,3X,'ANALYSIS TYPE SELECTED: DAMPER PERFORMANCE CURVE')
      WRITE(6,20)
   20 FORMAT(/,3X,'INPUT DATA:')
C
C        READ GENERALIZED FORCES FROM STRESS?
C        A1=1 YES
C        A1=2 NO
C
      READ(7,*) A1
      IF(A1 .EQ. 1.) THEN
```

```
      CALL READS
      ELSE
      CALL READGF
      ENDIF
C
C        READ DAMPER NORMAL LOAD
C
      READ(7,*) FN
      WRITE(6,30) FN
   30 FORMAT(/,7X,'NORMAL LOAD =',F12.7)
C
C        READ REFERENCE STRESS, COMPONENT NUMBER, AND MODE
C
      READ(7,*) NP,NC,NONMOD
      WRITE(6,40) NP,NC,NONMOD
   40 FORMAT(/,3X,'PEAK RESPONSE IS BASED ON',//,
     1          5X,'STRESS NUMBER     =',I3,/,
     2          5X,'COMPONENT NUMBER =',I3,/,
     2          5X,'MODE NUMBER       =',I3)
C
      CALL PERFOR(NONMOD,FN)
      RETURN
      END
C
      SUBROUTINE READGF
C
C        READS GENERALIZED FORCES
C
      IMPLICIT DOUBLE PRECISION (A-H,O-Z)
      COMMON/EXCIT/GF(10),MODE
      COMMON/NUMB/NBLADE,NEODER,NMODES,NRS,NCO
      DO 20 I=1,NMODES
      WRITE(6,10) I
   10 FORMAT(/,7X,'EXCITATION OF MODE NUMBER',1X,I2)
      READ(7,*) GF(I)
      WRITE(6,15) GF(I)
   15 FORMAT(/,7X,'GENERALIZED FORCE = ',1PE15.5,/)
   20 CONTINUE
      RETURN
      END
C
      SUBROUTINE READS
C
C        READ PEAK STRESS & MODAL STRESS THEN CALCULATE
C        GENERALIZED FORCE
C        PSTRESS = MAXIMUM UNDAMPED STRESS
C        SVRM = MODAL STRESS
C
      IMPLICIT DOUBLE PRECISION (A-H,O-Z)
      COMMON/EXCIT/GF(10),MODE
      COMMON/NUMB/NBLADE,NEODER,NMODES,NRS,NCO
      COMMON/BLADE/U(8,10),SR(15,10),EMASS(10),WMODAL(10),
     1  DAM(10)
      DO 50 I=1,NMODES
      READ(7,*) PSTRESS,SVRM
      WRITE(6,10) I
   10 FORMAT(/,7X,'EXCITATION OF MODE #',1X,I2)
      WRITE(6,20) PSTRESS,SVRM
   20 FORMAT(/,7X,'MAXIMUM UNDAMPED STRESS =',1PE15.5,/,
     1          7X,'MODAL STRESS             =',1PE15.5,/)
```

```
      GDRM = PSTRESS/SVRM
      GF(I) = 2.0*DAM(I)*WMODAL(I)**2*EMASS(I)*GDRM
   50 CONTINUE
      RETURN
      END
C
      SUBROUTINE FREQRP(WMIN,WMAX,DW,FN)
C
C          FIND STRESS VERSUS FREQUENCY OF EXCITATION FOR A GIVEN
C          INPUT.
C
C        WMIN - SMALLEST FREQUENCY
C        WMAX - LARGEST FREQUENCY
C        DW - REFERENCE FREQUENCY INCREMENT
C        FN - NORMAL LOAD
C
      IMPLICIT DOUBLE PRECISION (A-H,O-Z)
      COMMON/BLADE/U(8,10),SR(15,10),EMASS(10),WMODAL(10),
     1  DAM(10)
      COMMON/NUMB/NBLADE,NEODER,NMODES,NRS,NCO
      COMMON/MAIN/PHASE
      COMMON/RECEPE/RE1(2,2),RE2(2,2),RE3(2,2),RE4(2,2)
      COMMON/RECEPF/RF(8,8,2),CF(8,2)
      COMMON/DAMPER/SMTX11(2,2),SMTX12(2,2),SMTX21(2,2),SMTX22(2,2),
     1  S1(2,2),S2(2,2),FCOE11,FCOE12,FCOE21,FCOE22,FNM11,FNM12,
     1  FNM21,FNM22,FNMC11,FNMC12,FNMC21,FNMC22,COE1,COE2
      COMMON/NLOAD/FN1,FN2,ALPHA
      COMMON/EXCIT/GF(10),MODE
      COMMON/GSOLV/X(8),DX(8),XMAX(8),XMIN(8),DELMX(8),EPSI(8),
     1  A(8,8),B(8,1)
      COMMON/STICK/IS,SFN,SW
      COMMON/NITER/ITER
      DIMENSION PS(3),SM(3,2)
      DIMENSION PSS(500,5,3),WW(500),SMM(500,5,3,2)
      DIMENSION XI(8)
C
      WRITE(6,10)
   10 FORMAT(///,3X,'***** CALCULATE FREQUENCY RESPONSE *****')
C
      CALL GETRE(WMIN)
C
      MODE=1
      CALL DVALUE
      XI(1)=RE1(1,1)+RE4(1,1)
      XI(2)=RE1(1,2)+RE4(1,2)
      XI(3)=RE1(2,1)+RE4(2,1)
      XI(4)=RE1(2,2)+RE4(2,2)
      XI(5)=RE2(1,1)+RE3(1,1)
      XI(6)=RE2(1,2)+RE3(1,2)
      XI(7)=RE2(2,1)+RE3(2,1)
      XI(8)=RE2(2,2)+RE3(2,2)
      CALL DAMPR(FN)
      NOEQN=8
      MITER=20
      IC = 0
      NUMO = 0
      DW1=DW
      DW3=DW*3
      IW=2
   20 W = WMIN
```

```
   30 IC = IC + 1
   40 CALL GETRE(W)
      CALL GETRF(W)
      DO 50 I=1,8
   50 X(I) = XI(I)
      CALL GSLV(NOEQN,X,DX,XMAX,XMIN,DELMX,EPSI,20,0,IERR,A,B)
      IF(IERR.EQ.1)THEN
      IF(NUMO .EQ. 0) THEN
      WMIN=0.9*WMIN
      GO TO 20
      ENDIF
      DW1=DW1/IW
      W=W-DW1
      GO TO 40
      ENDIF
      DO 60 I=1,8
   60 XI(I) = X(I)
      NUMO = NUMO+1
      WW(NUMO)=W
      DO 80 J=1,NRS
      CALL OSTRESS(W,J,PS,SM)
      DO 70 JJ=1,NCO
      PSS(NUMO,J,JJ) = PS(JJ)
      SMM(NUMO,J,JJ,1)= SM(JJ,1)
   70 SMM(NUMO,J,JJ,2)= SM(JJ,2)
   80 CONTINUE
C
      IF(IC .GE. 10) THEN
      IC = IC-10
      ENDIF
      DW1=DW1*(3.0-8.0/3.0*ITER/MITER)
      IF(DW1 .GE. DW3) THEN
      DW1=DW3
      ENDIF
      W = W + DW1
      IF(W .LE. WMAX) THEN
      GO TO 30
      ENDIF
C
C
C        PRINT STRESS VS FREQUENCY
C
      DO 140 J=1,NRS
      DO 140 K=1,NCO
      WRITE(6,110) J,K
  110 FORMAT(1H1,1X,'FREQUENCY RESPONSE CURVE FOR STRESS NUMBER',
     1  I3,' COMPONENT NUMBER',I3,//,6X,'FREQUENCY',10X,'STRESS',/)
      DO 120 I=1,NUMO
  120 WRITE(6,130) WW(I),PSS(I,J,K)
  130 FORMAT(1X,1PE15.5,3X,1PE15.5)
  140 CONTINUE
  500 WRITE(6,510)
  510 FORMAT(/,3X,'***** END OF OUTPUT DATA *****')
      RETURN
      END
C
      SUBROUTINE OPTIM(NONMOD)
C
C        CALCULATES OPTIMUM NORMAL FORCE CURVE
C
```

```
C         FN = NORMAL LOAD
C
      IMPLICIT DOUBLE PRECISION (A-H,O-Z)
      COMMON/BLADE/U(8,10),SR(15,10),EMASS(10),WMODAL(10),
     1  DAM(10)
      COMMON/NUMB/NBLADE,NEODER,NMODES,NRS,NCO
      COMMON/MAIN/PHASE
      COMMON/DAMPER/SMTX11(2,2),SMTX12(2,2),SMTX21(2,2),SMTX22(2,2),
     1  S1(2,2),S2(2,2),FCOE11,FCOE12,FCOE21,FCOE22,FNM11,FNM12,
     2  FNM21,FNM22,FNMC11,FNMC12,FNMC21,FNMC22,COE1,COE2
      COMMON/NLOAD/FN1,FN2,ALPHA
      COMMON/RECEPE/RE1(2,2),RE2(2,2),RE3(2,2),RE4(2,2)
      COMMON/RECEPF/RF(8,8,2),CF(8,2)
      COMMON/FFORCE/F1(2,2),F2(2,2),F3(2,2),F4(2,2)
      COMMON/EXCIT/GF(10),MODE
      COMMON/GSOLV1/X1(1),DX1(1),XMAX1(1),XMIN1(1),DELMX1(1),EPSI1(1),
     1  A1(1,1),B1(1,1)
      COMMON/GSOLV/X(8),DX(8),XMAX(8),XMIN(8),DELMX(8),EPSI(8),
     1  A(8,8),B(8,1)
      COMMON/ERROR/IR,XI(8)
      COMMON/STICK/IS,SFN,SW
      COMMON/SWITCH/IM
      DIMENSION PS(3),SM(3,2)
      DIMENSION PSS(100,5,3),WW(100),SMM(100,5,3,2),FNO(100)
      DIMENSION SVALUE(2),RANGLE(2),PANGLE(2)
C
      WRITE(6,10)
   10 FORMAT(///,3X,'***** CALCULATE PEAK RESPONSE *****')
      MODE=NONMOD
      XII=WMODAL(MODE)*(1.0-2.0*DAM(MODE)**2)**0.5
      XIII=0.9*XII
      CALL GETRE1(XII)
      X(1)=RE1(1,1)+RE4(1,1)
      X(2)=RE1(1,2)+RE4(1,2)
      X(3)=RE1(2,1)+RE4(2,1)
      X(4)=RE1(2,2)+RE4(2,2)
      X(5)=RE2(1,1)+RE3(1,1)
      X(6)=RE2(1,2)+RE3(1,2)
      X(7)=RE2(2,1)+RE3(2,1)
      X(8)=RE2(2,2)+RE3(2,2)
      CALL DVALUE
      CALL DVALUE1
      DFNN=ABS(GF(MODE))
      MITER=20
      NF=0
      IC=0
      NUMO=0
      FN=0.0
      DFN=DFNN
   20 IC=IC+1
      NUMO=NUMO+1
      IT=0
      IN=3
   30 CALL DAMPR(FN)
      X1(1)=XII
      DO 40 I=1,8
   40 XI(I)=X(I)
      IM=1
      CALL GSLV1(1,X1,DX1,XMAX1,XMIN1,DELMX1,EPSI1,MITER,ITER,0,IERR,
     1 A1,B1)
```

```
      IF(IERR.EQ.1.OR.IR.EQ.1.OR.X1(1).LE.XII*0.99.OR.
     1  X1(1) .GT. XII*1.1) THEN
      IT=IT+1
      IF(IT .GE. 10) GO TO 100
      FN=FN-DFN*(IN-1)/IN
      DFN=DFN/IN
      GO TO 30
      ENDIF
      XII=X1(1)
      DO 50 I=1,8
   50 X(I)=XI(I)
      IM=2
      CALL GSLV1(1,X1,DX1,XMAX1,XMIN1,DELMX1,EPSI1,MITER,ITER,0,IERR,
     1 A1,B1)
      W = X1(1)
      FNO(NUMO)=FN
      WW(NUMO)=W
      DO 70 J=1,NRS
      CALL OSTRESS(W,J,PS,SM)
      DO 60 JJ=1,NCO
      PSS(NUMO,J,JJ)=PS(JJ)
      SMM(NUMO,J,JJ,1)=SM(JJ,1)
   60 SMM(NUMO,J,JJ,2)=SM(JJ,2)
   70 CONTINUE
      IF(IC.GE. 5) THEN
      IC = IC-5
      ENDIF
      DFN=DFN*(3.0-8.0/3.0*ITER/MITER)
      FN = FN +DFN
      CRIT=W/XIII-1.0
      IF(ABS(CRIT) .GE. 1.0D-07) THEN
      XIII=X1(1)
      GO TO 20
      ENDIF
C
      DO 80 I=1,2
      DO 80 J=1,2
      F1(I,J) = CF(I,J)
   80 F2(I,J) = CF(I+2,J)
      CALL ROTATE(F1,SVALUE,RANGLE,PANGLE)
      FN1 = SVALUE(1)/COE1
      CALL ROTATE(F2,SVALUE,RANGLE,PANGLE)
      FN2 = SVALUE(1)/COE2
C
      IF(ALPHA.EQ.0.0) THEN
      SFN = FN2
      GO TO 90
      ELSEIF(ALPHA.EQ.1.0)THEN
      SFN = FN1
      GO TO 90
      ENDIF
      FN1 = FN1/ALPHA
      FN2 = FN2/(1.0-ALPHA)
      IF(FN1.GT.FN2)THEN
      SFN = FN1
      GO TO 90
      ENDIF
C
      SFN = FN2
   90 FNO(NUMO-1)=SFN
```

```
      FNO(NUMO)=1.1*SFN
      GO TO 120
  100 WRITE(6,110)
  110 FORMAT(/,1X,'CONVERGEMENT FAILS; STOP COMPUTING|')
  120 CONTINUE
C
C        PRINT PEAK FREQUENCY
C
      WRITE(6,140)
  140 FORMAT(1H1,2X,'FREQUENCY OF PEAK RESPONSE AS A FUNCTION OF ',
     1 'NORMAL FORCE',//,4X,'NORMAL FORCE',5X,'FREQUENCY',/)
      DO 150 I=1,NUMO
  150 WRITE(6,160) FNO(I),WW(I)
  160 FORMAT(1X,1P2E15.5)
C
C        PRINT OPTIMUM CURVE
C
      DO 240 J=1,NRS
      DO 240 K=1,NCO
      WRITE(6,210) J,K
  210 FORMAT(1H1,1X,'OPTIMUM CURVE FOR STRESS NUMBER',I3,
     1   ' COMPONENT NUMBER',I3,//,4X,'NORMAL FORCE',9X,'STRESS',/)
      DO 220 I=1,NUMO
  220 WRITE(6,230) FNO(I),PSS(I,J,K)
  230 FORMAT(1X,1PE15.5,3X,1PE15.5)
  240 CONTINUE
  500 WRITE(6,510)
  510 FORMAT(/,3X,'***** END OF OUTPUT DATA *****')
      RETURN
      END
C
      SUBROUTINE PERFOR(NONMOD,FNN)
C
C        SUBROUTINE FINDS THE PEAK STRESS WITH THE DAMPER IN PLACE AS
C        A FUNCTION OF WHAT THE STRESS WOULD BE WITHOUT THE DAMPER.
C
C        FNN - GIVEN DAMPER NORMAL LOAD
C
      IMPLICIT DOUBLE PRECISION (A-H,O-Z)
      COMMON/BLADE/U(8,10),SR(15,10),EMASS(10),WMODAL(10),
     1  DAM(10)
      COMMON/NUMB/NBLADE,NEODER,NMODES,NRS,NCO
      COMMON/MAIN/PHASE
      COMMON/DAMPER/SMTX11(2,2),SMTX12(2,2),SMTX21(2,2),SMTX22(2,2),
     1  S1(2,2),S2(2,2),FCOE11,FCOE12,FCOE21,FCOE22,FNM11,FNM12,
     2  FNM21,FNM22,FNMC11,FNMC12,FNMC21,FNMC22,COE1,COE2
      COMMON/NLOAD/FN1,FN2,ALPHA
      COMMON/RECEPE/RE1(2,2),RE2(2,2),RE3(2,2),RE4(2,2)
      COMMON/RECEPF/RF(8,8,2),CF(8,2)
      COMMON/FFORCE/F1(2,2),F2(2,2),F3(2,2),F4(2,2)
      COMMON/EXCIT/GF(10),MODE
      COMMON/GSOLV1/X1(1),DX1(1),XMAX1(1),XMIN1(1),DELMX1(1),EPSI1(1),
     1  A1(1,1),B1(1,1)
      COMMON/GSOLV/X(8),DX(8),XMAX(8),XMIN(8),DELMX(8),EPSI(8),
     1  A(8,8),B(8,1)
      COMMON/ERROR/IR,XI(8)
      COMMON/STICK/IS,SFN,SW
      COMMON/SWITCH/IM
      DIMENSION PDN(100,5,3),FNO(100),SMN(100,5,3,2),WW(100),WWW(100)
      DIMENSION PDD(100,5,3),PUD(100,5,3),GFF(100),SMM(100,5,3,2)
```

```
      DIMENSION PS(3),SM(3,2)
      DIMENSION SVALUE(2),RANGLE(2),PANGLE(2)
C
      WRITE(6,10)
   10 FORMAT(/,3X,'***** CALCULATE PERFORMANCE CURVE *****')
C
      MODE = NONMOD
      XII=WMODAL(MODE)*(1.0-2.0*DAM(MODE)**2)**0.5
      XIII=XII*0.9
C
      CALL GETRE1(XII)
C
      X(1)=RE1(1,1)+RE4(1,1)
      X(2)=RE1(1,2)+RE4(1,2)
      X(3)=RE1(2,1)+RE4(2,1)
      X(4)=RE1(2,2)+RE4(2,2)
      X(5)=RE2(1,1)+RE3(1,1)
      X(6)=RE2(1,2)+RE3(1,2)
      X(7)=RE2(2,1)+RE3(2,1)
      X(8)=RE2(2,2)+RE3(2,2)
C
      CALL DVALUE
      CALL DVALUE1
      CALL DAMPR(FNN)
      MITER=20
      NF=0
      IC=0
      NUMO=0
      FN=0.0
      FN1 = ALPHA*FN
      FN2 = (1.0 - ALPHA)*FN
      DFN=ABS(GF(MODE))
   20 IC=IC+1
      NUMO=NUMO+1
      IT=0
      IN=3
   30 CONTINUE
      X1(1)=XII
      DO 40 I=1,8
   40 XI(I)=X(I)
      IM=1
      CALL GSLV1(1,X1,DX1,XMAX1,XMIN1,DELMX1,EPSI1,MITER,ITER,0,IERR,
     1  A1,B1)
      IF(IERR.EQ.1.OR.IR.EQ.1.OR.X1(1).LE.XII*0.99.OR.
     1  X1(1) .GT. XII*1.1) THEN
      IT=IT+1
      IF(IT .GE. 10) GO TO 100
      FN=FN-DFN*(IN-1)/IN
      DFN=DFN/IN
      FN1=ALPHA*FN
      FN2=(1.0-ALPHA)*FN
      GO TO 30
      ENDIF
      XII=X1(1)
      DO 50 I=1,8
   50 X(I)=XI(I)
      IM=2
      CALL GSLV1(1,X1,DX1,XMAX1,XMIN1,DELMX1,EPSI1,MITER,ITER,0,IERR,
     1  A1,B1)
      W = X1(1)
```

```
      FNO(NUMO)=FN
      WW(NUMO)=W
      DO 60 J=1,NRS
      CALL OSTRESS(W,J,PS,SM)
      DO 60 JJ=1,NCO
      SMN(NUMO,J,JJ,1)=SM(JJ,1)
      SMN(NUMO,J,JJ,2)=SM(JJ,2)
      PDN(NUMO,J,JJ)=PS(JJ)
   60 CONTINUE
      IF(IC .GE. 5) THEN
      IC = IC-5
      ENDIF
      DFN=DFN*(3.0-8.0/3.0*ITER/MITER)
      FN=FN+DFN
      FN1=ALPHA*FN
      FN2=(1.0-ALPHA)*FN
      CRIT=W/XIII-1.0
      IF(ABS(CRIT) .GE. 1.0D-7) THEN
      XIII=X1(1)
      GO TO 20
      ENDIF
C
C        PRINT FREQUENCY OF PEAK RESPONSE VS NORMAL FORCE
C
      WRITE(6,70)
   70 FORMAT(1H1,1X,'FREQUENCY OF PEAK RESPONSE AS A FUNCTION OF',
     1 ' NORMAL FORCE',//,3X,'NORMAL FORCE',5X,'FREQUENCY',/)
      WRITE(6,75) (FNO(I),WW(I),I=1,NUMO)
   75 FORMAT(1X,1P2E15.7)
      DO 80 I=1,2
      DO 80 J=1,2
      F1(I,J) = CF(I,J)
   80 F2(I,J) = CF(I+2,J)
      CALL ROTATE(F1,SVALUE,RANGLE,PANGLE)
      FN1 = SVALUE(1)/COE1
      CALL ROTATE(F2,SVALUE,RANGLE,PANGLE)
      FN2 = SVALUE(1)/COE2
C
      IF(ALPHA .EQ. 0.0) THEN
      SFN = FN2
      GO TO 90
      ELSE IF(ALPHA .EQ. 1.0) THEN
      SFN = FN1
      GO TO 90
      ENDIF
      FN1 = FN1/ALPHA
      FN2 = FN2/(1.0-ALPHA)
      IF(FN1 .GT. FN2) THEN
      SFN = FN1
      GO TO 90
      ENDIF
C
      SFN = FN2
   90 FNO(NUMO-1)=SFN
      FNO(NUMO)=1.1*SFN
C
      GO TO 120
  100 WRITE(6,110)
  110 FORMAT(/,1X,'CONVERGEMENT FAILS; STOP COMPUTING|')
  120 CONTINUE
```

```
      GFF(1)=0.0
      WWW(1)=WW(NUMO)
      DO 130 I=1,NRS
      DO 130 J=1,NCO
      SMM(1,I,J,1)=0.0
      SMM(1,I,J,2)=0.0
      PUD(1,I,J)=0.0
  130 PDD(1,I,J)=0.0
C
      DO 150 II=2,NUMO
      I1=NUMO-II+2
      GFF(II)=FNN/FNO(I1)
      WWW(II)=WW(I1)
      DO 150 I=1,NRS
      DO 140 J=1,NCO
      SMM(II,I,J,1) =SMN(II,I,J,1)*GFF(II)
      SMM(II,I,J,2) =SMN(II,I,J,2)*GFF(II)
      PUD(II,I,J)=PDN(1,I,J)*GFF(II)
  140 PDD(II,I,J)=PDN(I1,I,J)*GFF(II)
  150 CONTINUE
C
C        PRINT PEAK FREQUENCY AS A FUNCTION OF GENERALIZED FORCE
C
      WRITE(6,160)
  160 FORMAT(1H1,1X,'FREQUENCY OF PEAK RESPONSE AS A FUNCTION OF ',
     1 'GENERALIZED FORCE',//,3X,'GENERALIZED FORCE',5X,
     2 'FREQUENCY',/)
      DO 170 I=1,NUMO
  170 WRITE(6,180) FNO(I),WWW(I)
  180 FORMAT(3X,1PE15.7,4X,1PE15.7)
C
C        PRINT PERFORMANCE CURVE
C
      DO 250,J=1,NRS
      DO 250 K=1,NCO
      WRITE(6,220) J,K
  220 FORMAT(1H1,1X,'DAMPER PERFORMANCE CURVE FOR STRESS NUMBER',I3,
     1 ' COMPONENT NUMBER',I3,//,4X,'GEN. FORCE/NORMAL FORCE',10X,
     2 'STRESS',/)
      DO 230 I=1,NUMO
  230 WRITE(6,240) PUD(I,J,K),PDD(I,J,K)
  240 FORMAT(6X,1PE15.5,5X,1PE15.5)
  250 CONTINUE
  500 WRITE(6,510)
  510 FORMAT(/,3X,'***** END OF OUTPUT DATA *****')
      RETURN
      END
C
      SUBROUTINE OSTRESS(W,NREFER,PS,SM)
C
C        CALCULATE STRESS INFORMATION FOR A REFERENCE POINT
C
      IMPLICIT DOUBLE PRECISION (A-H,O-Z)
      COMMON/BLADE/U(8,10),SR(15,10),EMASS(10),WMODAL(10),
     1  DAM(10)
      COMMON/NUMB/NBLADE,NEODER,NMODES,NRS,NCO
      COMMON/MAIN/PHASE
      COMMON/RECEPF/RF(8,8,2),CF(8,2)
      COMMON/EXCIT/GF(10),MODE
      DIMENSION SS(10),FS(10)
```

```
      DIMENSION SM(3,2),PS(3)
C
      DO 100 I =1,NCO
      DO 10 J1=1,NMODES
      N1= NREFER-1
   10 SS(J1)=SR(NCO*N1+I,J1)
C
      CALL RESPNSE(SS,W,SM(I,1),SM(I,2))
C
      DO 30 K=1,8
      DO 20 J2=1,NMODES
   20 FS(J2)= U(K,J2)
C
      CALL STRESS(SS,FS,1.0D+0,W,SCA,SSA)
      SM(I,1) = SM(I,1) - CF(K,1)*SCA + CF(K,2)*SSA
      SM(I,2) = SM(I,2) - CF(K,2)*SCA - CF(K,1)*SSA
   30 CONTINUE
      PS(I)= (SM(I,1)**2+SM(I,2)**2)**0.5
  100 CONTINUE
      RETURN
      END
C
      SUBROUTINE DVALUE
C
C        SPECIFY NUMERICAL VALUES FOR THE PARAMETERS USED
C        IN GSOLV
C
      IMPLICIT DOUBLE PRECISION (A-H,O-Z)
      COMMON/BLADE/U(8,10),SR(15,10),EMASS(10),WMODAL(10),
     1  DAM(10)
      COMMON/GSOLV/X(8),DX(8),XMAX(8),XMIN(8),DELMX(8),EPSI(8),
     1  A(8,8),B(8,1)
      COMMON/EXCIT/GF(10),MODE
      COMMON/MAIN/PHASE
      COMMON/RECEPE/RE1(2,2),RE2(2,2),RE3(2,2),RE4(2,2)
      COMMON/CONVE/CEPSI
      DIMENSION XX(8)
      CALL GETRE(WMODAL(MODE))
      XX(1)=RE1(1,1)+RE4(1,1)
      XX(2)=RE1(1,2)+RE4(1,2)
      XX(3)=RE1(2,1)+RE4(2,1)
      XX(4)=RE1(2,2)+RE4(2,2)
      XX(5)=RE2(1,1)+RE3(1,1)
      XX(6)=RE2(1,2)+RE3(1,2)
      XX(7)=RE2(2,1)+RE3(2,1)
      XX(8)=RE2(2,2)+RE3(2,2)
      DO 10 I=1,2
      J1=4*I-3
      J2=4*I-2
      J3=4*I-1
      J4=4*I
      XX2=(XX(J1)**2+XX(J2)**2+XX(J3)**2+XX(J4)**2)**0.5
      EPSI(J1)=CEPSI*XX2
      EPSI(J2)=EPSI(J1)
      EPSI(J3)=EPSI(J1)
      EPSI(J4)=EPSI(J1)
      DX(J1)=0.000001*XX2
      DX(J2)=DX(J1)
      DX(J3)=DX(J1)
      DX(J4)=DX(J1)
```

```
      XMAX(J1)=1.0D15
      XMAX(J2)=XMAX(J1)
      XMAX(J3)=XMAX(J1)
      XMAX(J4)=XMAX(J1)
      XMIN(J1)=-10000.*XX2
      XMIN(J2)=XMIN(J1)
      XMIN(J3)=XMIN(J1)
      XMIN(J4)=XMIN(J1)
      DELMX(J1)=0.1*XX2
      DELMX(J2)=DELMX(J1)
      DELMX(J3)=DELMX(J1)
   10 DELMX(J4)=DELMX(J1)
      RETURN
      END
C
      SUBROUTINE DVALUE1
C
C        SPECIFY NUMERICAL VALUES FOR THE PARAMETERS USED
C        IN GSOLV1
C
      IMPLICIT DOUBLE PRECISION (A-H,O-Z)
      COMMON/BLADE/U(8,10),SR(15,10),EMASS(10),WMODAL(10),
     1  DAM(10)
      COMMON/GSOLV1/X1(1),DX1(1),XMAX1(1),XMIN1(1),DELMX1(1),EPSI1(1),
     1  A1(1,1),B1(1,1)
      COMMON/EXCIT/GF(10),MODE
      EPSI1(1)=0.01/WMODAL(MODE)
      DX1(1)=0.01*DAM(MODE)*WMODAL(MODE)
      XMAX1(1)=1.0D15
      XMIN1(1)=-10000.0
      DELMX1(1)=0.1*WMODAL(MODE)
      RETURN
      END
C
      SUBROUTINE DAMPR(FN)
C
C        CALCULATE DAMPER STIFFNESS AND FRICTION COEFF.
C        AT A GIVEN NORMAL LOAD
C
      IMPLICIT DOUBLE PRECISION (A-H,O-Z)
      COMMON/DAMPER/SMTX11(2,2),SMTX12(2,2),SMTX21(2,2),SMTX22(2,2),
     1  S1(2,2),S2(2,2),FCOE11,FCOE12,FCOE21,FCOE22,FNM11,FNM12,
     1  FNM21,FNM22,FNMC11,FNMC12,FNMC21,FNMC22,COE1,COE2
      COMMON/NLOAD/FN1,FN2,ALPHA
C
      FN1 = ALPHA*FN
      FN2 = (1.0-ALPHA)*FN
C
      BATA1 = (FN1-FNMC11)/(FNMC12-FNMC11)
      IF(BATA1.GT.1.0)THEN
      BATA1 = 1.0
      ELSEIF(BATA1.LT.0.0)THEN
      BATA1 = 0.0
      ENDIF
C
      BATA2 = (FN2-FNMC21)/(FNMC22-FNMC21)
      IF(BATA2.GT.1.0)THEN
      BATA2 = 1.0
      ELSEIF(BATA2.LT.0.0)THEN
      BATA2 = 0.0
```

```
      ENDIF
C
      COE1 = (1.0-BATA1)*FCOE11 + BATA1*FCOE12
      COE2 = (1.0-BATA2)*FCOE21 + BATA2*FCOE22
      BATA1 = (FN1-FNM11)/(FNM12-FNM11)
      IF(BATA1.GT.1.0)THEN
      BATA1 = 1.0
      ELSEIF(BATA1.LT.0.0)THEN
      BATA1 = 0.0
      ENDIF
C
      BATA2 = (FN2-FNM21)/(FNM22-FNM21)
      IF(BATA2.GT.1.0)THEN
      BATA2 = 1.0
      ELSEIF(BATA2.LT.0.0)THEN
      BATA2 = 0.0
      ENDIF
C
      S1(1,1) = (1.0-BATA1)*SMTX11(1,1)+BATA1*SMTX12(1,1)
      S1(1,2) = (1.0-BATA1)*SMTX11(1,2)+BATA1*SMTX12(1,2)
      S1(2,1) = (1.0-BATA1)*SMTX11(2,1)+BATA1*SMTX12(2,1)
      S1(2,2) = (1.0-BATA1)*SMTX11(2,2)+BATA1*SMTX12(2,2)
C
      S2(1,1) = (1.0-BATA2)*SMTX21(1,1)+BATA2*SMTX22(1,1)
      S2(1,2) = (1.0-BATA2)*SMTX21(1,2)+BATA2*SMTX22(1,2)
      S2(2,1) = (1.0-BATA2)*SMTX21(2,1)+BATA2*SMTX22(2,1)
      S2(2,2) = (1.0-BATA2)*SMTX21(2,2)+BATA2*SMTX22(2,2)
C
      RETURN
      END
C
      FUNCTION F(IEQ,NOEQN,X)
C
C        A SET OF NONLINEAR EQUATIONS WHICH DESCRIBE THE MOTION
C        AT THE CONTACTING POINT
C
      IMPLICIT DOUBLE PRECISION (A-H,O-Z)
      COMMON/DAMPER/SMTX11(2,2),SMTX12(2,2),SMTX21(2,2),SMTX22(2,2),
     1  S1(2,2),S2(2,2),FCOE11,FCOE12,FCOE21,FCOE22,FNM11,FNM12,
     1  FNM21,FNM22,FNMC11,FNMC12,FNMC21,FNMC22,COE1,COE2
      COMMON/NLOAD/FN1,FN2,ALPHA
      COMMON/EXCIT/GF(10),MODE
      COMMON/RECEPE/RE1(2,2),RE2(2,2),RE3(2,2),RE4(2,2)
      COMMON/RECEPF/RF(8,8,2),CF(8,2)
      COMMON/FFORCE/F1(2,2),F2(2,2),F3(2,2),F4(2,2)
      COMMON/MAIN/PHASE
      COMMON/STICK/IS,SFN,SW
      DIMENSION X(8),W1(2,2),W2(2,2)
      DIMENSION CFF(8,2),FF2(2,2),FF1(2,2)
      W1(1,1) = X(1)
      W1(1,2) = X(2)
      W1(2,1) = X(3)
      W1(2,2) = X(4)
      W2(1,1) = X(5)
      W2(1,2) = X(6)
      W2(2,1) = X(7)
      W2(2,2) = X(8)
C
      IF(IS.EQ.1)THEN
      CALL AB(S1,W1,2,F1)
```

```
      CALL AB(S2,W2,2,F2)
      GO TO 10
      ENDIF
      CALL FRIFORC(W1,S1,COE1,FN1,F1)
      CALL FRIFORC(W2,S2,COE2,FN2,F2)
   10 CALL PHASLAG(F1,PHASE,F4)
      CALL PHASLAG(F2,PHASE,F3)
C
      DO 20 I=1,2
      DO 20 J=1,2
      CF(I,J)= F1(I,J)
      CF(I+2,J) = F2(I,J)
      CF(I+4,J) = F3(I,J)
   20 CF(I+6,J) = F4(I,J)
C
      CALL PHASLAG(F1,-PHASE,FF1)
      CALL PHASLAG(F2,-PHASE,FF2)
C
      DO 30 I=1,2
      DO 30 J=1,2
      CFF(I,J)= -FF1(I,J)
      CFF(I+2,J) = -FF2(I,J)
      CFF(I+4,J) = -F2(I,J)
   30 CFF(I+6,J) = -F1(I,J)
C
      DO 50 I=1,2
      W1(I,1)=RE1(I,1)+RE4(I,1)
      W1(I,2)=RE1(I,2)+RE4(I,2)
      DO 40 K=1,8
      W1(I,1)= W1(I,1)-RF(I,K,1)*CF(K,1)+RF(I,K,2)*CF(K,2)
      W1(I,1)= W1(I,1)+RF(I+6,K,1)*CFF(K,1)-RF(I+6,K,2)*CFF(K,2)
      W1(I,2)= W1(I,2)-RF(I,K,2)*CF(K,1)-RF(I,K,1)*CF(K,2)
   40 W1(I,2)= W1(I,2)+RF(I+6,K,2)*CFF(K,1)+RF(I+6,K,1)*CFF(K,2)
   50 CONTINUE
C
      DO 70 I=1,2
      W2(I,1)= RE2(I,1)+RE3(I,1)
      W2(I,2)= RE2(I,2)+RE3(I,2)
      DO 60 K=1,8
      W2(I,1)= W2(I,1)-RF(I+2,K,1)*CF(K,1)+RF(I+2,K,2)*CF(K,2)
      W2(I,1)= W2(I,1)+RF(I+4,K,1)*CFF(K,1)-RF(I+4,K,2)*CFF(K,2)
      W2(I,2)= W2(I,2)-RF(I+2,K,2)*CF(K,1)-RF(I+2,K,1)*CF(K,2)
   60 W2(I,2)= W2(I,2)+RF(I+4,K,2)*CFF(K,1)+RF(I+4,K,1)*CFF(K,2)
   70 CONTINUE
C
      IF(IEQ.EQ.1) THEN
      F=X(1)-W1(1,1)
      ELSEIF(IEQ.EQ.2) THEN
      F=X(2)-W1(1,2)
      ELSEIF(IEQ.EQ.3) THEN
      F=X(3)-W1(2,1)
      ELSEIF(IEQ.EQ.4) THEN
      F=X(4)-W1(2,2)
      ELSEIF(IEQ.EQ.5) THEN
      F=X(5)-W2(1,1)
      ELSEIF(IEQ.EQ.6) THEN
      F=X(6)-W2(1,2)
      ELSEIF(IEQ.EQ.7) THEN
      F=X(7)-W2(2,1)
      ELSEIF(IEQ.EQ.8) THEN
```

```
      F=X(8)-W2(2,2)
      ENDIF
      RETURN
      END
C
      FUNCTION F1(IEQ,NOEQN,X1)
C
C        A NONLINEAR EQUATION WHICH DEFINES THE PEAK RESPONSE
C        OF AN OPTIMAL CURVE
C
      IMPLICIT DOUBLE PRECISION (A-H,O-Z)
      COMMON/EXCIT/GF(10),MODE
      COMMON/BLADE/U(8,10),SR(15,10),EMASS(10),WMODAL(10),
     1  DAM(10)
      COMMON/RECEPE/RE1(2,2),RE2(2,2),RE3(2,2),RE4(2,2)
      COMMON/RECEPF/RF(8,8,2),CF(8,2)
      COMMON/GSOLV/X(8),DX(8),XMAX(8),XMIN(8),DELMX(8),EPSI(8),
     1  A(8,8),B(8,1)
      COMMON/ERROR/IR,XI(8)
      COMMON/STICK/IS,SFN,SW
      COMMON/SWITCH/IM
      DIMENSION X1(1)
C
      W = X1(1)
      IT = 30
      IF(IS.EQ.1)THEN
      IT = 50
      ENDIF
      IF(IM .EQ. 1) THEN
      CALL GETRE(W)
      ELSE IF(IM .EQ. 2) THEN
      CALL GETRE1(W)
      ENDIF
      CALL GETRF(W)
      CALL GSLV(8,XI,DX,XMAX,XMIN,DELMX,EPSI,IT,0,IR,A,B)
      IF(IR.EQ.1) GO TO 10
      IF(IEQ.EQ.1) THEN
      F1=F9(W,.001*DAM(MODE)*WMODAL(MODE),XI)
      ENDIF
   10 RETURN
      END
C
      FUNCTION F9(W,DW,XI)
C
C        CALCULATE THE SLOPE OF AN OPTIMAL CURVE AT A GIVEN FREQUENCY
C
      IMPLICIT DOUBLE PRECISION (A-H,O-Z)
      COMMON/BLADE/U(8,10),SR(15,10),EMASS(10),WMODAL(10),
     1  DAM(10)
      COMMON/NUMB/NBLADE,NEODER,NMODES,NRS,NCO
      COMMON/MAIN/PHASE
      COMMON/EXCIT/GF(10),MODE
      COMMON/RECEPF/RF(8,8,2),CF(8,2)
      COMMON/GSOLV/X(8),DX(8),XMAX(8),XMIN(8),DELMX(8),EPSI(8),
     1  A(8,8),B(8,1)
      COMMON/OPTIMUM/NP,NC
      DIMENSION XI(8),WW(2),FF(2)
      DIMENSION PS(3),SM(3,2)
C
      WW(2)=W+0.01*DW
```

```
      WW(1)=W-0.01*DW
      DO 10 II=1,2
      CALL GETRE(WW(II))
      CALL GETRF(WW(II))
      X(1) = XI(1)
      X(2) = XI(2)
      X(3) = XI(3)
      X(4) = XI(4)
      X(5) = XI(5)
      X(6) = XI(6)
      X(7) = XI(7)
      X(8) = XI(8)
      CALL GSLV(8,X,DX,XMAX,XMIN,DELMX,EPSI,50,0,IERR,A,B)
      CALL OSTRESS(WW(II),NP,PS,SM)
   10 FF(II)=PS(NC)
      F9=(FF(2)-FF(1))/(0.02*DW)
      RETURN
      END
C
      SUBROUTINE GETRE(W)
C
C        CALCULATE VIBRATORY DISPLACEMENTS OF THE FOUR CONTACT
C        POINTS WHEN ASSUMING ZERO NORMAL LOAD (NO FRICTION FORCE)
C        AND MULTI-MODE EXCITATION
C
      IMPLICIT DOUBLE PRECISION (A-H,O-Z)
      COMMON/NUMB/NBLADE,NEODER,NMODES,NRS,NCO
      COMMON/BLADE/U(8,10),SR(15,10),EMASS(10),WMODAL(10),
     1  DAM(10)
      COMMON/RECEPE/RE1(2,2),RE2(2,2),RE3(2,2),RE4(2,2)
      COMMON/FFORCE/F1(2,2),F2(2,2),F3(2,2),F4(2,2)
      COMMON/MAIN/PHASE
      COMMON/EXCIT/GF(10),MODE
      DIMENSION RE5(2,2),RE6(2,2)
      DIMENSION GD(10)
C
      DO 50 I=1,2
      DO 10 J=1,NMODES
   10 GD(J) = U(I,J)
      CALL RESPNSE(GD,W,RE1(I,1),RE1(I,2))
      DO 20 J=1,NMODES
   20 GD(J) = U(I+2,J)
      CALL RESPNSE(GD,W,RE2(I,1),RE2(I,2))
      DO 30 J=1,NMODES
   30 GD(J) = U(I+4,J)
      CALL RESPNSE(GD,W,RE5(I,1),RE5(I,2))
      DO 40 J=1,NMODES
   40 GD(J) = U(I+6,J)
   50 CALL RESPNSE(GD,W,RE6(I,1),RE6(I,2))
      CALL PHASLAG(RE5,-PHASE,RE3)
      CALL PHASLAG(RE6,-PHASE,RE4)
      RETURN
      END
C
      SUBROUTINE GETRE1(W)
C
C        CALCULATE VIBRATORY DISPLACEMENTS OF THE FOUR CONTACT
C        POINTS WHEN ASSUMING ZERO NORMAL LOAD (NO FRICTION FORCE)
C        AND SINGLE-MODE EXCITATION
C
```

```
      IMPLICIT DOUBLE PRECISION (A-H,O-Z)
      COMMON/NUMB/NBLADE,NEODER,NMODES,NRS,NCO
      COMMON/BLADE/U(8,10),SR(15,10),EMASS(10),WMODAL(10),
     1  DAM(10)
      COMMON/RECEPE/RE1(2,2),RE2(2,2),RE3(2,2),RE4(2,2)
      COMMON/FFORCE/F1(2,2),F2(2,2),F3(2,2),F4(2,2)
      COMMON/MAIN/PHASE
      COMMON/EXCIT/GF(10),MODE
      DIMENSION RE5(2,2),RE6(2,2)
      DIMENSION GD(10)
C
      DO 50 I=1,2
      DO 10 J=1,NMODES
   10 GD(J) = 0.0
      GD(MODE)=U(I,MODE)
      CALL RESPNSE(GD,W,RE1(I,1),RE1(I,2))
      DO 20 J=1,NMODES
   20 GD(J) = 0.0
      GD(MODE)=U(I+2,MODE)
      CALL RESPNSE(GD,W,RE2(I,1),RE2(I,2))
      DO 30 J=1,NMODES
   30 GD(J) = 0.0
      GD(MODE)=U(I+4,MODE)
      CALL RESPNSE(GD,W,RE5(I,1),RE5(I,2))
      DO 40 J=1,NMODES
   40 GD(J) = 0.0
      GD(MODE)=U(I+6,MODE)
   50 CALL RESPNSE(GD,W,RE6(I,1),RE6(I,2))
      CALL PHASLAG(RE5,-PHASE,RE3)
      CALL PHASLAG(RE6,-PHASE,RE4)
      RETURN
      END
C
      SUBROUTINE GETRF(W)
C
C        CALCULATE RECEPTANCE MATRIX
C
      IMPLICIT DOUBLE PRECISION (A-H,O-Z)
      COMMON/BLADE/U(8,10),S(15,10),EMASS(10),WMODAL(10),
     1  DAM(10)
      COMMON/NUMB/NBLADE,NEODER,NMODES,NRS,NCO
      COMMON/MAIN/PHASE
      COMMON/RECEPF/RF(8,8,2),CF(8,2)
      DIMENSION DSHAPE(10),FSHAPE(10)
C
      DO 20 I=1,8
      DO 20 J=1,8
C
      DO 10 K=1,NMODES
      DSHAPE(K) = U(I,K)
   10 FSHAPE(K) = U(J,K)
C
      CALL RECEPTN(DSHAPE,FSHAPE,1.0D+0,W,RF(I,J,1),RF(I,J,2))
   20 CONTINUE
      RETURN
      END
C
      SUBROUTINE RECEPTN(DSHAPE,FSHAPE,FC,W,RC,RS)
C
C        CALCULATE RECEPTANCE (DISPLACEMENT)
```

```
C
      IMPLICIT DOUBLE PRECISION (A-H,O-Z)
      COMMON/BLADE/U(8,10),S(15,10),EMASS(10),WMODAL(10),
     1  DAM(10)
      COMMON/NUMB/NBLADE,NEODER,NMODES,NRS,NCO
      DIMENSION DSHAPE(10),FSHAPE(10)
      RC = 0.0
      RS = 0.0
      DO 10 J=1,NMODES
      GFC = FSHAPE(J)*FC/EMASS(J)/WMODAL(J)**2
      DEN1 = 1.0 - (W/WMODAL(J))**2
      DEN2 = 2.0*DAM(J)*W/WMODAL(J)
      RC = RC + DSHAPE(J)*DEN1*GFC/(DEN1**2+DEN2**2)
      RS = RS + DSHAPE(J)*(DEN2*GFC)/(DEN1**2+DEN2**2)
   10 CONTINUE
      RETURN
      END
C
      SUBROUTINE STRESS(SSHAPE,FSHAPE,FC,W,SC,SS)
C
C        CALCULATE RECEPTANCE (STRESS)
C
      IMPLICIT DOUBLE PRECISION (A-H,O-Z)
      COMMON/BLADE/U(8,10),S(15,10),EMASS(10),WMODAL(10),
     1  DAM(10)
      COMMON/NUMB/NBLADE,NEODER,NMODES,NRS,NCO
      DIMENSION SSHAPE(10),FSHAPE(10)
C
      SC = 0.0
      SS = 0.0
      DO 10 J=1,NMODES
      GFC = FSHAPE(J)*FC/EMASS(J)/WMODAL(J)**2
      DEN1 = 1.0 - (W/WMODAL(J))**2
      DEN2 = 2.0*DAM(J)*W/WMODAL(J)
      SC = SC + SSHAPE(J)*DEN1*GFC/(DEN1**2+DEN2**2)
      SS = SS + SSHAPE(J)*(DEN2*GFC)/(DEN1**2+DEN2**2)
   10 CONTINUE
      RETURN
      END
C
      SUBROUTINE RESPNSE(GD,W,RC,RS)
C
C        CALCULATE VIBRATORY RESPONSE OF A NODE POINT WHOSE
C        MODAL DISPLACEMENT/STRESS IS GIVEN
C
      IMPLICIT DOUBLE PRECISION (A-H,O-Z)
      COMMON/NUMB/NBLADE,NEODER,NMODES,NRS,NCO
      COMMON/BLADE/U(8,10),S(15,10),EMASS(10),WMODAL(10),
     1   DAM(10)
      COMMON/EXCIT/GF(10),MODE
      DIMENSION GD(10)
C
      RC = 0.0
      RS = 0.0
      DO 10 J=1,NMODES
      GFC = GF(J)/EMASS(J)/WMODAL(J)**2
      DEN1 = 1.0 - (W/WMODAL(J))**2
      DEN2 = 2.0*DAM(J)*W/WMODAL(J)
      RC = RC + GD(J)*DEN1*GFC/(DEN1**2+DEN2**2)
      RS = RS + GD(J)*(DEN2*GFC)/(DEN1**2+DEN2**2)
```

```
   10 CONTINUE
      RETURN
      END
C
      SUBROUTINE PHASLAG(F1,PHASE,F2)
C
C        CALCULATE PHASE ANGLE BETWEEN ADJACENT BLADES
C
      IMPLICIT DOUBLE PRECISION (A-H,O-Z)
      DIMENSION F1(2,2),F2(2,2)
C
      C = COS(PHASE)
      S = SIN(PHASE)
      F2(1,1) = -C*F1(1,1) + S*F1(1,2)
      F2(2,1) = -C*F1(2,1) + S*F1(2,2)
      F2(1,2) = -S*F1(1,1) - C*F1(1,2)
      F2(2,2) = -S*F1(2,1) - C*F1(2,2)
      RETURN
      END
C
      SUBROUTINE FRIFORC(DMATRX,SMATRX,FCOE,FNORM,FFMATRX)
C
C        CALCULATE FRICTION FORCE MATRIX WHEN RELATIVE
C        DISPLACEMENT MATRIX OF THE CONTACT POINTS
C        IS GIVEN
C
      IMPLICIT DOUBLE PRECISION (A-H,O-Z)
      DIMENSION DMATRX(2,2),SMATRX(2,2),FFMATRX(2,2)
      DIMENSION SVALUE(2),RANGLE(2),PANGLE(2),U(2,2),V(2,2)
      DIMENSION FFSTIC(2,2),FFSLIP(2,2),RFFSLIP(2,2)
      CALL AB(SMATRX,DMATRX,2,FFSTIC)
      CALL ROTATE(FFSTIC,SVALUE,RANGLE,PANGLE)
      IF(SVALUE(1).EQ.0.0) THEN
      DO 10 I=1,2
      DO 10 J=1,2
   10 FFMATRX(I,J) = 0.0
      GO TO 100
      ENDIF
      FLIMIT = FCOE*FNORM
      SLIP = FLIMIT/SVALUE(1)
      IF(SLIP.LT.1.0) GO TO 20
C
      CALL EMATRX(FFSTIC,FFMATRX,2)
C
      GO TO 100
   20 CONTINUE
C
      CALL ROTATE(DMATRX,SVALUE,RANGLE,PANGLE)
      R = SVALUE(2)/SVALUE(1)
      CALL ELLIPI(R,BSIN,BCOS)
      FOURDPI = 4.0/3.1415927
      RFFSLIP(1,1) = 0.0
      RFFSLIP(1,2) = -FLIMIT*FOURDPI*BSIN
      RFFSLIP(2,1) = FLIMIT*FOURDPI*BCOS
      RFFSLIP(2,2) = 0.0
C
      CALL RTMATRX(RANGLE(1),U)
      CALL RTMATRX(-PANGLE(1),V)
      CALL ABC(U,RFFSLIP,V,2,FFSLIP)
C
```

```
C INTERPOLATION COEFFICIENTS
C
      CSTHETA = 1.0 - 2.0*SLIP
      THETA = ACOS(CSTHETA)
      CSTIC = (THETA - 0.5*SIN(2.0*THETA))/3.1415927
      CSLIP = 1.0 - SLIP
      CALL COMATRX(CSTIC,FFSTIC,CSLIP,FFSLIP,2,FFMATRX)
  100 CONTINUE
      RETURN
      END
C
      FUNCTION ELLIP1 (T)
C
C ELLIP1  - COMPLETE ELLIPTIC INTEGRAL OF THE FIRST KIND.
C
C T  - INPUT PARAMETER; 0 < T < 1.0
C
      IMPLICIT DOUBLE PRECISION (A-H,O-Z)
      A0 = 1.38629436112
      A1 = 0.09666344259
      A2 = 0.03590092383
      A3 = 0.03742563713
      A4 = 0.01451196212
      B0 = 0.5
      B1 = 0.12498593597
      B2 = 0.06880248576
      B3 = 0.03328355346
      B4 = 0.00441787012
      T1 = 1.0 - T
      T2 = T1**2
      T3 = T1**3
      T4 = T1**4
      ELLIP1 = (A0+A1*T1+A2*T2+A3*T3+A4*T4)
      ELLIP1 = ELLIP1 + (B0+B1*T1+B2*T2+B3*T3+B4*T4)*LOG(1.0/T1)
      RETURN
      END
C
      FUNCTION ELLIP2 (T)
C
C ELLIP2  - COMPLETE ELLIPTIC INTEGRAL OF THE SECOND KIND.
C
C T  - INPUT PARAMETER; 0 < T < 1.0
C
      IMPLICIT DOUBLE PRECISION (A-H,O-Z)
      A0 = 1.0
      A1 = 0.44325141463
      A2 = 0.06260601220
      A3 = 0.04757383546
      A4 = 0.01736506451
      B1 = 0.24998368310
      B2 = 0.09200180037
      B3 = 0.04069697526
      B4 = 0.00526449639
      T1 = 1.0 - T
      T2 = T1**2
      T3 = T1**3
      T4 = T1**4
      ELLIP2 = (A0+A1*T1+A2*T2+A3*T3+A4*T4)
      ELLIP2 = ELLIP2 + (B1*T1+B2*T2+B3*T3+B4*T4)*LOG(1.0/T1)
      RETURN
```

```
      END
C
      SUBROUTINE ROTATE (A,SVALUE,RANGLE,PANGLE)
C
C        CALCULATE SINGULAR VALUES AND VECTORS OF A MATRIX A
C
      IMPLICIT DOUBLE PRECISION (A-H,O-Z)
      DIMENSION A(2,2),SVALUE(2),RANGLE(2),PANGLE(2)
C
      DS = A(1,1) + A(2,2)
      DD = A(1,1) - A(2,2)
      CS = A(1,2) + A(2,1)
      CD = A(2,1) - A(1,2)
      SDS = DS*DS
      SDD = DD*DD
      SCS = CS*CS
      SCD = CD*CD
      SVALUE(1) = 0.5*((SDS+SCD)**0.5 + (SDD+SCS)**0.5)
      SVALUE(2) = 0.5*((SDS+SCD)**0.5 - (SDD+SCS)**0.5)
      IF(SVALUE(1).EQ.SVALUE(2)) GO TO 10
      SRAP = ATAN2(CS,DD)
      GO TO 20
   10 SRAP = 0.0
   20 IF(SVALUE(1).EQ.(-SVALUE(2))) GO TO 30
      DRAP = ATAN2(CD,DS)
      GO TO 40
   30 DRAP = 0.0
   40 CONTINUE
      RANGLE(1) = 0.5*(SRAP + DRAP)
      RANGLE(2) = RANGLE(1)*180.0/3.1415927
      PANGLE(1) = 0.5*(SRAP - DRAP)
      PANGLE(2) = PANGLE(1)*180.0/3.1415927
      RETURN
      END
C
      SUBROUTINE RTMATRX (RANGLE,U)
C
C        GIVE TWO DIMENSIONAL ROTATION MATRIX WHEN ROTATIONAL
C        ANGLE IS GIVEN
C
      IMPLICIT DOUBLE PRECISION (A-H,O-Z)
      DIMENSION U(2,2)
      U(1,1) = COS(RANGLE)
      U(2,1) = SIN(RANGLE)
      U(1,2) = -U(2,1)
      U(2,2) = U(1,1)
      RETURN
      END
C
      SUBROUTINE ELLIPI(R,BSIN,BCOS)
C
      IMPLICIT DOUBLE PRECISION (A-H,O-Z)
      IF(ABS(R) .LE. 1.0D-04) GO TO 25
      IF(ABS(R) .EQ. 1.0) GO TO 20
      IF(ABS(R).GT.1.0) GO TO 10
      T = 1.0 - R*R
      E1 = ELLIP1(T)
      E2 = ELLIP2(T)
      BSIN = (E2 - (1.0-T)*E1)/T
      BCOS = (E1 - E2)*R/T
```

```
      GO TO 30
   10 CONTINUE
      T = 1.0 - 1/(R*R)
      E1 = ELLIP1(T)
      E2 = ELLIP2(T)
      BCOS = (E2 - (1.0-T)*E1)/T
      BSIN = (E1 - E2)/R/T
      GO TO 30
   20 CONTINUE
      BSIN = 3.1415927/4.0
      BCOS = R*BSIN
      GO TO 30
   25 BSIN = 1.0
      BCOS = 0.0
   30 CONTINUE
C
      RETURN
      END
C
      SUBROUTINE AB(A,B,N,C)
C
C        C = AB (MATRIX MULTIPLICATION)
C
      IMPLICIT DOUBLE PRECISION (A-H,O-Z)
      DIMENSION A(2,2),B(2,2),C(2,2)
      DO 10 I=1,N
      DO 10 J=1,N
      C(I,J) = 0.0
      DO 20 K=1,N
   20 C(I,J) = C(I,J) + A(I,K)*B(K,J)
   10 CONTINUE
C
      RETURN
      END
C
      SUBROUTINE ABC(A,B,C,N,D)
C
C        D = ABC (MATRIX MULTIPLICATION)
C
      IMPLICIT DOUBLE PRECISION (A-H,O-Z)
      DIMENSION A(2,2),B(2,2),C(2,2),D(2,2),E(2,2)
      CALL AB(A,B,N,E)
      CALL AB(E,C,N,D)
      RETURN
      END
C
      SUBROUTINE EMATRX(A,B,N)
C
C        DUPLICATES A MATRIX  A = B
C
      IMPLICIT DOUBLE PRECISION (A-H,O-Z)
      DIMENSION A(2,2),B(2,2)
      DO 10 I=1,N
      DO 10 J=1,N
   10 B(I,J) = A(I,J)
      RETURN
      END
C
      SUBROUTINE COMATRX(CA,A,CB,B,N,C)
C
```

```
C         LINEAR COMBINATION OF TWO MATRICES  C = CA*A + CB*B
C
      IMPLICIT DOUBLE PRECISION (A-H,O-Z)
      DIMENSION A(2,2),B(2,2),C(2,2)
      DO 10 I=1,N
      DO 10 J=1,N
   10 C(I,J) = CA*A(I,J) + CB*B(I,J)
      RETURN
      END
C
      SUBROUTINE GSLV (NOEQN,X,DX,XMAX,XMIN,DELMX,EPSI,MITER,
     1                 IPARTL,IERR,A,B)
C
C
C   GSOLV  - SOLVES A NONLINEAR EQUATIONS SET BY NEWTON-RAPHSON'S
C            METHOD.
C
C   PROGRAM DESCRIPTION
C     SOLVES A NONLINEAR EQUATION SET BY NEWTON-RAPHSON'S
C     METHOD. (UP TO 100 X 100 EQUATIONS SET).
C
      IMPLICIT DOUBLE PRECISION (A-H,O-Z)
      COMMON/NITER/ITER
      DIMENSION X(NOEQN),XMAX(NOEQN),XMIN(NOEQN),
     1      DELMX(NOEQN),DX(NOEQN),EPSI(NOEQN)
      DIMENSION A(NOEQN,NOEQN),B(NOEQN,1)
      DIMENSION LW(300),XN(100),FV(10)
      EXTERNAL F
C
C   INITIALIZE DATA
C
      IERR=0
      IHALT=0
      ITER=0
C
C  SOLVE THE EQUATION USING THE NEWTON'S METHOD
C
   10 CONTINUE
C
C  IF NO. OF ITERATIONS ARE GREATER THAN MITER,  DIVERGES
C
      ITER=ITER+1
      IF(ITER.GT.MITER) THEN
      IERR=1
      GO TO 70
      ENDIF
C
C  GET THE FUNCTION VALUE FOR THE CURRENT VARIABLE VALUES
C
      DO 40 I=1,NOEQN
      IENUMB= I
      VALF= F(IENUMB,NOEQN,X)
      B(I,1)= -VALF
      FV(I)=VALF
C
C  GET THE PARTIAL DIFFERENCE VALUE FOR THE CURRENT VARIABLE VALUES
C
      DO 30 J=1,NOEQN
      IVNUMB=J
C
```

```
C  STOP WHEN THE VALUE OF THE VARIABLE IS LESS THAN XMIN
C  OR  GREATER THAN XMAX.
C
      IF(X(IVNUMB).LT.XMIN(IVNUMB)) THEN
      X(IVNUMB)=X(IVNUMB)+500.
      GO TO 10
      ELSEIF(X(IVNUMB).GT.XMAX(IVNUMB)) THEN
      IERR=2
      GO TO 70
      ENDIF
C
C  CALCULATE THE PARTIAL DERIVATIVES NUMERICALLY.
C
      IF(IPARTL.EQ.0) THEN
      DO 20 K=1,NOEQN
      XN(K) = X(K)
   20 CONTINUE
      XN(IVNUMB)=X(IVNUMB)+DX(IVNUMB)
      FNEW = F(IENUMB,NOEQN,XN)
      A(I,J) = (FNEW-VALF)/DX(IVNUMB)
C
C  CALCULATE THE PARTIAL DERIVATIVES ANALYTICALLY.
C
      ELSEIF(IPARTL.EQ.1) THEN
C     A(I,J)= PARTL(IENUMB,IVNUMB,N,X)
      ENDIF
C
   30 CONTINUE
   40 CONTINUE
      IHALT=1
      DO 44 I=1,NOEQN
      DAA=ABS(FV(I))
      IF(DAA.GT.EPSI(I)) THEN
      IHALT=0
      ENDIF
   44 CONTINUE
      IF(IHALT.EQ.1) GO TO 70
C
C  SOLVE THE NOEQN BY NOEQN METRICS
C
      CALL ULNEQ2(A,NOEQN,NOEQN,B,1,NOEQN,LW,0.,LRR)
      IF(LRR.EQ.1) THEN
      IERR=3
      GO TO 70
      ENDIF
C
C  IF THE CHANGE OF VARIABLE IS GREATER THAN THE ALLOWABLE
C  MAXIMUM VALUE,LIMIT THE CHANGE OF THE VARIABLES.
C
      DO 50 I=1,NOEQN
      IVNUMB=I
      IF(ABS(B(I,1)).GT.DELMX(IVNUMB)) THEN
      SIGN=B(I,1)/ABS(B(I,1))
      B(I,1)=SIGN*DELMX(IVNUMB)
      ENDIF
   50 CONTINUE
C
C  GET THE NEW VALUES OF THE VARIABLES
C
      IHALT=1
```

```
      DO 60 I=1,NOEQN
      DELX = B(I,1)
      XNEW = X(I)+B(I,1)
      X(I)= XNEW
C
   60 CONTINUE
      GO TO 10
   70 RETURN
      END
C
      SUBROUTINE GSLV1 (NOEQN,X,DX,XMAX,XMIN,DELMX,EPSI,MITER,ITER,
     1                  IPARTL,IERR,A,B)
C
      IMPLICIT DOUBLE PRECISION (A-H,O-Z)
      COMMON/ERROR/IR,XI(8)
      DIMENSION X(NOEQN),XMAX(NOEQN),XMIN(NOEQN),
     1       DELMX(NOEQN),DX(NOEQN),EPSI(NOEQN)
      DIMENSION A(NOEQN,NOEQN),B(NOEQN,1)
      DIMENSION LW(300),XN(100),FV(10)
       EXTERNAL F1
C
C  INITIALIZE DATA
C
      IERR=0
      IHALT=0
      ITER=0
C
C  SOLVE THE EQUATION USING THE NEWTON'S METHOD
C
   10 CONTINUE
C
C  IF NO. OF ITERATIONS ARE GREATER THAN MITER,  DIVERGES
C
      ITER=ITER+1
      IF(ITER.GT.MITER) THEN
      IERR=1
      GO TO 70
      ENDIF
C
C  GET THE FUNCTION VALUE FOR THE CURRENT VARIABLE VALUES
C
      DO 40 I=1,NOEQN
      IENUMB= I
      VALF= F1(IENUMB,NOEQN,X)
      IF(IR.EQ.1) GO TO 70
      B(I,1)= -VALF
      FV(I)=VALF
C
C  GET THE PATIAL DIFFERENCE VALUE FOR THE CURRENT VARIABLE VALUES
C
      DO 30 J=1,NOEQN
      IVNUMB=J
C
C  STOP WHEN THE VALUE OF THE VARIABLE IS LESS THAN XMIN
C  OR GREATER THAN XMAX.
C
      IF(X(IVNUMB).LT.XMIN(IVNUMB)) THEN
      X(IVNUMB)=X(IVNUMB)+500.
      GO TO 10
      ELSEIF(X(IVNUMB).GT.XMAX(IVNUMB)) THEN
```

```
      IERR=2
      GO TO 70
      ENDIF
C
C  CALCULATE THE PARTIAL DERIVATIVES NUMERICALLY.
C
      IF(IPARTL.EQ.0) THEN
      DO 20 K=1,NOEQN
      XN(K) = X(K)
   20 CONTINUE
      XN(IVNUMB)=X(IVNUMB)+DX(IVNUMB)
      FNEW = F1(IENUMB,NOEQN,XN)
      A(I,J) = (FNEW-VALF)/DX(IVNUMB)
C
C  CALCULATE THE PARTIAL DERIVATIVES ANALYTICALLY.
C
      ELSEIF(IPARTL.EQ.1) THEN
C     A(I,J)= PARTL(IENUMB,IVNUMB,N,X)
      ENDIF
C
   30 CONTINUE
   40 CONTINUE
      IHALT=1
      DO 44 I=1,NOEQN
      DAA=ABS(FV(I))
      IF(DAA.GT.EPSI(I)) THEN
      IHALT=0
      ENDIF
   44 CONTINUE
      IF(IHALT.EQ.1) GO TO 70
C
C  SOLVE THE NOEQN BY NOEQN METRICS
C
      CALL ULNEQ2(A,NOEQN,NOEQN,B,1,NOEQN,LW,0.,LRR)
      IF(LRR.EQ.1) THEN
      IERR=3
      GO TO 70
      ENDIF
C
C  IF THE CHANGE OF VARIABLE IS GREATER THAN THE ALLOWABLE
C  MAXIMUM VALUE,LIMIT THE CHANGE OF THE VARIABLES.
C
      DO 50 I=1,NOEQN
      IVNUMB=I
      IF(ABS(B(I,1)).GT.DELMX(IVNUMB)) THEN
      SIGN=B(I,1)/ABS(B(I,1))
      B(I,1)=SIGN*DELMX(IVNUMB)
      ENDIF
50    CONTINUE
C
C  GET THE NEW VALUES OF THE VARIABLES
C
      IHALT=1
      DO 60 I=1,NOEQN
      DELX = B(I,1)
      XNEW = X(I)+B(I,1)
      X(I)= XNEW
C
   60 CONTINUE
      GO TO 10
```

```
70    RETURN
      END
C
      SUBROUTINE ULNEQ2 (A,N,IDIMA,B,M,IDIMB,LWORK,EPS,IERR)
C
C     ULNEQ2 - SOLVES A SET OF DOUBLE-PRECISION LINEAR EQUATIONS.
C
C
C     PROGRAM DESCRIPTION
C       THIS SUBROUTINE SOLVES THE MATRIX EQUATION A * X = B,
C       OVERWRITING B WITH THE SOLUTION MATRIX X.  A  MUST BE SQUARE
C       AND NON-SINGULAR. B MUST HAVE THE SAME NUMBER OF ROWS AS A.
C       BOTH A AND B ARE DESTROYED.  BOTH  A  AND  B  ARE DOUBLE-
C       PRECISION MATRICES.
C
C     ACCESS
C     CALL ULNEQ2 (A,N,IDIMA,B,M,IDIMB,LWORK,EPS,IERR)
C       A       -DP ARY-U/R-DIM(IDIMA,N)- COEFFICIENT MATRIX OF THE
C                MATRIX EQUATION  A * X = B.  THE N X N  PORTION OF  A
C                MUST CONTAIN THE SQUARE COEFFICIENT MATRIX.  THE
C                CONTENTS OF THIS PORTION ARE DESTROYED BY THIS ROUTINE.
C       N       -IN VBL-USD- THE ORDER OF COEFFICIENT MATRIX  A .  N MUST
C                BE LESS THAN OR EQUAL TO IDIMA,LESS THAN OR EQUAL TO
C                THE SECOND DIMENSION OF  A  IN THE CALLING ROUTINE,AND
C                LESS THAN OR EQUAL TO IDIMB.
C     IDIMA   -IN VBL-USD- FIRST DIMENSION OF A IN THE CALLING ROUTINE.
C       B       -DP ARY-U/R-DIM(IDIMB,M)- CONSTANT-TERM (RIGHT-HAND-SIDE)
C                MATRIX.  THE N X M  PORTION OF  B  MUST CONTAIN THE
C                RIGHT-HAND-SIDE MATRIX.  UPON RETURN FROM THIS ROUTINE,
C                THIS PORTION OF  B  CONTAINS THE SOLUTION MATRIX.
C       M       -IN VBL-USD- THE NUMBER OF COLUMNS IN B.  M MUST BE LESS
C                THAN OR EQUAL TO THE SECOND DIMENSION OF  B  IN THE
C                CALLING ROUTINE.
C     IDIMB   -IN VBL-USD- FIRST DIMENSION OF B IN THE CALLING ROUTINE.
C       LWORK   -IN ARY-WRK-DIM(3*N)- WORKING ARRAY FOR SOLUTION
C                ALGORITHM.  LWORK MAY BE ANY INTEGER ARRAY WITH AT LEAST
C                3N ELEMENTS.  THE FIRST THIRD IS RESERVED FOR PIVOT
C                COLUMN INDICES. THE FIRST NP POSITIONS OF THIS THIRD
C                LIST THE PIVOT COLUMN INDICES IN ORDER OF USE.  THE
C                SECOND THIRD IS RESERVED FOR PIVOT ROW INDICES. THE
C                FIRST NP POSITIONS OF THIS THIRD LIST THE PIVOT ROW
C                INDICES IN ORDER OF USE.  THE LAST THIRD IS USED FOR
C                TEMPORARY STORAGE FOR INTERCHANGE OF PIVOT ROW AND
C                COLUMN INDICES.
C     EPS      -RL VBL-USD- VALUE ALL PIVOT ELEMENTS MUST EXCEED FOR
C                MATRIX  A  TO BE CONSIDERED NONSINGULAR.  IF IN DOUBT,
C                USE THE VALUE 0.0 .
C     IERR    -IN VBL-RTD- PIVOT-SEARCH ERROR CODE (SEE BELOW).
C
C     COMMON BLOCK VARIABLES
C       NONE
C
C     ERROR CONDITIONS
C       PIVOT-SEARCH ERRORS ARE RETURNED THROUGH IERR AS FOLLOWS-
C     IERR=0 IF ALL COLUMNS OF X ARE FOUND,NO TROUBLE BEING DETECTED.
C     IERR=1 IF NO COLUMNS OF X ARE FOUND,THE ELIMINATION PROCESS
C       BEING HALTED BECAUSE THE CURRENT PIVOT FAILS TO EXCEED EPS IN
C       MAGNITUDE.
C
C     EXTERNAL REFERENCES
```

```
C       NONE
C
C     COMMENTS
C       THE METHOD CONSISTS OF GAUSSIAN ELIMINATION FOLLOWED BY BACK
C       SUBSTITUTIONS. THIS IS MORE EFFICIENT THAN SOLUTION BY MATRIX
C     INVERSION REGARDLESS OF THE NUMBER OF COLUMNS IN B. BOTH ROWS
C       AND COLUMNS ARE SEARCHED FOR MAXIMAL PIVOTS. INTERCHANGING OF
C       ROWS OR COLUMNS OF A IS AVOIDED. CHAPTER 1 OF E.L. STIEFLE,
C     INTRODUCTION TO NUMERICAL MATHEMATICS,ACADEMIC PRESS,N.Y.,1963,
C       SHOULD BE HELPFUL IN FOLLOWING THE CODE.
C
C     LOCAL VARIABLES
C       ABSEPS -DP VBL- ABSOLUTE VALUE OF EPS.
C       ABSPIV -DP VBL- ABSOLUTE VALUE OF PIV.
C     IPIV    -IN VBL- ACTUAL ROW OF CURRENT PIVOT ELEMENT.
C     ITEMP   -IN VBL- TEMPORARY SPACE FOR INTERCHANGE OF PIVOT
C                INDICES.
C       JPIV    -IN VBL- ACTUAL COLUMN OF CURRENT PIVOT ELEMENT.
C       KPIV    -IN VBL- LOCATION IN SECOND THIRD OF LWORK (ROW PIVOTS)
C                CORRESPONDING TO CURRENT PIVOT.
C       LPIV    -IN VBL- LOCATION IN FIRST THIRD OF LWORK (COLUMN PIVOTS)
C                CORRESPONDING TO CURRENT PIVOT.
C       NP      -IN VBL- NUMBER OF PIVOT ELEMENT CURRENTLY BEING
C                COMPUTED.
C       NPN     -IN VBL- N PLUS N (I.E. 2N).
C       NPP     -IN VBL- NP PLUS 1 .
C       PIV     -DP VBL- VALUE OF THE CURRENT PIVOT.
C       TEMP    -DP VBL- TEMPORARY SPACE FOR INTERCHANGE OF ELEMENTS OF
C                SOLUTION MATRIX.
C
      DIMENSION A(IDIMA,N),B(IDIMB,M),LWORK(300)
      DOUBLE PRECISION A,B
C
      DOUBLE PRECISION ABSEPS,ABSPIV,PIV,TEMP
C
C
C     INITIALIZATIONS
C
      IERR=1
      NPN=N+N
      ABSEPS=ABS(EPS)
      DO 1 I=1,N
      LWORK(I+N)=I
      LWORK(I)=I
    1 CONTINUE
C
C     BEGIN ELIMINATION PROCESS
C
      DO 10 NP=1,N
C
C        SELECT PIVOT
C
      ABSPIV=0.0
      DO 3 K=NP,N
      I=LWORK(K+N)
      DO 2 L=NP,N
      J=LWORK(L)
      IF (ABS(A(I,J)).LE.ABSPIV) GOTO 2
      KPIV=K
      LPIV=L
```

```
      IPIV=I
      JPIV=J
      PIV=A(I,J)
      ABSPIV=ABS(PIV)
    2 CONTINUE
    3 CONTINUE
C
C        EXIT IF PIVOT TOO SMALL
C
C
      IF (ABSPIV.LE.ABSEPS) GOTO 19
C
C        UPDATE PIVOT ROW AND COLUMN LISTS
C
      ITEMP=LWORK(NP+N)
      LWORK(NP+N)=LWORK(KPIV+N)
      LWORK(KPIV+N)=ITEMP
      ITEMP=LWORK(NP)
      LWORK(NP)=LWORK(LPIV)
      LWORK(LPIV)=ITEMP
C
C        MODIFY PIVOT ROW OF A AND B (ELEMENTS IN PRESENT OR PREVIOUS
C        PIVOT COLUMNS OF A ARE SKIPPED)
C
      IF (NP.EQ.N) GOTO 5
      NPP=NP+1
      DO 4 L=NPP,N
      J=LWORK(L)
      A(IPIV,J)=-A(IPIV,J)/PIV
    4 CONTINUE
    5 DO 6 J=1,M
      B(IPIV,J)=-B(IPIV,J)/PIV
    6 CONTINUE
C
C        MODIFY NON-PIVOT ROWS OF A AND B (ELEMENTS IN PRESENT OR
C        PREVIOUS PIVOT ROWS OR COLUMNS ARE SKIPPED)
C
      IF (NP.EQ.N) GOTO 10
      DO 9 K=NPP,N
      I=LWORK(K+N)
      TEMP=A(I,JPIV)
      IF (TEMP.EQ.0.0) GOTO 9
      DO 7 L=NPP,N
      J=LWORK(L)
      A(I,J)=A(I,J)+A(IPIV,J)*TEMP
    7 CONTINUE
      DO 8 J=1,M
      B(I,J)=B(I,J)+B(IPIV,J)*TEMP
    8 CONTINUE
    9 CONTINUE
   10 CONTINUE
C
C     END  ELIMINATION PROCESS
C
C     BEGIN BACK SUBSTITUTIONS
C
      DO 13 J=1,M
      DO 12 K=2,N
      KK=N-K+1
      I=LWORK(KK+N)
```

```
      DO 11 L=2,K
      LL=N-L+2
      II=LWORK(LL+N)
      JJ=LWORK(LL)
      B(I,J)=B(I,J)+B(II,J)*A(I,JJ)
   11 CONTINUE
   12 CONTINUE
   13 CONTINUE
C
C     UNSCRAMBLE ROWS OF SOLUTION MATRIX
C
      DO 14 I=1,N
      L=LWORK(I+N)
      LWORK(L+NPN)=LWORK(I)
   14 CONTINUE
      DO 17 I=1,N
   15 K=LWORK(I+NPN)
      IF (I.EQ.K) GOTO 17
      DO 16 J=1,M
      TEMP=B(I,J)
      B(I,J)=B(K,J)
      B(K,J)=TEMP
   16 CONTINUE
      LWORK(I+NPN)=LWORK(K+NPN)
      LWORK(K+NPN)=K
      GO TO 15
   17 CONTINUE
C
      DO 18 J=1,M
      DO 18 I=1,N
      B(I,J)=-B(I,J)
   18 CONTINUE
      IERR=0
   19 RETURN
      END
```

NASA
National Aeronautics and Space Administration

Report Documentation Page

1. Report No.	2. Government Accession No.	3. Recipient's Catalog No.
RI/RD 91-230		

4. Title and Subtitle

Airfoil Vibration Dampers Program
Final Report

5. Report Date
11 November1991

6. Performing Organization Code

7. Author(s)

Robert M. Cook

8. Performing Organization Report No.

10. Work Unit No.

9. Performing Organization Name and Address

Rocketdyne Division, Rockwell International Corporation
6633 Canoga Avenue
Canoga Park , CA 91304

11. Contract or Grant No.
NAS8 - 36720

13. Type of Report and Period Covered
Final Report

12. Sponsoring Agency Name and Address

National Aeronautics and Space Administration
George C. Marshall Space Flight Center
Huntsville , AL 35812

14. Sponsoring Agency Code

15. Supplementary Notes

16. Abstract

The Airfoil Vibration Damper program has consisted of an analysis phase and a testing phase. During the analysis phase, a state-of-the-art computer code was developed, which can be used to guide designers in the placement and sizing of friction dampers. The use of this computer code was demonstrated by performing representative analyses on turbine blades from the High Pressure Oxidizer Turbopump (HPOTP) and High Pressure Fuel Turbopump (HPFTP) of the Space Shuttle Main Engine (SSME). The testing phase of the program consisted of performing friction damping tests on two different cantilever beams. Data from these tests provided an empirical check on the accuracy of the computer code developed in the analysis phase.

Results of the analysis and testing showed that the computer code can accurately predict the performance of friction dampers. In addition, a valuable set of friction damping data was generated, which can be used to aid in the design of friction dampers, as well as provide benchmark test cases for future code developers.

17. Key Words (Suggested by Author(s))	18. Distribution Statement

19. Security Classif. (of this report)	20. Security Classif. (of this page)	21. No. of Pages	22. Price
UNCLASS	UNCLASS	239	A11

NASA FORM 1626 Oct 86